Durham University

# Durham E-Theses

## *Non-isothermal plasma treatment of organic and inorganic polymers*

Oliver Davey Greenwood

**How to cite:**

Greenwood, Oliver Davey (1997) Non-isothermal plasma treatment of organic and inorganic polymers. Doctoral thesis, Durham University.

**Use policy**

The full-text may be used and/or reproduced, and given to third parties in any format or medium, without prior permission or charge, for personal research or study, educational, or not-for-profit purposes provided that:

- a full bibliographic reference is made to the original source
- a https://etheses.durham.ac.uk/id/eprint/5065/ is made to the metadata record in Durham E-Theses
- the full-text is not changed in any way

The full-text must not be sold in any format or medium without the formal permission of the copyright holders.

Please consult the full Durham E-Theses policy for further details.

Academic Support Office, The Palatine Centre, Durham University, Stockton Road, Durham, DH1 3LE
e-mail: e-theses.admin@durham.ac.uk Tel: +44 0191 334 6107
https://etheses.durham.ac.uk

# Non-isothermal Plasma Treatment Of Organic And Inorganic Polymers

**PhD Thesis**

**Oliver Davey Greenwood**

**University of Durham**

**Department of Chemistry**

**1997**

The copyright of this thesis rests with the author. No quotation from it should be published without the written consent of the author and information derived from it should be acknowledged.

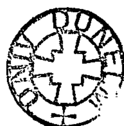

1 2 AUG 1998

## Abstract

Increased understanding of plasma-polymer interactions is required to further the technological use of such processes, and elucidates heterogeneous physico-chemical reactions which occur under bombardment by complex combinations of energetic species. This thesis presents a systematic investigation into the effect of exposing organic and inorganic polymeric surfaces to controlled non-isothermal plasmas. Concurrently, a novel process is presented by which metal oxide gas barrier coatings are synthesized on polymer substrates by non-isothermal plasma treatment.

Organic polymers exhibiting a range of structures were modified using non-isothermal plasmas at atmospheric and low pressure. The extent of atmospheric discharge oxygenation, measured by X-ray photoelectron spectroscopy (XPS), correlated with the polymers' ozonolysis rate constants. Surface physical disruption, studied using atomic force microscopy (AFM), after atmospheric discharge treatment was more pronounced than after low pressure plasma treatment. During low pressure oxygen plasma treatment, polymers containing phenyl groups were oxygenated to an extent which varied with the strength of $\pi$–$\pi^*$ valence band excitation in XPS C(1s) spectra of the untreated polymers, suggesting a dominance of reaction of plasma atomic oxygen at polymer radical sites excited by plasma vacuum ultraviolet radiation. The size of globules, observed by AFM, on the plasma modified surfaces correlated with the extent of surface chemical modification, inkeeping with a mechanism of chemically driven agglomeration of plasma oxidized low molecular weight polymer material.

Oxygen plasma was more effective than water plasma in chemically modifying the surface of films of zirconium-normal-butoxide spin coated on polyester substrates, and the resulting optimized treatment produced a significant reduction in gas permeation of the substrate. XPS studies showed that oxygen plasma treatment of a polyphenylsilsesquioxane film on polyester film created a $SiO_2$ layer less than 8 nm thin, which reduced $O_2$ and Ar permeation of the coated film by 37.5 % and 31.6% respectively.

## Statement of Copyright

The copyright of this thesis rests with the author. No quotation from it should be published without prior written consent from the author, and information derived from it should be acknowledged.

## Declaration of Originality

The work presented in this thesis was carried out in the Department of Chemistry at the University of Durham between September 1992 and October 1995. This work has not previously been submitted for any degree with the exception of AFM images of polysulfone and polyethersulfone in chapter 3, which formed part of the PhD thesis of Janet Hopkins entitled "Plasma treatment of polysulfone gas separation membranes". The work is the original work of the author except where otherwise acknowledged. The author would like to officially register that: AFM images in chapters 2 and 3 were recorded by J. P. S. Badyal; the AFM images in chapter 4 were recorded by R. D. Boyd in collaboration with the author; and all data interpretation was carried out in collaboration with J. P. S. Badyal.

## Publications Arising From This Thesis

Work presented in chapters 2 and 3 of this thesis has appeared in the following publications.

1. Greenwood, O. D.; Wells, R. K.; Badyal, J. P. S. "A comparative study of the silent discharge treatment of polyethylene, polypropylene, polyisobutylene and polystyrene," *Proc. 11th Int. Symp. Plasma Chem.* **1993**, *3*, 1168.

2. Greenwood, O. D.; Tasker, S.; Badyal, J. P. S. "A comparative study of the silent discharge treatment of saturated and unsaturated hydrocarbon polymers," *J. Polymer Sci.: Part A: Polymer Chem.* **1994**, *32*, 2479.

3. Greenwood, O. D.; Boyd, R. D.; Hopkins, J.; Badyal, J. P. S. "Atmospheric silent discharge treatment versus low pressure plasma treatment of polyethylene, polypropylene, polyisobutylene and polystyrene," *Int. Symp. Polymer Surface Mod., Las Vegas*, **1993**; *J. Adh. Sci. & Tech.* **1995**, *9*, 311.

4. Greenwood, O. D.; Hopkins, J.; Badyal, J. P. S "Non-isothermal $O_2$ plasma treatment of phenyl-containing polymers," *Macromolecules*, **1997**, *30*, 1091.

## Other Publication

1. Boyd, R. D.; Greenwood, O. D.; Hopkins, J.; Badyal, J. P. S. "Silent discharge treatment of biaxially orientated polypropylene" *Proc. 12th Int. Symp. Plasma Chem.*, **1995**, *1*, 239.

## Acknowledgements

I gratefully acknowledge support, practical help and teaching given to me in my thesis work by my supervisor, Professor Jas Pal Badyal; by each of the surface science group members and the technical staff of the Chemistry Department at the University of Durham; and by Brian Simmons at my industrial sponsor company, Pira International.

I was able to carry out and write up this work through the inspiration, love and patient support of my wife Catherine, and I thank the rest of my family for their generosity in supporting and encouraging me during my research. My thanks also goes to Mary Boreham for her help in submitting this thesis while I was working in the USA.

# Table Of Contents


**Title** i

**Abstract** ii

**Statement of Copyright** iii

**Declaration of Originality** iii

**Publications Arising From This Thesis** iv

**Other Publication** iv

**Acknowledgements** v

**Table of Contents** vi

**List of Figures** xi

**List of Tables** xvii

**Chapter One : Introduction to Gas Barrier Materials and Plasma Surface Modification** 1

**1.1 GAS BARRIER MATERIALS** 1

*1.1.1 Introduction* 1

*1.1.2 Requirements For Food Packaging Materials* 1

*1.1.3 Solution, Diffusion and Permeation* 2

*1.1.4 Reducing Gas Permeability* 3

*1.1.5 Barrier Coating Technology* 5

**1.2 PLASMA MODIFICATION OF POLYMER SURFACES** 5

*1.2.1 Advantages Of Plasma Surface Modification* 5

*1.2.2 Plasma Parameters* 6

1.2.2.1 Definition and Parameter Range 6

1.2.2.2 Thermal and Non-equilibrium Plasmas 8

1.2.2.3 Debye Shielding 9

1.2.2.4 Plasma Frequency 10

1.2.2.5 Plasma Sheath 10

1.2.2.6 Supply Frequency 11

*1.2.3 Chemical Physics of Plasma-Polymer Modification* 12

1.2.3.1 Introduction 12

1.2.3.2 Homogeneous Plasma Reactions 13

1.2.3.3 Polymer-Plasma Heterogeneous Reactions 14
1.2.3.4 Plasma Physical Modification of Polymer Surfaces 14
1.2.3.5 Synergistic Processes 15
*1.2.4 Polymer Properties Modified By Plasma Treatment* *16*
1.2.4.1 Wettability and Adhesion 16
1.2.4.2 Gas Permeability and Selectivity 16
1.2.4.3 Biocompatibility 17
1.2.4.4 Roughness and Friction 17
1.2.4.5 Hardness and Wear 17
1.2.4.6 Electromagnetic Properties 17
*1.2.5 Summary* *18*
**1.3 REFERENCES** **18**

**Chapter Two : Silent Discharge Versus Low Pressure Plasma Treatment Of Five Hydrocarbon Polymers** **24**
**2.1 INTRODUCTION** **24**
*2.1.1 Atmospheric Pressure Air Discharge* *24*
*2.1.2 Low Pressure Air Discharge* *26*
**2.2 EXPERIMENTAL** **27**
**2.3 RESULTS** **30**
**2.4 DISCUSSION** **46**
*2.4.1 Silent Discharge Chemical Modification* *46*
*2.4.2 Low Pressure Plasma Chemical Modification* *49*
*2.4.3 Topographical Modification* *49*
**2.5 CONCLUSIONS** **49**
**2.6 REFERENCES** **50**

**Chapter Three: Non-Isothermal Oxygen Plasma Treatment Of Phenyl Containing Polymers** **54**
**3.1 INTRODUCTION** **54**
**3.2 EXPERIMENTAL** **54**
**3.3.RESULTS** **56**
*3.3.1 XPS* *56*

*3.3.2 AFM* 67

**3.4 DISCUSSION** 80

**3.5 CONCLUSIONS** 85

**3.6 REFERENCES** 85

**Chapter Four : Plasma Modification Of Zirconium Butoxide Films** 87

**4.1 INTRODUCTION** 87

**4.2 EXPERIMENTAL** 88

***4.2.1 $Zr(OBu)_4$ Solution Preparation*** 88

***4.2.2 Substrate Preparation*** 89

***4.2.3 Spin Coating $Zr(OBu)_4$ Solution*** 89

***4.2.4 Plasma Treatments Of Spin Coated Films*** 90

***4.2.5 Analysis Of Coatings*** 90

**4.3 RESULTS** 93

***4.3.1 XPS*** 93

*4.3.1.1 $Zr(OBu)_4$ Spin Coated On Glass, PET and Silent Discharge Treated PET* 93

*4.3.1.2 Silent Discharge Treated $Zr(OBu)_4$ Spin Coated On Glass Substrates* 98

*4.3.1.3 Plasma Treated $Zr(OBu)_4$ Spin Coated On Glass Substrates* 98

*4.3.1.4 Oxygen Plasma Power Variation* 103

*4.3.1.5 Oxygen Plasma Duration Variation* 104

*4.3.1.6 Water Plasma Power Variation* 106

*4.3.1.7 Water Plasma Duration Variation* 107

*4.3.1.8 Plasma Treated $Zr(OBu)_4$ Spin Coated On PET Substrates* 109

*4.3.1.9 Oxygen Plasma Power Variation* 113

*4.3.1.10 Oxygen Plasma Duration Variation* 114

*4.3.1.11 Water Plasma Power Variation* 116

*4.3.1.12 Water Plasma Duration Variation* 117

*4.3.2 Argon Ion Etch Depth Profiles* 119

*4.3.3 FTIR* 123

*4.3.4 Gas Permeability Of $Zr(OBu)_4$ Coatings On PET Substrates* 125

*4.3.5 Film Thickness Estimation* 125

*4.3.5 AFM* 126

4.4 DISCUSSION 127

4.5 CONCLUSION 134

4.6 REFERENCES 135

**Chapter Five : Plasma Modification Of Polyphenylsilsesquioxane Films** 139

5.1 INTRODUCTION 139

5.2 EXPERIMENTAL 140

5.3 RESULTS 141

5.4 DISCUSSION 156

5.5 CONCLUSIONS 160

5.6 REFERENCES 160

**Chapter Six: Conclusions** 163

**Appendix One: Surface Analysis Techniques** 166

A1.1 INTRODUCTION 166

A1.2 X-RAY PHOTOELECTRON SPECTROSCOPY 166

*A1.2.1 Introduction* 166

*A1.2.2 Instrumentation* 167

*A1.2.3 Spectral Interpretation* 168

*A1.2.4 Valence Band Spectral Features* 168

*A1.2.5 Sampling Depth* 169

*A1.2.7 XPS Depth Profiling* 170

*A1.2.7 Advantages and Disadvantages of XPS* 171

A1.3 SURFACE INFRARED SPECTROSCOPY 171

*A1.3.1 Introduction* 171

*A1.3.2 Instrumentation* 173

*A1.3.3 Attenuated Total Internal Reflection (ATR)* 174

**A1.4 ATOMIC FORCE MICROSCOPY** 174

*A1.5.1 Introduction* 174

*A1.5.2 Modes of Operation* 174

**A1.5 REFERENCES** 175

**Appendix Two: Courses, Conferences Colloquia, Lectures and Seminars Attended** 189

## List of Figures

Figure 1.1 Regimes of plasma particle density and energy. 7
Figure 1.2 Maxwellian electron energy distribution model. 9
Figure 1.3 Plasma coupling configurations (a) Capacitative and (b) Inductive. 12
Figure 2.1 Concentration of silent discharge species as a function of time after start of a microdischarge. 25
Figure 2.2 Structures of hydrocarbon polymers treated in this study. 27
Figure 2.3 Silent discharge reactor. 28
Figure 2.4 Low pressure plasma reactor. 29
Figure 2.5 C(1s) XPS spectra of untreated: (a) polystyrene; (b) polyethylene; (c) polypropylene; (d) polyisobutylene; and (e) polyisoprene. 31
Figure 2.6 C(1s) XPS spectra of silent discharge treated: (a) polystyrene; (b) polyethylene; (c) polypropylene; (d) polyisobutylene; and (e) polyisoprene. 33
Figure 2.7 C(1s) XPS spectra of air plasma treated: (a) polystyrene; (b) polyethylene; (c) polypropylene; (d) polyisobutylene; and (e) polyisoprene. 34
Figure 2.8(a) AFM of untreated polystyrene. 36
Figure 2.8(b) AFM of air plasma treated polystyrene. 36
Figure 2.8(c) AFM of silent discharge treated polystyrene. 37
Figure 2.9(a) AFM of untreated polyethylene. 37
Figure 2.9(b) AFM of air plasma treated polyethylene. 38
Figure 2.9(c) AFM of silent discharge treated polyethylene. 38
Figure 2.10(a) AFM of untreated polypropylene. 39
Figure 2.10(b) AFM of air plasma treated polypropylene. 39
Figure 2.10(c) AFM of silent discharge treated polypropylene. 40
Figure 2.11(a) AFM of untreated polyisobutylene. 40
Figure 2.11(b) AFM of air plasma treated polyisobutylene. 41
Figure 2.11(c) AFM of silent discharge treated polyisobutylene. 41
Figure 2.12 AFM of air plasma treated polyisoprene. 42

Figure 2.13 ATR-FTIR spectra of (a) untreated PIP and (b) silent discharge treated PIP. 45

Figure 3.1(a) C(1s) XPS spectra of untreated polymers 57

Figure 3.1(b) C(1s) XPS spectra of $O_2$ plasma treated polymers 59

Figure 3.1(c) C(1s) XPS spectra of solvent washed $O_2$ plasma treated polymers 61

Figure 3.2 Variation in XPS O:C ratio with parent polymer structure for: untreated, $O_2$ plasma treated, and solvent washed $O_2$ plasma treated polymers. 63

Figure 3.3 Atomic force micrographs of untreated: (a) polystyrene; (b) polyethyleneterephthalate 68

Figure 3.3 Atomic force micrographs of untreated (c) polyetheretherketone; (d) polybisphenolcarbonate 69

Figure 3.3 Atomic force micrographs of untreated (e) polybisphenolsulfone; (f) polyethersulfone 70

Figure 3.3 Atomic force micrograph of untreated (g) polydimethylphenyleneoxide 71

Figure 3.4 Atomic force micrographs of $O_2$ plasma treated: (a) polystyrene; (b) polyethyleneterephthalate 72

Figure 3.4 Atomic force micrographs of $O_2$ plasma treated: (c) polyetheretherketone; (d) polybisphenolcarbonate 73

Figure 3.4 Atomic force micrographs of $O_2$ plasma treated: (e) polybisphenolsulfone; (f) polyethersulfone 74

Figure 3.4 Atomic force micrograph of $O_2$ plasma treated: (g) polydimethylphenyleneoxide 75

Figure 3.5 Atomic force micrographs of solvent washed $O_2$ plasma treated: (a) polystyrene; (b) polyethyleneterephthalate 76

Figure 3.5 Atomic force micrographs of solvent washed $O_2$ plasma treated: (c) polyetheretherketone; (d) polybisphenolcarbonate 77

Figure 3.5 Atomic force micrographs of solvent washed $O_2$ plasma treated: (e) polybisphenolsulfone; (f) polyethersulfone 78

Figure 3.5 Atomic force micrographs of solvent washed $O_2$ plasma treated: (g) polydimethylphenyleneoxide 79

Figure 3.6 Percentage $\pi-\pi^*$ shake-up of total XPS C(1s) intensity versus percentage of carbon centres in phenyl environments for untreated polymers. 81

Figure 3.7 Extent of oxidative attack versus percentage $\pi-\pi^*$ shake-up of total XPS C(1s) intensity for the untreated polymer. 82

Figure 3.8 Extent of oxidative attack versus mean globule size. 84

Figure 4.1 Structure of zirconium butoxide, $Zr(OBu)_4$. 87

Figure 4.2 Coordinate bond responsible for polymerization in zirconium butoxide[15]. 88

Figure 4.3 Apparatus for mass spectrometric gas permeability measurement. 92

Figure 4.4 C(1s) spectra of $Zr(OBu)_4$ spin coated on: (a) PET; (b) SDT PET; and (c) glass. 95

Figure 4.5 Zr(3d) spectra of $Zr(OBu)_4$ spin coated on: (a) PET; (b) SDT PET; and (c) glass. 96

Figure 4.6 O(1s) spectra of $Zr(OBu)_4$ spin coated on: (a) PET; (b) SDT PET; and (c) glass. 97

Figure 4.7 Surface composition of $Zr(OBu)_4$ films on glass: (a) untreated; (b) $H_2O$ plasma treated (40 W, 2 min); and (c) $O_2$ plasma treated (60 W, 2 min). 99

Figure 4.8 C(1s) XP spectra of $Zr(OBu)_4$ films on glass: (a) untreated; (b) $H_2O$ plasma treated (30W, 5 min); and (c) $O_2$ plasma treated (30 W, 5 min). 100

Figure 4.9 Zr(3d) XP spectra of $Zr(OBu)_4$ films on glass: (a) untreated; (b) $H_2O$ plasma treated (30W, 5 min); and (c) $O_2$ plasma treated (30 W, 5 min). 101

Figure 4.10 O(1s) XP spectra of $Zr(OBu)_4$ films on glass: (a) untreated; (b) $H_2O$ plasma treated (30W, 5 min); and (c) $O_2$ plasma treated (30 W, 5 min). 102

Figure 4.11 Carbon, zirconium and oxygen content of $Zr(OBu)_4$ films on glass versus power of $O_2$ plasma treatment. 103

Figure 4.12 Carbon, zirconium and oxygen content of $Zr(OBu)_4$ films

on glass versus duration of $O_2$ plasma treatment. 105
Figure 4.13 Carbon, zirconium and oxygen content of $Zr(OBu)_4$ films
on glass versus power of $H_2O$ plasma treatment. 106
Figure 4.14 Carbon, zirconium and oxygen content of $Zr(OBu)_4$ films
on glass versus duration of $H_2O$ plasma treatment. 108

Figure 4.15 Surface composition of $Zr(OBu)_4$ films on SDT PET:

(a) untreated; (b) $H_2O$ plasma treated (50W, 2 min); and

(c) $O_2$ plasma treated (2 W, 2 min). 109

Figure 4.16 C(1s) XP spectra of $Zr(OBu)_4$ films on SDT PET:

(a) untreated; (b) $H_2O$ plasma treated (20W, 2 min); and

(c) $O_2$ plasma treated (20 W, 2 min). 110

Figure 4.17 Zr(3d) XP spectra of $Zr(OBu)_4$ films on SDT PET:

(a) untreated; (b) $H_2O$ plasma treated (20W, 2 min); and

(c) $O_2$ plasma treated (20 W, 2 min). 111

Figure 4.18 O(1s) XP spectra of $Zr(OBu)_4$ films on SDT PET:

(a) untreated; (b) $H_2O$ plasma treated (20W, 2 min); and

(c) $O_2$ plasma treated (20 W, 2 min). 112
Figure 4.19 Carbon, zirconium and oxygen content of $Zr(OBu)_4$ films
on SDT PET versus power of $O_2$ plasma treatment. 113
Figure 4.20 Carbon, zirconium and oxygen content of $Zr(OBu)_4$ films
on SDT PET versus duration of $O_2$ plasma treatment. 115
Figure 4.21 Carbon, zirconium and oxygen content of $Zr(OBu)_4$ films
on SDT PET versus power of $H_2O$ plasma treatment. 116
Figure 4.22 Carbon, zirconium and oxygen content of $Zr(OBu)_4$ films
on SDT PET versus duration of $H_2O$ plasma treatment. 118
Figure 4.23 Ar Ion Etch Composition Depth Profile of $Zr(OBu)_4$
Spin Coated On Glass. 119

Figure 4.24 O(1s) spectra as a function of cumulative Ar ion etch time for untreated $Zr(OBu)_4$ spin coated on glass. 120
Figure 4.25 Zr(3d) spectra as a function of cumulative Ar ion etch time for untreated $Zr(OBu)_4$ spin coated on glass. 121
Figure 4.26 XPS Ar Ion Etch Depth Profile of Oxygen Plasma Treated $Zr(OBu)_4$ Spin Coated on Glass. 122
Figure 4.27 Transmission FTIR spectra of $Zr(OBu)_4$ spin coated on KBr: (a) untreated; and (b) $O_2$ plasma treated for 2 minutes at 30 W. 123
Figure 4.28 ATR-FTIR spectra of (a) clean PET; (b) SDT PET; and (c) $Zr(OBu)_4$ spin coated on SDT PET. 124
Figure 4.29 Atomic force micrographs of $O_2$ plasma treated $Zr(OBu)_4$ films spin coated on PET (1 μm per x-axis division). 126
Figure 4.30 Atomic force micrograph of $O_2$ plasma treated $Zr(OBu)_4$ film spin coated on PET (0.2 μm per x-axis division). 127
Figure 4.31. Structure of a trimeric solvated coordination complex of $Zr(OR)_4$ in alcohol solution. 128
Figure 5.1 Ladder structure of polyphenylsilsesquioxane (PPSQ). 139
Figure 5.2 Surface % carbon for (a) untreated, (b) oxygen plasma treated and (c) silent discharge treated PPSQ 142
Figure 5.3 Surface % silicon for (a) untreated, (b) oxygen plasma treated and (c) silent discharge treated PPSQ 142
Figure 5.4 Surface % oxygen for (a) untreated, (b) oxygen plasma treated and (c) silent discharge treated PPSQ 142
Figure 5.5 C(1s) spectra of untreated PPSQ: (a) powder; (b) spin coated on PET; (c) spin coated on SDT PET; and (d) evaporated on PET. 145
Figure 5.6 Si(2p) spectra of untreated PPSQ: (a) powder; (b) spin coated on PET; (c) spin coated on SDT PET; and (d) evaporated on PET. 146
Figure 5.7 O(1s) spectra of untreated PPSQ: (a) powder; (b) spin coated on PET; (c) spin coated on SDT PET; and (d) evaporated on PET. 147
Figure 5.8 C(1s) spectra of $O_2$ plasma treated PPSQ: (a) powder; (b) spin coated on PET; (c) spin coated on SDT PET; and (d) evaporated on PET. 149
Figure 5.9 Composition of PPSQ evaporated on PET as a function of $O_2$ plasma treatment power. 150
Figure 5.10 Composition of PPSQ spin coated on PET as a function of

$O_2$ plasma treatment power. 151
Figure 5.11 O(1s) XPS spectra of PPSQ evaporated on untreated PET and $O_2$ plasma treated at RF powers of (a) 20 W and (b) 30 W. 152
Figure 5.12 O(1s) XPS spectra of PPSQ evaporated on untreated PET and $O_2$ plasma treated at 50 W collected at electron take-off angles of (a) 15°, (b) 30°, and (c) 45°. 154
Figure 5.13 O(1s) XPS spectra collected at an electron take-off angle of 45° from PPSQ evaporated on untreated PET and $O_2$ plasma treated at 50 W in (a) 0.2 mbar $O_2$ and (b) 0.5 mbar $O_2$. 155
Figure A1.1 Variation of electron mean free path with kinetic energy[9]. 170
Figure A1.2 Modes of molecular excitation following infrared absorption.

## List of Tables

Table 1.1 Oxygen and water vapour permeability of some common substrate and metallized packaging polymers. 4

Table 2.1 Plasma parameter ranges for silent and low pressure discharges. 24

Table 2.2 Compilation of O : C ratios following electrical discharge treatment (± 0.01). 32

Table 2.3 Relative amounts of carbon functionalities following low pressure plasma and silent discharge (S.D.) treatment (± 0.8). 35

Table 2.4 Surface roughness following electrical discharge treatment. 43

Table 4.1 Surface composition of spin coated $Zr(OBu)_4$ films compared with theoretical $Zr(OBu)_4$ composition. 93

Table 4.2 O(1s) XP peak positions and area proportions (± 2 %) for $Zr(OBu)_4$ films spin coated on glass, PET and SDT PET. 94

Table 4.3 Surface composition (± 1.2 %) of untreated and silent discharge treated $Zr(OBu)_4$ spin coated on glass. 98

Table 4.4 Peak fit area proportions (errors ≤ 2 %) of $Zr(OBu)_4$ coated on glass as a function of $O_2$ plasma treatment power. 104

Table 4.5 Peak fit area proportions (errors ≤ 2 %) of $Zr(OBu)_4$ coated on glass as a function of $O_2$ plasma treatment duration. 105

Table 4.6 Peak fit area proportions (errors ≤ 2 %) of $Zr(OBu)_4$ coated on glass as a function of $H_2O$ plasma treatment power. 107

Table 4.7 Peak fit area proportions (errors ≤ 2 %) of Zr(OBu 114

Table 4.9 Peak fit area proportions (errors ≤ 2 %) of $Zr(OBu)_4$ coated on SDT PET as a function of $O_2$ plasma treatment duration. 115

Table 4.10 Peak fit area proportions (errors ≤ 2 %) of $Zr(OBu)_4$ coated on SDT PET as a function of $H_2O$ plasma treatment power. 117

Table 4.11 Peak fit area proportions (errors ≤ 2 %) of $Zr(OBu)_4$ coated on SDT PET as a function of $H_2O$ plasma treatment duration. 118

Table 4.12 Mean equilibrium permeant partial pressures (MEPPPs) of $O_2$, Ar and He for untreated PET, silent discharge treated (SDT) PET and $O_2$ plasma treated $Zr(OBu)_4$ on SDT PET. 125

Table 5.1 Composition of $O_2$ Plasma Treated PPSQ films evaporated on PET analyzed at XPS electron take off angles of 15°, 30° and 45°. 153

Table 5.2. Mean equilibrium partial pressures of $O_2$, Ar and He for untreated PET and PPSQ evaporated on PET and $O_2$ plasma treated. 156

# Chapter One : Introduction to Gas Barrier Materials and Plasma Surface Modification

## 1.1 GAS BARRIER MATERIALS

### *1.1.1 Introduction*

Polymers are characteristically cheap, light, tough and easily processed, ideally suiting them to packaging for electronics, pharmaceuticals, speciality chemicals and food products[1]. However, the high degree of molecular motion of polymers which accounts for many of their attractive physical properties also makes them greatly more gas permeable than dense materials such as metals and ceramics[2].

The shelf lives of many food products rely heavily on the gas permeability of their packaging[3]. Improvement of polymer gas barrier properties through chemical and morphological tailoring of materials[3], or coating with an effective gas barrier film[5], therefore greatly enhances the value of such products.

### *1.1.2 Requirements For Food Packaging Materials*

Each food has specific gas barrier requirements; some foods require certain gases to permeate their pack in order to remain fresh[3] whilst some are packed in modified gas atmospheres which need to be maintained[4]. The main gases of concern are: oxygen, which causes fats to go rancid but is required by fruit and vegetables for continued respiration and ripening; water vapour, which can spoil the texture of foods and accelerate microbial spoilage; and carbon dioxide, containment of which is required for carbonated drinks.

The list of requirements for food packaging materials is demanding, and often can only be fulfilled by combining several materials in a multilayer structure which is expensive to make and difficult to separate for recycling[6]. The ideal food packaging material would be stable to high temperatures, chemically resistant, transparent, microwaveable, metal detector compatible, printable, not

damaged by strain and crumpling, impermeable to specific odours and gases, and would selectively allow some gases to permeate. Recent legislation has also put environmental demands on packaging materials[7-9], so that alternatives are sought for widely used halogen containing gas barrier polymers, such as polyvinylidinechloride, PVdC, which release halo-carbons upon incineration.

Thin ceramic coatings, such as alumina and silica, can match the high gas barrier performance of metallized polymer films[10-13], and solve many of the problems inherent in metallized packaging. The latter suffers from being opaque, unreclaimable, unmicrowaveable[14], and expensive and energy intensive to produce[6]. Metal oxide coated film can be recycled, the thin coating becoming an inorganic filler in subsequent conversions[6]. Current draw-backs of these coatings include yellow colouration of substoichiometric oxides[15] and brittleness which makes them susceptible to barrier loss through physical damage during conversion and transportation[11,13,14,16].

### *1.1.3 Solution, Diffusion and Permeation*

Permeation is the passage of species through a material under the driving force of a concentration gradient[17]. This process can be regarded as activated diffusion[3], the activation being the sorption and solution of species in the material. The solution step favours permeation of more condensable molecules whilst diffusion favours more concentrated and smaller molecules[18,19].

The steady state flux of a certain gas through a particular material is determined by three variables[20,21]: diffusivity, D, solubility, S, and pressure gradient, $dp/dx$, of the permeating species, Equation 1.

$$J = DS\, dp/dx \qquad \text{Equation 1}$$

Diffusivity, D, relates the permeant flux, J, to the concentration gradient, Equation 2, expressing Fick's First Law of diffusion[22].

$$J = -D\,(dC/dx) \qquad \text{Equation 2}$$

Solubility, S, relates the concentration, C, of a permeant in the material to the partial pressure of that permeant, p, in the gas phase, Equation 3; this relationship holds for sorption in which Henry's Law is obeyed[23,24].

$$C = S\,p \qquad \text{Equation 3}$$

Solubility and diffusivity data are available for most gas-polymer systems[25,26]. These coefficients combine to give an overall permeability coefficient, P = DS, for the solution-diffusion process[27,28], Equation 4.

$$J = P\,{}^{dp}/_{dx} \qquad \text{Equation 4}$$

### *1.1.4 Reducing Gas Permeability*

Polymers with pinholes, cracks or voids are highly permeable due to gas phase diffusion, and attempts to model permeation assume the absence of these imperfections[25,26]. Polymer characteristics which favour low gas permeability include low free volume fraction[29,30], high cohesive energy density (strong inter-chain forces)[25], high chain stiffness[26], high degree of chain alignment[31,32], high crystallinity and high glass transition temperature[31,33,34], high polarity[3] and weak interaction with the permeant[3]. The permeabilities of a range of common polymeric substrates and coated polymers to oxygen and water vapour are presented in Table 1.1[35].

| | Low Density Polyethylene | Oriented Polypropylene | Polyethylene-terephthalate (PET) | Polyvinyl-idinechloride Coated PET |
|---|---|---|---|---|
| Base Polymer $O_2$ Transmission Rate (cc $m^{-2}$ $day^{-1}$) | 5000 | 1600 | 58 | 9 |
| Metallized Polymer $O_2$ Transmission Rate (cc $m^{-2}$ $day^{-1}$) | 38 | 20 | 1.6 | 0.8 |
| Base Polymer $H_2O$ Transmission Rate (cc $m^{-2}$ $day^{-1}$) | 17 | 6 | 46 | 11 |
| Metallized Polymer $H_2O$ Transmission Rate (cc $m^{-2}$ $day^{-1}$) | 0.8 | 1.5 | 0.7 | 0.5 |

Table 1.1 Oxygen and water vapour permeability of some common substrate and metallized packaging polymers[35].

Gas barrier coatings reduce the rate of permeation by frustrating the solution and diffusion of gas species in the substrate[36]. This can be achieved by a combination of blocking polymer pinholes and amorphous regions, providing a surface in which the gas is only sparingly soluble[37], providing only tortuous diffusion paths through film defects and grain boundaries[36-39], and 'pinning' otherwise flexible groups which allow diffusion in the substrate polymer[40]. Investigations have suggested that gas barrier performance is highly sensitive to both physico-chemical structure and adhesion at the polymer-coating interface[14,40,41], and that polymer surface preparation before coating is of prime importance[5].

*1.1.5 Barrier Coating Technology*

Gas barrier coatings have been produced on polymers using a variety of techniques: inert and reactive evaporation of metals and metal oxides[14,42]; electron-beam[43-45] and magnetron[11] sputtering of a target material; plasma polymerization of oxygen containing organic barrier films[46,47] and plasma enhanced chemical vapour deposition from siloxanes[11,15]. The cost competitiveness of films coated using these methods is limited by low line speeds[11], the cost of raw materials such as silica[44] and batch operation in complicated, expensive vacuum equipment[44].

A novel gas barrier film production method is explored in this thesis, in which a polymer substrate is coated with a solid layer of precursor material and subsequently exposed to a non-isothermal gas plasma environment to form an inorganic surface layer. This process shows potential for fast barrier coating of organic substrates at low temperatures using cheap, non-toxic precursor materials, and the possibility of an atmospheric pressure continuous coating process.

## 1.2 PLASMA MODIFICATION OF POLYMER SURFACES

### *1.2.1 Advantages Of Plasma Surface Modification*

Polymer-gas interfaces are typically characterized by a low-energy, smooth, pin-holey, permeable and unfunctionalized polymer surface which is unsuitable for many industrial applications[48]. The value of polymer film may be greatly enhanced, without mechanical compromise of the underlying bulk material, by selective physical and chemical modification of the outer few molecular layers.

Of the various competing surface-selective modification techniques that exist, plasma treatment often proves to be the most suitable method due to a number of advantages detailed below.

1) Plasmas react with surfaces to modify only the outermost atomic layers (less than 1 μm) whilst the bulk is not deformed nor degraded from its originally engineered specification[49-52].

2) Ions, electrons and metastable excited particles in plasmas possess energies of 1 eV to 5 eV, which are ideal for bond breaking and are not attainable in conventional or photo-chemical reactions[53].

3) Non-equilibrium plasmas allow energetic reactions to occur at the surface of temperature sensitive substrates without heat damage[53].

4) Levels of modification can be obtained within seconds of plasma treatment compared to many minutes for conventional modification techniques[54].

5) Plasma treatment can modify the entire surface of irregularly shaped objects[55].

6) Hazardous substances need neither be used nor produced.

In summary, plasma modification is a quick, precise, clean, solventless process in which low electrical powers are used efficiently to achieve surface-selective modification.

### *1.2.2 Plasma Parameters*

#### 1.2.2.1 Definition and Parameter Range

Plasmas, usually recognizable as regions of glowing gas, are familiar in nature in the form of stars, lightning and flames, and throughout modern buildings as fluorescent lighting. In their range of particle density and energy, Figure 1.1, plasmas vastly outweigh solids, liquids and gases[56], however, they have only relatively recently gained classification as the 'fourth state of matter.' Understanding of the interactions between plasmas and solid surfaces, meanwhile, is in its very early stages.

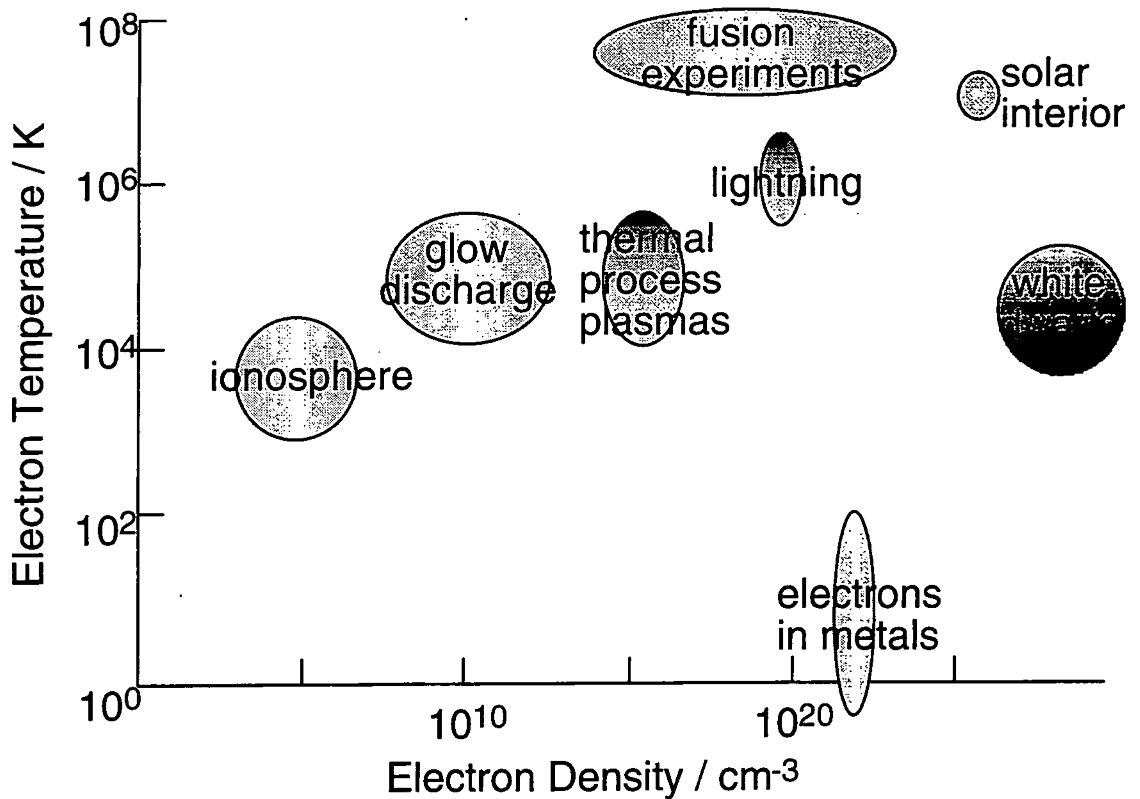


Figure 1.1 Regimes of plasma particle density and energy.

A plasma is defined as a volume of quasi-neutral ionized gas, meaning that the overall numbers of positive and negative charge in a plasma are equal[55], in which local concentrations of charge dominate the motion of particles giving rise to collective behaviour[57].

A discharge is initiated by the acceleration of randomly occurring free electrons in an applied electric field[58]. When sufficient energy is available for free electrons to ionize gas molecules by inelastic collision[59], the discharge current rises and an equilibrium is established between ion production, through ionization, and ion loss, through recombination with electrons and diffusion to surrounding surfaces[56].

Sections 1.2.2.2 through to 1.2.2.6 introduce physical parameters and conditions which describe plasmas.

### 1.2.2.2 Thermal and Non-equilibrium Plasmas

Regimes of number density and 'temperature' (average energy) of plasma particles characterize particular types of gas discharges[56], Figure 1.1. Electromagnetic energy used to initiate and sustain discharges causes greater acceleration of electrons than of massive charged particles[57]. In a low pressure ($10^{-5}$ to 1 mbar) plasma the low rate of electron-neutral collisions ensures energy non-equilibrium, and a cold plasma is produced[58].

In such non-isothermal plasmas, electrons with temperatures, $T_e$, of up to 10 eV (equivalent to a mean temperature of $1.2 \times 10^5$ K) initiate a broad range of excitation and ionization processes. However, the temperatures of neutral and ionized gas species, $T_g$ and $T_i$ respectively, remain sufficiently low, Inequality 1, to allow temperature-sensitive materials to be immersed in the reactive plasma medium without thermal damage[56].

$$T_g < T_i << T_e \qquad \text{Inequality 1}$$

The distribution of energy amongst plasma electrons determines the rate of electron induced reactions. This distribution function, modelled by a Maxwellian function for equilibrium plasmas, Figure 1.2, and a Druyvesteyn function for non-equilibrium plasmas, shows that significant numbers of electrons are available in the plasma to initiate processes with activation energies well above the most probable electron energy[56].

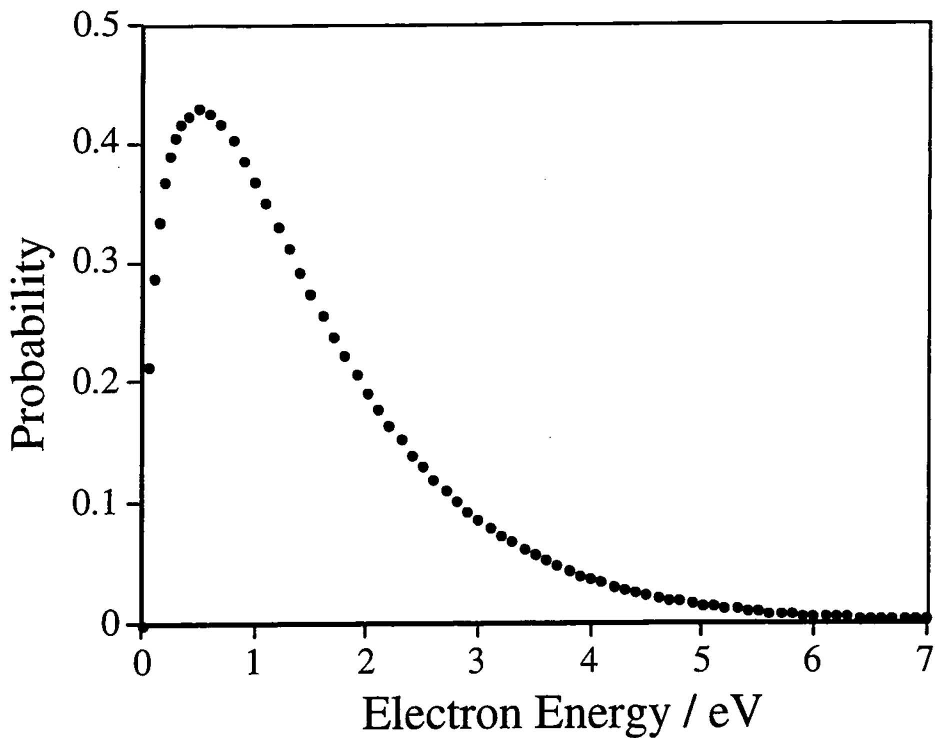


Figure 1.2 Maxwellian electron energy distribution model[56].

1.2.2.3 Debye Shielding

Plasma quasi-neutrality is ensured by mobile electrons which rapidly redistribute to cancel any charge imbalance; a process known as Debye shielding[57].

The Debye length, $\lambda_D$, is the distance over which charge imbalance can exist in a plasma[56], Equation 1.

$$\lambda_D = (\varepsilon_o k T_e / ne^2)^{1/2} \qquad \text{Equation 1}$$

where $\varepsilon_o$ = permittivity of free space; $k$ = Boltzmann's constant

$T_e$ = electron temperature; $n$ = electron number density

$e$ = charge of an electron

The potential, $V(x)$, produced by a local charge in the plasma, $q$, is attenuated exponentially by electron shielding with a decay length of $\lambda_D$[56], Equation 2.

$$V(x) = (q/4\pi\varepsilon_o x) \exp(-x/\lambda_D)$$ Equation 2

For Debye shielding to be effective in restricting charge imbalance to small volumes of the overall quasi-neutral plasma, the characteristic dimension of the discharge, L, must be large compared to the Debye length[58], Inequality 2.

$$L >> \lambda_D$$ Inequality 2

1.2.2.4 Plasma Frequency

Movement of electrons to shield charge imbalances results in their oscillation with a characteristic frequency called the plasma frequency[57], $\omega_p$, Equation 3.

$$\omega_p = (ne^2/m_e\varepsilon_o)^{1/2}$$ Equation 3

where $m_e$ = mass of an electron

Electrons of average thermal velocity $v_e$ travel a distance $\lambda_D$ in one oscillation[57], Equation 4.

$$\omega_p = v_e/\lambda_D$$ Equation 4

If an electric perturbation with a frequency less than the plasma frequency is applied, then electrons can respond fast enough to shield the plasma from the applied field[57].

1.2.2.5 Plasma Sheath

Plasmas are maintained at a mean equipotential positive with respect to earth, referred to as the plasma potential[56]. An electrically isolated object placed in a plasma receives a greater flux of electrons than of ions, since the average

electron velocity is much larger than the average ion velocity. A net negative charge builds on the object until it reaches a potential which repels electrons enough to balance their greater flux: this potential is called the floating potential[56] which is negative with respect to the plasma potential.

The lack of energetic free electrons in the region around the charged object reduces the intensity of electron impact excited radiation processes, producing a visible dark space or *plasma sheath* between the plasma and the surface of the object[57].

The plasma sheath acts as an active filter, modifying the majority of neutral species diffusing from the plasma and a proportion of the ions by reactive collisions, accelerating positive ions towards the negatively charged surfaces and allowing up to 70% of plasma emitted vacuum ultraviolet radiation through to surrounding surfaces[60].

#### 1.2.2.6 Supply Frequency

Direct current (dc) diode plasmas may be used in sputter deposition processes, however insulating samples may not be used as a sputter source since these materials build up charge which quickly extinguishes the discharge[57]. In such situations a continuous discharge is obtained for alternating current (ac) supplies above 100 kHz; this also allows inductive or capacitative coupling of electrical power into the plasma, in which electrodes may be external to the discharge chamber, Figure 1.3. The industrial standard radio frequency of 13.56 MHz has been widely adopted; such radio frequency plasmas can operate at pressures as low as 0.1 mTorr with much more efficient ionization than dc discharges[57]. For alternating current plasmas, the impedances of the signal generator and the coupling device need to be matched using an electronic network, and radio frequency shielding of the discharge may be required to protect other sensitive electronic equipment[58].

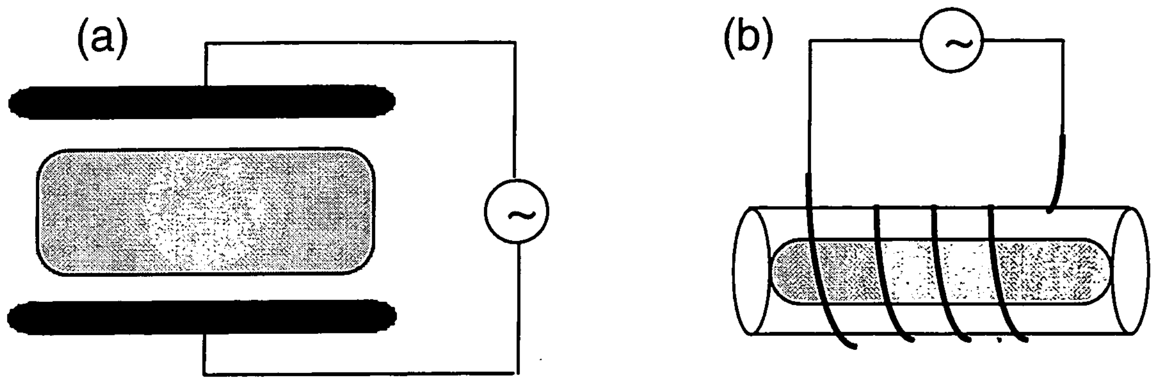


Figure 1.3 Plasma coupling configurations (a) Capacitative and (b) Inductive.

Higher frequency plasmas, supplied by microwave sources at 2.45 GHz, are more efficient still at producing ionization, however radio frequency plasmas may produce a higher proportion of a desired chemically reactive species so that both of these frequencies have been used simultaneously[61]. Magnetic fields have been used to electromagnetically confine and densify plasmas, and can be used to sustain electron cyclotron resonance (ECR) above a critical field threshold[62].

### *1.2.3 Chemical Physics of Polymer-Plasma Interactions*

#### 1.2.3.1 Introduction

To understand how plasmas interact with polymer surfaces requires a knowledge of the natures, energies and fluxes of species within the plasma bulk and at the surface of interest. A substrate exposed to energetic electrons, ions, atoms, radicals, metastable excited species and photons from a plasma usually undergoes a great variety of chemical reactions and physical modification processes. Processes by which plasma species react homogeneously, within the gas phase, and heterogeneously, with solid surfaces, are discussed in sections 1.2.3.2 and 1.2.3.3 respectively, and physical modification of polymer surfaces is introduced in 1.2.3.4.

#### 1.2.3.2 Homogeneous Plasma Reactions

Gas phase reactions consist of those between electrons and heavier species, and between the heavier species: ions, molecules, atoms and radicals [56].

Inelastic collisions of electrons with gas species form a wide range of reactive plasma species even for simple gases: free radicals, excited metastable molecules and ions[56,59]. Electrons may attach to gas species with or without dissociation of the latter, forming ions; gas species may be dissociated into neutral fragments through an excited intermediate; gas species may lose an electron forming atomic or molecule positive ions, and electrons may recombine either with molecular ions with dissociation of the molecule, or with atomic ions (rare), emitting a quantum of radiation.

Excitation of atomic or molecular species by electrons, Reaction 1, is followed rapidly for most species by radiative relaxation, producing the plasma's wide range of electromagnetic emission which extends into the soft X-ray region[60]. Some species are promoted into metastable excited states which exist long enough to undergo further reactions.

$$e + AB \rightarrow e + AB^* \qquad \text{Reaction 1}$$

Reactions between ions, molecules, atoms and radicals are dominated by radical-molecule events, since ions are relatively rare compared to complete and dissociated gas molecules[56]. These reactions allow interchanges between molecular groupings, the creation and neutralization of ionic species and the release of excess reaction energy as electromagnetic radiation[56,58,59].

### 1.2.3.3 Polymer-Plasma Heterogeneous Reactions

Chemisorption of, and energetic bombardment by, gas phase plasma species at exposed surfaces leads to competition between chemical modification and chemical etching of the substrate[63]. Radicals are about 1000 times more abundant than ions in a non-isothermal plasma, have a high probability for chemisorption on surfaces[55] and have high reactivity with many surface species. Heterogeneous reaction between radicals can form polymers (termed 'plasma

polymerization') or chemically functionalized groups at the substrate surface[56,64]. Volatile reaction products desorb into the plasma-boundary layer completing the process of surface chemical etching.

Molecular positive ions are accelerated to the substrate surface by the floating potential. A proportion of the ions' kinetic energy is transformed into internal energy often causing dissociation into their constituent atoms and radicals. These dissociated species react with surface groups forming new chemical species, such as oxides, nitrides and carbides from $O_2^+$, $N_2^+$ and $CH_4^+$ ions respectively[56,65].

Only electrons from the high energy tail of the population are able to transverse the negative potential gradient of the sheath: those still possessing kinetic energy above the threshold for surface reactions may break surface bonds, forming radicals and new molecular species[65]. Electron beams have been used in this mode to cross-link polymer surfaces[66].

Surfaces allow de-excitation of metastable molecules through collisions and recombination of plasma atoms at catalytic adsorption sites, both processes donating thermal energy to the substrate[56].

Radiation, ranging from visible photons to soft X-rays, bombards surfaces immersed in low pressure plasmas[60] since at this pressure the mean free path of photons are typically many times greater than reactor dimensions[56]. UV photons are strongly adsorbed by organic surface groups, creating reactive radical sites which initiate subsequent chemical functionalization and cross-linking reactions[67].

#### 1.2.3.4 Plasma Physical Modification of Polymer Surfaces

Collisions of low energy (about 1 eV) plasma species of all types with surfaces provides thermal energy allowing migration or desorption of surface species. The former process may improve step coverage and density of a growing surface film and promote growth of a well defined microstructure whilst the latter may lower the level of volatile contaminants in the film[68].

Plasma positive ions are accelerated towards surfaces at energies up to the sheath potential[69]. Collision cascades of neutralized ions in the surface region

cause lattice damage, ejection of secondary material (sputtering)[70] and implantation[71]. Sputtering of electrically biased surfaces is highly anisotropic, preferentially removing material in a direction normal to the surface; high aspect-ratio features can therefore be plasma-etched to produce ultra large scale integrated circuit patterns[72,73]. Material removal through energetic ion collision may be used to clean surfaces[74], and may lead to surface roughening or smoothing[75].

Polymer etch rate in plasmas depends upon plasma conditions and polymer composition and structure; the rate is higher when discharge parameters favour electrons in the high energy tail of the energy distribution[70], at long treatment times[76,77], at high powers[77], and when a moderate fraction (about 10%) of fluorine containing gases are present in the plasma[78,79]. Plasma etch rate increases with polymer chain oxygen content[80], is greater for aliphatic than for aromatic polymers[72], and can be greatly reduced by the presence of metals such as silicon and tin in the plasma treated surface since refractory oxides are formed[81]. Molecular orbital modelling of the attack of plasma species at saturated and unsaturated polymer sites confirms that aromatic polymers are relatively resistant to etching compared to aliphatic polymers[81, 83].

Substrate molecular weight may be increased during plasma treatment, as a result of radical recombinations in the surface, or decreased by chain scission, as in the case of oxygen plasma treatment of polymers[72].

Depth of penetration of plasma species into the surface varies with substrate material, and is typically 10 to 100 nm for massive particles with energies of about 1 eV[83,84], and a few microns for photons in the ultraviolet region[85, 67].

#### 1.2.3.5 Synergistic Processes

It has been observed that bombardment of surfaces by a combination of energetic radicals and photons[86], or ions and photons[87], produces greater chemical functionalization and material removal than the sum of the individual components. The overall effect of plasma surface treatment is thus a complex synergistic modification[88].

### *1.2.4 Polymer Properties Modified By Plasma Treatment*

#### 1.2.4.1 Wettability and Adhesion

The ability of plasma treatment to increase adhesion to a variety of materials[78,89-97] is particularly important in the industrial use of polymer surfaces and other inert, hydrophobic materials. Contact with an oxygen containing plasma introduces chemical groups into the surface which increase surface energy and provide polar groups for hydrogen bonding[98]. Other adhesive benefits may be gained from the ablative cleaning effect which removes weakly bound surface layers, and crosslinking of polymer chains which increases internal strength and cohesion of the surface[99,100].

Plasma surface functionalization increases surface free energy and therefore can be used to obtain surfaces with a controlled degree of wettability[101] or with wettability gradients[102]. Bond strengths between polymers and metals are increased several times within seconds of He - $O_2$ plasma treatment[93].

#### 1.2.4.2 Gas Permeability and Selectivity

Alteration of polymer membrane gas permeability by plasma treatment may be due to surface cross-linking, chemical functionalization or topographical changes[103]. Changes in permeation selectivity of polymers occur during $CF_4$ plasma fluorination[104], however, the absolute barrier to oxygen and water vapour achieved by non-polymerizable gas plasma treatment does not compete successfully with deposited films[105]. Gas barrier applications in which a laminated layer of metal[106], metal oxide[95,96] or polymer[107] is used as the barrier component, often use substrate plasma pre-treatment to increase coating adhesion.

Organic gas barrier films have been deposited onto polymer substrates by plasma polymerization[108] and inorganic gas barrier films by plasma enhanced chemical vapour deposition (PECVD)[15,16,61,95,109].

#### 1.2.4.3 Biocompatibility

Bulk material chosen for a biochemical engineering application can be rendered cell-compatible[110], hydrophilic[111], ion permeable[112] and crosslinked[112] by plasma surface treatment. This allows the material's use in biologically sensitive situations such as tissue trays[110], immuno-sensors[111], ion exchange membranes[112] and catheters[110].

#### 1.2.4.4 Roughness and Friction

Plasma sputtering modifies surface topography, as observed by various microscopies[53,73,81]. Plasma treatment can be used to roughen surfaces to increase friction[51], or to improve coverage of lubricants for low friction surfaces[112,115].

#### 1.2.4.5 Hardness and Wear

Plasma surface nitriding of metals, at high substrate temperatures and with very high voltage (40 kV) thermal plasma pulses, is used to case-harden machine tools and other hard wearing mechanical components[55]. Polymer surfaces may be hardened by silane low temperature plasma treatment of an organo-polysiloxane coating; the composite structure is heat, weather and wear resistant and is used in building materials and as rollers for copying machines[116].

#### 1.2.4.6 Electromagnetic Properties

Surface plasma oxidation by plasma treatment alters electromagnetic properties through modification of the surface material's electronic structure. Applications include haze-proof optical coatings for lenses and windows[117], semiconductor films for carbon monoxide detection[118], magnetic polymer films[119], and deposition of solar cells, waveguides and light modulators[120].

### *1.2.5 Summary*

Plasma is a complex, energetic state of matter which has many advantages for a variety of surface engineering applications. Non-isothermal plasmas induce novel combinations of chemical and physical surface modifications, and may be applied successfully in a number of industrial processes.

## 1.3 REFERENCES


1. Cowie, J. M. G. *Polymers: Chemistry and Physics of Modern Materials;* 2nd Ed.; Blackie: New York, **1991**.
2. Comyn, J. *Polymer Permeability*, Preface, J. Comyn, Ed.; Elsevier Applied Science Publishers Ltd: London, **1985**.
3. Ashley, R. J. *Polymer Permeability;* Ch 7, Comyn, J. Ed.; Elsevier Applied Science Pubishers Ltd: London, **1985**.
4. Church, I. J.; Parsons, A. L. *J. Sci. Food and Agriculture* **1995**, *67*, 143.
5. Benmalek, M.; Dunlop, H. M. *Surf. Coatings Tech.* **1995**, *77*, 821.
6. Fritschel, S. J. *ACS Symp Ser* **1992**, *513*, 266.
7. Heidegger, U. *JOCCA - Surf Coatings Int.* **1993**, *76*, 496.
8. Mullin, R. *Chem Week* **1994**, *155*, 16.
9. Overton, B. W. *Food Additives and Contaminates* **1994**, *11*, 285.
10. Wood, L.; Chatham, H. *Proc. Soc. Vac. Coaters 35th Ann. Tech. Conf.*, **1992**, 59.
11. Missiano, C.; Simonetti, E.; Staffetti, F.; Taglioni, G.; Rimediotti, F. *Proc. Soc. Vac. Coaters 35th Ann. Tech. Conf.*, **1992**, 28.
12. Nelson, R. J. *Proc. Soc. Vac. Coaters 35th Ann. Tech. Conf.*, **1992**, 75.
13. Charoudi, D. *Paper, Film and Foil Converter* **1991**, October.
14. Barker, C. P.; Kochem, K.-H.; Revell, K. M.; Kelly, R. S. A.; Badyal, J. P. S. *Thin Solid Films*, **1995**, *259*, 46.
15. Ang, P. *Proc. Soc. Vac. Coaters 36th Ann. Tech. Conf.*, **1993**, 518.
16. Felts, J. T. *Transparent Barrier Coatings Update: Flexible Substrates,* Airco Coating, **1991**.
17. Kesting, R. E. *Synthetic Polymer Membranes*, 2nd Ed., Wiley: New York, **1985**.

18. Koros, W. J.; Fleming, G. K. *J. Membrane Sci.* **1993**, *83*, 1.

19. Mazid, M. A.; Matsura,T. *Sep. Sci. Technology* **1993**, *28*, 2287.

20. Henema, E. R. *Adv. Mater.* **1994**, *6*, 264.

21. Rogers, C. E. *Polymer Permeability*, Ch. 2, J. Comyn, Ed.; Elsevier Applied Science Pubishers Ltd: London, **1985**.

22. Crank, J. *The Mathematics of Diffusion*, 2nd Ed.; Oxford Uni. Press: Oxford, **1975**.

23. Naylor, T. *Comprehensive Polymer Science, Vol. 2, Polymer Properties*, Ch. 20; Permagon Press: New York, **1989**.

24. Osado, Y.; Nakagawa, T. *Membrane Science and Tech.*; Marcel Dekker: New York, **1992**.

25. Pace, R. J.; Datyner, A. *J. Polym. Sci. Polym. Phys.* **1979**, *17*, 437.

26. Muller-Plathe, F.; Rogers, S. C.; van Gunsteren, W. F. *Macromolecules* **1992**, *25*, 6722.

27. Jia, L.; Xu, J. *Polym. J.* **1991**, *23*, 417.

28. Crank, J.; Park, G. S. *Diffusion in Polymers*, Ch. 1; Academic Press: London, **1968**.

29. Stern, S. A.; Sampat, S. R.; Kullarmi, S. S. *J. Polym Sci.: Part B: Polym. Phys.* **1986**, *24*, 2149.

30. Sha, H.; Harrison, I. R. *J. Polym Sci.: Part B: Polym. Phys.* **1992**, *30*, 915.

31. Holden, P. S.; Orchard, G. A. J.; Ward, I. M. *J. Polym Sci.: Part B: Polym. Phys.* **1985**, *23*, 709.

32. Paulos, J. P.; Thomas, E. L. *J. Appl. Polym. Sci.* **1980**, *25*, 15.

33. Schlotter, N. E.; Furlan, P. Y. *Polymer* **1992**, *33*, 3323.

34. Booth, C.; Price, C. Eds. In *Comp. Polym. Sci. Vol. Two*; Ch. 2; Permagon Press: New York, 1989.

35. Barker, C. P. Private Communication, **1996**.

36. Mercea, P ;Muresan, L.; Mercea, V. *Rev. Roum. Phys.* **1985**, *30*, 241.

37. Mercea, P.; Muresan, L.; Mercea, V. *J. Membrane Sci.* **1985**, *24*, 297.

38. Mercea, P.; Muresan, L.; Mercea, V.; Silipas, D.; Ursu, I. *J. Membrane Sci.* **1988**, *35*, 291.

39. Beu, T. A.; Mercea, P. V. *Mater. Chem. Phys.* **1990**, *26*, 309.

40. Barker, C. P.; Kochem, K.-H.; Revell, K. M.; Kelly, R. S. A.; Badyal, J. P. S. *Thin Solid Films*, **1995**, *257*, 77.

41. Mittal, K. L. *J. Vac. Sci. Tech.* **1976**, *13*, 19.
42. Kelly, R. S. A.; Revell, K. M. UK Patent Appl. 2210826.
43. Schiller, S.; Neumann, M.; Morgner, H.; Schiller, N. *Proc. Soc. Vac. Coaters 36th Ann. Tech. Conf.*, **1993**, 278.
44. Krug, T.; Ludwig, R.; Steiniger, G *Proc. Soc. Vac. Coaters 36th Ann. Tech. Conf.*, **1993**, 302.
45. Krug, T.; Ludwig, R. *Packaging* **1991**, *April*, 11.
46. Wertheimer, M. R.; Klemberg-Sapieha, J. E.; Schreiber, H. P. *Thin Solid Films* **1984**, *115*, 109.
47. Crawley, R. L.; Evans, J. L. *J. Vac. Sci. Tech.* **1991**, *A9*, 824.
48. Garbassi, F.; Morra, M.; Occhiello, E. In *"Polymer Surfaces from Physics to Technology"*; John Wiley & Sons: Chichester, **1994**.
49. Strobel, M.; Corn, S; Lyons, C. S.; Korba, G. A. *J. Polym. Sci.: Polym. Chem. Ed.* **1985**, *23*, 1125.
50. Gerenser, L. *J. Adh. Sci Tech.* **1987**,*1*, 303.
51. Nakayama, Y.; Soeda, F.; Ishitani, A. *Polym. Eng. & Sci.* **1991**, *31*, 812.
52. Coopes, I. H.; Grifkins, K. J. *J. Macromol. Sci. Chem. Ed.* **1982**, *17*, 217.
53. Suhr, H. *Plasma Chemistry and Processing* **1989**, *9*, 7S.
54. Foerch, R.; McIntyre, N. S.; Hunter, D. H. *J. Polm. Sci. Part A: Polym. Chem. Ed.* **1990**, *28*, 193.
55. Coburn, J. W. *IEEE Trans On Plasma Sci.* **1991**, *19*, 1048.
56. Grill, A. In "*Cold Plasma In Materials Fabrication*" Ch. 1; IEEE Press: New York, 1994.
57. Chapman, B. In *"Glow Dishcarge Processes"*; Wiley-Interscience: New York, 1980.
58. Bell, A. T. In "Techniques & Applications of Plasma Chemistry"; Ch. 1; Hollohan, J. R.; Bell A. T. J. Wiley & Sons: New York, 1974.
59. Liston, E. M. *Proc. ISPC-9* **1989**, *3*, L7.
60. Wertheimer, M. R.; Moisan, M. *J. Vac. Sci. Tech.* **1983**, *A3*, 2643.
61. Rossnagel, S. M. In *"Thin Solid Film Processes II"*; Ch. II-1; Vossen, J. L.; Kern W. Eds.; Academic Press: London, 1991.
62. McTaggart, F. K. *"Plasma Chemistry In Electrical Discharges"*; Elsevier: Amsterdam, 1967.
63. Shard, A.; Badyal, J. P. S. *Macromol.* **1992**, *25*, 2053.

64. Yasuda, H. *"Plasma Polymerisation"*; Academic Press: London, **1985**.

65. Winters, H. F. in *"Topics In Current Chemistry: Plasma Chemistry III"*; Veprek, S.; Venugoplan, M. Eds.; Springer-Verlag: Berlin, **1980**.

66. Onyiriuka, E. C. *J. Adh. Sci. Tech.* **1994**, *8*, 1.

67. Clark, D. T; Dilks, A. *J. Polym. Sci.: Polym. Chem. Ed.* **1980**, *18*, 1233.

68. Reif, R. In *Thin Solid Film Processes II*; Ch. IV-1; Vossen, J. L.; Kern W. Eds.; Academic Press: London, **1991**.

69. Graves, D.; Jenson, K. *IEEE Trans. Plasma Sci.* **1986**, *14*, 78.

70. Anderson, H. M.; Merson, J. A.; Light, R. W. *IEEE Trans. Plasma Sci.* **1986**, *14*, 156.

71. Briggs, D; Brown, A.; Vickermann, J. C. *"Handbook of Static Secondary Ion Mass Spectrometry"*; Ch. 1; J. Wiley & Sons: Chichester, **1989**.

72. Hand, B.; Long, T.; Dems, B. C.; Rodriguez, F. *J. Appl. Polym. Sci.* **1993**, *47*, 2135.

73. MacDonald, S. A.; Schlosser, H.; Ito, H.; Clecak, N. J.; Wilson, C. G. *Chem. Mater.* **1991**, *3*, 435.

74. Lucovsky, G.; Tsu, D. V.; Rudder, R. A.; Markunas, R. J. In *Thin Solid Film Processes II*; Ch. IV-2; Vossen, J. L.; Kern W. Eds.; Academic Press: London, **1991**.

75. Greenwood, O. D.; Boyd, R. D.; Hopkins, J.; Badyal, J. P. S. *J. Adh. Sci. Tech.* **1995**, *9*, 311.

76. Poncin-Epaillard, F.; Chevet, B.; Brosse, J. C. *Europ. Polym. J.* **1990**, *26*, 333.

77. Morra, M.; Occhiello, E.; Garbassi, F. *Langmuir* **1989**, *5*, 872.

78. Wu, S-Y.; Denton, D. D. *J. Vac. Sci. Tech.* **1993**, *11*, 291.

79. Egitto, F. D. *Pure & Appl. Chem.* **1990**, *62*, 1699.

80. Gokan, H.; Esho, S.; Ohnishi, Y. *Solid State Tech.* **1985**, *28*, 163.

81. Dems, B. C.; Rodriguez, F.; Solbrig, C. M.; Namaste, Y. M. N.; Obendorf, S. K. *Int. Polym. Proc.* **1989**, *4*, 183.

82. Cain, S. R.; Egitto, F. D.; Emmi, F. *J. Vac. Sci. & Tech.* **1987**, *A5*, 1578.

83. Liston, E. M. J. Adh. 1989, 30, 199.

84. Clark, D. T.; Dilks, A. *J. Polym. Sci.: Chemistry Ed.* **1977**, *15*, 2321.

85. Steinhauser, H.; Ellinghorst, G. *Die Ange. Makromol.* **1984**, *120*, 177.

86. Veprek, S.; Webb, A. P.; Oswald, H. R. *J. Nucl. Mater.* **1977**, *68*, 32.

87. Liston, E. M.; Martinu, L.; Wertheimer, M. R. *J. Adh. Sci. Tech* **1993**, *7*, 1091.

88. Hopkins, J.; Badyal, J. P. S. submitted for publication, 1995.

89. F.F.I. Ho, Hercules Inc., Patent No.s EP-282094-A, AU8813018-A, BR8801152-A, JP63258938-A, **1988**, and US4897305-A, **1990**.

90. Furukawa Electric Co., Patent No. JP01031958-A, **1989**.

91. Haque, R.; Smith, E. F.; Kadija, I. V., Olin Corp., Patent No. US4598022-A, **1986**.

92. Hitachi Ltd., Patent No.s JP60235844-A, **1985**, and JP92042416-B, **1992**.

93. Hall, J. R.; Westerdahl, C. A. L.; Bodnar, M. J.; Levi, D. W. *J. Appl. Polym. Sci.* **1972**, *16*, 1465.

94. Burkstrand, J. M. *J. Vac. Sci. Tech.* **1978**, *15*, 223.

95. Toray Ind Inc, Patent No. JP63319141, **1988**.

96. Toyo Metallising KK, Patent No.s JP62101428-A, **1987**, JP92020383-B, **1992**.

97. Nippon Paint KK, Patent No.s JP1315474-A, **1989**, EP-388547-A, **1990**, and US4996076-A, **1991**.

98. Owens, D. K. *J. Appl. Polym. Sci.* **1975**, *19*, 3315.

99. Lanauze, J. A.; Myers, D. L. *J. Appl. Polym. Sci.* **1990**, *40*, 595.

100. Bezigian, T. *TAPPI Journal* **1992**, *March*, 139.

101. Kogoma, M.; Kasi, H.; Kakahashi, T.; Moriwaki, T.; Okazaki, S. *J. Appl. Phys.* **1986**, *46*, 147.

102. Ho, K. W. *J. Polym. Sci. Polym. Chem. Ed.* **1986**, *24*, 2467.

103. Mohr, J. M.; Paul, D. R.; Pinnau, J.; Koros, W. K. *J. Membr. Sci.* **1991**, *56*, 77.

104. Lin, X.; Xiao, J.; Yu, Y.; Chen, J.; Zheng, G.; Xu, J. *J. Appl. Polym. Sci.* **1993**, *48*, 231.

105. Pira International C412 Committee Report, *New Packaging Material Combinations*; Pira International: Leatherhead, September, **1995**.

106. Ho F.F.I. Hercules Inc., Patent No.s EP-282094-A, AU8813018-A, BR8801152-A, JP63258938-A, **1988**, and US4897305-A, **1990**.

107. Imada, K.; Ueno, S.; Nishina, Y.; Nomura, H. Shinetsu Chem Ind KK, Patent No.s NL8003934-A, GB2053027-A, JP56011247-A, FR2460783-A, DE3025861-A, **1981**, US4372986-A, GB2053027-B, **1983**, NL-182482-B **1987**.

108. Hercules Inc., Patent No. RD-316056-A, **1990**.

109. Morra, M.; Occhiello, E.; Garbassi, F. *J. Appl. Polym. Sci.* **1993**, *48*, 1331.

110. Chatelier, R. C.; Griesser, H. J.; Steele, J. G.; Johnson, G. Commonwealth Sci. and In. Res. Org., Patent No.s WO9116378-A, AU9177439-A, **1991**, and EP-487661-A1, **1992**.

111. Wang, Y. W.; Chen, C. H.; Yeh, M. L.; Hsiue, G. H.; Yu, B. C. *J. Membrane Sci.* **1990**, *53*, 275.

112. Karakelle, M.; Zdrahala, R. J. Becton Dickinson Co., Patent No. S4885077-A, **1989**.

113. Kuraray Co. Ltd., Patent No.s JP59203951-A, **1984**, and JP93002940-B , **1993**.

114. Nippon Oil Seal Ind., Patent No.s JP59202227-A, 1984, and JP91015663-B, **1991**.

115. Hu, C. B.; Solomon, D. D.; Williamiti, V. A. Becton Dickinson Co., Patent No.s EP-302625-A, JP01070536-A, US4842889, 1**989**.

116. Shinetsu Chem. Ind. KK, Patent No. JP03164246-A, **1991**.

117. Nishikawa, A., Patent No. JP3035031-A, **1991**.

118. Inagaki, N.; Tasaka, S.; Nozue, Y. *J. Appl. Polym. Sci.* **1992,** *45*, 1041.

119. Sumitomo Elec Ind KK, Patent No. JP03161908-A, **1991**.

120. Major, S.; Kumar, S.; Bhatnagar, M.; Chopra, K. L. *Appl. Phys. Lett* **1986**, *49*, 394.

# Chapter Two : Silent Discharge Versus Low Pressure Plasma Treatment Of Five Hydrocarbon Polymers

## 2.1 INTRODUCTION

Electrical discharge treatments of polymeric substrates for improved adhesion and printability[1-3] rely upon chemical[4,5] and topographical[6,7] surface modification. Plasma parameters in atmospheric and low pressure electrical discharges differ strongly, Table 2.1, and are expected to strongly affect the modes of surface modification using these two types of discharge.

| Parameter | Atmospheric Pressure R. F. Discharge | Low Pressure R. F. Discharge |
|---|---|---|
| Pressure range | 0.1 to 10 bar | $10^{-3}$ to $10^{-1}$ bar |
| Electric field range | 0.1 to 100 kV/cm | 1 to 100 V/cm |
| Average electron energy | 1 to 10 eV | 1 to 3 eV |
| Electron density | $10^{14}$ $cm^{-3}$ | $10^{12}$ to $10^{13}$ $cm^{-3}$ |
| Degree of ionization | $10^{-4}$ | $10^{-5}$ |
| Radiation wavelengths | visible to 300 nm | visible to 100 nm |

Table 2.1 Plasma parameter ranges for silent and low pressure discharges[8].

### *2.1.1 Atmospheric Pressure Air Discharge*

A 'silent' discharge, also referred to as a 'dielectric barrier' discharge, is an atmospheric pressure non-equilibrium plasma. It consists of a large number of bright, filamentary microdischarges extending between parallel plate electrodes, at least one of which is covered by a dielectric[9]. Within the microdischarges, free electrons ionize and excite gas molecules which relax to create a purple glow and

visible streamers[9]. Charge accumulates at the dielectric surface and reduces the local applied field, terminating each microdischarge within 100 ns of initiation[10]. The dielectric barrier thus serves to limit the discharge current, preventing spark formation, and to distribute microdischarges evenly over the sample surface[9].

In contrast to a low pressure glow discharge, electrons in a silent discharge are in electrostatic equilibrium with the applied alternating field[11], which allows calculation of the concentrations of various species present as a function of time after the microdischarge was initiated, figure 2.1[9]. Such calculations show that ozone in a silent discharge is typically one hundred times more concentrated than free electrons or ions, and ten times more concentrated than any other excited molecular species, *e.g.* $N_2$, $O_2$, singlet oxygen etc.[9-11]. A combination of electron[14-16] and photon[9-10] surface impact with ozone chemistry therefore governs the characteristics of an air dielectric-barrier surface treatment reactor.

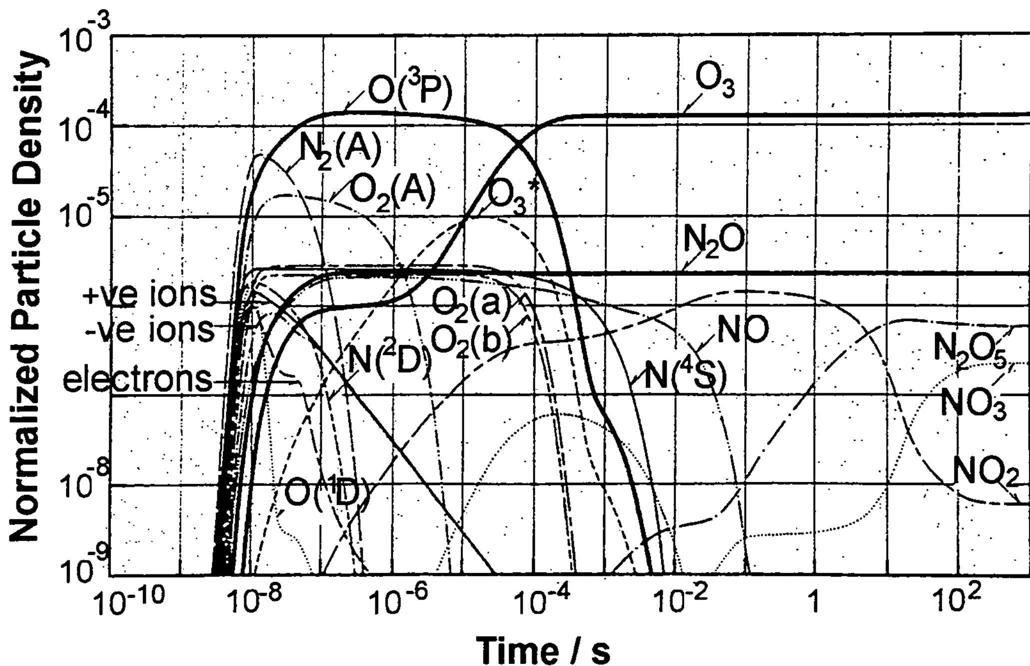


Figure 2.1 Concentration of silent discharge species as a function of time after start of a microdischarge[9].

Ozone is formed in a silent discharge in a two-step process[11]: firstly, dissociation of molecular oxygen by electrons in a microdischarge

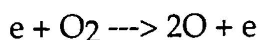

$$e + O_2 \text{ ---> } 2O + e$$

and, subsequently, a three-body reaction

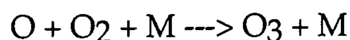

$$O + O_2 + M \text{ ---> } O_3 + M$$

where M can be O, $O_2$, $O_3$, or $N_2$.

*2.1.2 Low Pressure Air Discharge*

If air pressure in a silent discharge is reduced, the diameter of its microdischarges increases, from about 100 µm at atmospheric pressure, until a homogeneous glow discharge is generated at a pressure of about $10^{-1}$ bar[9,10]. This discharge is an oxygen containing, low pressure plasma, in which vacuum-ultraviolet light[17,18] and atomic oxygen radicals[19] are reported to be the chemically prominent species. In such a plasma a substrate is exposed to energetic photons, which easily cleave organic bonds[20], and highly reactive atomic oxygen, which reacts with polymer surfaces in the presence or absence of UV light[19]. The major limitation in application of this technique is that a vacuum system is required, which restricts it to batch mode operation.

Previous investigations of the effect of plasma parameters have used a single type of discharge and only one or two polymers at a time[21-25]. This chapter attempts to quantify how strongly the substrate structure of five hydrocarbon polymer films, Figure 2.2, influences the plasma / surface chemistry for both atmospheric pressure and low pressure electrical discharges.

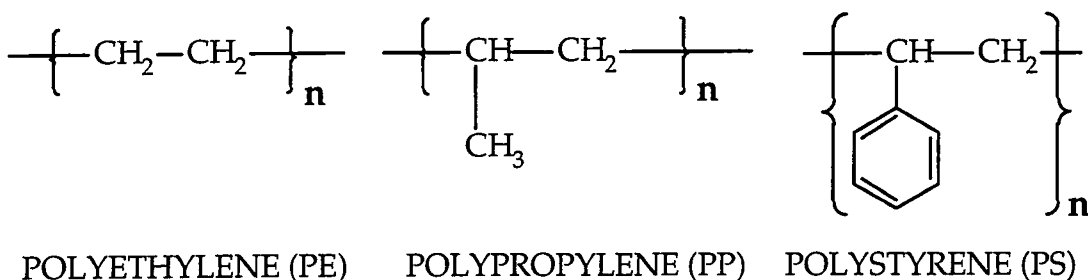

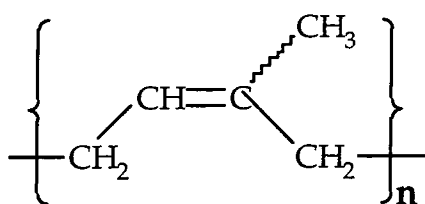


POLYISOPRENE (PIP)

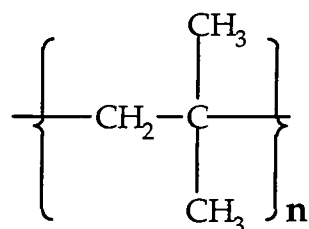


POLYISOBUTYLENE (PIB)

Figure 2.2 Structures of hydrocarbon polymers treated in this study.

## 2.2 EXPERIMENTAL

Small strips of low density polyethylene (ICI), polypropylene (ICI), and polystyrene (ICI) were ultrasonically cleaned for 30 seconds in a 1:1 ratio mixture cyclohexane and propan-1-ol solvents (analytical reagent grade, Aldrich). Polyisobutylene (Exxon) and polyisoprene (Exxon) were spin coated onto ultrasonically cleaned glass slides from 2% weight/volume toluene solution.

Silent discharge treatment of each sample in air was carried out for 30 seconds using a home-built parallel-plate dielectric barrier discharge cell with an inter-electrode gap of 3.00 ± 0.05 mm, Figure 2.3. The discharge was supplied with a maximum peak to peak voltage of 11 kV at a frequency of 3 KHz[26].

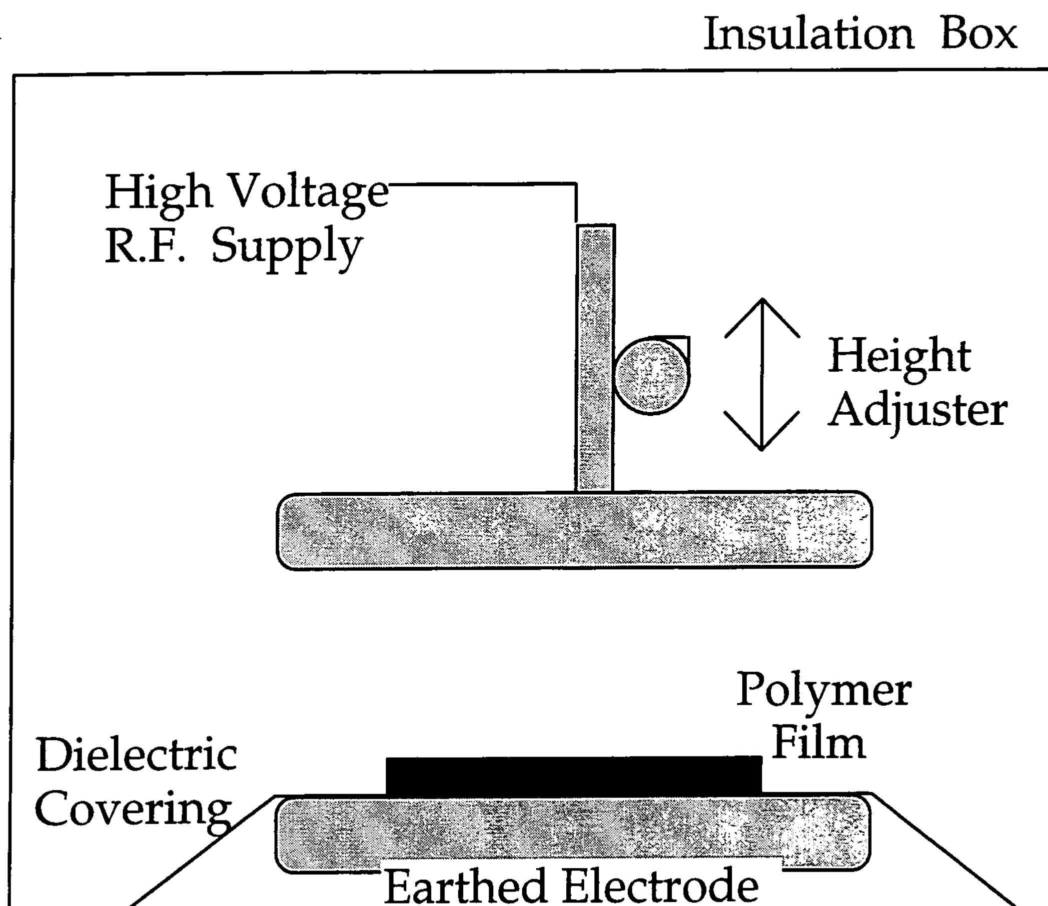


Figure 2.3 Silent discharge reactor.

Low pressure plasma treatments were carried out in an electrodeless cylindrical reactor (4.5 cm diameter, 460 $cm^3$ volume, with a leak rate better than 4 x $10^{-3}$ $cm^3$ $min^{-1}$) enclosed in a Faraday cage[27], Figure 2.4. This was fitted, using grease-free joints, with a gas inlet, a Pirani pressure gauge, and a 27 L $min^{-1}$ two-stage rotary pump connected to the reactor through a liquid nitrogen cold trap. Gas and leak mass flow rates were measured by assuming ideal gas behaviour[28]. A 13.56 MHz radio frequency (RF) generator was impedance matched to a copper coil (4 mm diameter, 9 turns, spanning from 8 cm to 15 cm from the gas inlet), wound around the reactor for inductive plasma coupling. A typical experimental run comprised of initially scrubbing the reactor with detergent, rinsing with isopropyl alcohol, and oven drying, followed by a 60 min high power (50 W) air plasma cleaning treatment. At this stage, a polymer sample was inserted into the centre of the reactor (*i.e.* the glow region), and

pumped down to a base pressure of 1.5 x $10^{-3}$ Torr. Air was subsequently introduced into the reaction chamber at 2 x $10^{-1}$ Torr pressure, and a flow rate of 1.0 $cm^3$ $min^{-1}$. After purging for 5 min, the glow discharge was ignited at 20 W for 30 seconds. Upon termination of treatment, the RF generator was switched off, and the system was purged to atmospheric pressure.

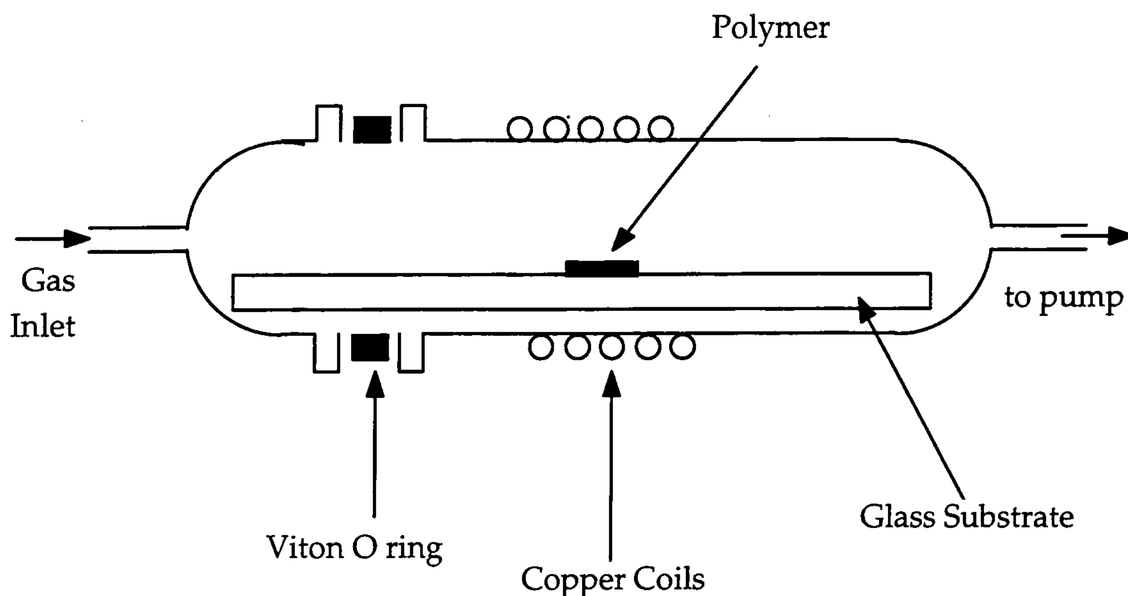


Figure 2.4 Low pressure plasma reactor.

A Kratos ES300 electron spectrometer equipped with a Mg Kα X-ray source (photon energy of 1253.6 eV), and a hemispherical analyser, was used for surface analysis by X-ray photoelectron spectroscopy (XPS). Photo-emitted electrons were collected at a take-off angle of 30° from the substrate normal, corresponding to a sampling depth of approximately 5 Å to 20 Å in polymers[29], with electron detection in the fixed retarding ratio (FRR, 22:1) mode. XPS spectra were accumulated on an interfaced IBM PC computer. Sensitivity factors for unit stoichiometry of C(1s) : O(1s) were determined to be 1.00 : 0.62. The cleanliness of each substrate and the absence of any surface-active non-hydrocarbon additives was verified by XPS. Each polymer was characterized immediately after each type of electrical discharge treatment.

Infrared absorption spectra of each clean and treated polymer were taken using a variable angle attenuated total reflection (ATR) cell fitted with a KRS-5 crystal on a Mattson Polaris instrument. 100 scans were acquired at a resolution of 4 $cm^{-1}$ using an incident beam angle of 45°, which corresponds to an ATR-FTIR sampling depth in polymers of approximately 0.1 μm[30].

Atomic force microscopy offers structural characterization of surfaces in the $10^{-4}$ - $10^{-10}$ m range without the prerequisite of special sample preparation, such as metallization, which can modify surface structure[31]. A Digital Instruments Nanoscope III atomic force microscope was used for examining the topographical nature of each substrate surface prior to and after electrical discharge exposure. All of the AFM images were acquired in air using the tapping mode and are presented as unfiltered data. Surface roughness measurements were taken directly from the stored AFM data.

## 2.3 RESULTS

Wide-scan XPS spectra of the treated and untreated polymer substrates yielded only carbon and oxygen features for low pressure plasma modification, whilst an additional small amount of nitrogen (less than 3 atomic %) was measurable following dielectric barrier exposure. C(1s) XPS spectra were fitted with Gaussian peaks of equal full width at half maximum (FWHM)[32], using a Marquardt minimisation computer program. Energies distinctive of different types of oxidised carbon moieties were referenced to the hydrocarbon peak (-$\underline{C}_xH_y$-) at 285.0 eV[33,34]: carbon adjacent to a carboxylate group (>$\underline{C}$-$CO_2$-) at 285.7 eV, carbon singly bonded to one oxygen atom (>$\underline{C}$-O-) at 286.6 eV, carbon doubly bonded to one oxygen atom or carbon singly bonded to two oxygen atoms (>$\underline{C}$=O / -O-$\underline{C}$-O-) at 287.9 eV, carboxylate groups (-O-$\underline{C}$=O) at 289.0 eV, and carbonate carbons (-O-$\underline{C}$O-O-) at 290.4 eV. The π–π* shake-up satellite around 291.5 eV for polystyrene and polyisoprene was fitted with a Gaussian peak of

different FWHM[35] in order to assess the level of aromaticity present before and after electrical discharge exposure, Figure 2.5.

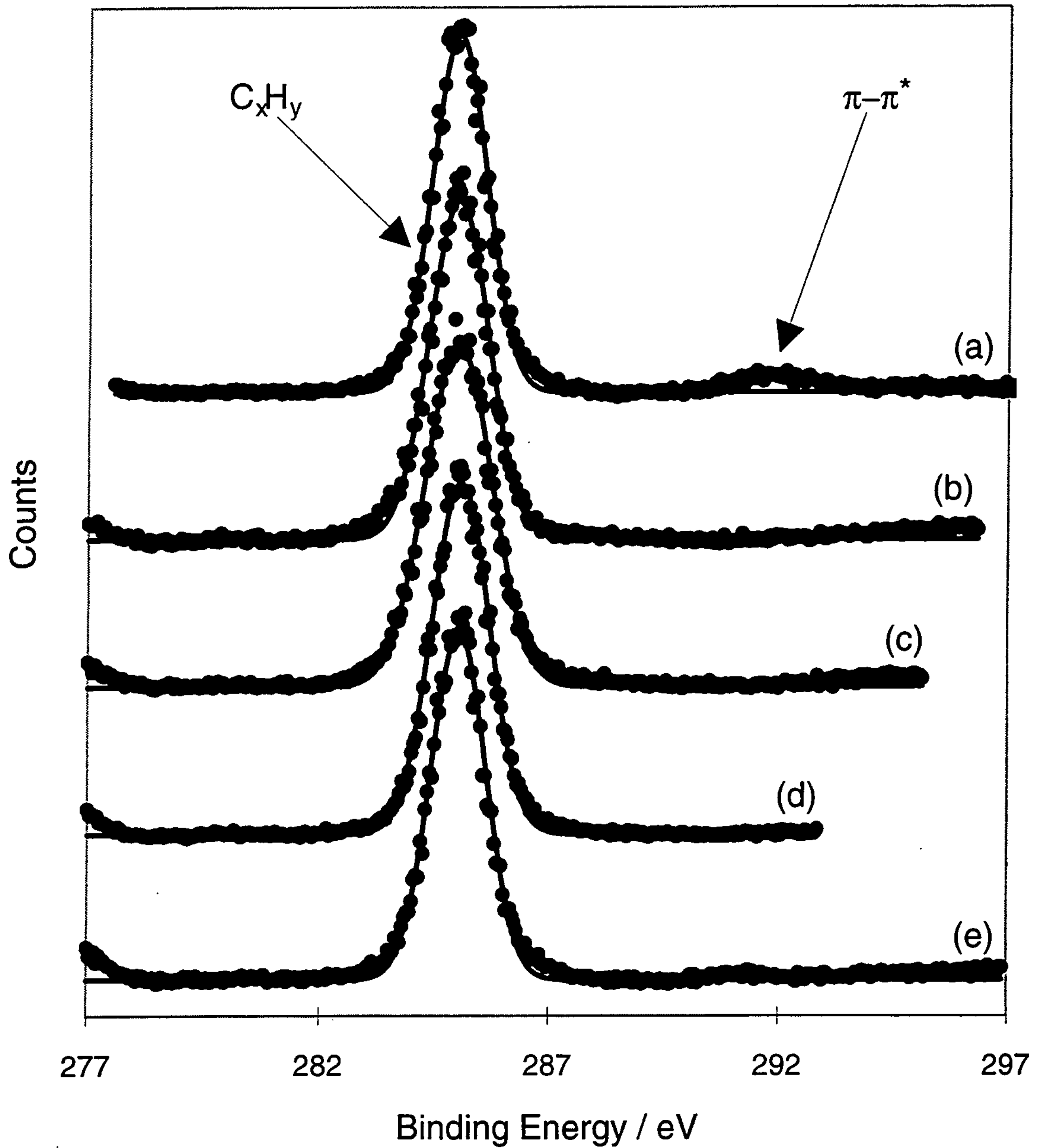


Figure 2.5 C(1s) XPS spectra of untreated: (a) polystyrene; (b) polyethylene; (c) polypropylene; (d) polyisobutylene; and (e) polyisoprene.

XPS spectra of untreated saturated polyolefins (PE, PP, and PIB) displayed a single C(1s) peak at 285.0 eV arising from -$\underline{C}_xH_y$-, Figure 2.5. For PE and PP, both types of electrical discharge used in this study resulted in similar O:C ratios, Table 2.2, and >$\underline{C}$-O- groups are the predominant reaction product, Figures 2.6 and 2.7 and Table 2.3. Oxidation levels are comparable to those previously noted for atmospheric[36,37] and low pressure plasma[38] treatments. However, in contrast to the lack of any topographical change reported for plasma modification of polyolefins[38], there is a definite change in the surface roughness of PE and PP following the electrical discharge exposures employed in this study, Figures 2.9-2.10. Surface roughness on the local scale is reduced, giving way to roughness at the macroscopic level, Table 2.4. This effect is most prominent for the dielectric barrier treatment, for which 'globules' are observed.

| Treatment | PE | PP | PIB | PIP | PS |
|---|---|---|---|---|---|
| Clean | 0.00 | 0.00 | 0.00 | 0.00 | 0.00 |
| Low Pressure Plasma | 0.21 | 0.29 | 0.05 | 0.24 | 0.42 |
| Silent Discharge | 0.21 | 0.29 | 0.12 | 0.51 | 0.34 |
| Ozonolysis Rate Constant ($L\ mol^{-1}\ s^{-1}$) | 0.046 | 0.080 | 0.012 | $10^5$ | 0.120 |

Table 2.2 Compilation of O : C ratios following electrical discharge treatment (± 0.01) and literature ozonolysis rate constants[47].

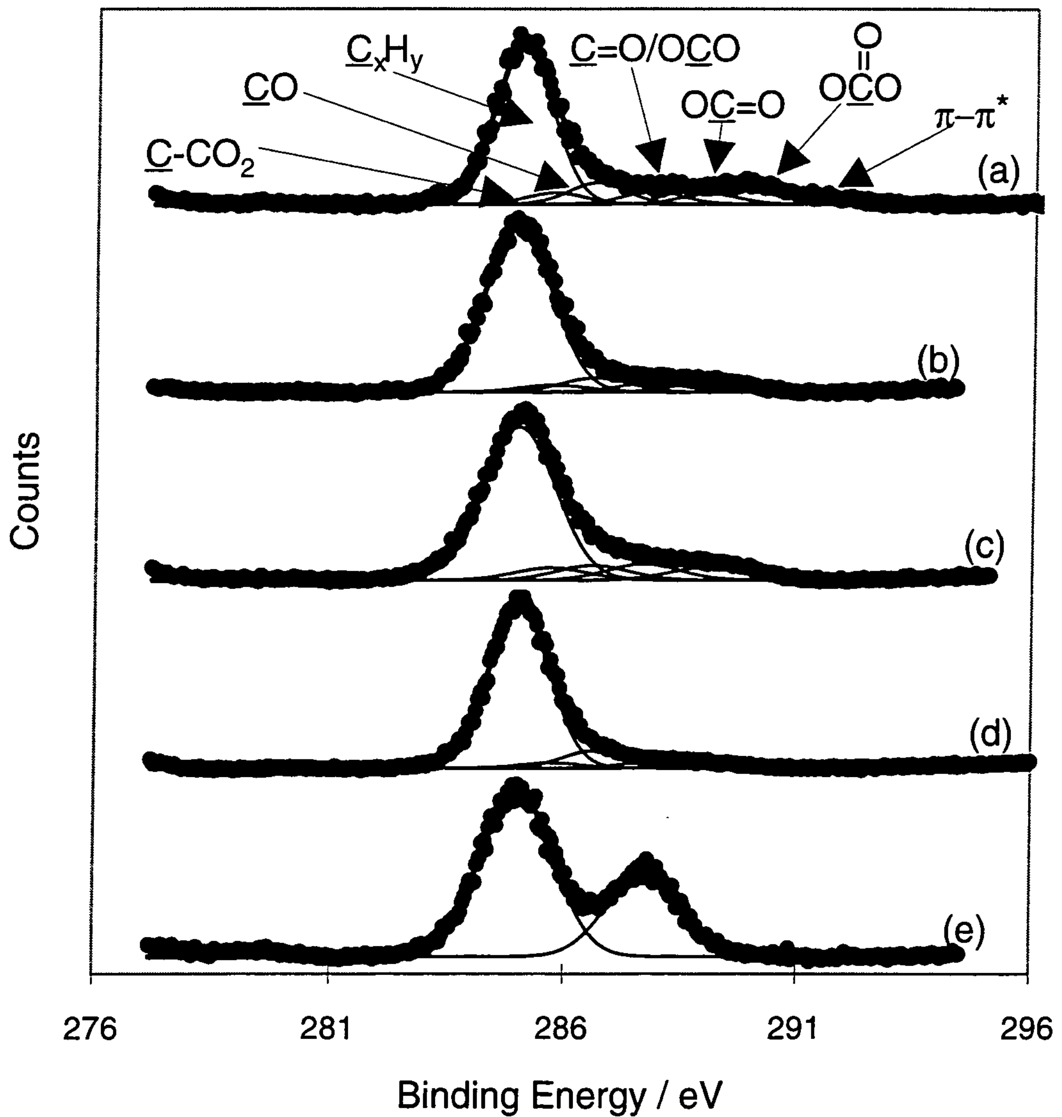


Figure 2.6 C(1s) XPS spectra of silent discharge treated: (a) polystyrene; (b) polyethylene; (c) polypropylene; (d) polyisobutylene; and (e) polyisoprene.

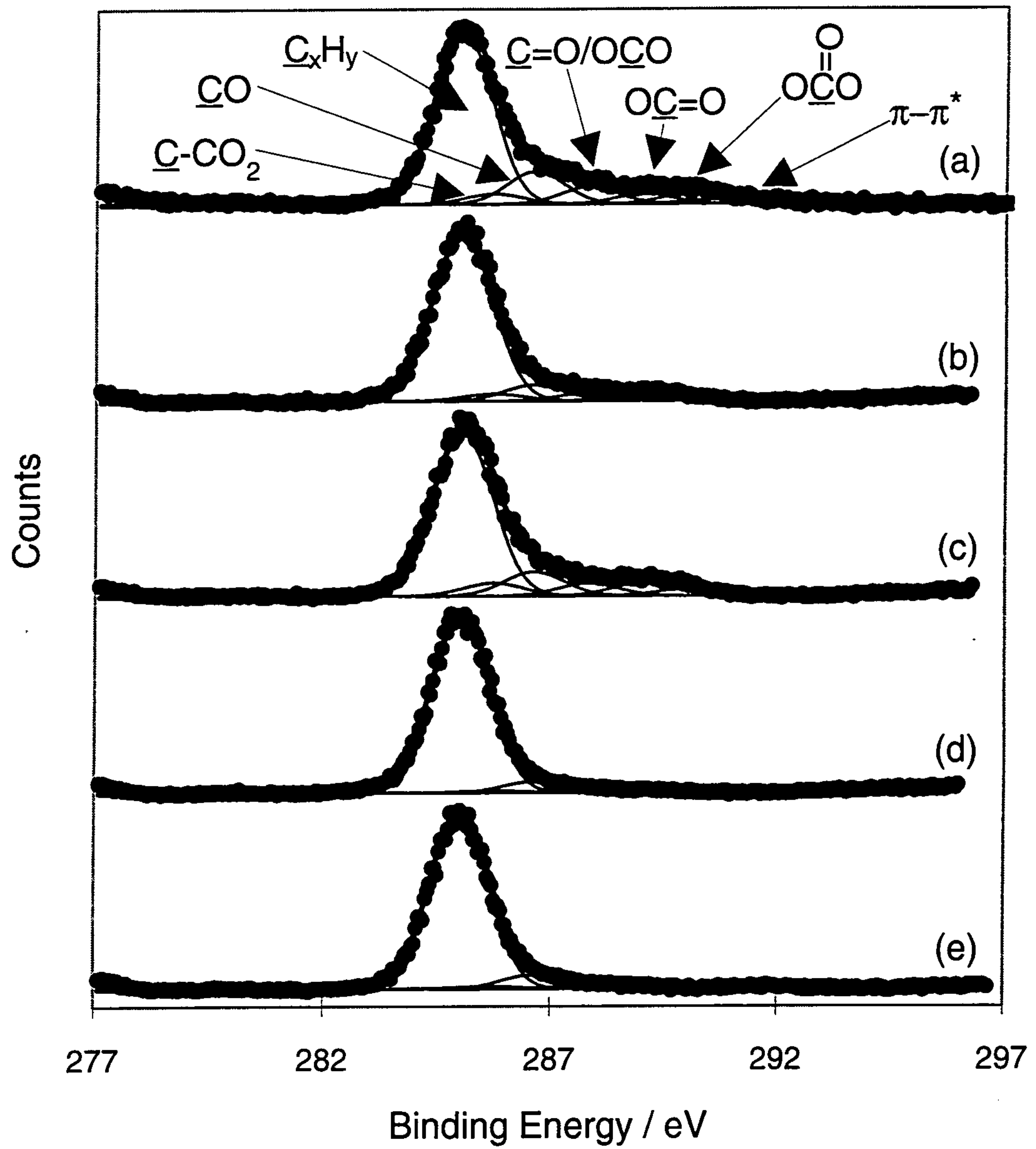


Figure 2.7 C(1s) XPS spectra of air plasma treated: (a) polystyrene; (b) polyethylene; (c) polypropylene; (d) polyisobutylene; and (e) polyisoprene.

| Treatment | -C-H- | -C-$CO_2$- | >C-O- | >C=O / -O-C-O- | -O-C=O | -O-CO-O- | $\pi-\pi^*$ |
|---|---|---|---|---|---|---|---|
| Plasma PE | 78.1 | 4.0 | 7.5 | 3.9 | 4.2 | 2.3 | - |
| S.D. PE | 76.2 | 4.5 | 8.5 | 4.5 | 4.5 | 1.8 | - |
| Plasma PP | 70.5 | 5.3 | 9.8 | 5.1 | 5.3 | 4.0 | - |
| S.D. PP | 67.1 | 5.9 | 11.4 | 7.7 | 5.9 | 1.9 | - |
| Plasma PIB | 90.8 | 1.1 | 5.3 | 1.5 | 1.1 | 0.2 | - |
| S.D. PIB | 83.2 | 2.5 | 8.6 | 2.9 | 2.5 | 0.3 | - |
| Plasma PS | 63.9 | 4.1 | 13.2 | 7.0 | 4.1 | 4.8 | 2.9 |
| S.D. PS | 67.3 | 3.9 | 9.3 | 6.1 | 3.9 | 6.6 | 2.8 |
| Plasma PIP | 71.6 | 4.8 | 10.6 | 3.2 | 4.8 | 3.5 | 1.5 |
| S.D. PIP | 61.3 | - | - | 38.7 | - | - | - |

Table 2.3 Relative amounts of carbon functionalities following low pressure plasma and silent discharge (S.D.) treatment (± 0.8).

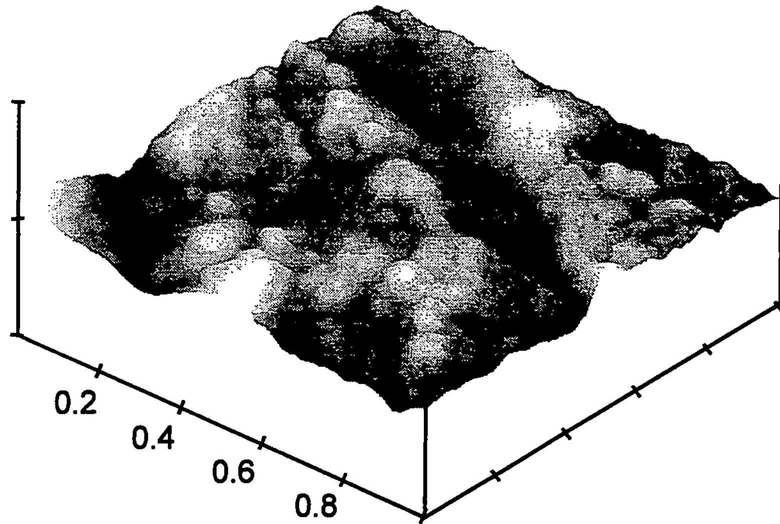


Figure 2.8(a) AFM of untreated polystyrene.

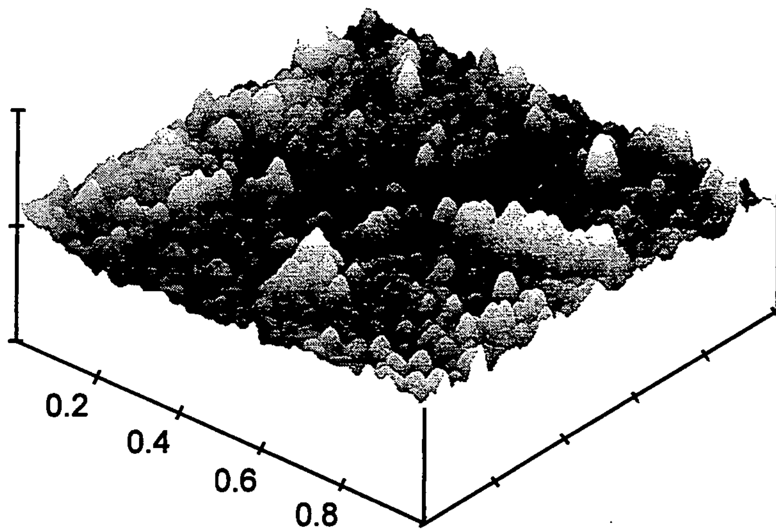


Figure 2.8(b) AFM of air plasma treated polystyrene.

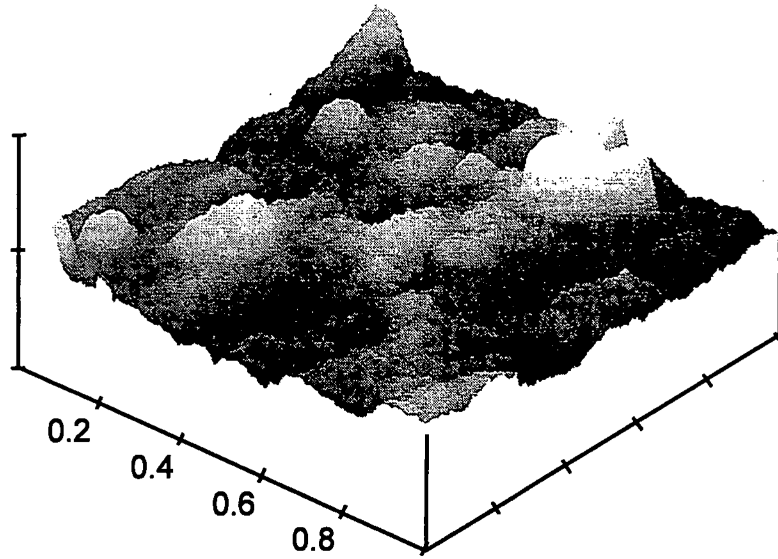


Figure 2.8(c) AFM of silent discharge treated polystyrene.

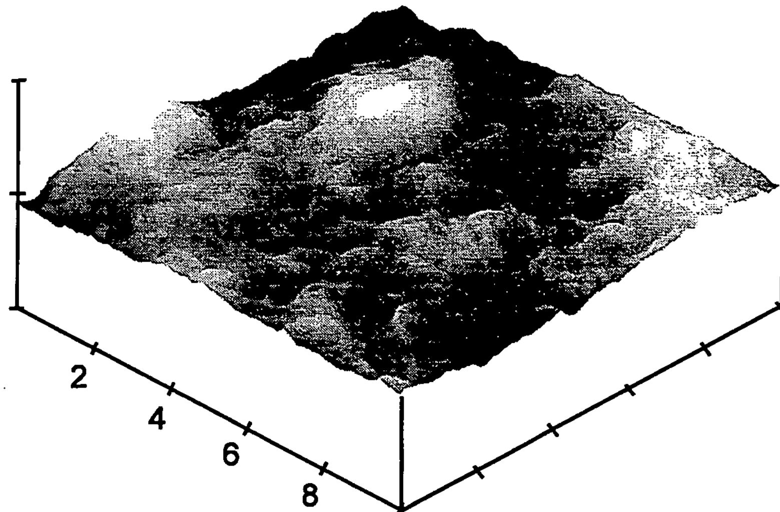


Figure 2.9(a) AFM of untreated polyethylene.

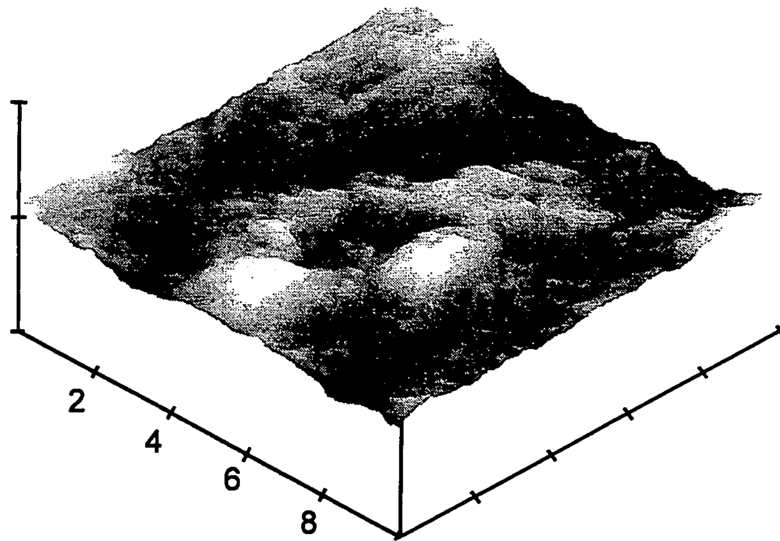


Figure 2.9(b) AFM of air plasma treated polyethylene.

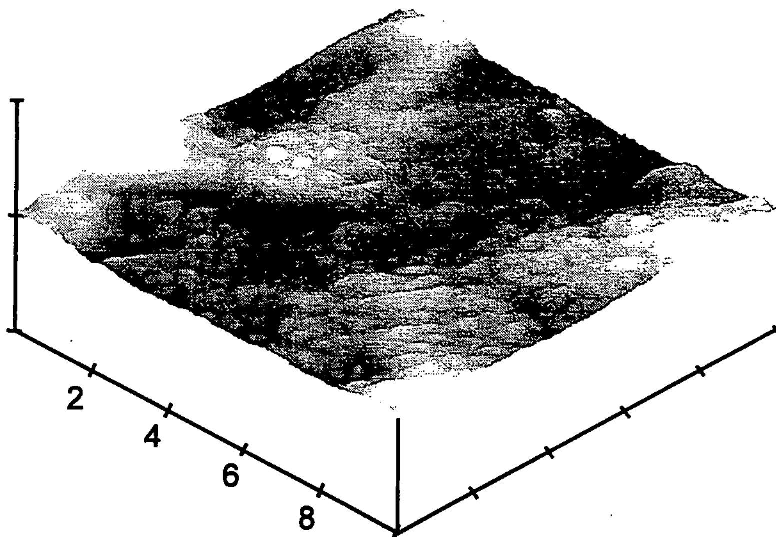


Figure 2.9(c) AFM of silent discharge treated polyethylene.

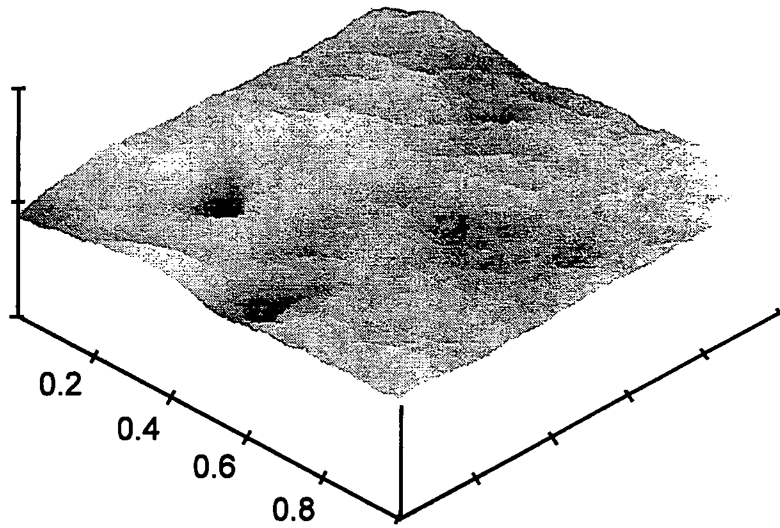


Figure 2.10(a) AFM of untreated polypropylene.

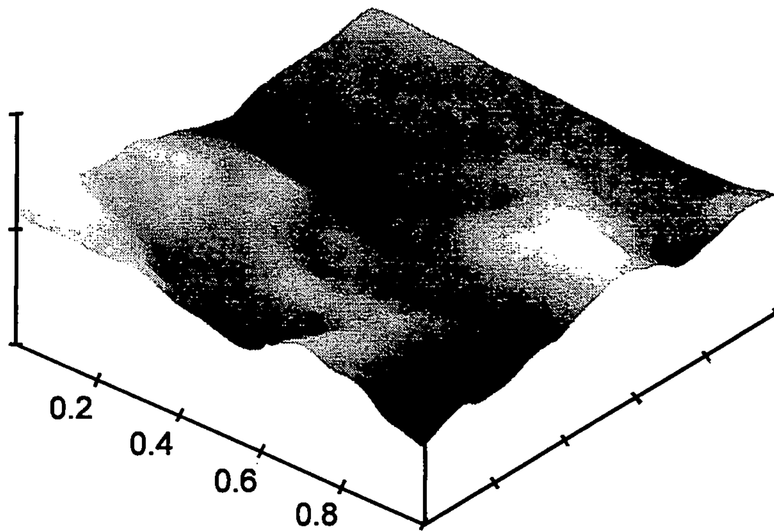


Figure 2.10(b) AFM of air plasma treated polypropylene.

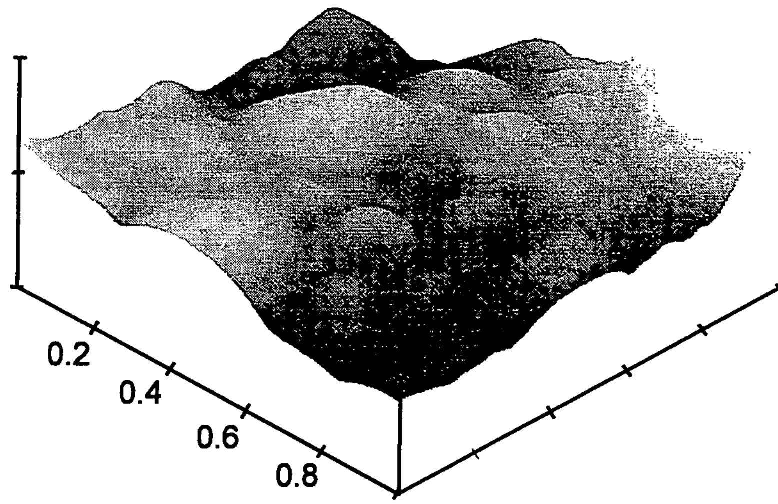


Figure 2.10(c) AFM of silent discharge treated polypropylene.

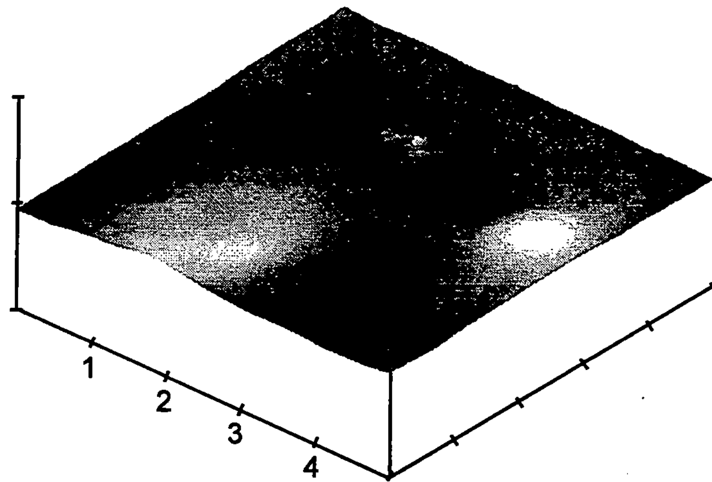


Figure 2.11(a) AFM of untreated polyisobutylene.

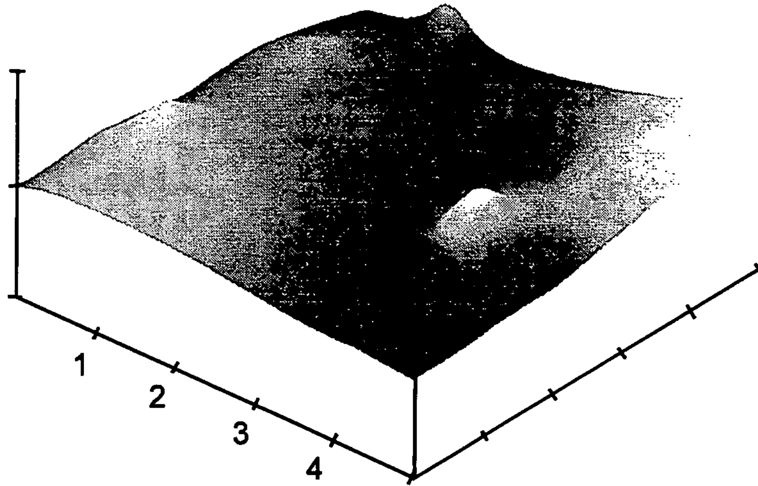


Figure 2.11(b) AFM of air plasma treated polyisobutylene.

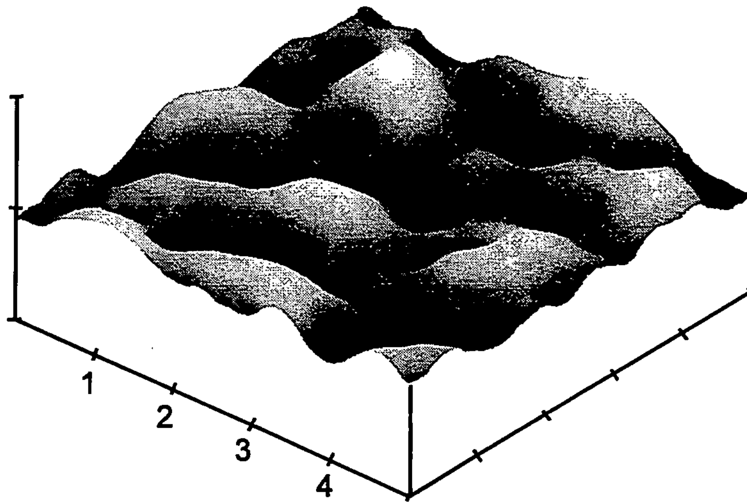


Figure 2.11(c) AFM of silent discharge treated polyisobutylene.

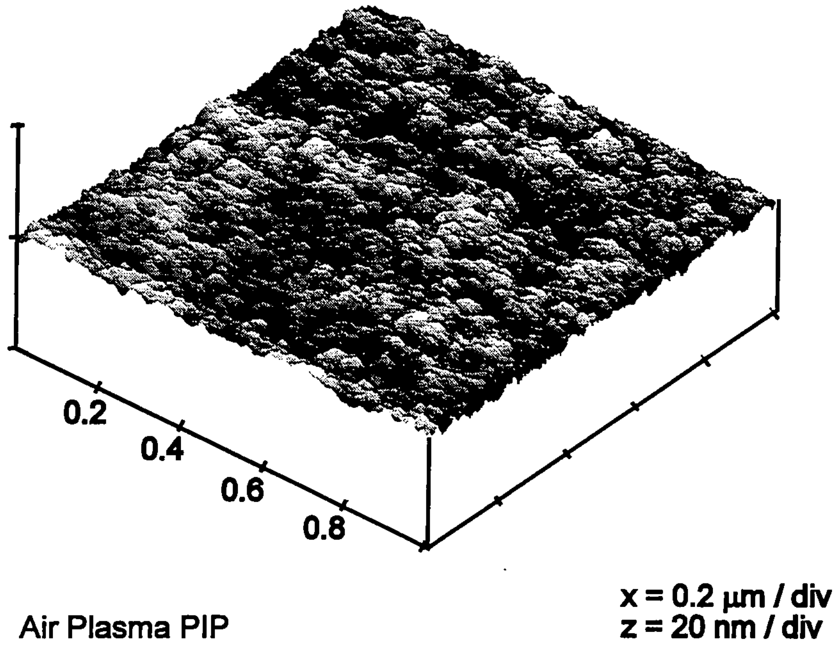


Figure 2.12 AFM of air plasma treated polyisoprene.

| Substrate | Area Analysed / μm | RMS Roughness / nm |
|---|---|---|
| Clean PE | 10 x 10 | 129 |
| Plasma PE | 10 x 10 | 117 |
| Silent Discharge PE | 10 x 10 | 98 |
| Clean PP | 1 x 1 | 9 |
| Plasma PP | 1 x 1 | 24 |
| Silent Discharge PP | 1 x 1 | 45 |
| Clean PIB | 5 x 5 | 6 |
| Plasma PIB | 5 x 5 | 19 |
| Silent Discharge PIB | 5 x 5 | 23 |
| Clean PS | 1 x 1 | 7 |
| Plasma PS | 1 x 1 | 9 |
| Silent Discharge PS | 1 x 1 | 13 |

Table 2.4 Surface roughness following electrical discharge treatment.

Polyisobutylene (PIB) is more susceptible to both chemical and topographical attack by silent discharge treatment than by low pressure plasma exposure, Table 2.2; more oxygen is incorporated into PIB for the former, together with the formation of a highly modulated topography, Figure 2.11. As in the case of PE and PP, >C-O- groups are the predominant reaction product for both treatments of PIB, Table 2.3.

Clean polystyrene C(1s) spectra showed a pure hydrocarbon peak with 5.3 ± 0.2 % of total intensity due to the aromatic $\pi$–$\pi^*$ shake-up satellite, Figure 2.5(a). There is a greater level of oxygen incorporation into PS during low pressure plasma exposure than during silent discharge treatment, whilst the aromaticity was approximately halved in both cases. As with the saturated polyolefins, >C-O- groups are the predominant oxidized carbon functionality, however, carbonate group (-O-CO-O-) concentration is greater for treated

polystyrene than that measured for the other modified polymers. Again for PS, atomic force microscopy illustrates the more energetic nature of the silent discharge treatment compared to low pressure plasma modification, Figure 2.8. These results are contrary to previous SEM studies concerning the low pressure oxygen plasma treatment of polystyrene, in which no change in surface topography was reported[39].

The C(1s) region of untreated polyisoprene comprises a main hydrocarbon peak, and a weak valence band $\pi$-$\pi^*$ shake-up feature (3% of the total C(1s) intensity) shifted by 6.5 eV towards higher binding energy, Figure 2.5(e). For polyisoprene, low pressure plasma treatment incorporates mainly >C̲-O- groups, and causes a similar amount of oxygenation as for PE. Silent discharge treatment of PIP creates the most highly oxidised surface found in this study. Chemical modification was selective to >C̲=O / -O-C̲-O- groups; the C(1s) XPS spectrum of silent discharge treated PIP can be fitted with just two Gaussian peaks: hydrocarbon (-$\underline{C}_xH_y$-) at 285.0 eV, and carbonyl / double ether (>C̲=O / -O-C̲-O-) at 287.8 eV, Figure 2.6. The O:C ratio of the treated surface was found to be 0.51 ± 0.01, and the ratio of oxygen to oxidised carbon was calculated to be 1.54 ± 0.02.

ATR-FTIR characterisation showed a difference between clean and treated polymer surfaces only for silent discharge exposed polyisoprene. Spin coated PIP exhibits the following absorbances[40-42], Figure 2.13(a): 2962 $cm^{-1}$ (antisymmetric $CH_3$ stretching), 2916 $cm^{-1}$ (antisymmetric $CH_2$ stretching), 2852 $cm^{-1}$ (symmetric $CH_2$ stretching), 1448 $cm^{-1}$ ($CH_3$ symmetric bending) and 1375 $cm^{-1}$ (antisymmetric $CH_3$ bending), and 835 $cm^{-1}$ (tri-substituted >C=C< double bond stretch). No residual solvent was discernible. The following extra features were observed for silent discharge treated polyisoprene, Figure 2.13(b): 3384 $cm^{-1}$ (OH stretching[40]), 1714 $cm^{-1}$ (ketone C=O stretching[40]), 1215 $cm^{-1}$ (ketone group vibration[40]), 1105 $cm^{-1}$ (C-O-O ozonide stretch[43,44]), 1084 $cm^{-1}$ (C-O ozonide stretch[40]), 1026 $cm^{-1}$ (C-O ozonide stretch[40]) 1008 $cm^{-1}$ (trans CH=CH stretching[40]).

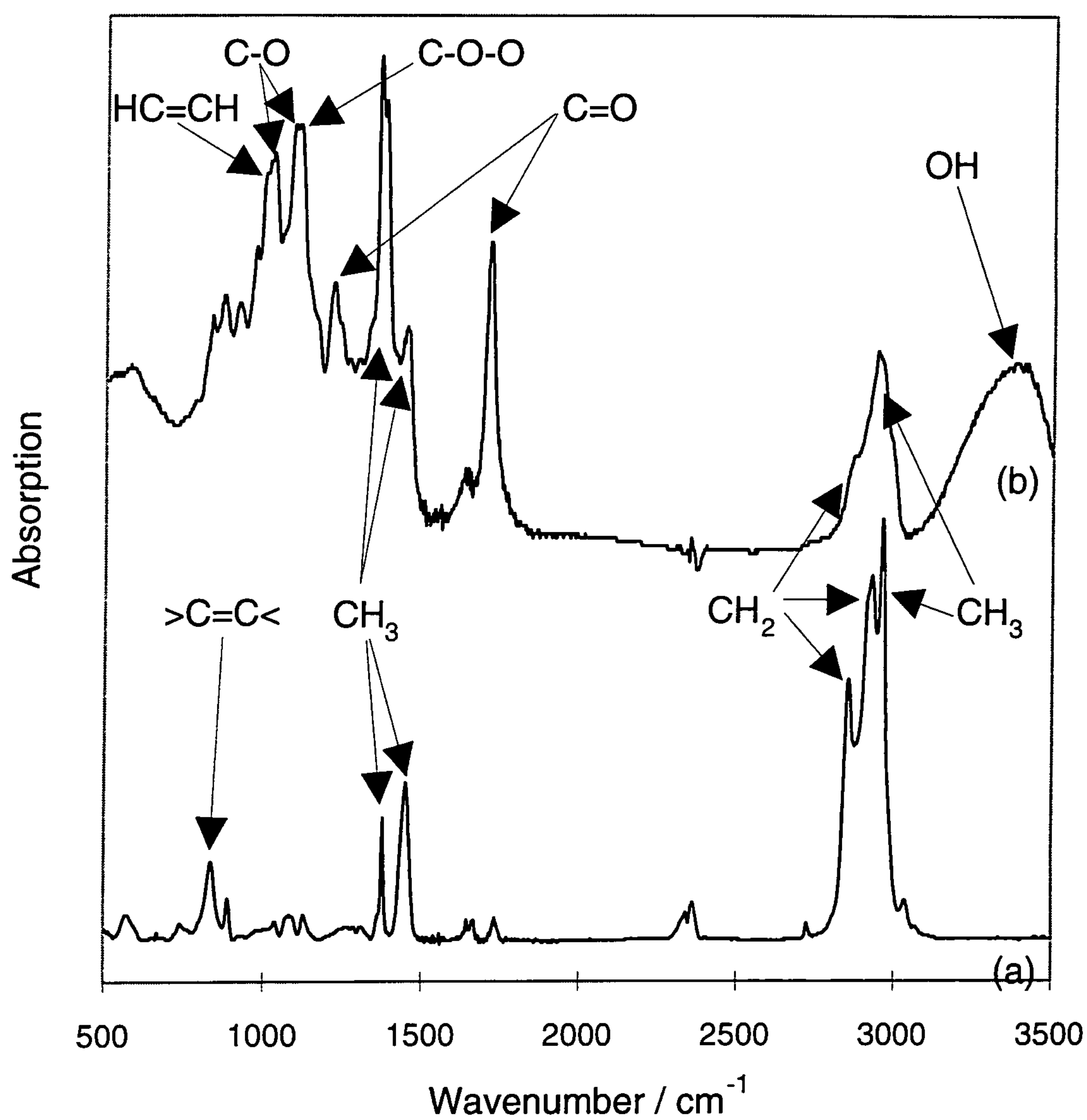


Figure 2.13 ATR-FTIR spectra of (a) untreated PIP and (b) silent discharge treated PIP.

## 2.4 DISCUSSION

### *2.4.1 Silent Discharge Chemical Modification*

Reaction of ozone, which is predominant in the silent discharge reactor[45], with polymer surfaces is expected to govern chemistry of silent discharge surface modification. Silent discharges in air contain nitrogen ions, dinitrogen ions and oxides of nitrogen ranging from NO to $N_2O_5$, in addition to atomic oxygen and ozone produced in pure oxygen discharges[11]. During silent discharge treatment, reaction of the polymer surface with activated nitrogen containing species must compete with vigorous oxidation reactions, explaining the low level of nitrogen incorporation observed.

Electron spin resonance (ESR) studies have demonstrated that saturated hydrocarbon polymers ozonize via a peroxy radical mechanism[46] to yield a wide variety of oxidised carbon groups, including carbonyl, alcohol and acid moeties, Scheme 1.

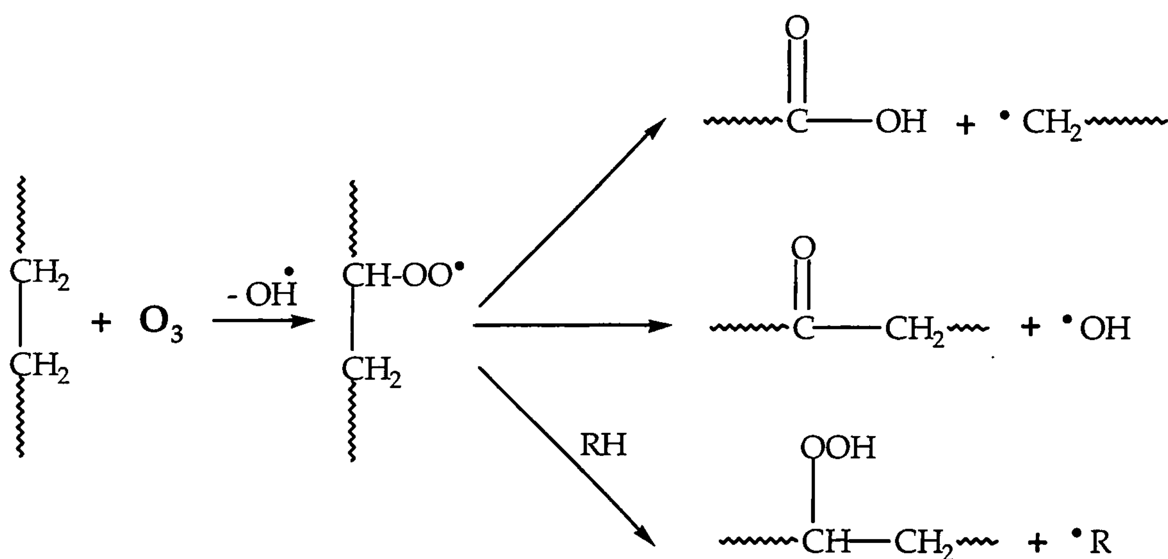


Scheme 1 Ozonolysis of saturated hydrocarbons[47].

In contrast, unsaturated polymers yield ozonides via the Criegee addition mechanism[51,52] in which ozone attacks a carbon double bond, Scheme 2.

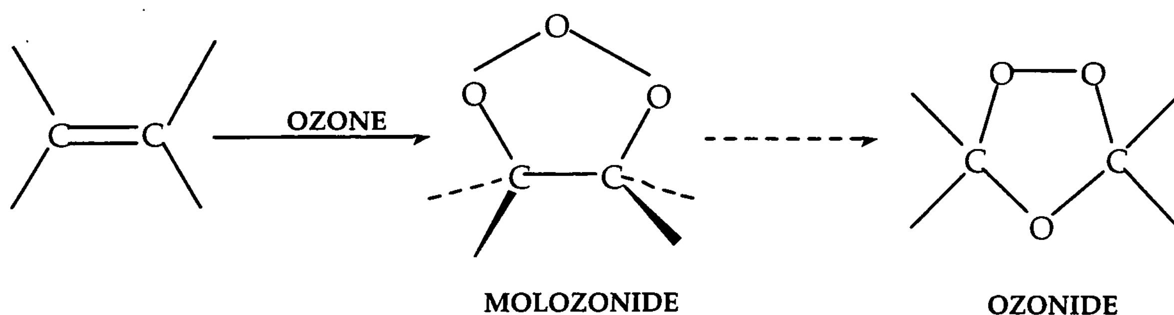


Scheme 2 Ozonolysis of unsaturated hydrocarbons[41].

The unstable primary ozonide (molozonide) decomposes into a zwitter ion of carbonyl oxide, and an aldehyde / ketone group[53,54], followed by a 3 + 2 cyclo-addition of spatially re-arranged zwitter ions with carbonyl groups to give the stable ozonide. At room temperature, ozonides are stable enough for isolation[43].

The relative degree of silent discharge oxidation of polymers in this study is PIP > PS > PP > PE > PIB; this order is entirely consistent with the rate constants reported in the literature for the ozonation of these polymers[46], Table 2.2. Comparison with previous studies where polyethylene[48,13], and polystyrene[27] substrates were exposed to ozone for exposure times similar to those employed in this work, however, indicates that surface oxidation is an order of magnitude greater in the case of silent discharge treatment. It is clear that silent discharge treatment offers an additional means of enhancing the rate of surface oxidation, such as the direct activation of the polymer substrate by electron[14-16] and / or photon bombardment[9,10].

Amongst all of the polymers studied both electrical discharge treatments of polyisobutylene exhibits the highest selectivity towards >C-O- groups Table 2.3, which is possibly due to the stabilizing influence of the dimethyl groups located along the polyisobutylene backbone. The largest number of carbonate groups are produced for silent discharge treatment of polystyrene film. In this case, there is the additional reaction pathway available which involves the formation of aromatic ozonides[44], which also accounts for the attenuation in the polystyrene $\pi-\pi^*$ feature.

A highly selective mode of surface oxidation is in operation during the dielectric barrier discharge treatment of polyisoprene, yielding exclusively >C̲=O / -O-C̲-O- functionalities. This result is remarkable in the context of non-equilibrium plasma treatments, which typically produce a variety of oxygenated functionalities[55]. Polyisoprene is reported to have an abnormally high rate coefficient for reaction with ozone[46], Table 2.2, and would therefore be expected to undergo rapid reaction with ozone generated in a dielectric barrier air discharge. Ozonation of double bonds along the polyisoprene backbone to form a polyozonide structure corresponds to a value of 1.50 for the oxygen to oxidized carbon XPS ratio; this is very close to the oxygen to oxidized carbon XPS ratio of $1.54 \pm 0.02$ measured for silent discharge treated PIP.

The ATR-FTIR spectrum for silent discharge treated PIP, Figure 2.13(b), indicates modification to a much greater depth than for any of the other polymers and the creation of a variety of molecular environments. This result confirms a strong reaction between PIP and ozone, since the depth of oxidation for combined ozone and ultraviolet light treatment of polymers is reported to be greater than that for discharge treatments[56]. The apparent disagreement with the XPS data in terms of molecular environments can be explained by the sampling depth of each technique; ATR-FTIR samples down to 1000 Å[30], whereas XPS accesses only the topmost 5 - 20 Å of the surface[29]. Dielectric barrier discharge treatment of polyisoprene appears to yield a polyozonide structure in the uppermost surface region, where spatial rearrangement of zwitter ions will occur in a similar fashion to that found in solution, and a mixture of ozonide and trapped carbonyl oxide zwitter ion / aldehyde / ketone intermediates in the sub-surface, where spatial rearrangement of zwitter ions in the bulk phase is sterically restricted.

### *2.4.2 Low Pressure Plasma Chemical Modification*

In contrast to ozone dominated chemistry in the silent discharge, vacuum-ultraviolet light[17,18] and atomic oxygen radicals[19] are the chemically predominant components in low pressure oxygen-containing plasmas. During this treatment, highly energetic photons cause chemical modification at the polymer substrate; atoms and unactivated molecules of oxygen may react with photo-generated polymer radicals[18,20]. Atomic oxygen may also react with unactivated polymer chains[57]. The greater oxygen incorporation into polystyrene observed for low pressure plasma treatment may be attributed to its chromophoric phenyl rings[58], whilst the low level of oxygenation in low pressure plasma treated polyisobutylene can be explained in terms of this polymer lacking any strong UV absorbing centres in its parent structure[59].

### *2.4.3 Topographical Modification*

Both free-radical photo-oxidation[14,15] and electron- or photon- activated ozonolysis mechanisms[11-13,60] are highly energetic. This is especially evident in the case of dielectric barrier modification, for which AFM has shown a high level of disruption in the polymer substrate topography. In the case of silent discharge treatment, low molecular weight oxidised material remains on the polymer surface and rearranges to minimise interfacial surface energy[61] forming globules[62,63], whereas, in the low pressure plasma environment volatile reaction products are more likely to desorb and be pumped away from the reactor. The depth resolution of SEM analysis used in previous studies may have been insufficient to detect topographical changes of PE[38] and PS[39] arising from plasma treatment.

## 2.5 CONCLUSIONS

Electrical discharge treatment of polymers results in textural changes and oxygenation at the substrate surface, and highlights the differences in physical and chemical nature between non-isothermal atmospheric and low pressure plasmas.

Topographical modification is more extreme for a discharge at atmospheric pressure than at low pressure, whilst the extent of oxygen incorporated by these discharges varies strongly with the original polymer chemical structure. An activated ozonolysis mechanism for silent discharge treatment is suggested by the XPS data O:C ratio, for all the polymers, and by the selective modification of PIP to a polyozonide structure. The chromophoric phenyl ring of polystyrene accounts for its stronger oxidation by low pressure plasma treatment, confirming the importance of vacuum ultraviolet surface photochemistry in this type of discharge.

## 2.6 REFERENCES


1. Lanauze, J. A.; Myers, D. L. *J. Appl. Polym. Sci.* **1990**, *40*, 595.
2. Morra, M.; Occhiello, E.; Garbassi, F. *Metallized Plastics 2*, Mittal K L Ed.; Plenum: New York, **1991**, 363.
3. Wade, W. L.; Mammone, R. J.; Binder, M. *J. Appl. Polym. Sci.* **1991**, *43*, 1589.
4. Owens, D. K. *J. Appl. Polym. Sci.* **1975**, *19*, 3315.
5. Blythe, A.; Briggs, D. *Polymer* **1978**, *19*, 1274.
6. Blais, P.; Carlssen, D. J.; Wiles, D. M. *J. Appl. Polym. Sci.* **1971**, *15*, 129.
7. Kim, C. Y.; Goring, D. A. I. *J. Appl. Polym. Sci.* **1971**, *15*, 1357.
8. Coburn, J. W. *IEEE Trans On Plasma Sci.* **1991**, *19*, 1048.
9. Eliason, B.; Kogelschatz, U. *IEEE Trans. Plasma Sci.* **1991**, *19*, 1063.
10. Eliason, B.; Kogelschatz, U. *IEEE Trans. Plasma Sci.* **1991**, *19*, 309.

11. Eliasson, B.; Hirth, M.; Kogelschatz, U. *J. Phys. D: Appl. Phys.* **1987**, *20*, 1421.

12. Honda, K.; Naito, Y. *J. Phys. Soc. Jpn.* **1955**, *10*, 1007.

13. Landers, E. *Proc. IEE* **1978**, *125*, 1069.

14. Skalny, J.; Luknarova, M.; Dindosova, D. *Czech. J. Phys.* **1988**, *B38*, 329.

15. Steinhauser, H.; Ellinghorst, G. *Angew. Makrom. Chem.* **1984**, *120*, 177.

16. Leclerq, B.; Sotton, M. *Polymer* **1977**, *18*, 675.

17. Clark, D. T.; Dilks, A. *J. Polym. Sci., Polym. Chem. Ed.* **1977**, *15*, 2321.

18. Shard, A. G.; Badyal, J. P. S. *Macromolecules* **1992**, *25*, 2053.

19. Yasuda, H. *J. Macromol.Sci., Chem.* **1976**, *A 10*, 383.

20. Liston, E. M. *J. Adhes.* **1989**, *30*, 199.

21. Briggs, D.; Kendall C.; Blythe, A. R.; Wootton, A. B. *Polymer* **1979**, *20*, 1053.

22. Briggs, D.; Kendall C.; Blythe, A. R.; Wootton, A. B. *Polymer* **1983**, *24* , 47.

23. Iwata, H.; Kishida, A.; Suzuki, M.; Hata, Y.; Ikada, Y. *J. Polym. Sci: Part A: Polym. Chem. Ed.* **1988**, *26*, 3309.

24. Pochan, J.; Gerenser, L *Polymer* **1986**, *27*, 1058.

25. Stradal, M. *Canad J. Chem. Eng.* **1975**, *53*, 427.

25a. Beer, H. F. *PhD Thesis*, Department of Chemistry, University of Durham, **1985**.

27. Shard, A. G.; Munro, H. S.; Badyal, J. P. S. *Polym. Comm.* **1991**, *32* , 152.

28. Ehrlich, C. D.; Basford, J. A. *J. Vac. Sci. Technol.* **1992**, *A10*, 1.

29. Roberts, R. F.; Allara, D. L.; Pryde, C. A.; Buchanan, D. N. E.; Hobbins, N. D. *Surf. Interface Anal.* **1980**, *2*, 5.

30. Harrick, N. J. *"Internal Reflection Spectroscopy"*; Harrick Sci. Corp: New York, 1967.

31. Binnig, G.; Quate, C. F.; Gerber, C. *Phys. Rev. Lett.* **1986**, *56*, 930.

32. Evans, J. F.; Gibson, J. H.; Moulder, J. F.; Hammond, J. S.; Goretzki, H. *Fresenius Z. Anal. Chem.* **1984**, *319*, 841.

33. Clark, D. T.; Dilks, A. *J. Polym. Sci. Polym. Chem. Ed.* **1978**, *16*, 991.

34. Johansson, G.; Hedman, J.; Berndtsson, A.; Klasson, M.; Nilsson, R. *J. Electron Spectr.* **1973**, *2*, 295.
35. Clark, D. T.; Thomas, H. R. *J. Polym. Sci: Polym. Chem. Ed.* **1978**, *16*, 791.
36. Lee, J. H.; Kim, H. G.; Khang, G. S.; Lee, H. B.; Jhon, M. S. *J. Colloid Interface Sci.* **1992**, *152*, 563.
37. Gerenser, L. J.; Elman, J. F.; Mason, M. G.; Pochan, J. M. *Polymer* **1985**, *26*, 1162.
38. Gerenser, L. J. *J. Adhesion. Sci. Tech.* **1987**, *1*, 303.
39. Onyiriuka, E. C.; Hersh, L. S.; Hertl, W. *J. Colloid Interface Sci.* **1991**, *144*, 98.
40. Bellamy, L. J. *"The Infrared Spectra of Complex Molecules"*; Chapman and Hall: London, 1975.
41. Williams, D. H.; Flemming, I. *"Spectroscopic Methods In Organic Chemistry"*; McGraw-Hill: London, 1980.
42. Amram, B.; Bokobza, L.; Quesel, J. P.; Monnerie, L. Polymer **1986**, *27*, 877.
43. Hon, Y.-S.; Lu, L.; Chang, R.-C.; Chu, K.-P. *Heterocycles* **1991**, *32*, 437.
44. Witkop, B. *J. Am. Chem. Soc.* **1953**, *75*, 4273.
45. Yagi, S.; Kumumoto, M. *Australian J. Phys.* **1995**, *48*, 411.
46. Razumovskii, S. D.; Kefeli, A. A.; Zaikov, G. E. *Euro. Polym. J.* **1971**, *7*, 275.
47. Pokholak, T. N.; Vohlyaev, P. M.; Karpukhin, O. N.; Razumovskii, S. D. *Vysokomol. Soedin. B* **1969**, *11*, 692.
48. Peeling, J.; Clark, D. T. *J. Polym. Sci Polym. Chem. Ed.* **1983**, *21*, 2047.
49. Foerch, R.; McIntyre, N. S.; Hunter, D. H. *J. Polym. Sci. Polym. Chem. Ed.* **1990**, *28*, 193.
50. Peeling, J.; Jazzar, M. S.; Clark, D. T. *J. Polym. Sci Polym. Chem. Ed.* **1982**, *20*, 1797.
51. Criegee, R. *Adv. Chem Ser.* **1959**, *21*, 133.
52. Bailey, P. S. *Ozonation in Organic Chemistry Vol.1*; Academic Press: New York, **1978**.
53. Kuczkowski, R. L. *Chem. Soc. Rev.* **1992**, *21*, 79.

54. Ho, K. W. *J. Polym. Sci. Polym. Chem. Edn.* **1986**, *24*, 2467.

55. Clark, D. T.; Dilks, A. *J. Polym. Sci. Polym. Chem. Edn.* **1979**, *17*, 957.

56. Strobel, M.; Walzak, M. J.; Hill, J. M.; Lin, A.; Karbaskewski, E.; Lyons, C. S. *J. Adh. Sci. Tech.* **1995**, *9*, 365.

57. Cain, S. R.; Egitto, F. D.; Emmi, F. *J. Vac. Sci. & Tech.* **1987**, *A5*, 1578.

58. Wells, R. K.; Drummond, I. W.; Robinson, K. S.; Street, F. J.; Badyal, J. P. S. *Polymer* **1993**, *34*, 3611.

59. Guillet, J. *"Polymer Photophysics and Photochemistry"*; Chapter 1; Cambridge Uni. Press: Cambridge, 1985.

60. Eliasson, B. *IEEE Trans. Plasma Sci.* **1991**, *19*, 309.

61. Good, R. S. *Contact Angles, Wettability and Adhesion*; Ed. Mittal K. L.; VSP: Utrecht, **1993**.

62. Overney, R. M.; Guntherodt H.-J.; Hild S. *J. Appl. Phys.* **1994**, *75*, 1401.

63. Overney, R. M.; Luthi R.; Haefke H.; Frommer J.; Meyer E.; Guntherodt H.-J. *Appl. Surf. Sci.* **1993**, *64*, 197.

# Chapter Three: Non-Isothermal Oxygen Plasma Treatment Of Phenyl Containing Polymers

---

## 3.1 INTRODUCTION

Non-isothermal plasma processing offers many advantages over traditional methods for altering polymer surfaces, such as chemical, hot press, flame, abrasion, and graft treatments[1-4], section 1.2.1. During cold plasma treatment of polymeric materials, bombardment of the substrate surface by a wide variety of energetic species, section 1.2.3, leads to chemical functionalisation and disruption of polymer topography, making non-isothermal plasma a suitable pre-treatment for polymer printing, painting, metallizing or laminating[5,6].

Most of the previous investigations in this field[7-9] have studied only one or two polymers at a time under comparable experimental conditions, making it difficult to draw any valid mechanistic conclusions concerning the importance of substrate structure.

A recent study based on contact angle measurements reported that $O_2$ plasma treatment improves aluminium adhesion to a variety of phenyl containing polymers[10]; however the relative variations in chemical and topographical nature were not correlated to parent polymer structure. In this article, the interdependence between surface reactivity and parent polymer structure during low pressure non-isothermal $O_2$ plasma treatment is investigated for seven phenyl containing polymers using X-ray photoelectron spectroscopy (XPS) and atomic force microscopy (AFM).

## 3.2 EXPERIMENTAL

Small strips of polystyrene (BP), polyethyleneterephthalate (Hoechst). polyetheretherketone (ICI), polybisphenolcarbonate (General Electric Plastics), polybisphenolsulfone (Westlake Plastics Company) and polyethersulfone

(Westlake Plastics Company) were ultrasonically cleaned in a 50 : 50 non-polar (cyclohexane) : polar (propan-2-ol) solvent mixture for 30 s. Polydimethylphenyleneoxide (Aldrich) was spin coated onto clean glass slides from a 2% chloroform solution.

Low pressure plasma treatments were carried out in a electrodeless cylindrical reactor which was set up and cleaned exactly as described in section 2.2. A polymer sample was inserted into the centre of the reactor (i.e. the glow region), and pumped down to a base pressure of $3 \times 10^{-3}$ mbar. Subsequently $O_2$ (99.9% purity, BOC) was introduced into the reaction chamber at $2 \times 10^{-1}$ mbar pressure, and a flow rate of 1.0 $cm^3 min^{-1}$. After purging with $O_2$ gas for 5 min, the glow discharge was ignited at 20 W for 30 s. Upon termination of treatment, the RF generator was switched off, and the reactor was flushed with $O_2$ gas for a further 5 min in order to allow quenching of residual reactive centres at the surface, and then finally vented to air prior to surface characterization.

In addition, $O_2$ plasma treated polymer strips were rinsed for 2 min in a 50 : 50 mixture of cyclohexane : propan-2-ol (a non-polar and a polar solvent respectively) and dried in air prior to surface analysis. None of the parent polymers are soluble in either of these washing solvents[11].

X-ray photoelectron spectroscopy (XPS), and atomic force microscopy (AFM), were used, exactly as described in section 2.2, to examine each of the polymer substrates at the three stages: clean, $O_2$ plasma treated, and solvent washed $O_2$ plasma treated. XPS sensitivity factors for unit stoichiometry were experimentally determined to be C(1s) : O(1s) : S(2p) equals 1.00 : 0.62 : 0.54. Root-mean-square (RMS) roughness values were obtained from unfiltered 1 μm x 1 μm atomic force micrographs (this statistic is equivalent to the power spectrum value for RMS roughness recommended by the ASTM subcommittee for analyzing and reporting surface roughness[12]). The mean diameter of features on the micrographs was calculated from ten typical feature diameters, obtained using the microscope software's image cross-section facility.

## 3.3.RESULTS

### 3.3.1 XPS

The cleanliness of each substrate and the absence of any surface-active inorganic additives was verified by XPS wide-scan spectra. $O_2$ plasma treated polymer substrates yielded only carbon and oxygen features (with additional signals for sulphur in the cases of polysulfone and polyethersulfone). Mg $K\alpha_{1,2}$ C(1s) XPS core level spectra were peak fitted as described in section 2.3, with the addition of a peak for carbon singly bonded to one sulphur atom (>$\underline{C}$-S) at 285.6 eV[13] in the cases of polysulfone and polyethersulfone. The $\pi$–$\pi^*$ phenyl ring shake-up satellite present at ~291.7 eV for all of the substrates under investigation was fitted with a Gaussian peak of different FWHM in order to assess the level of aromaticity present in the untreated polymers[14].

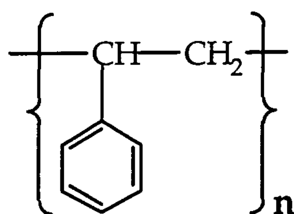


Polystyrene (PS)

The C(1s) XPS envelope for untreated polystyrene can be assigned to a hydrocarbon component, -$\underline{C}_xH_y$- at 285.0 eV, and a $\pi$–$\pi^*$ shake-up satellite feature is discernible at 291.7 ± 0.1 eV which accounts for approximately 5.3 ± 0.2 % of the total C(1s) peak area[14-17], Figure 3.1. Low pressure $O_2$ electrical discharge treatment of polystyrene produced the greatest uptake of oxygen amongst all of the polymers under investigation, Figure 3.2, this was accompanied by an attenuation of the of the $\pi$–$\pi^*$ shake-up satellite intensity to 3.3 ± 0.5 % of the total C(1s) peak area. 37 ± 5 % of the incorporated oxidized carbon functionalities were removed by solvent washing, Figures 3.1-3.2, with negligible variation in the intensity of the $\pi$–$\pi^*$ shake-up satellite.

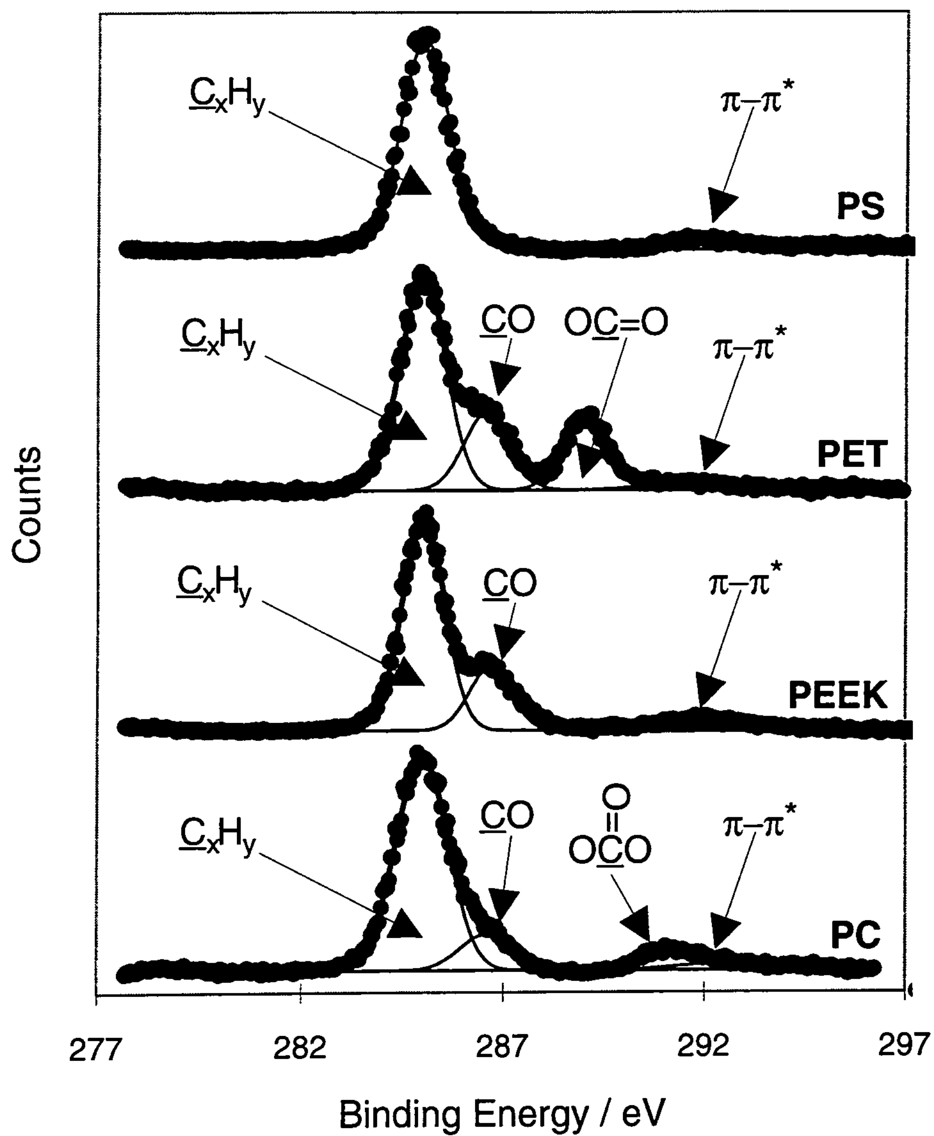


Figure 3.1(a) C(1s) XPS spectra of untreated polymers

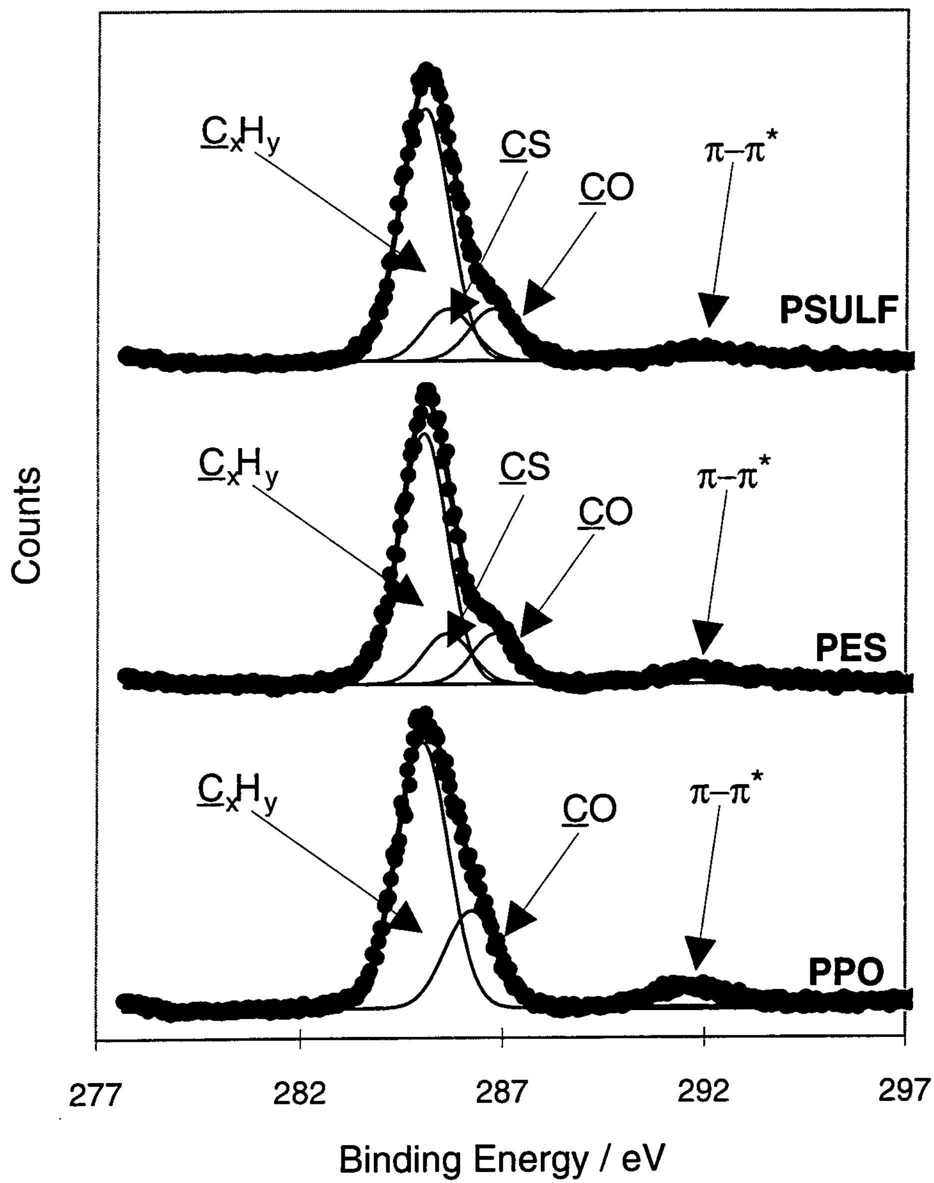


Figure 3.1(a) continued C(1s) XPS spectra of untreated polymers

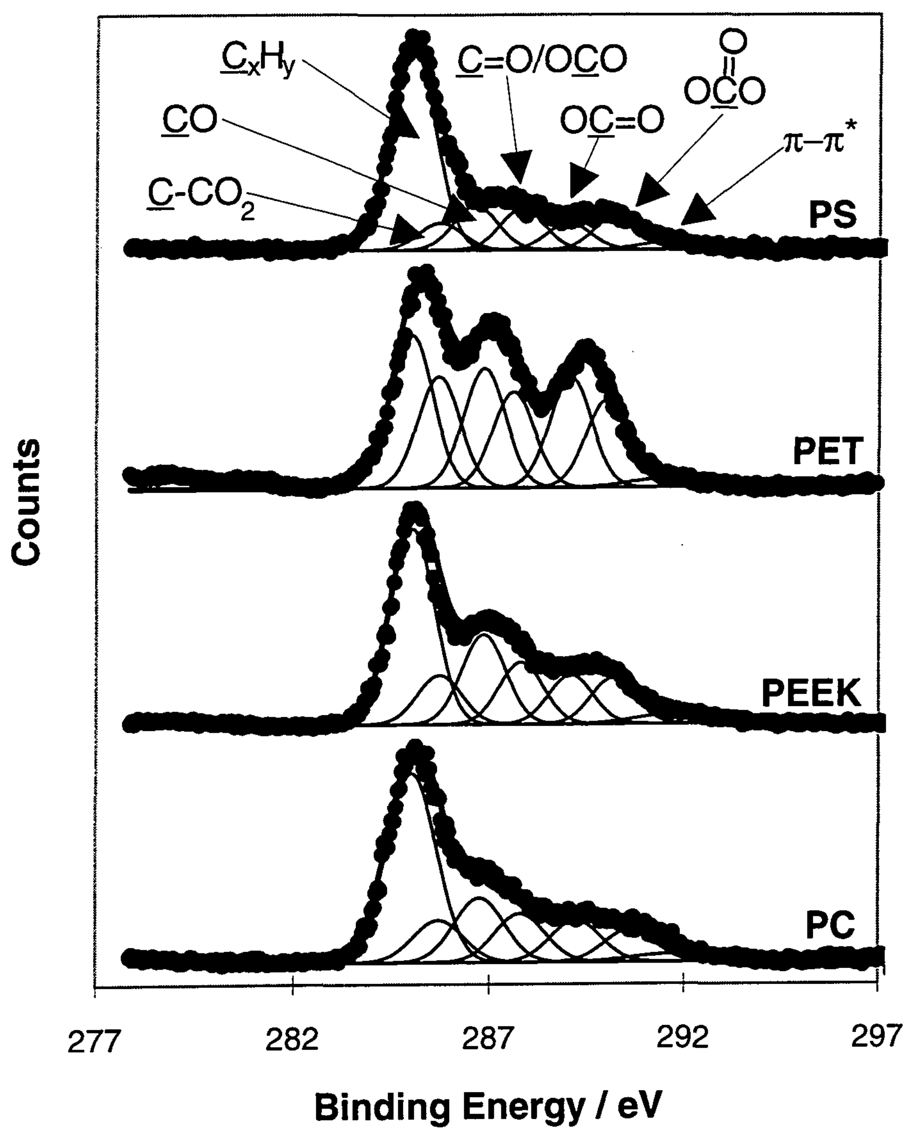


Figure 3.1(b) C(1s) XPS spectra of $O_2$ plasma treated polymers

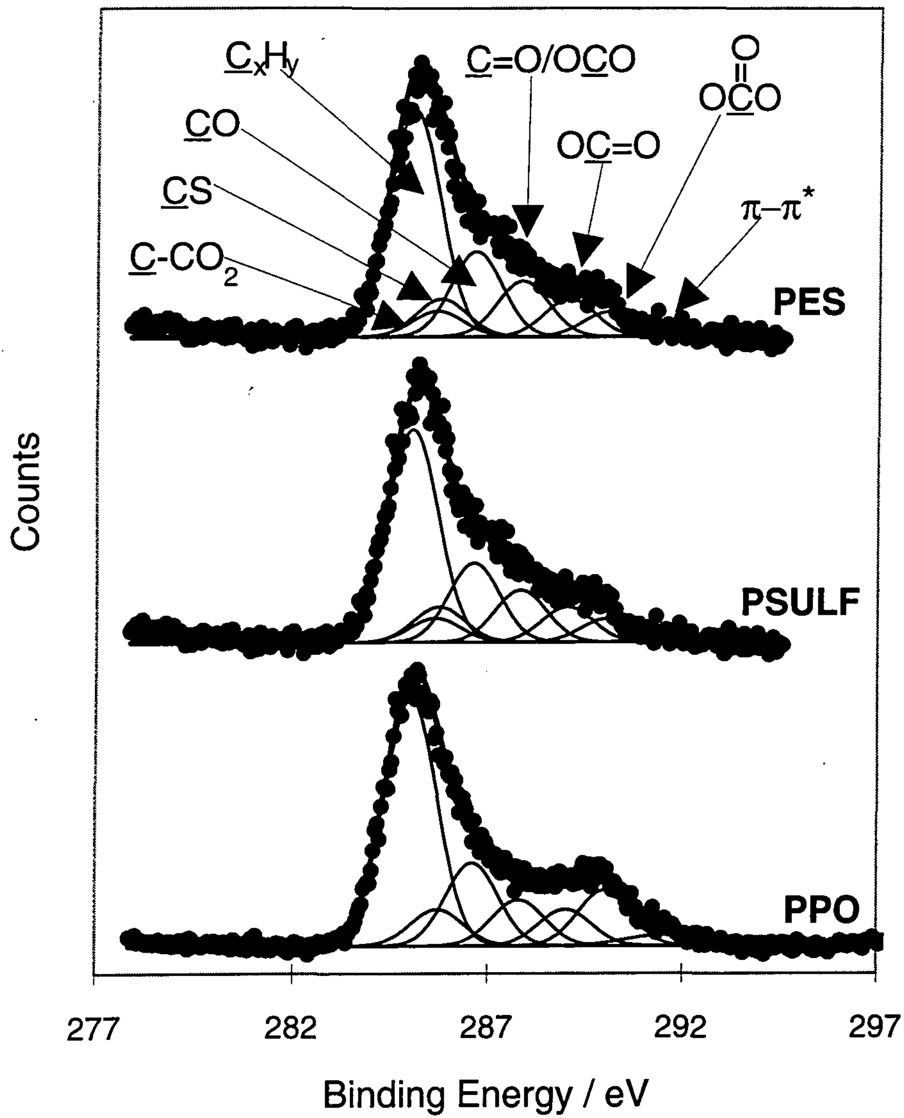


Figure 3.1(b) continued C(1s) XPS spectra of $O_2$ plasma treated polymers

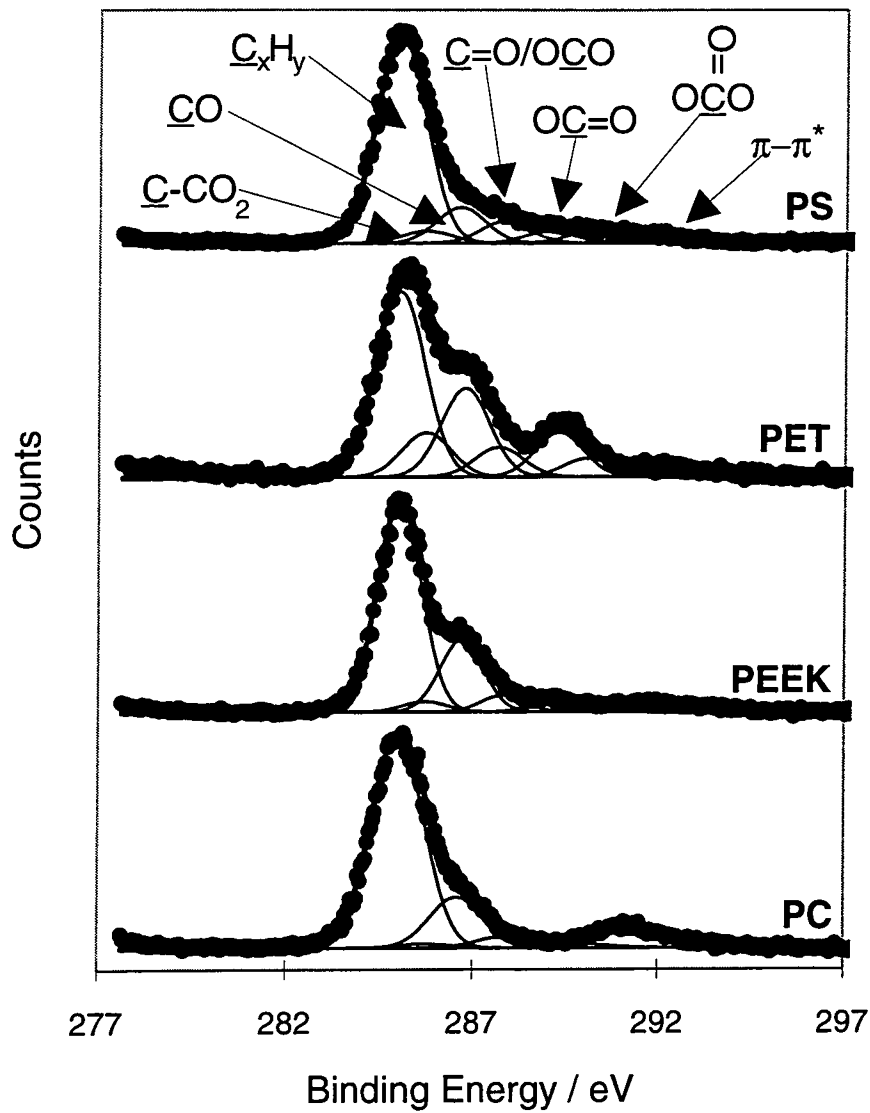


Figure 3.1(c) C(1s) XPS spectra of solvent washed $O_2$ plasma treated polymers

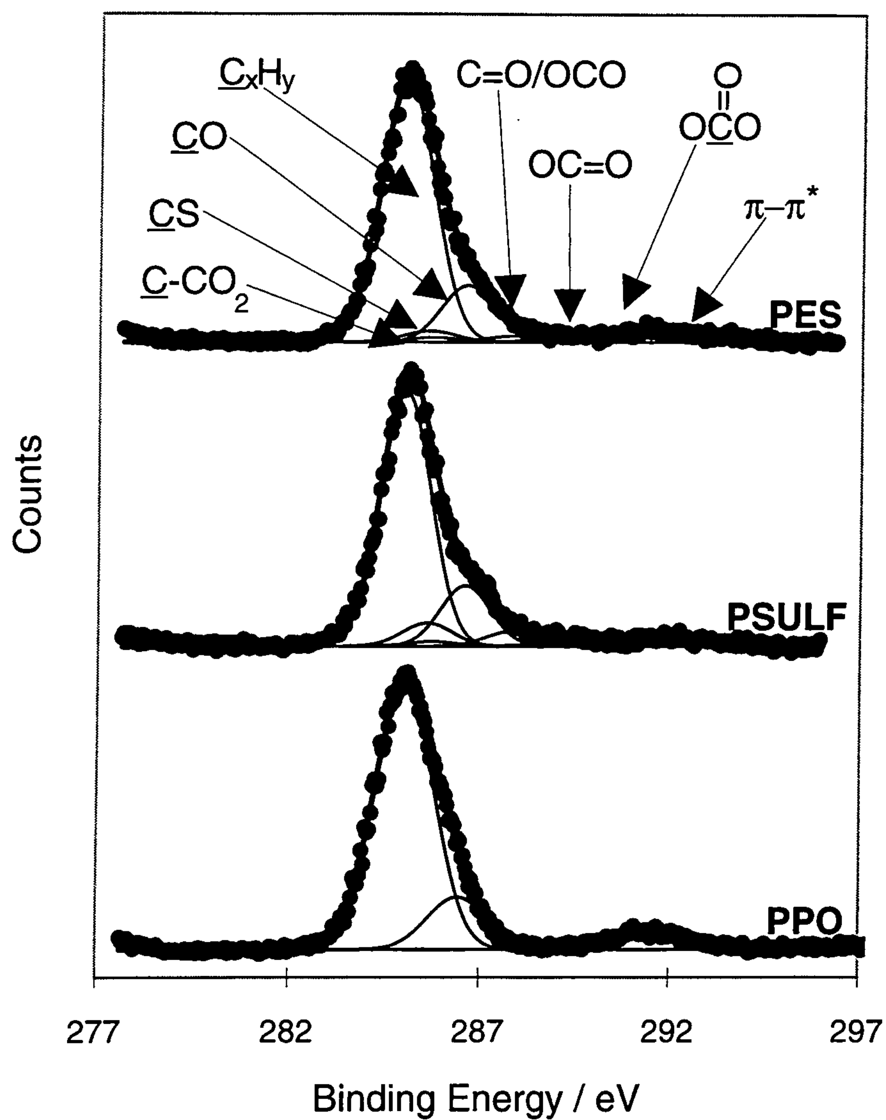


Figure 3.1(c) continued C(1s) XPS spectra of solvent washed $O_2$ plasma treated polymers.

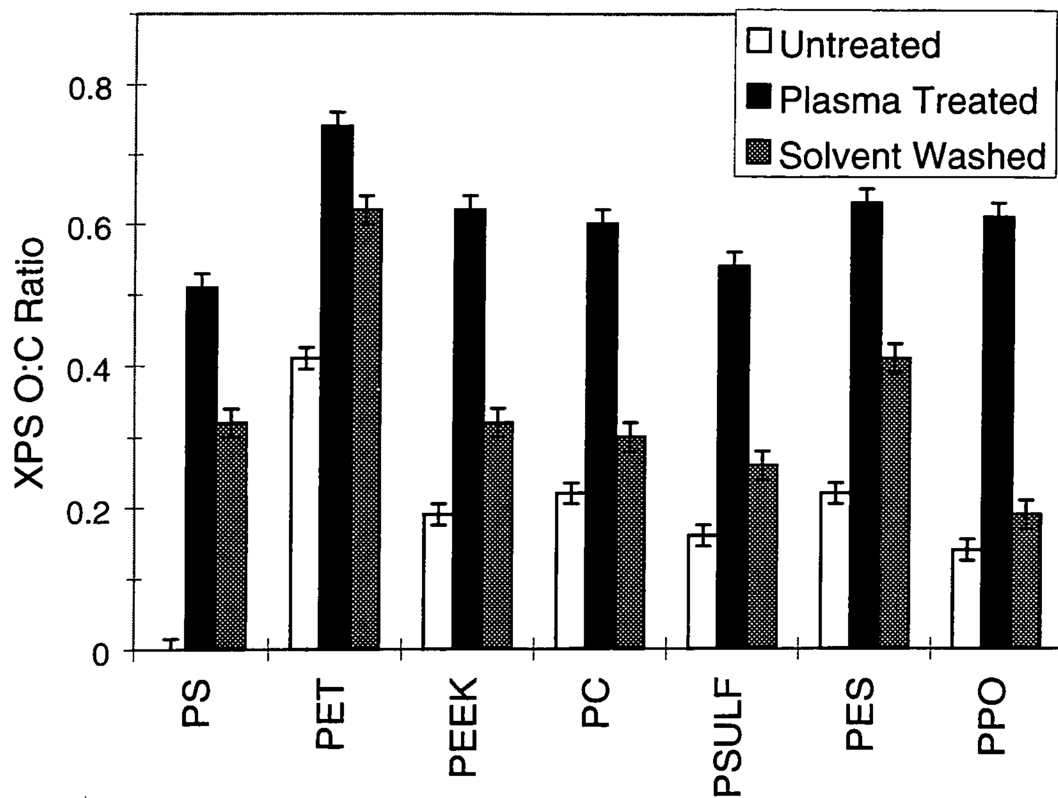


Figure 3.2 Variation in XPS O:C ratio with parent polymer structure for: untreated, $O_2$ plasma treated, and solvent washed $O_2$ plasma treated polymers.

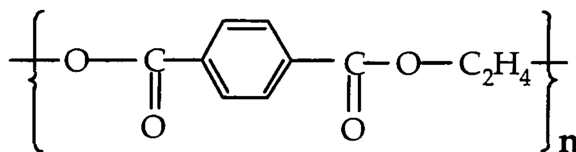

Polyethyleneterephthalate (PET)

In the case of untreated polyethyleneterephthalate (PET), the C(1s) envelope comprises -$\underline{C}_xH_y$-, -$\underline{C}$-O-, and -O-$\underline{C}$=O functionalities in a 3:1:1 ratio, Figure 3.1. The π–π* shake-up satellite accounts for 3.5 ± 0.2 % of the overall C(1s) envelope[18]. $O_2$ plasma treatment of PET produced the highest O:C ratio amongst all the polymers screened in the present study; this was despite the relative change with respect to the untreated polymer being the smallest, Figure 3.2. Plasma oxidation was accompanied by a loss in the π–π* shake-up satellite intensity to 2.3 ± 0.5 % of the total C(1s) envelope. The various types of oxygenated functionalities were noted to be fairly evenly distributed, Figure 3.1. Solvent washing of the $O_2$ plasma treated PET surface removed 36 ± 5 % of the oxygen added by plasma treatment, Figure 3.2.

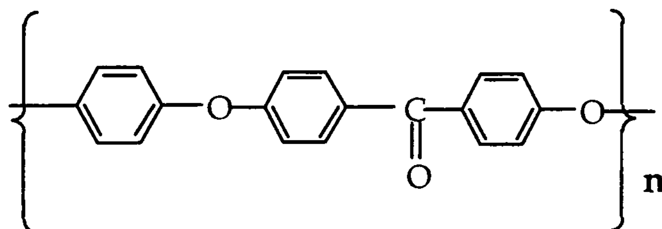

Polyetheretherketone (PEEK)

Polyetheretherketone (PEEK) contains two phenyl centres linked by ether groups and one benzophenone group per polymer repeat unit. Each of these carbon environments is clearly discernible in the C(1s) spectrum, Figure 3.1. $O_2$ plasma treatment of PEEK led to a large increase in O:C ratio, Figure 3.2, combined with a reduction in the π–π* shake-up satellite signal from 5.9 ± 0.2 % to 3.5 ± 0.5 % of total C(1s) peak area. Solvent washing of the PEEK surface removed 71 ± 5 % of the oxygen added by $O_2$ plasma treatment, accompanied by a large increase in the proportion of -$\underline{C}$-O- groups at the expense of the other three types of oxidized carbon environments (*i.e.* $\underline{C}$=O / O-$\underline{C}$-O, O-$\underline{C}$=O, and O-$\underline{C}$O-O), Figure 3.1.

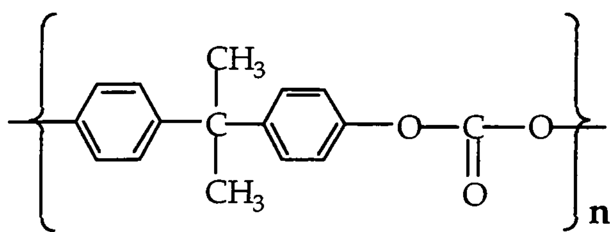

Polybisphenolcarbonate (PC)

Clean polycarbonate displays a π–π* shake-up satellite amounting to 4.2 ± 0.2 % of the total C(1s) signal intensity, Figure 3.1. Attenuation of the C(1s) π–π* shake-up satellite to 3.2 ± 0.5 %, and an increase in oxygen content occurred during $O_2$ glow discharge treatment, Figure 3.2. The rise in the proportion of -$\underline{C}$-O- and >$\underline{C}$=O / -O-$\underline{C}$-O- groups was accompanied by a drop in the proportion of carbonate centres. These results are in agreement with previous reports which have shown that polycarbonate is more susceptible to plasma oxidation than PET and less so than polystyrene[19]. Solvent washing the treated polycarbonate surface removed 79 ± 5 % of the oxygen added by $O_2$ plasma treatment. Once again, structural environments originating from the parent polymer became more prominent upon solvent washing, Figure 3.1, *i.e.* a large increase in the proportion of -$\underline{C}$-O- groups was observed in conjunction with a decrease in the proportion of >$\underline{C}$=O / -O-$\underline{C}$-O- functionalities.

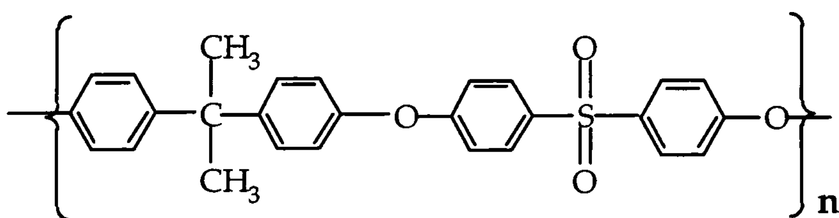

Polybisphenolsulfone (PSF)

The surface of untreated polysulfone (PSF) was found to contain 82 ± 2 % carbon, 15 ± 2 % oxygen, and 3 ± 1 % sulfur, in-keeping with the parent polymer structure (the theoretical composition being 84.4 % carbon, 12.5 % oxygen, and 3.1 % sulfur). Ether (-$\underline{C}$-O-) linkages constitute the only oxidized carbon groups in untreated polysulfone, whilst oxygen is also present doubly bonded to sulfur. The π–π* shake up intensity accounted for 4.4 ± 0.2% of total C(1s) intensity,

Figure 3.1. A significant level of oxygen incorporation was noted during $O_2$ plasma treatment, Figure 3.2, combined with an attenuation of the $\pi$–$\pi^*$ shake-up satellite intensity to 1.6 ± 0.5 % of the total C(1s) signal. Solvent washing the polysulfone surface removed 73 ± 5 % of the oxygen added by $O_2$ plasma treatment. A large increase in the -C̲-O- group contribution was seen at the expense of the other types of oxidized carbon environments, Figure 3.1, together with an increase in the $\pi$–$\pi^*$ shake-up satellite intensity to 4.0 ± 0.5 % of the total C(1s) signal, almost restoring its original contribution.

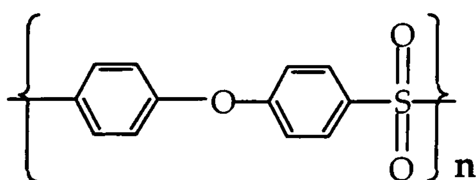


Polyethersulfone (PES)

Polyethersulfone (PES) has a greater oxygen (20 ± 2 %) and sulfur (6 ± 2 %) content compared to its structurally related polysulfone counterpart, since the former contains no dimethyl carbon linkage in its repeat unit. Also, the $\pi$–$\pi^*$ shake-up satellite was found to be more intense for polyethersulfone, Figure 3.1, constituting 5.8 ± 0.2 % of the total C(1s) peak intensity. $O_2$ plasma treatment of polyethersulfone caused a large increase in the oxygen content, Figure 3.2, and complete disappearance of the $\pi$–$\pi^*$ shake-up satellite[20], Figure 3.1. Solvent washing polyethersulfone removed 54 ± 2 % of the oxygen incorporated during $O_2$ plasma treatment, accompanied by the C(1s) envelope reverting back towards the parent polymer spectrum, Figure 3.1, and about two thirds of the original percentage of $\pi$–$\pi^*$ shake-up satellite intensity being recovered. The absolute value of the change in O:C ratio upon solvent washing, Δ(O:C) = -0.25 ± 0.02, is the same for both sulfur containing polymers.

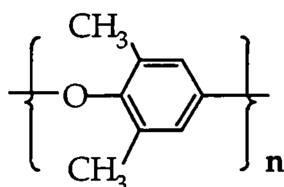


Polydimethylphenyleneoxide (PPO)

Poly(2,6-dimethyl-1,4-phenyleneoxide) (PPO) contains one backbone phenyl ring with two pendant methyl groups and one ether linkage per polymer repeat unit. The C(1s) XPS spectrum comprised 28 ± 2% of carbon atoms in <u>C</u>-O environments, which is consistent with the parent polymer structure, Figure 3.1, and the $\pi$-$\pi^*$ shake-up satellite peak constituted 6.9 ± 0.2% of C(1s) peak area. $O_2$ plasma treatment of PPO produced a large increase in O:C ratio, Figure 3.2, accompanied by an attenuation of the C(1s) $\pi$-$\pi^*$ shake-up signal to about half of its original value, Figure 3.1. A significant proportion (89 ± 2%) of the oxygen added during $O_2$ plasma treatment was lost from the PPO surface during solvent rinsing, leading to the largest change in O:C upon washing. Once again the C(1s) peak shape reverted to being reminiscent of the untreated polymer, Figure 3.1.

### *3.3.2 AFM*

Atomic force micrographs of clean, $O_2$ plasma treated, and solvent washed $O_2$ plasma treated polymers are shown in Figures 3.3, 3.4 and 3.5 respectively. The relatively smooth untreated surfaces were roughened by $O_2$ plasma treatment to produce an even distribution of more or less hemispherical protrusions.

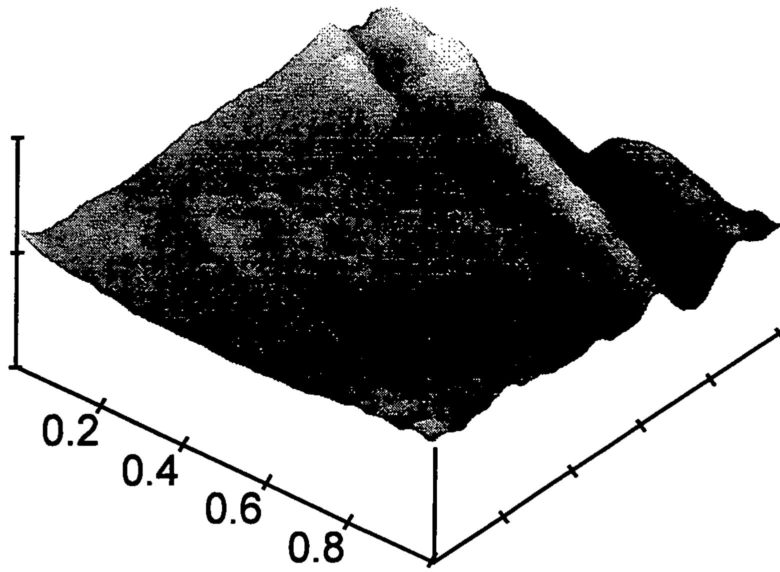


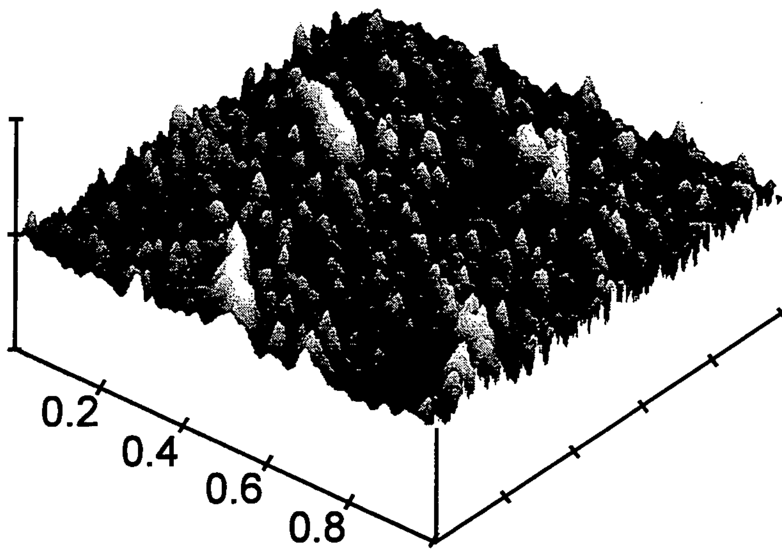


Figure 3.3 Atomic force micrographs of untreated: (a) polystyrene; (b) polyethyleneterephthalate

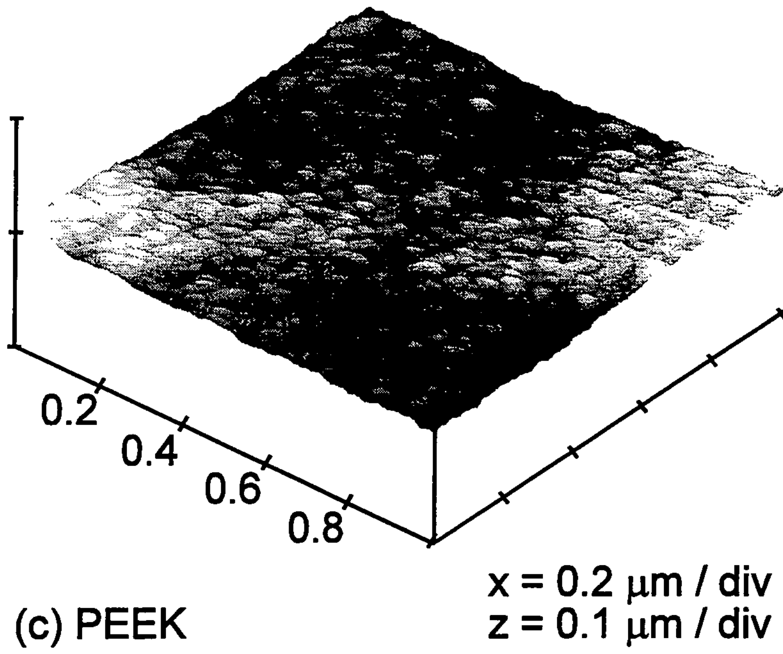


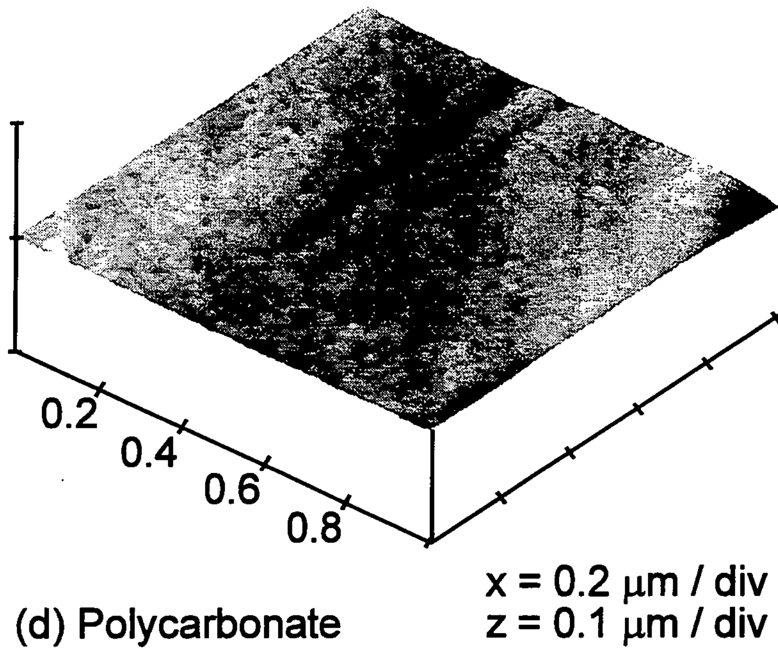


Figure 3.3 Atomic force micrographs of untreated (c) polyetheretherketone; (d) polybisphenolcarbonate

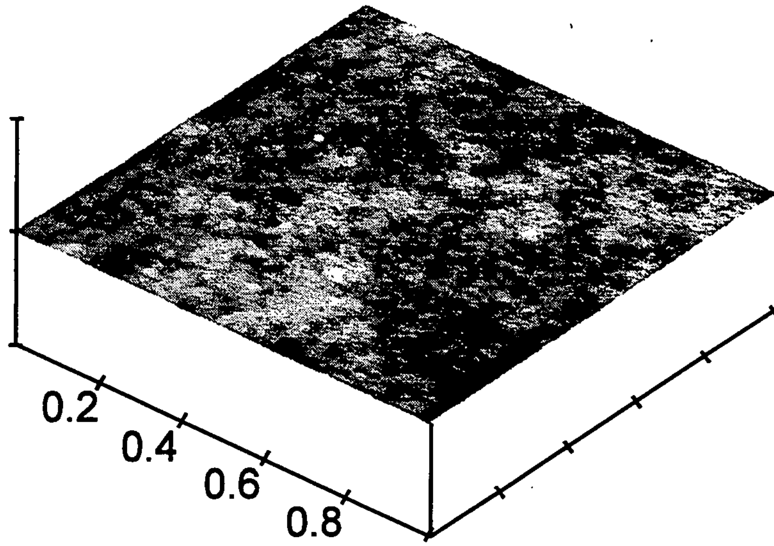


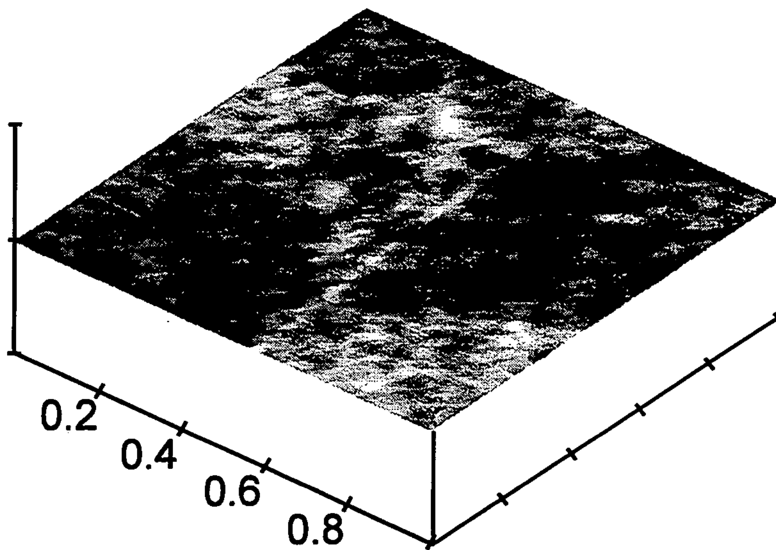


Figure 3.3 Atomic force micrographs of untreated (e) polybisphenolsulfone; (f) polyethersulfone

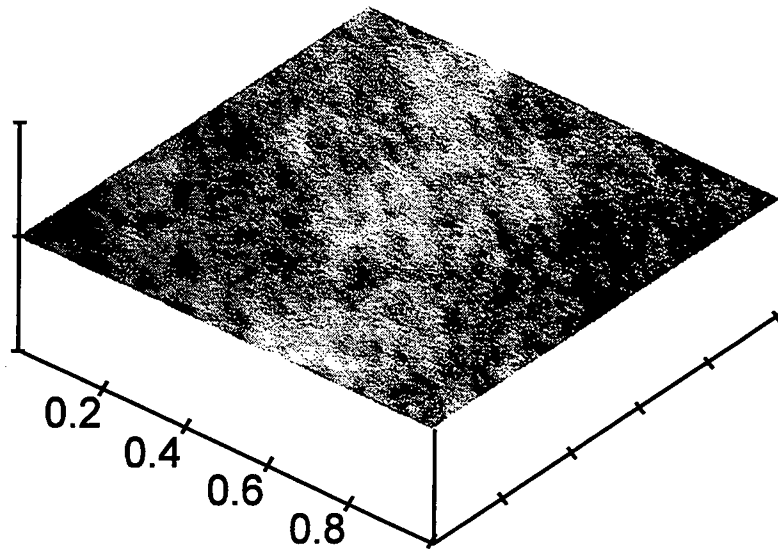


Figure 3.3 Atomic force micrograph of untreated (g) polydimethylphenyleneoxide

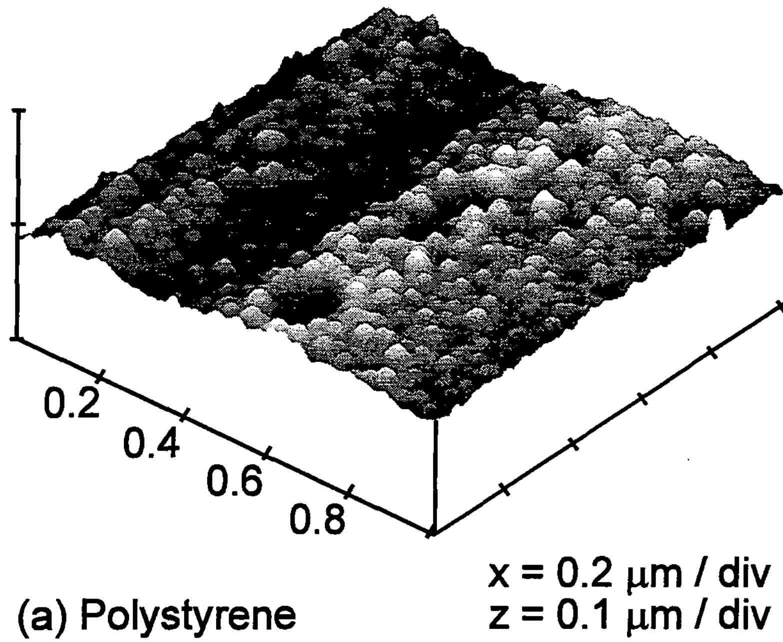


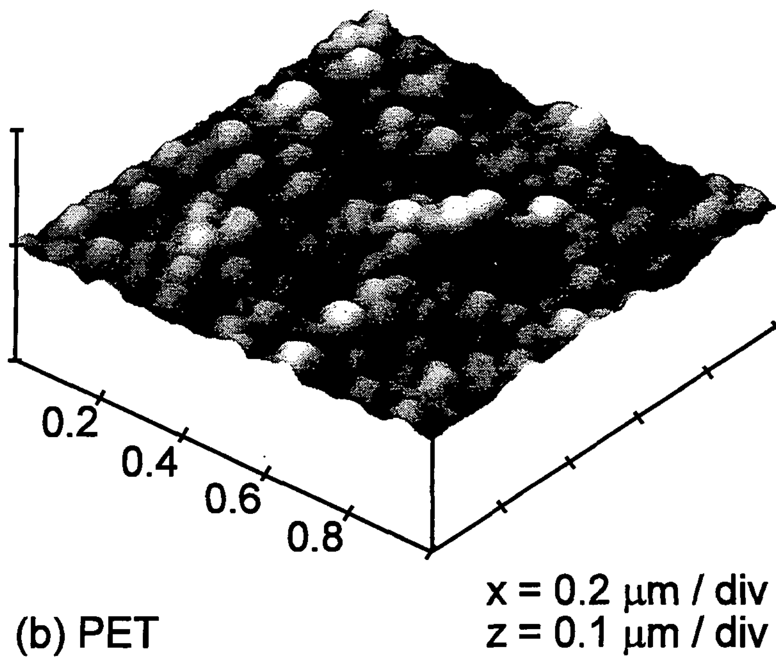


Figure 3.4 Atomic force micrographs of $O_2$ plasma treated: (a) polystyrene; (b) polyethyleneterephthalate

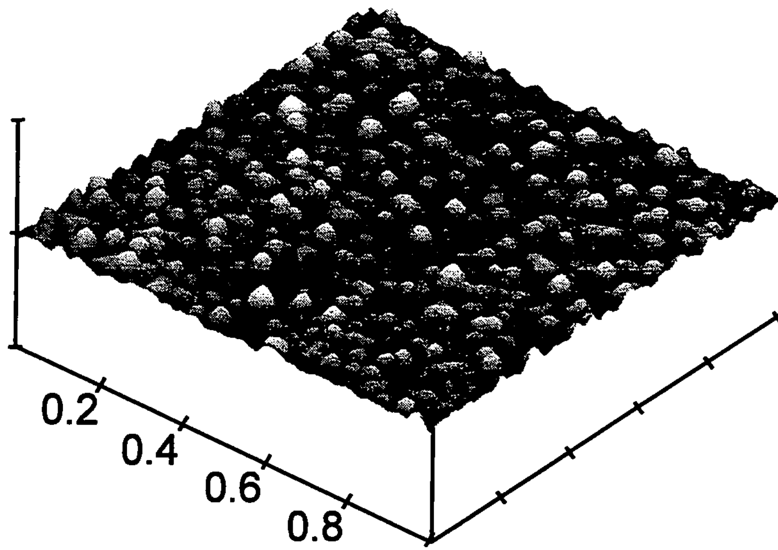


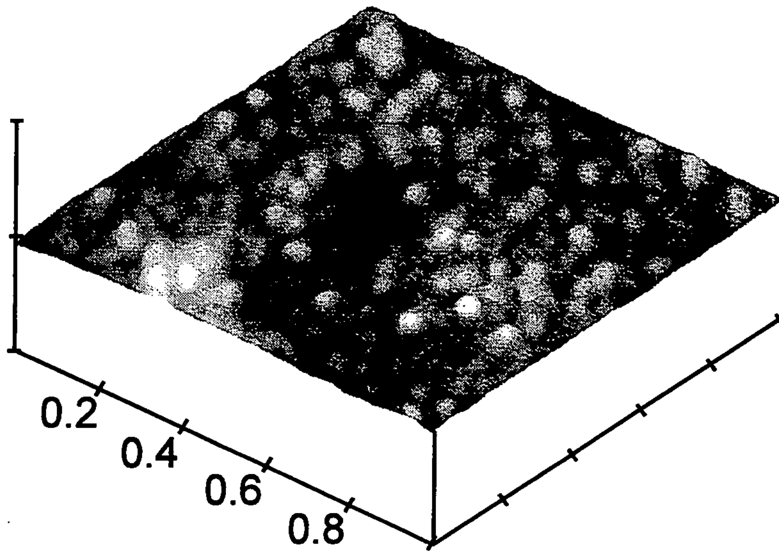


Figure 3.4 Atomic force micrographs of $O_2$ plasma treated: (c) polyetheretherketone; (d) polybisphenolcarbonate

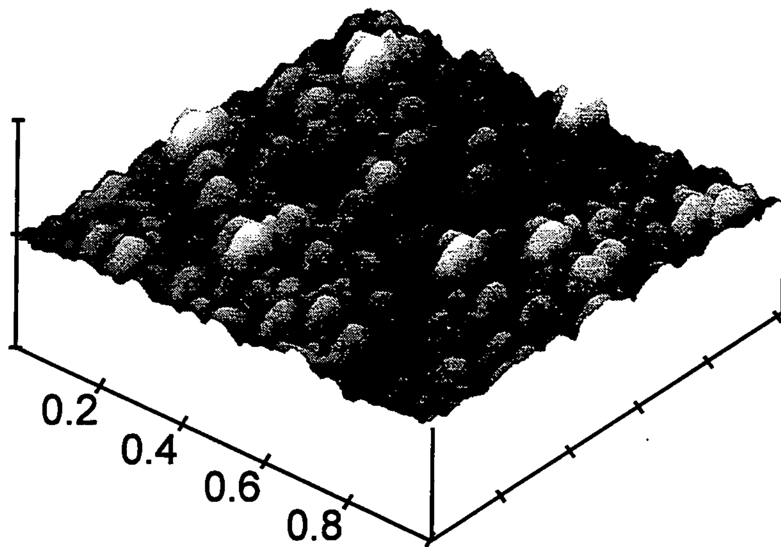


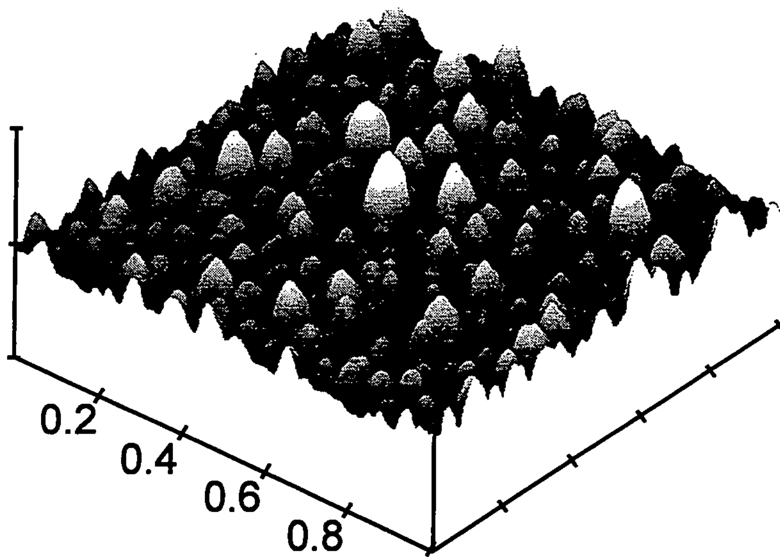


Figure 3.4 Atomic force micrographs of $O_2$ plasma treated: (e) polybisphenolsulfone; (f) polyethersulfone

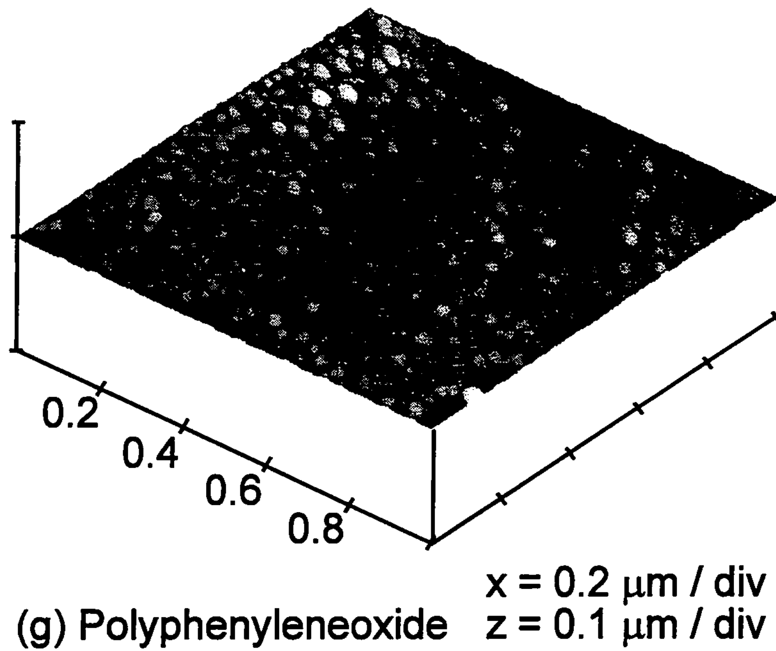


Figure 3.4 Atomic force micrograph of $O_2$ plasma treated: (g) polydimethylphenyleneoxide

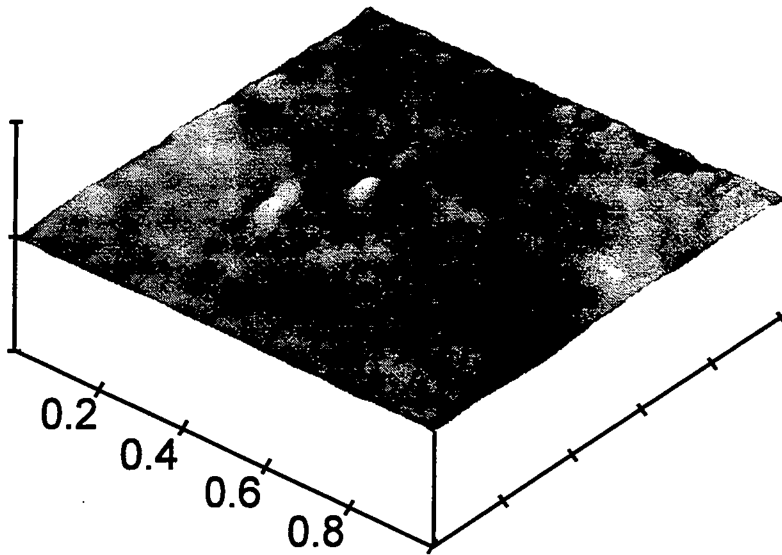


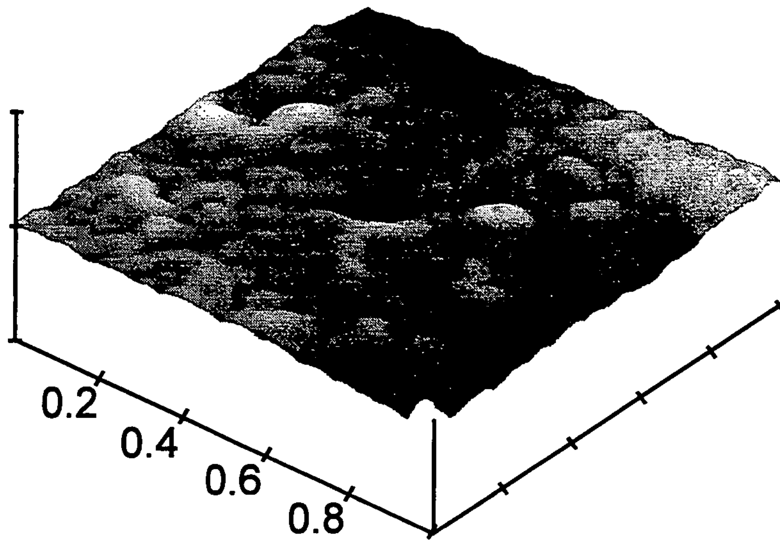


Figure 3.5 Atomic force micrographs of solvent washed $O_2$ plasma treated: (a) polystyrene; (b) polyethyleneterephthalate

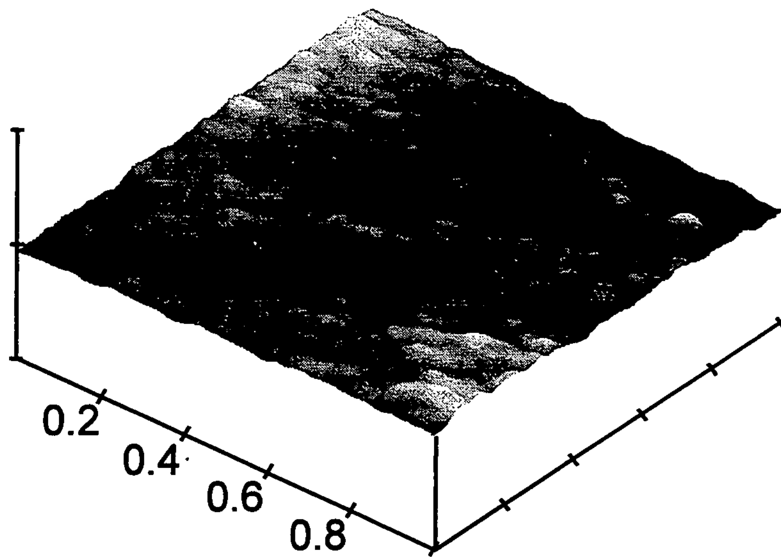


(c) PEEK

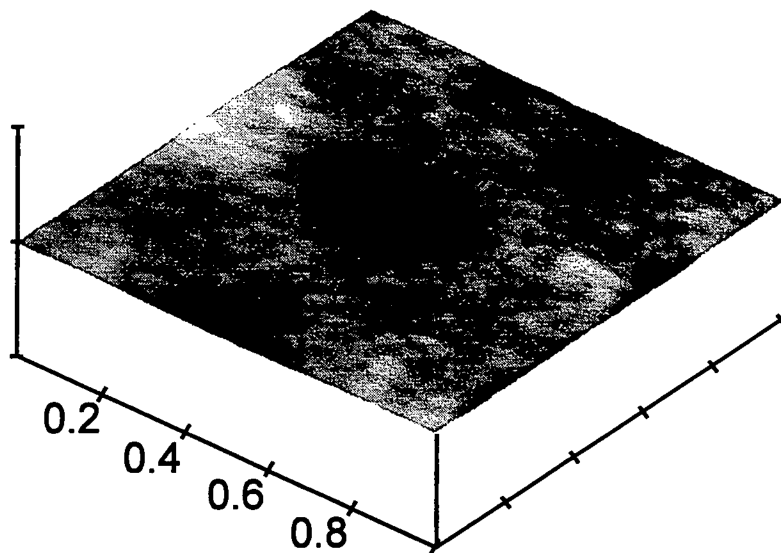


(d) Polycarbonate

Figure 3.5 Atomic force micrographs of solvent washed $O_2$ plasma treated: (c) polyetheretherketone; (d) polybisphenolcarbonate

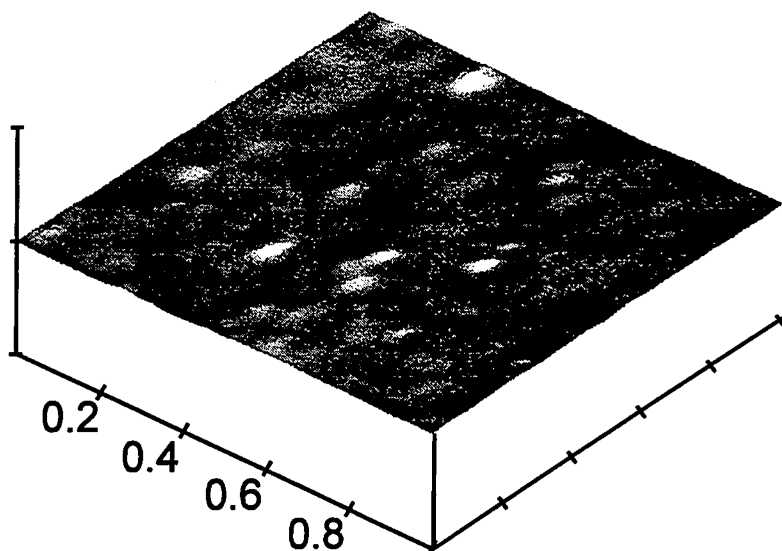


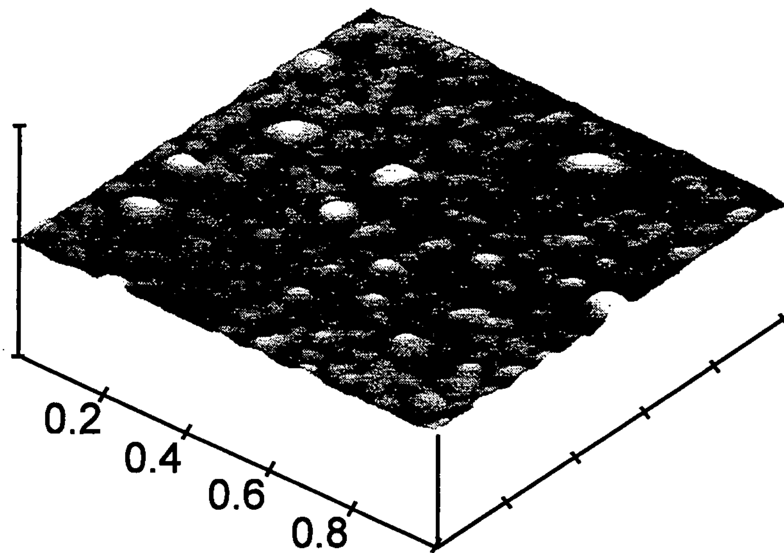


Figure 3.5 Atomic force micrographs of solvent washed $O_2$ plasma treated: (e) polybisphenolsulfone; (f) polyethersulfone

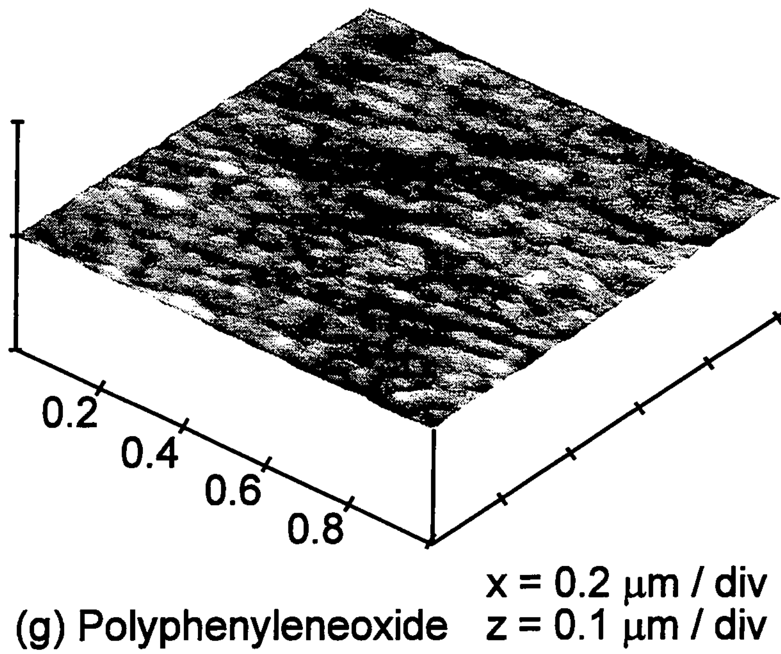


Figure 3.5 Atomic force micrographs of solvent washed $O_2$ plasma treated: (g) polydimethylphenyleneoxide

Polystyrene, PET and PEEK displayed topographical features prior to plasma treatment which were most probably introduced into the surface during film manufacture, Figure 3.3: PET has an even distribution of narrow, non-hemispherical protrusions; PEEK has an array of relatively low height, circular features; and polystyrene has a small number of relatively low height ridges. Following $O_2$ plasma treatment, the surfaces of the plasma treated polymers, Figure 3.4, all showed hemispherical-dome shaped globules whose mean diameter are in the order PET > PSF > PES > PC > PEEK > PS > PPO. The globules on $O_2$ plasma treated polysulfone were found to be irregular in shape[20] compared to those on the other $O_2$ plasma treated polymers. Solvent washing of $O_2$ plasma treated polymer surfaces resulted in a diminishing of the globular features accompanied by an overall smoothing of the surface texture, Figure 3.5.

## 3.4 DISCUSSION

Satellite 'shake-up' lines appear on the high binding energy side of core photoelectron lines for unsaturated systems, due to valence orbital excitations during the ejection of core level photoelectrons[21,22]. The high degree of delocalization in phenyl $\pi$ ring orbital systems yields particularly intense C(1s) $\pi$–$\pi^*$ shake-up structures[23]. A correlation is found between the C(1s) $\pi$–$\pi^*$ shake-up intensity for clean polymers and the proportion of carbon centres located in a phenyl environment for the untreated polymer structure, Figure 3.6. The anomalously high $\pi$–$\pi^*$ shake-up peak observed for polydimethylphenyleneoxide may result from a greater net charge density on the phenyl carbon atoms, due to electron donation into the aromatic ring system from the adjacent methyl groups[24,25].

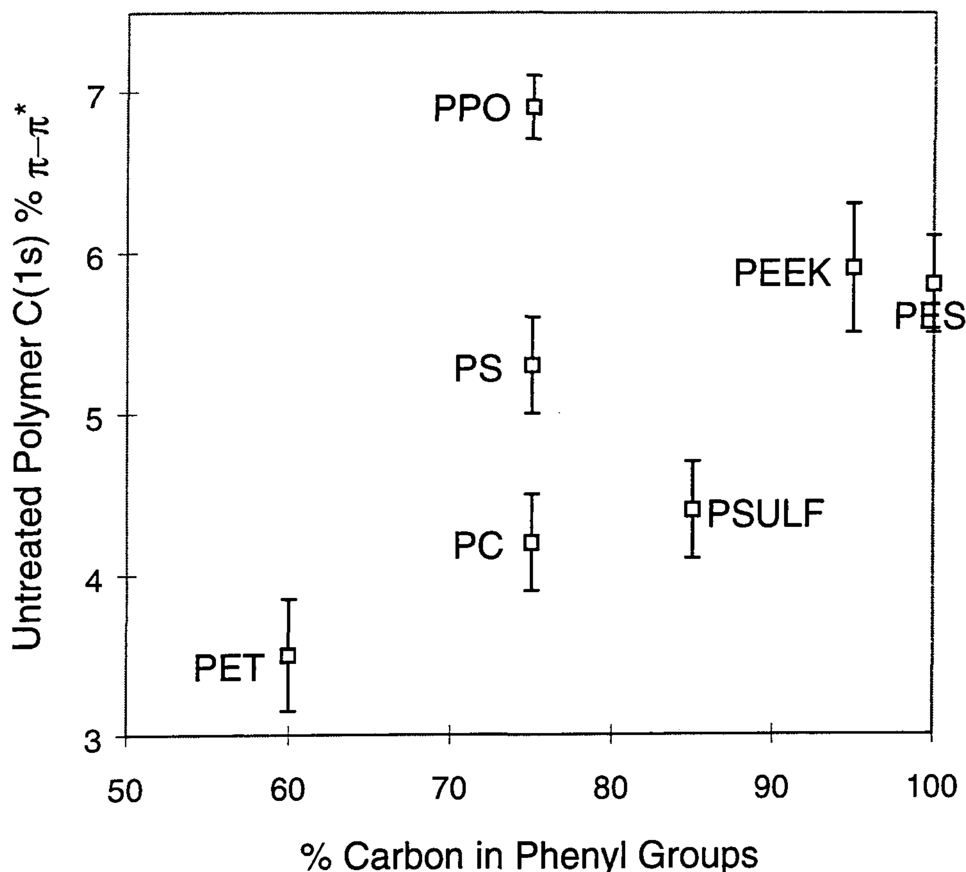


Figure 3.6 Percentage $\pi$–$\pi^*$ shake-up of total XPS C(1s) intensity versus percentage of carbon centres in phenyl environments for untreated polymers.

Substrate-plasma reactivity can be expected to be influenced by the chemical structure[26] and aromaticity[27] of the underlying polymer. Previous extended Huckel molecular orbital calculations have predicted that phenyl containing polymers are more resistant towards oxygen plasma etching compared to saturated polymers, and are therefore more likely to become highly oxygenated during oxygen plasma treatment[28]. Our results have shown that the extent of oxygenation obtained during $O_2$ plasma treatment is directly dependent upon $\pi$–$\pi^*$ shake-up intensity measured in the C(1s) XPS spectrum for the untreated polymer, Figure 3.7.

Low pressure $O_2$ plasmas contain a range of energetic species which are capable of reacting with polymer surfaces: molecular, atomic, and electronically

excited oxygen moieties, in addition to electrons, ions and electromagnetic radiation[29]. Oxygen atoms are mainly produced by collisions of ions, electrons and photons with $O_2$ molecules in the plasma, and are believed to be the prominent reactive species[30]. Since the level of gas ionization[31] is less than 1 in $10^5$ and retarding collisions in the plasma boundary further attenuate the chance of ions reacting with the polymer surface[32], it is probable that a combination of VUV irradiation and oxygen atoms gives rise to most of the observed polymer oxidation.

Electromagnetic radiation generated by the $O_2$ glow discharge includes an intense line at 130 nm[33,34], which can give rise to photo-excitation of π electrons in polymer phenyl rings to anti-bonding π* orbitals[24,35]. Such singly occupied π orbitals are highly susceptible to attack by incident nucleophiles (e.g. atomic oxygen)[32,36]. The ease of π-π* transitions observed by XPS for each untreated polymer can therefore be used as a good measure of polymer reactivity towards an $O_2$ plasma, Figure 3.6. Attenuation of the π–π* shake-up signal during $O_2$ plasma treatment of all of the polymers studied confirms substantial oxidative attack of phenyl groups[37,38].

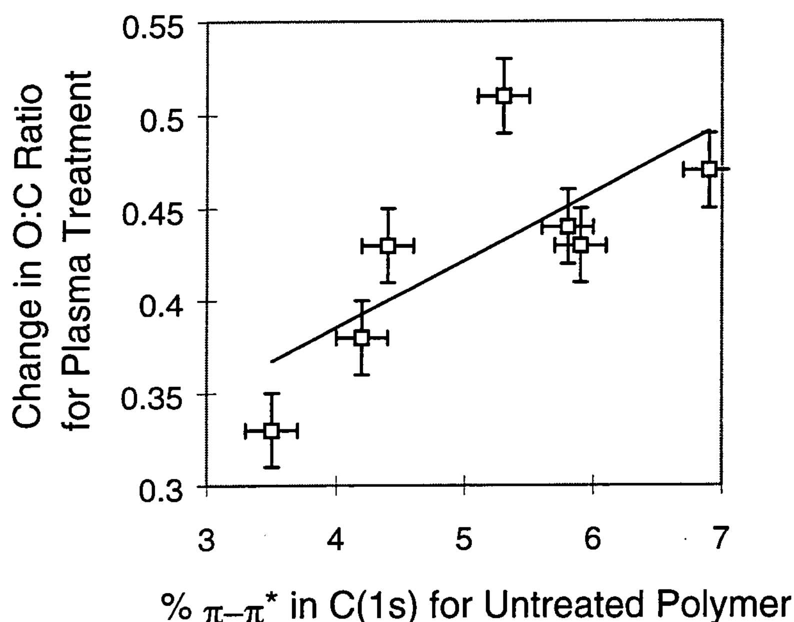


Figure 3.7 Extent of oxidative attack versus percentage π–π* shake-up of total XPS C(1s) intensity for the untreated polymer.

A correlation is evident between the mean diameter of globules, from AFM images, Figure 3.4, and the extent of plasma oxidative attack, Δ(O:C), measured by XPS for each treated polymer, Figure 3.8, suggesting that the degree of oxygenation determines the final surface morphology. The height of globular features (~ 4 nm) ensures that the majority of the XPS signal (sampling depth ~ 2 nm[39]) is measured from the $O_2$ plasma generated surface texture. No trend was established between $O_2$ plasma modified surface topography and parent polymer melting point[40] or glass transition temperature[41]; this confirms that surface physical modification does not occur exclusively via a polymer melting mechanism.

Modification of surface morphology by $O_2$ plasma treatment is reported to be due to vigorous reactions of the polymer with atomic oxygen[42], photon and ion induced physical degradation[42], melting and recrystallization[44], or conglomeration of surface species formed during plasma oxidation and chain scission into globules[44,45]. Conglomeration of plasma oxidized polymer material is driven by minimization of polar surface energy at the interface with the underlying unmodified substrate[46]. The contact angle between functionalized polymeric material and the low energy substrate therefore increases, and the mean diameter of globules decreases, with increasing level of oxygenation[47], Figure 3.8.

The removal of oxidized surface species upon solvent washing of discharge treated polymers has been attributed to solvation of low molecular weight oxidized material formed by electrical discharge treatment[48-50]. The proportion of oxygenated material and globular features which remained on the surface during rinsing in a polar / non-polar solvent mixture must have undergone extensive crosslinking and minimal chain scission[46,50-52].

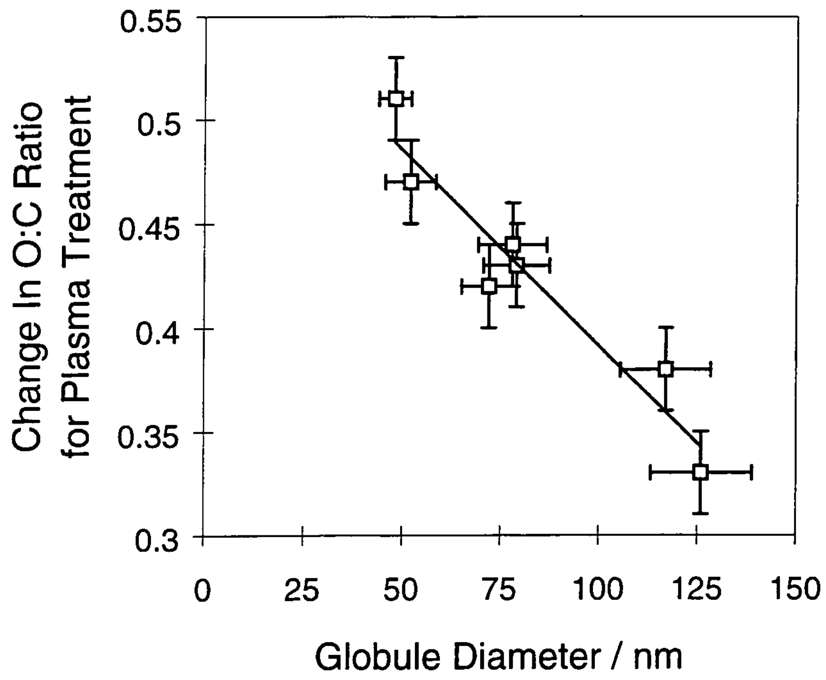


Figure 3.8 Extent of oxidative attack versus mean globule size.

## 3.5 CONCLUSIONS

Initial polymer chemical structure can bear a strong influence upon the level of oxygenation attained during $O_2$ plasma treatment of phenyl containing polymers. The C(1s) $\pi$–$\pi^*$ shake-up intensity measured for the initial polymer is a good measure of its reactivity towards an $O_2$ glow discharge; this can be accounted for in terms of VUV photo-excitation of phenyl rings followed by reaction with plasma generated oxygen atoms.

$O_2$ plasma treatment of phenyl containing polymers forms surface globules, the diameter of which is inversely proportional to the extent of surface oxygenation. This correlation is inkeeping with the conglomeration of oxidized low molecular weight material in order to minimize surface polar energy. Oxidized species and globular features remaining on the plasma treated surface following solvent washing may be attributed to unscissioned phenyl ring oxidation products and crosslinked polymer chains. Oxygen glow discharge treatment of PET gives rise to the most stable oxidized surface whilst plasma modified PPO loses the greatest amount of incorporated oxygen functionalities during solvent washing.

## 3.6 REFERENCES


1. Lanauze, J. A.; Myers, D. L. *J. Appl. Polym. Sci.* **1990**, *40*, 595.
2. Coburn, J. W. *IEEE Trans. Plasma Sci.* **1991**, *19*, 1048.
3. Nakayama, Y.; Soeda, F.; Ishitani, A. *Polym. Eng. & Sci.* **1991**, *31*, 812.
4. Suhr, H. *Plasma Chem. & Plasma Processing* **1989**, *9*, 7S.
5. Nippon Paint KK, Patent No.s JP1315474-A, **1989**, EP-388547-A, **1990**, and US4996076-A, **1991**.
6. Toyo Metallising KK, Patent No.s JP62101428-A, **1987**, JP92020383-B, **1992**.
7. Garby, L.; Chabert, B.; Sage, D.; Soulier, J. P. *Ange. Makro. Chemie* **1995**, *230*, 73.
8. Lianos, L.; Parrat, D.; Hoc, T. Q.; Duc, T. M. *J. Vac. Sci. Tech. A* **1994**, *12*, 2491.
9. Occhiello, E.; Morra, M.; Garbassi, F. *Ange. Makro. Chemie* **1979**, *173*, 183.

10. Wade, W. L.; Mammone, R.J.; Binder M. *J. Appl. Polym. Sci.* **1991**, *43*, 1589.

11. Burrell, H. *"Polymer Handbook"*; 2$^{nd}$ Edition; Brandrup J.; Immergut E. H. Eds.; J. Wiley: New York, **1975**.

12. ASTM E-42.14 STM / AFM subcommittee recommendation for analyzing and reporting surface roughness.

13. Clark, D. T.; Dilks, A.; Peeling, J.; Thomas, H. R. *Trans. Faraday Soc. Faraday Disc.* **1975**, *60*, 183.

14. Clark, D. T.; Dilks, A. *J. Polym. Sci, Polym. Chem Ed.* **1977**, *15*, 15.

15. Tepermeister, I. ; Sawin, H. H. *J. Vac. Sci. & Tech. A* **1992**, *10*, 3149.

16. Clark, D. T.; Feast, J. *Macromolecules C* **1975**, *12*, 191.

17. Triolo, P. M.; Andrade, J. D. *J. Biomed. Mater. Research* **1983**, *17*, 129.

18. Beamson, G.; Briggs, D. *High Resolution XPS of Organic Polymers, The Scienta ESCA300 Database*; J. Wiley and Sons: New York, **1992**.

19. Clark, D. T.; Wilson, R. *J. Polym. Sci, Polym. Chem Ed.* **1987**, *25*, 2643.

20. Hopkins, J.; Badyal, J. P. S. *Macromolecules* **1994**, *27*, 5498.

21. Clark, D. T.; Dilks, A. *J. Polym. Sci: Polym. Chem. Ed.* **1976**, *14*, 533.

22. Clark, D. T.; Thomas, H. R. *J. Polym. Sci: Polym. Chem. Ed.* **1978**, *16*, 791.

23. Keane, M. P.; Naves de Brito, A.; Correia, N.; Svensson, S.; Lunell, S. *Chem Phys.* **1991**, *155*, 379.

24. Flemming, I. *"Frontier Orbitals And Chemical Reactions"*; J. Wiley & Sons: London, **1976**, 80.

25. Sjogren, B.; Svensson, S.; Naves de Brito, A.; Correia, N.; Keane, M. P.; Enkvist, C.; Lunell, S. *J. Chem. Phys.* **1992**, *96*, 6389.

26. Greenwood, O. D.; Boyd, R. D.; Hopkins, J.; Badyal, J. P. S. *J. Adh. Sci. & Tech.* **1995**, *9*, 311.

27. Reed, N. M.; Vickerman, J. C. *"Surface Characterization Of Advanced Polymers"*; Sabbatini, L.; Zambonin, P. G. Eds.; VCH: Weinheim, **1993**, 138.

28. Cain, S. R.; Egitto, F. D.; Emmi, F. *J. Vac. Sci. & Tech.* **1987**, *A5*, 1578.

29. Bell A. T. In *"Techniques and Applications Of Plasma Chemistry"*; Hollahan J.; Bell A. T. Eds.; Wiley: New York, **1974**.

30. McTaggart, F. K. *"Plasma Chemistry In Electrical Discharges"*; Elsevier: Amsterdam **1967**.

31. Grill, A. *"Cold Plasma In Material Fabrication"*; IEEE Press: New York, **1993**, 7.

32. Liston, E. M. *Proc. ISPC-9* **1989**, 3, L7.

33. Hollander, A.; Klemberg-Sapieha, J. E.; Wertheimer, M. R. *Macromolecules* **1994**, *27*, 2893.

34. Clark, D. T.; Dilks, A. *J. Polym. Sci, Polym. Chem. Ed.* **1980**, *18*, 1233.

35. Pearson, R. G. *"Symmetry Rules For Chemical Reactions"*; J. Wiley & Sons: New York, **1976**, Chapter 6.

36. Bellas, M.; Bryce-Smith, D.; Gilbert, A. *Chem. Comm.* **1967**, 263 and 862.

37. Clark, D. T.; Dilks, A. *J. Polym. Sci, Polym. Chem. Ed.* **1979**, *17*, 957.

38. Wells, R. K.; Badyal, J. P. S.; Drummond, I. W.; Robinson, K. S.; Street, F. J. *Polymer* **1993**, *34*, 3611.

39. Roberts, R. F.; Allara, D. L.; Pryde, C. A.; Buchanan, D. N. E.; Hobbins, N. D. *Surf. Interface Anal.* **1980**, *2*, 5.

40. Cowie, J. M. G. *"Polymers: Chemistry and Physics of Modern Materials"*; 2nd Ed.; Blackie: London, **1991**.

41. Lee, W. A.; Rutherford, R. A. in *"Polymer Handbook"*; Ch. III; Brandrup J.; Immergut E. H. Eds.; J. Wiley Sons: New York, **1975**.

42. Yasuda, H. *J. Macromol.Sci., Chem. A* **1976**, *10*, 383.

44. Overney, R. M.; Guntherodt, H.-J.; Hild, S. *J. Appl. Phys.* **1994**, *75*, 1401.

45. Overney, R. M.; Luthi, R.; Haefke, H.; Frommer, J.; Meyer E.; Guntherodt H.-J. *Appl. Surf. Sci.* **1993**, *64*, 197.

46. Occhiello, E.; Morra, M.; Garbassi, F. *Die Angewandte Makromol. Chemie* **1989**, *173*, 183.

47. Good, R. S. *Contact Angles, Wettability and Adhesion*; Ed. Mittal K. L.; VSP: Utrecht, **1993**.

48. Pawson, D. J.; Ameen, A. P.; Short, R. D.; Denison, P.; Jones, F. R. *Surf. & Interface Anal.* **1992**, *18*, 13.

49. Strobel, M.; Dunatov, C.; Strobel, J. M.; Perron, S. J.; Morgen, M. C. *J. Adh. Sci. Tech.* **1989**, *3*, 321.

50. Xiao, G. Z. *J. Mater. Sci.* **1995**, *14*, 761.

51. Liston, E. M.; Martinu, L.; Wertheimer, M. *J. Adh. Sci. & Tech.* **1993**, *7*, 1091.

52. Clark, D.; Wilson, R. *J. Polym. Sci. A Polym. Chem.* **1987**, *25*, 2643.

# Chapter Four : Plasma Modification Of Zirconium Butoxide Films

---

## 4.1 INTRODUCTION

Zirconium oxide ($ZrO_2$) ceramic thin films are presently used as hard wearing coatings[1], thermal barrier films[2], catalysts and catalyst supports[3,4], buffer layers for high $T_c$ superconducting films[5] and in electronics as an inert, ion impermeable material of high dielectric constant[6]. Although dense $ZrO_2$ is impervious to $O_2$ at temperatures below 500 °C[7], its potential for gas barrier coatings on polymers has not been investigated.

Common methods of producing $ZrO_2$ thin films include spray pyrolysis[8], PVD[9], CVD[10] and sol-gel[11] processing of ceramic precursors. From the numerous possible organo-zirconium precursors, zirconium butoxide ($Zr(OBu)_4$), Figure 4.1, is often chosen for a number of reasons: the compound may easily be highly purified by distillation[12]; $Zr(OBu)_4$ is non-corrosive and may be stored indefinitely out of water contact[12]; $Zr(OBu)_4$ readily produces $ZrO_2$ by hydrolysis and thermolysis[13]; and zirconium is already directly bonded to excess oxygen, promoting oxide nuclei formation[14].

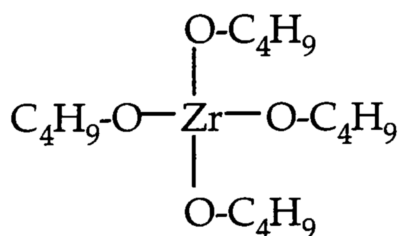


Figure 4.1 Structure of zirconium butoxide, $Zr(OBu)_4$.

In addition to its good oxide forming ability, $Zr(OBu)_4$ forms coordinatively bridged polymeric molecules in solution[13,15], Figure 4.2. The structure and degree of polymerization of transition metal normal alkoxides has

been extensively researched[13,15,16-18]; D. C. Bradley et. al. suggested a pentameric structure for $Zr(OBu^n)_4$ in which zirconium atoms are surrounded octahedrally by oxygen atoms, and five octahedra share edges or faces[16]. $Zr(OBu)_4$ films are deposited from solution containing polymeric ceramic precursor molecules, and these films are expected to cover substrates more completely than disperse monomeric centres.

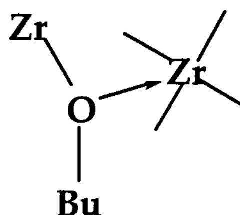


Figure 4.2 Coordinate bond responsible for polymerization in zirconium butoxide[15].

Surface treatment of $Zr(OBu)_4$ solid films in low pressure non-isothermal plasmas is a novel low temperature alternative to conventional sol-gel calcination of ceramic precursors. Such a process would allow temperature sensitive substrates, such as organic polymers, to be coated with ceramic gas barrier film.

The surface physico-chemistry of spin coated films of $Zr(OBu)_4$ treated in oxygen containing plasmas has been investigated, and the resultant coated PET substrate has been assessed for use as a gas barrier film.

## 4.2 EXPERIMENTAL

### *4.2.1 $Zr(OBu)_4$ Solution Preparation*

Commercially supplied 80% weight/volume butanol solution of zirconium-normal-butoxide $Zr(OBu)_4$ (Aldrich, 99.99% purity), stored under dry nitrogen (< 5 ppm $H_2O$), was diluted to 2% weight/volume concentration with propan-1-ol (analytical reagent grade, Aldrich). Each solution batch was used

within 8 hours of air contact, to limit the extent of atmospheric hydrolysis of $Zr(OBu)_4$.

### 4.2.2 Substrate Preparation

Glass slides were employed as an initial substrate on which to study plasma modification of $Zr(OBu)_4$ without the complication of plasma-polymer interactions present for the gas barrier coated PET film. 0.5 mm thick boro-silicate glass (Corning), was cut into 7 mm x 12 mm slides and cleaned in detergent followed by ultrasonically cleaning in a 1:1 ratio mixture of acetone and propan-1-ol solvents (both analytical reagent grade, Aldrich) for 10 minutes.

Additive free polyethyleneterephthalate (PET, ICI) film, of 100μm thickness, was cut into 10mm x 70 mm strips and ultrasonically cleaned in a 1:1 ratio mixture of acetone and propan-1-ol solvents (analytical grade, Aldrich) for 30 seconds.

Initial XPS results for spin coated $Zr(OBu)_4$ on as-cleaned PET substrates and on silent discharge treated PET substrates indicated a larger $Zr(OBu)_4$ coverage for the latter, therefore, each PET substrate was treated for 30 seconds in the silent discharge cell as described in section 2.2, Figure 2.3, using an inter-electrode distance of 3.0 mm and an applied peak-to-peak voltage of 11 kV at 3 kHz[19].

### 4.2.3 Spin Coating $Zr(OBu)_4$ Solution

Cleaned substrates were mounted on a glass plate using double sided adhesive tape and the plate was held on the vacuum chuck of a commercial spin coater (Cammax). A jet of dry nitrogen was blown over the substrate to remove any particulate contamination, and 4 drops of $Zr(OBu)_4$ solution were dropped from a distance of about 1 cm onto the centre of the stationary substrate from a clean glass pipette. Immediately after application of the $Zr(OBu)_4$ solution, the substrate was rotated at 1800 rpm (minimum speed and acceleration settings) for 30 seconds, under a jet of dry nitrogen jet to aid solvent evaporation[20].

### *4.2.4 Plasma Treatments Of Spin Coated Films*

Silent discharge treatment of substrates spin coated with $Zr(OBu)_4$ was carried out in air in the home-built parallel-plate reactor, described in section 2.1, for 30 seconds, using an inter-electrode distance of 3 mm and an applied peak-to-peak voltage of 8.6 kV at 3 kHz frequency.

For low pressure plasma treatments, a substrate was placed in the cylindrical glass reactor, described in section 2.2, immediately after spin coating with $Zr(OBu)_4$ solution, and pumped down to a pressure of $\leq 5 \times 10^{-3}$ torr. The reactor was purged for 10 minutes with the processing gas at a pressure of $2 \times 10^{-1}$ torr. The processing gas was either oxygen (99.6% purity, BOC) or water vapour from a monomer tube containing de-ionized water which had been frozen and thawed three times at base pressure to remove dissolved impurity gases. The power and duration of inductively coupled RF discharge treatment of the coating were systematically varied to investigate the roles of these parameters in modification of the precursor surface. Following plasma treatment, the chamber was purged with the processing gas for 5 minutes and then vented to atmospheric pressure.

### *4.2.5 Analysis Of Coatings*

Immediately after coating or treatment, surface chemical analysis was performed using XPS, as described in section 2.2. Sensitivity factors for unit stoichiometry were determined for the core levels C(1s) : Zr(3d) to be 1 : 0.16, using zirconium (IV) oxide powder (Aldrich); for C(1s) : Si(2p) to be 1 : 1.02 using zirconium (IV) silicate powder (Aldrich); and for the core levels C(1s) : O(1s) to be 1.00 : 0.62 using additive free polyethyleneterephthalate film (ICI).

Linear background intensity removal of XPS data was employed, which used consistently gives proportional results for all peaks from insulating materials[21]. A least squares linear regression routine[22] was then used to optimize

the width and intensity of gaussian peaks added manually and fixed at binding energies known from the literature.

C(1s) XPS core level spectra were fitted with peaks for carbon bound to carbon, hydrogen and oxygen as described in section 2.3, referencing the hydrocarbon peak to 285.0 eV to offset the XPS binding energy scale for sample charging[23]. An additional C(1s) peak for a carbide carbon environment was fitted at 282.1 eV[24]. The asymmetric envelopes of O(1s) spectra were fitted with 3 peaks at binding energies of 530.5 eV, 532.3 eV and 534.2 eV, which was the minimum number of peaks needed to fit the data with Gaussian peaks of equal full-width-at-half-maximum (FWHM).

Zr(3d) core level doublet spectra from untreated $Zr(OBu)_4$ films were fitted with Gaussian peaks at binding energies of 183.0 eV, 2.0 eV wide (FWHM), and 185.4 eV, 2.2 eV wide (FWHM), respectively. The Zr(3d) spectral envelope for treated $Zr(OBu)_4$ films were fitted with two pairs of doublet peaks, each doublet having the same binding energy separation (2.40 eV), widths and intensity ratio ($^5/_2$:$^3/_2$ = 3:2) as the Zr 3d doublet from untreated $Zr(OBu)_4$ films.

FTIR transmission spectra were recorded from freshly pressed KBr disks spin coated with $Zr(OBu)_4$ solution, and from coated KBr disks which had been oxygen plasma treated for 5 minutes at a RF power of 30 W. Attenuated total reflection infrared (ATR-IR) absorption spectra of cleaned PET substrates, $Zr(OBu)_4$ spin coated on PET substrates and plasma treated $Zr(OBu)_4$ coatings on PET substrates were recorded, using the method described in section 2.2.

Spin coated film thickness on glass and PET substrates was estimated by weighing substrates before and after spin coating, using an electronic balance (Mettler). A Tencor Instruments α-step 200 profilometer, with an 11 mg stylus scanned at 10 μm/s, provided cross-section profiles of the edge of spin coated films on glass substrates, having used a glass cover slide attached to the glass substrate as an edge mask.

XPS sputter etch depth profiles were performed in a Vacuum Generators CLAM 100 chamber (base pressure 1 x 10-10 mbar) using an hemispherical electron energy analyser in constant analyzer energy ($E_{pass}$ = 50 eV) mode.

Sputtering was achieved with a cold cathode ion gun operated in $5 \times 10^{-6}$ mbar of argon, accelerating an ion current of 1.5 μA to an energy of 3 keV.

Oxygen, argon and helium gas permeability of uncoated, coated and oxygen plasma treated coated PET films were determined using a laboratory-built mass spectrometric instrument[25,26]. A 1 cm radius disc of polymer sample was clamped between a copper gasket and a stainless steel flange, Figure 4.3. The coated side of the polymer sample was exposed to a pressure of 1000 Torr of the gas permeant to be measured; oxygen, argon or helium (99.6%, 99.995% and 99.999% purity respectively, BOC). The uncoated side of the polymer sample, supported by an electron microscopy grid, was connected to the preparation chamber of a Kratos ES300 spectrometer, which was monitored by an UHV ionization gauge and a computer-interfaced quadrupole mass spectrometer (Vacuum Generators, model SX200). The mass spectrometer signal intensity was calibrated in terms of pressure by admitting into the mass spectrometer chamber $10^{-7}$ Torr of each permeant gas, taking into account ion gauge sensitivity factors[27]. The mean equilibrium partial pressure of a permeant gas was calculated from mean mass spectrometer signal after equilibrium was attained.

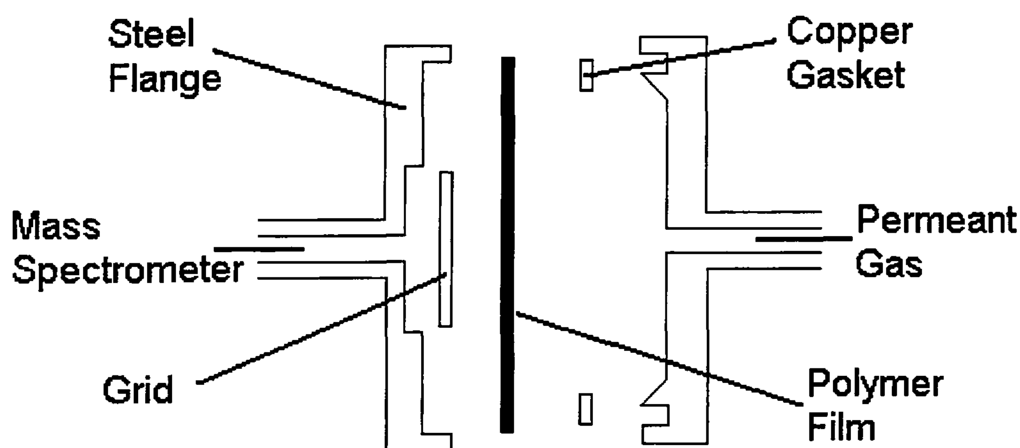


Figure 4.3 Apparatus for mass spectrometric gas permeability measurement[25,26].

The surface topography of oxygen plasma treated $Zr(OBu)_4$ spin coated on SDT PET was characterized by AFM in air, as described in section 2.1, using a Digital Instruments Nanoscope III in Tapping Mode[28].

## 4.3 RESULTS

### *4.3.1 XPS*

#### *4.3.1.1 $Zr(OBu)_4$ Spin Coated On Glass, PET and Silent Discharge Treated PET*

Spin coated films of $Zr(OBu)_4$ on substrates of glass, PET and silent discharge treated (SDT) PET yielded only photoelectron peaks for zirconium, oxygen, and carbon. The Si(2p) spectral region of films on glass showed no photoelectron peak, indicating complete coverage of the glass slide. Good coverage of PET and SDT PET by $Zr(OBu)_4$ was indicated by the C(1s) spectral lineshapes from films on these substrates, Figure 4.4, which resembled the C(1s) shape of $Zr(OBu)_4$ films on glass rather than that of bare PET substrates.

Elemental composition of coating surfaces, calculated from XPS peak areas using instrumentally determined sensitivity factors, indicated a large loss in carbon content from zirconium butoxide molecules during spin coating, Table 4.1. The change in composition is largest in the case of glass substrates and smallest for untreated PET.

| | % Carbon | % Zirconium | % Oxygen |
|---|---|---|---|
| Theoretical $Zr(OBu)_4$ | 76.2 | 4.8 | 19.0 |
| Spin Coated On Glass | 18.8 ± 1.2 | 23.4 ± 0.5 | 57.8 ± 1.2 |
| Spin Coated On PET | 35.0 ± 1.4 | 21.8 ± 0.8 | 43.2 ± 1.3 |
| Spin Coated On SDT PET | 30.2 ± 0.9 | 18.8 ± 0.4 | 51.0 ± 0.7 |

Table 4.1 Surface composition of spin coated $Zr(OBu)_4$ films compared with theoretical $Zr(OBu)_4$ composition.

C(1s) spectra, shown unnormalized due to the low signal to noise of the weak C(1s) counts, Figure 4.4, indicated a predominance of hydrocarbon centres, and the presence of oxidized carbon atoms, in $Zr(OBu)_4$ spin coated film surfaces on all three substrates. Zr(3d) doublet spectra from all three spin coated films, shown normalized to equal height for most intense data point, Figure 4.5, were fitted closely by just two peaks, at 183.0 eV and 185.4 eV, indicating a single oxygen bound zirconium environment to be present at film surfaces. O(1s) spectra, shown normalized to equal height for most intense data point, Figure 4.6, indicated the presence of three oxygen environments, since this was the minimum number of Gaussian peaks of equal width required to closely fit the data. The peaks are inkeeping with the presence of oxygen in the chemical environments: covalently bound to zirconium[24,29,30]; hydroxide and adsorbed water[31,32]; and oxidized carbon species[24,29]. Table 4.2 shows how the proportion of the three oxygen environments differs amongst films spin coated on the three different substrates.

| Assigned Chemical Environment | Zr<u>O</u> | <u>O</u>H/H$_2$<u>O</u> | C$_x$<u>O</u>$_y$ |
|---|---|---|---|
| Binding Energy / eV (± 0.1 eV) | 530.5 | 532.3 | 534.2 |
| $Zr(OBu)_4$ spin coated on glass | 58 % | 39 % | 3 % |
| $Zr(OBu)_4$ spin coated on PET | 53 % | 42 % | 5 % |
| $Zr(OBu)_4$ spin coated on SDT PET | 51 % | 45 % | 4 % |

Table 4.2 O(1s) XP peak positions and area proportions (± 2 %) for $Zr(OBu)_4$ films spin coated on glass, PET and SDT PET.

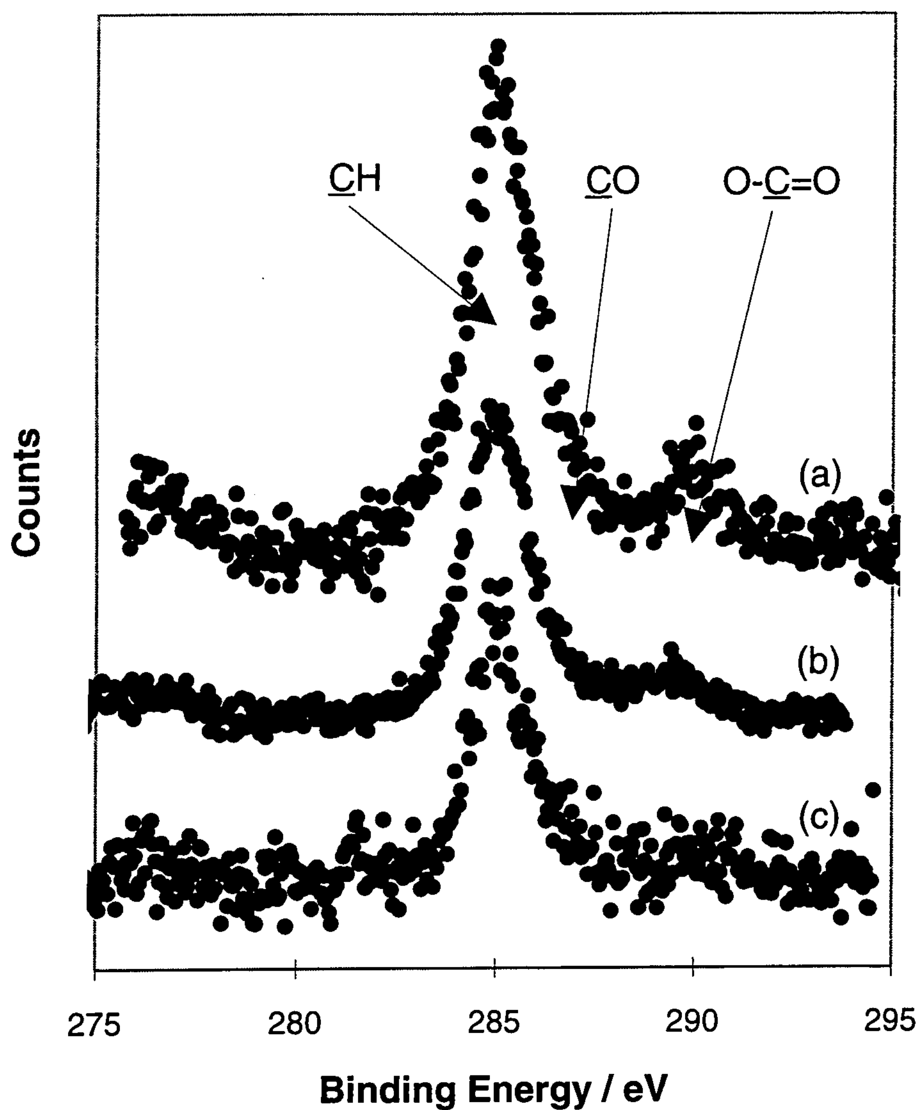


Figure 4.4 C(1s) spectra of $Zr(OBu)_4$ spin coated on: (a) PET; (b) SDT PET; and (c) glass.

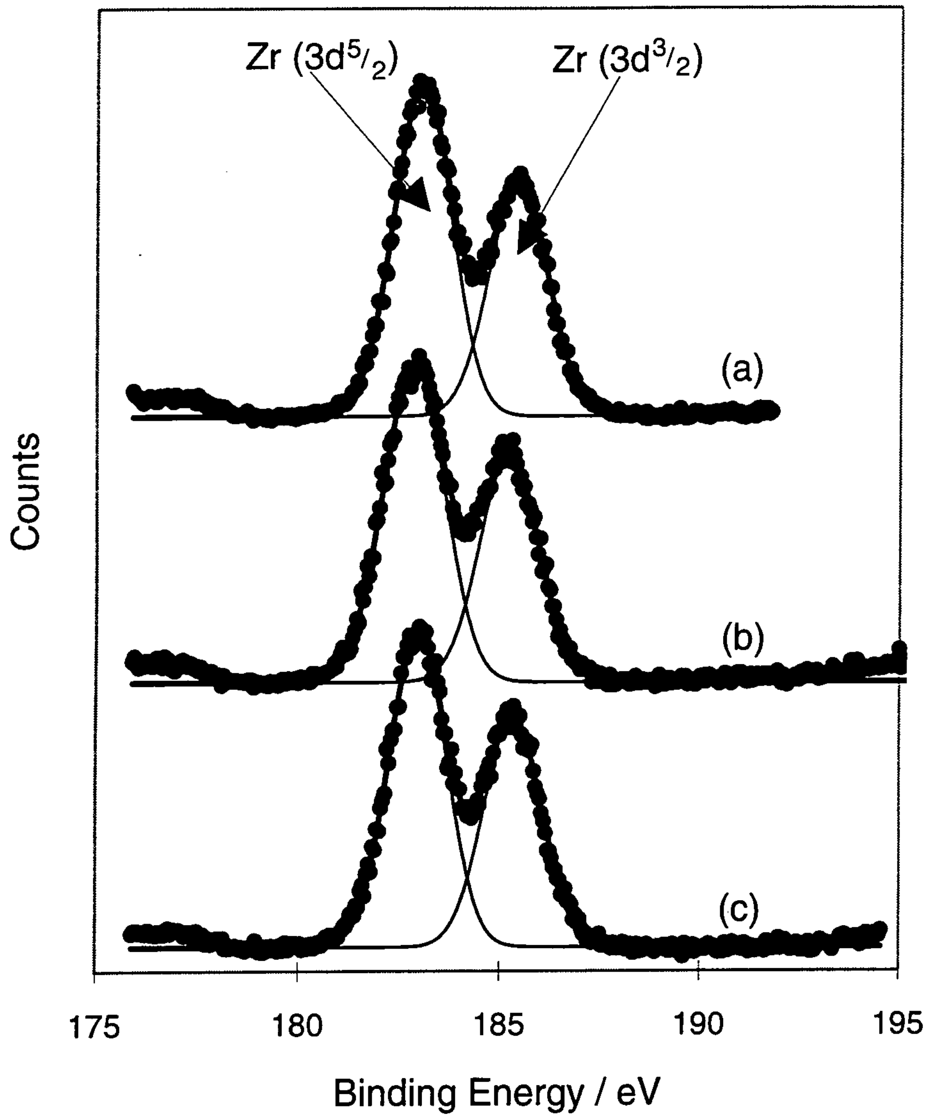


Figure 4.5 Zr(3d) spectra of $Zr(OBu)_4$ spin coated on: (a) PET; (b) SDT PET; and (c) glass.

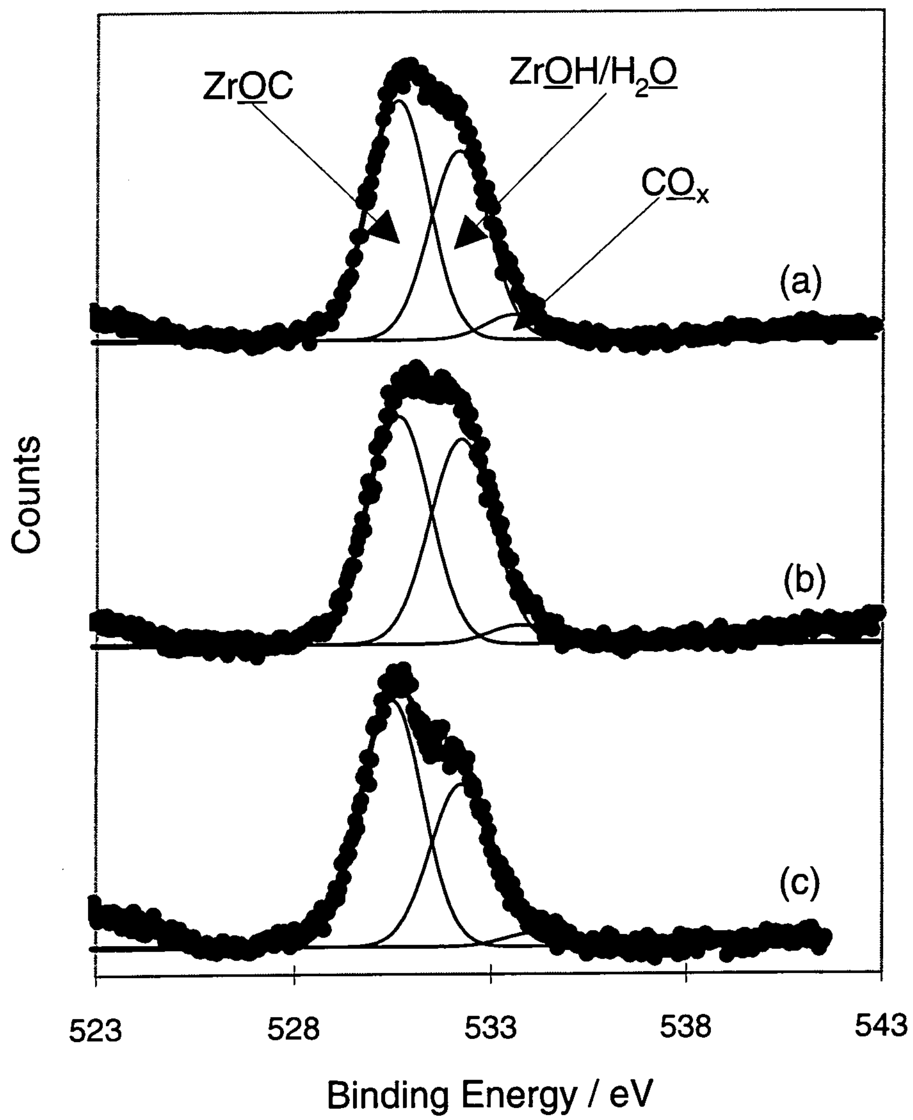


Figure 4.6 O(1s) spectra of $Zr(OBu)_4$ spin coated on: (a) PET; (b) SDT PET; and (c) glass.

*4.3.1.2 Silent Discharge Treated $Zr(OBu)_4$ Spin Coated On Glass Substrates*

XPS analysis revealed that the surface composition of $Zr(OBu)_4$ films spin coated on glass was barely altered by silent discharge treatment in air at a single set of conditions, Table 4.3, and that C(1s), O(1s) and Zr(3d) spectral lineshapes were not significantly modified. The Si(2p) spectral region showed only the background electron count, confirming that underlying glass had not been exposed by silent discharge treatment.

| | % Carbon | % Zirconium | % Oxygen |
|---|---|---|---|
| $Zr(OBu)_4$ / Glass | 19 | 23 | 58 |
| SDT $Zr(OBu)_4$ / Glass | 17 | 20 | 63 |

Table 4.3 Surface composition (± 1.2 %) of untreated and silent discharge treated $Zr(OBu)_4$ spin coated on glass.

*4.3.1.3 Plasma Treated $Zr(OBu)_4$ Spin Coated On Glass Substrates*

Oxygen gas and water vapour non-isothermal plasma treatments of $Zr(OBu)_4$ films spin coated onto glass substrates resulted in decreased surface carbon content, and increased oxygen content, Figure 4.7. An increase in the proportion of carbide carbon centres (C̲-Zr peak at 282 eV) and a decrease in the proportion of hydrocarbon during plasma treatments in both gases is indicated by C(1s) spectra, Figure 4.8. Zr(3d) spectra show that a new, more highly oxidized zirconium environment was created during plasma treatments, Figure 4.9. O(1s) spectra indicate that, of the three oxygen environments present, the lowest binding state was predominant in the surface of untreated films, whereas the middle binding energy environment was most populated in the plasma treated films surface, Figure 4.10.

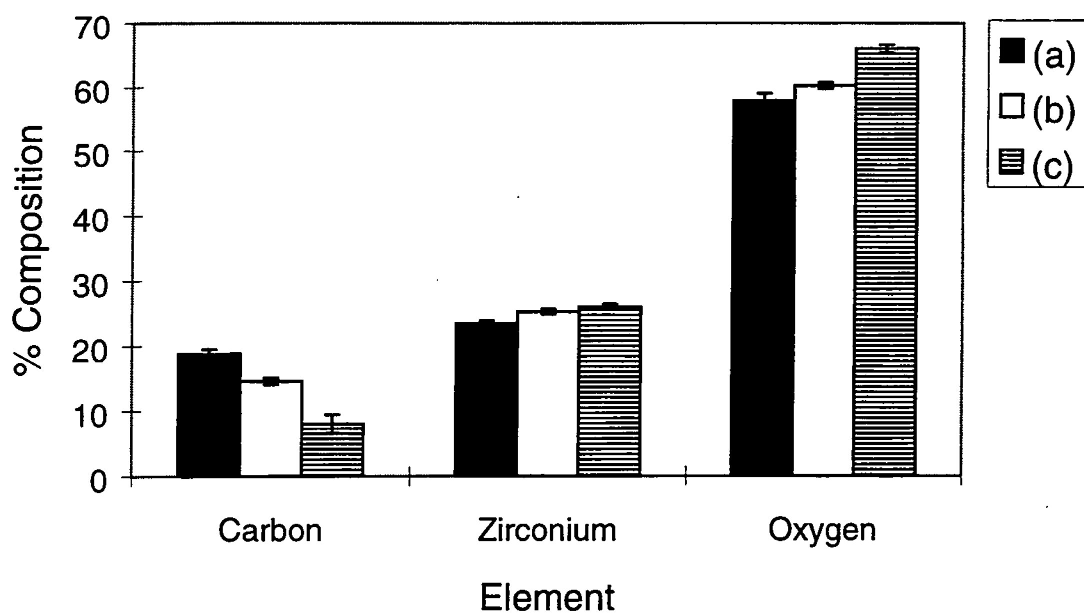


Figure 4.7 Surface composition of $Zr(OBu)_4$ films on glass: (a) untreated; (b) $H_2O$ plasma treated (40 W, 2 min); and (c) $O_2$ plasma treated (60 W, 2 min).

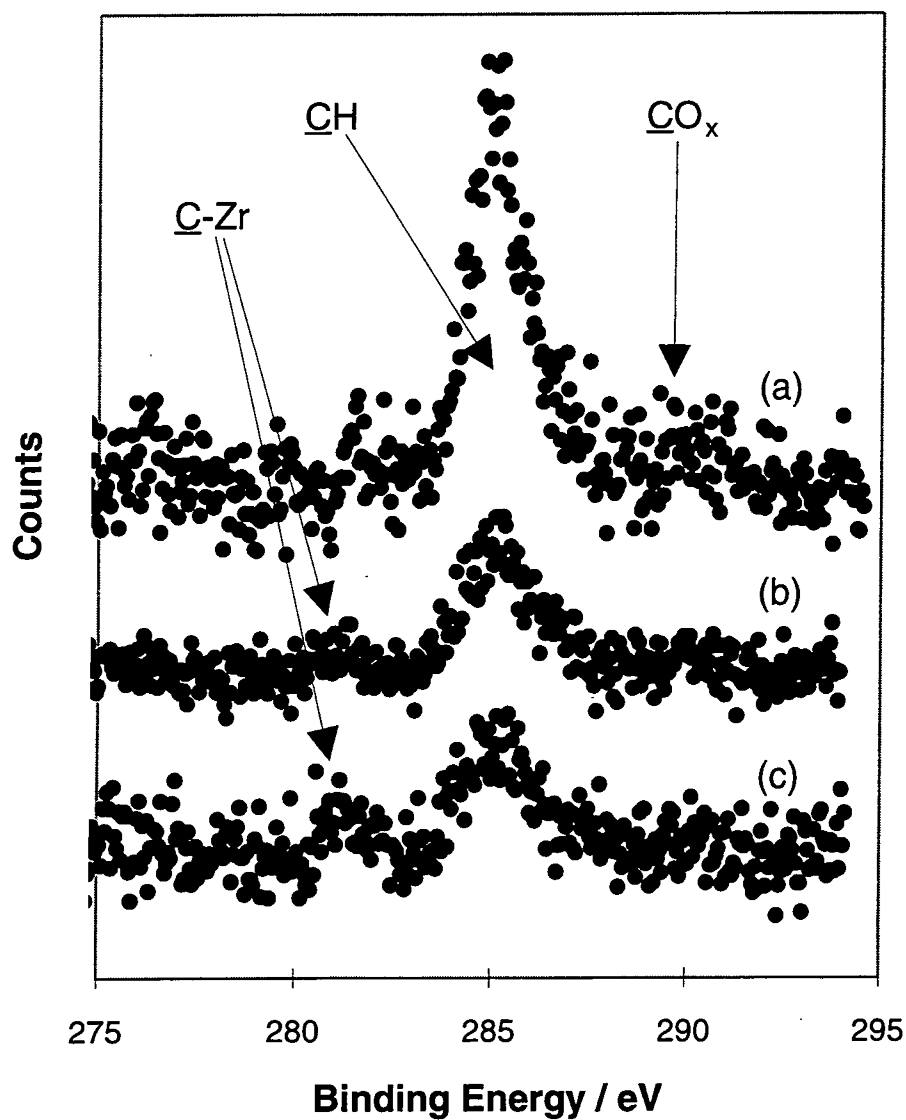


Figure 4.8 C(1s) XP spectra of $Zr(OBu)_4$ films on glass: (a) untreated; (b) $H_2O$ plasma treated (30W, 5 min); and (c) $O_2$ plasma treated (30 W, 5 min).

Figure 4.9 Zr(3d) XP spectra of $Zr(OBu)_4$ films on glass: (a) untreated; (b) $H_2O$ plasma treated (30W, 5 min); and (c) $O_2$ plasma treated (30 W, 5 min).



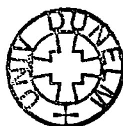

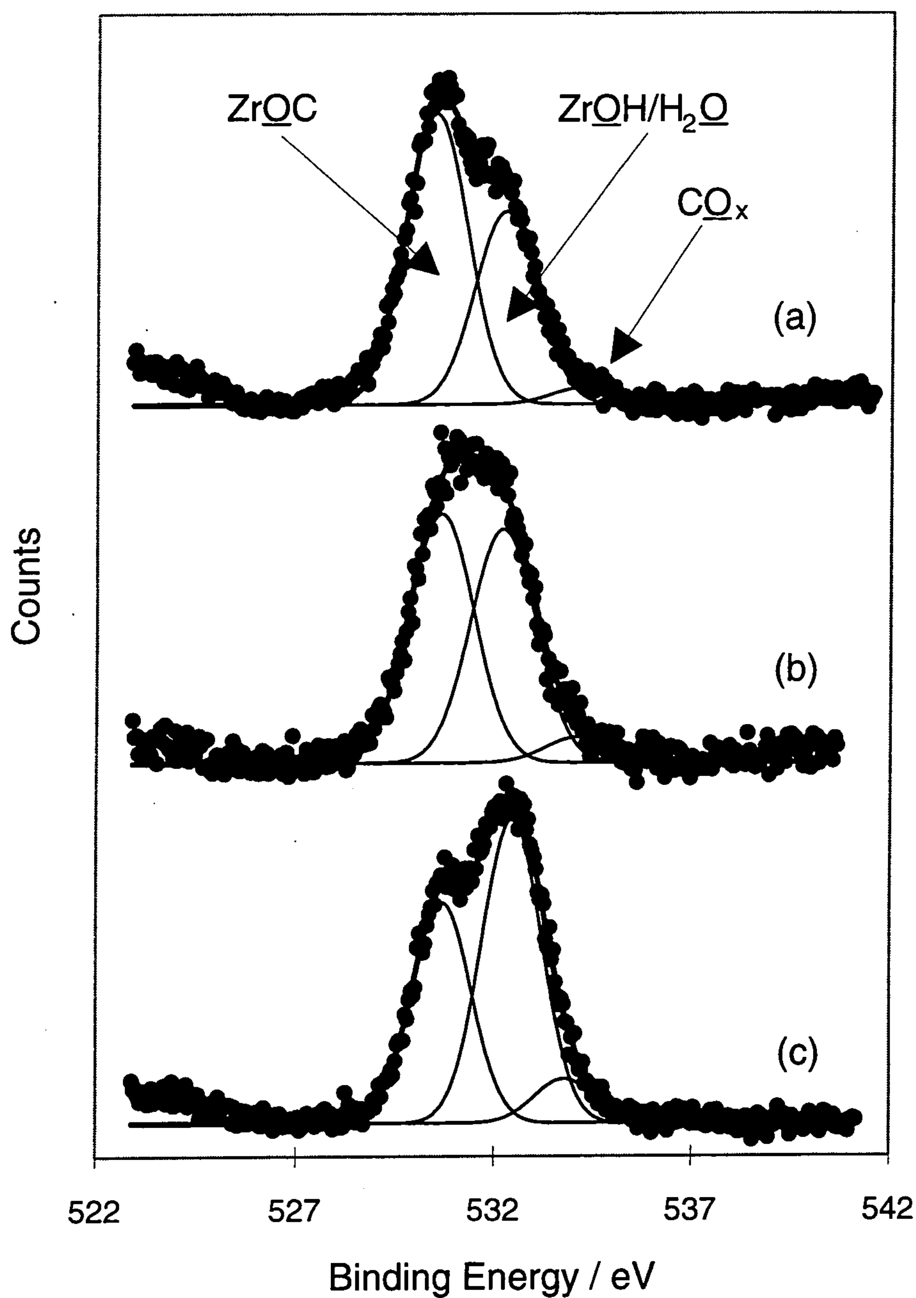


Figure 4.10 O(1s) XP spectra of $Zr(OBu)_4$ films on glass: (a) untreated; (b) $H_2O$ plasma treated (30W, 5 min); and (c) $O_2$ plasma treated (30 W, 5 min).

*4.3.1.4 Oxygen Plasma Power Variation*

The variation of surface elemental composition, Figure 4.11, and C(1s), Zr(3d) and O(1s) XP spectral peakfits, Table 4.4, with oxygen plasma RF power was determined for 2 minute long treatments of $Zr(OBu)_4$ films on glass. Increase in plasma power above 10 W had no additional significant effect on film surface composition, Figure 4.11. However, the proportion of the more highly oxidized zirconium environment (Zr II), the middle binding energy oxygen environment and carbide carbon centres increased with plasma power up to 60 W, Table 4.4.

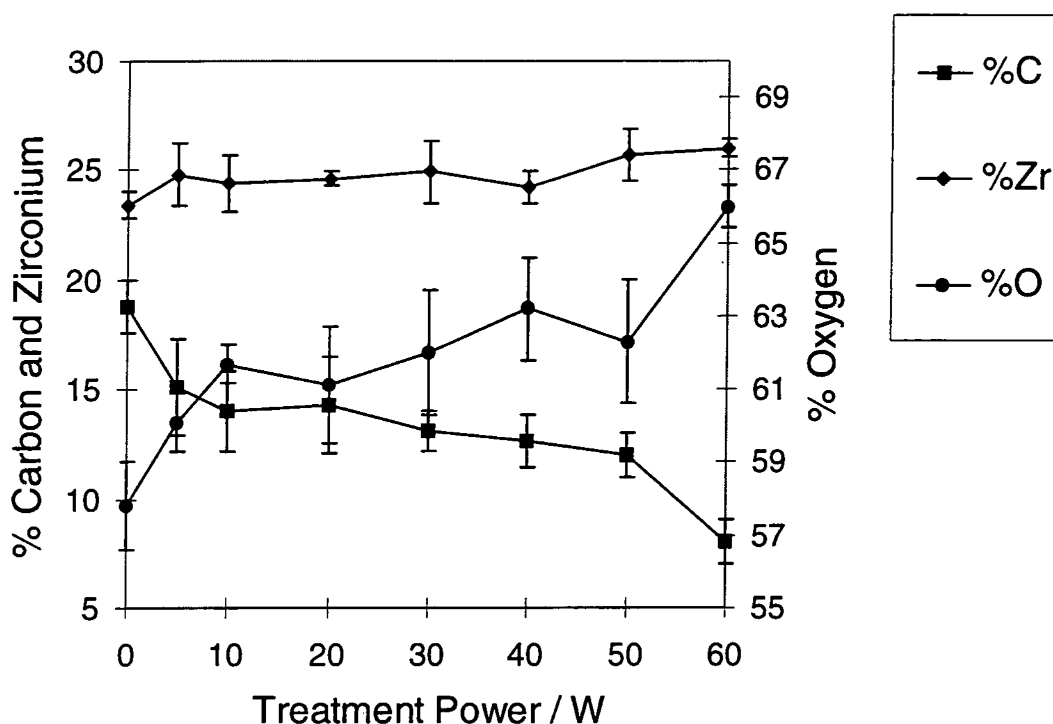


Figure 4.11 Carbon, zirconium and oxygen content of $Zr(OBu)_4$ films on glass versus power of $O_2$ plasma treatment.

| Power / W | % Zr II | % O I | % O II | % O III | % CxHy | % C-Zr |
|---|---|---|---|---|---|---|
| 0 | 0 | 58.3 | 38.4 | 3.3 | 63.7 | 7.3 |
| 5 | 9.5 | 40.3 | 50.9 | 8.7 | 60.0 | 10.2 |
| 10 | 5.8 | 46.0 | 46.1 | 7.9 | 61.7 | 11.2 |

| 20 | 12.9 | 48.1 | 44.1 | 7.8 | 58.1 | 12.7 |
|---|---|---|---|---|---|---|
| 30 | 15.6 | 43.7 | 45.9 | 10.4 | 63.4 | 11.4 |
| 40 | 14.8 | 48.1 | 43.2 | 8.7 | 56.7 | 13.1 |
| 50 | 10.5 | 49.6 | 44.8 | 5.6 | 55.2 | 13.7 |
| 60 | 18.2 | 48.2 | 48.4 | 3.4 | 55.0 | 16.9 |

Table 4.4 Peak fit area proportions (errors ≤ 2 %) of $Zr(OBu)_4$ coated on glass as a function of $O_2$ plasma treatment power.

*4.3.1.5 Oxygen Plasma Duration Variation*

$Zr(OBu)_4$ films on glass were treated in a 30 W $O_2$ plasma for durations up to 10 minutes. XPS analysis showed that the film surface was continuously enriched in oxygen and depleted of carbon between treatment times of about 2 and 8 minutes, Figure 4.12. A maximum of 29.1 % of surface zirconium atoms were modified to the higher binding energy environment after 5 minutes treatment, Table 4.5. Additionally, after 5 minutes treatment, no further increase in the O II peak nor carbide carbon was observed, Table 4.5.

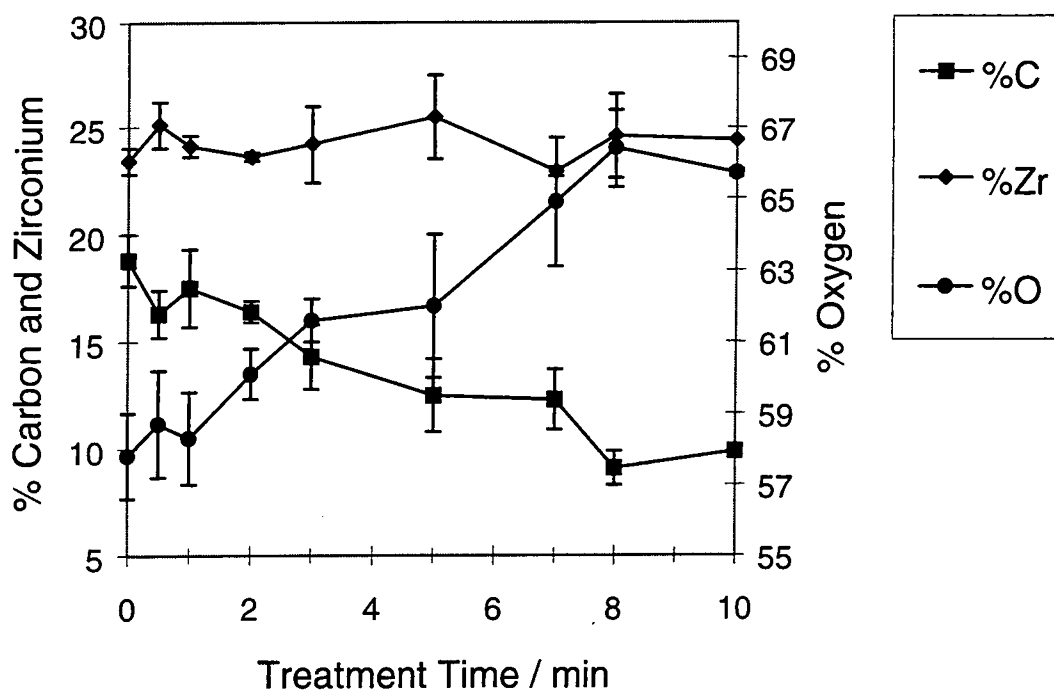


Figure 4.12 Carbon, zirconium and oxygen content of $Zr(OBu)_4$ films on glass versus duration of $O_2$ plasma treatment.

| Duration / min | % Zr II | % O I | % O II | % O III | % CxHy | % C-Zr |
|---|---|---|---|---|---|---|
| 0 | 0 | 58.3 | 38.4 | 3.3 | 63.7 | 7.3 |
| 0.5 | 5.3 | 43.8 | 43.5 | 12.7 | 63.4 | 16.2 |
| 1 | 18.8 | 47.2 | 44.1 | 8.7 | 68.4 | 7.7 |
| 2 | 15.6 | 43.7 | 45.9 | 10.4 | 63.4 | 11.3 |
| 5 | 29.1 | 38.9 | 53.7 | 7.5 | 56.3 | 14.2 |
| 7 | 18.2 | 39.1 | 54.6 | 6.3 | 68.6 | 10.0 |
| 8 | 24 | 37.7 | 54.0 | 8.3 | 66.0 | 15.6 |
| 10 | 18.3 | 40.8 | 50.9 | 8.3 | 59.6 | 14.5 |

Table 4.5 Peak fit area proportions (errors $\leq 2$ %) of $Zr(OBu)_4$ coated on glass as a function of $O_2$ plasma treatment duration.

*4.3.1.6 Water Plasma Power Variation*

$Zr(OBu)_4$ coated glass slides were purged in 0.2 mbar pressure of $H_2O$ vapour for 10 minutes prior to $H_2O$ plasma treatment for 2 minutes at RF powers up to 50 W. XPS analysis showed that the purge in water vapour caused a 5 % increase in surface carbon content and the same decrease in oxygen content, Figure 4.13. Water plasma treatment at 5 W power returned the surface composition to pre-purged values, and carbon content decreased further up to a power of 30 W above which no change was observed, Figure 4.13. The proportion of high binding energy zirconium environments and oxygen atoms giving rise to peak O II reached a maximum at about 20 W water plasma treatment, above which a smaller proportion of these species were detected, Table 4.6.

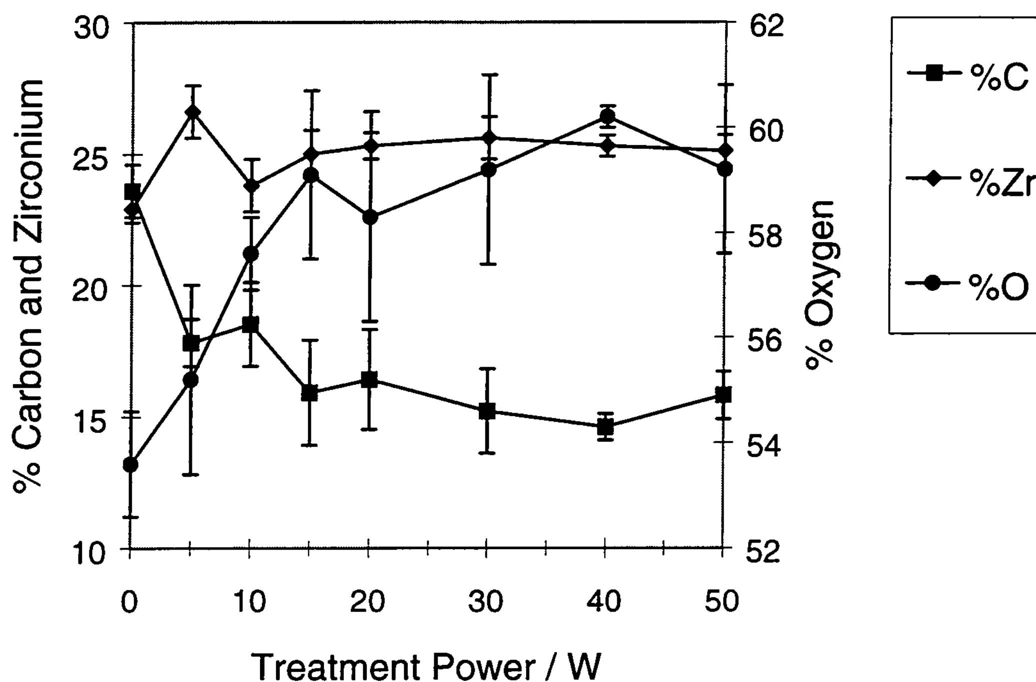


Figure 4.13 Carbon, zirconium and oxygen content of $Zr(OBu)_4$ films on glass versus power of $H_2O$ plasma treatment.

| Power / W | % Zr II | % O I | % O II | % O III | % CxHy | % C-Zr |
|---|---|---|---|---|---|---|
| 0 | 0 | 52.3 | 43.1 | 4.7 | 57.7 | 9.0 |
| 5 | 5.6 | 40.3 | 51.1 | 8.6 | 81.3 | 9.5 |
| 10 | 13.2 | 46.3 | 49.6 | 4.1 | 64.6 | 9.2 |
| 15 | 10.4 | 40.5 | 55.9 | 3.6 | 76.7 | 11.1 |
| 20 | 17.7 | 46.7 | 49.8 | 3.2 | 70.2 | 10.7 |
| 30 | 13 | 50.4 | 45.9 | 3.7 | 66.5 | 10.3 |
| 40 | 15.5 | 48.9 | 42.3 | 3.6 | 68.3 | 10.4 |
| 50 | 11.1 | 51.5 | 44.3 | 4.2 | 63.7 | 9.9 |

Table 4.6 Peak fit area proportions (errors ≤ 2 %) of $Zr(OBu)_4$ coated on glass as a function of $H_2O$ plasma treatment power.

#### *4.3.1.7 Water Plasma Duration Variation*

Following a purge in 0.2 mbar pressure of water vapour for 10 minutes, water plasma treatments of coated glass slides at 30 W power were performed for durations up to 10 minutes. A smoothly varying decrease of carbon content and increase of oxygen content was observed with increasing plasma treatment times up to 3 minutes, after which film surface composition remained unchanged, Figure 4.14. Zr(3d) and O(1s) peak fit area proportions are continuously modified until the longest studied treatment times, Table 4.7.

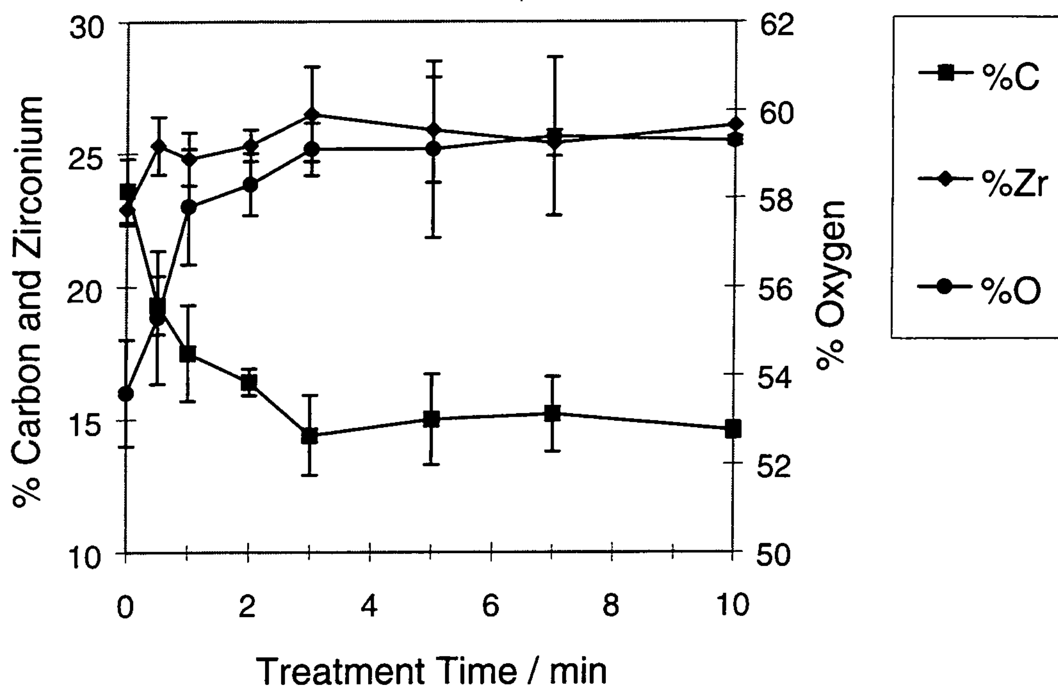


Figure 4.14 Carbon, zirconium and oxygen content of $Zr(OBu)_4$ films on glass versus duration of $H_2O$ plasma treatment.

| Duration / min | % Zr II | % O I | % O II | % O III | % CxHy | % C-Zr |
|---|---|---|---|---|---|---|
| 0 | 0 | 52.3 | 43.1 | 4.7 | 57.7 | 9.0 |
| 0.5 | 7.7 | 47.6 | 48.9 | 3.5 | 67.8 | 8.7 |
| 1 | 6.3 | 45.5 | 51.0 | 3.6 | 64.9 | 13.2 |
| 2 | 13 | 50.4 | 45.9 | 3.7 | 66.5 | 10.3 |
| 3 | 9 | 44.2 | 50.5 | 5.2 | 75.1 | 11.2 |
| 5 | 22.2 | 49.1 | 46.0 | 4.9 | 76.5 | 17.1 |
| 7 | 13.8 | 35.2 | 58.0 | 6.8 | 79.0 | 19.4 |
| 10 | 21.9 | 38.0 | 55.4 | 6.7 | 75.2 | 18.2 |

Table 4.7 Peak fit area proportions (errors ≤ 2 %) of $Zr(OBu)_4$ coated on glass as a function of $O_2$ plasma treatment duration.

*4.3.1.8 Plasma Treated $Zr(OBu)_4$ Spin Coated On PET Substrates*

Silent discharge treated PET was used as a substrate to investigate the effect of oxygen and water plasma treatments of $Zr(OBu)_4$ films spin coated onto PET film. As observed for plasma treatments of films spin coated on glass, surface content of carbon was decreased and that of oxygen was increased by plasma treatment, Figure 4.15; Zr(3d) spectra showed a new more highly oxidized chemical environment, Figure 4.17; and O(1s) spectra, Figure 4.18, showed that the chemical environment of oxygen atoms altered in favour of middle binding energy sites.

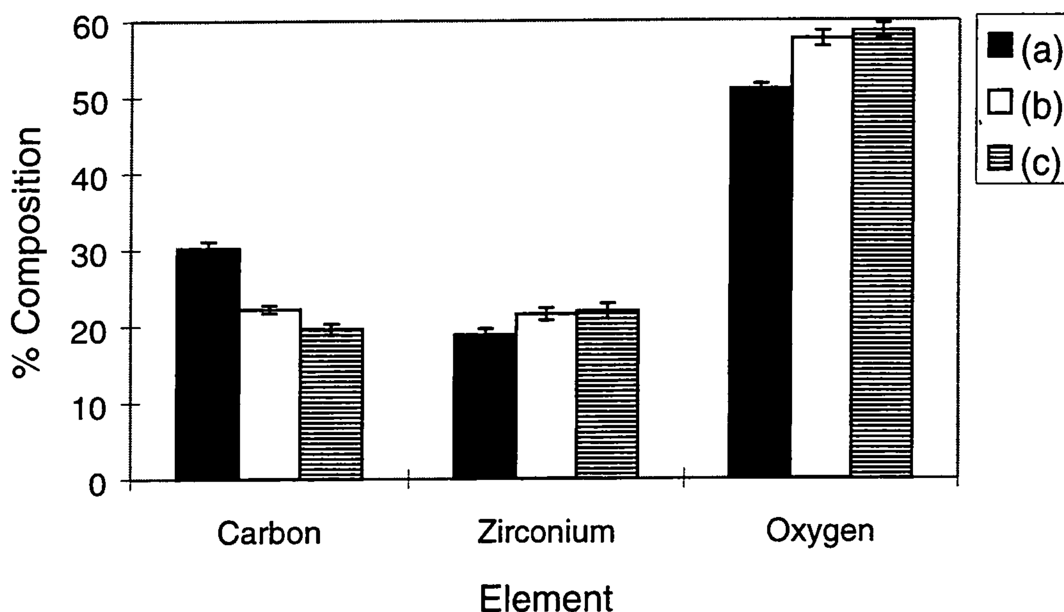


Figure 4.15 Surface composition of $Zr(OBu)_4$ films on SDT PET: (a) untreated; (b) $H_2O$ plasma treated (50W, 2 min); and (c) $O_2$ plasma treated (2 W, 2 min).

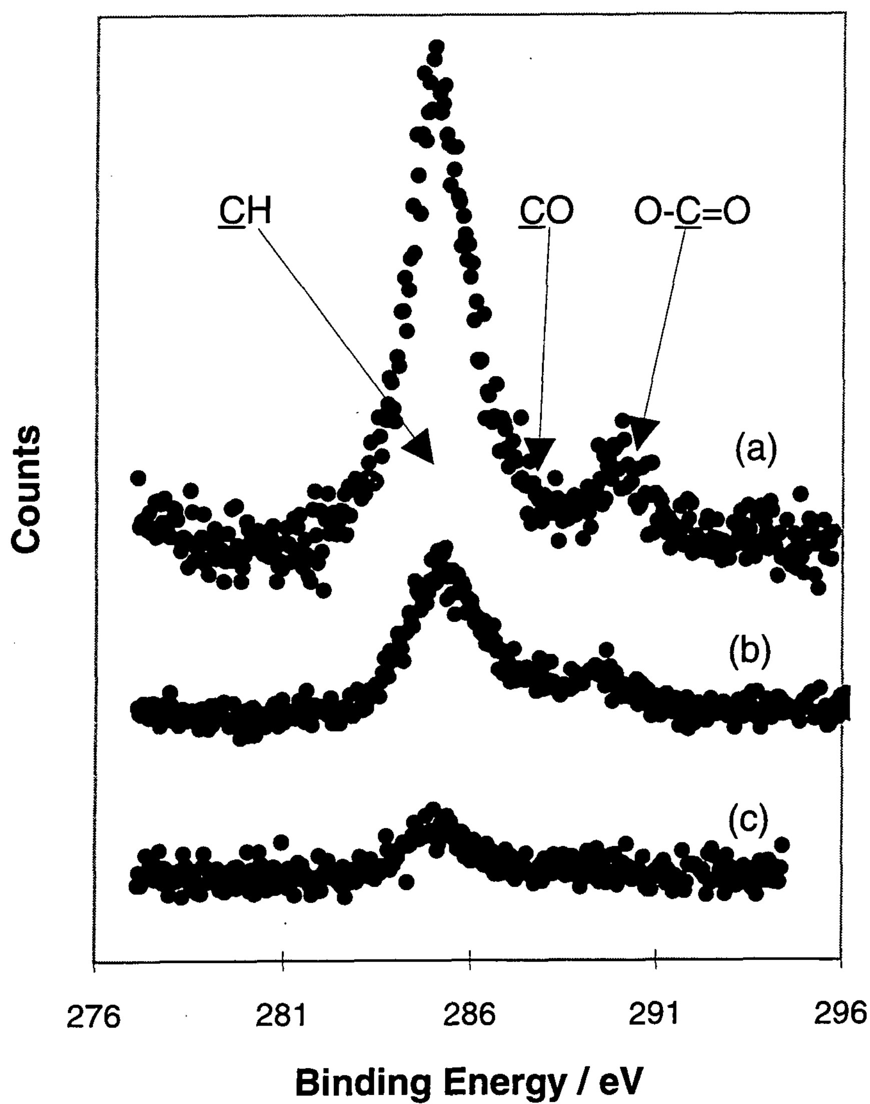


Figure 4.16 C(1s) XP spectra of $Zr(OBu)_4$ films on SDT PET: (a) untreated; (b) $H_2O$ plasma treated (20W, 2 min); and (c) $O_2$ plasma treated (20 W, 2 min).

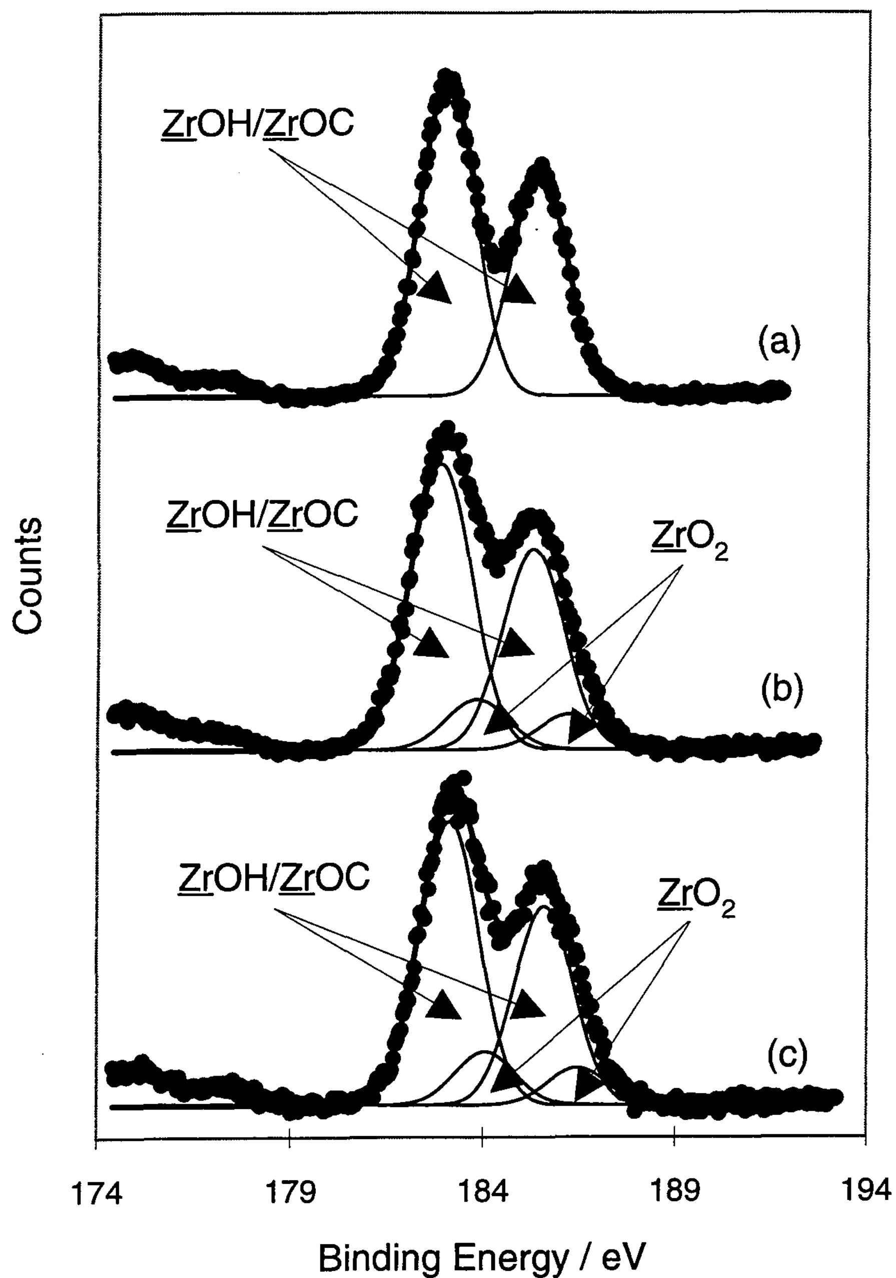


Figure 4.17 Zr(3d) XP spectra of $Zr(OBu)_4$ films on SDT PET: (a) untreated; (b) $H_2O$ plasma treated (20W, 2 min); and (c) $O_2$plasma treated (20 W, 2 min).

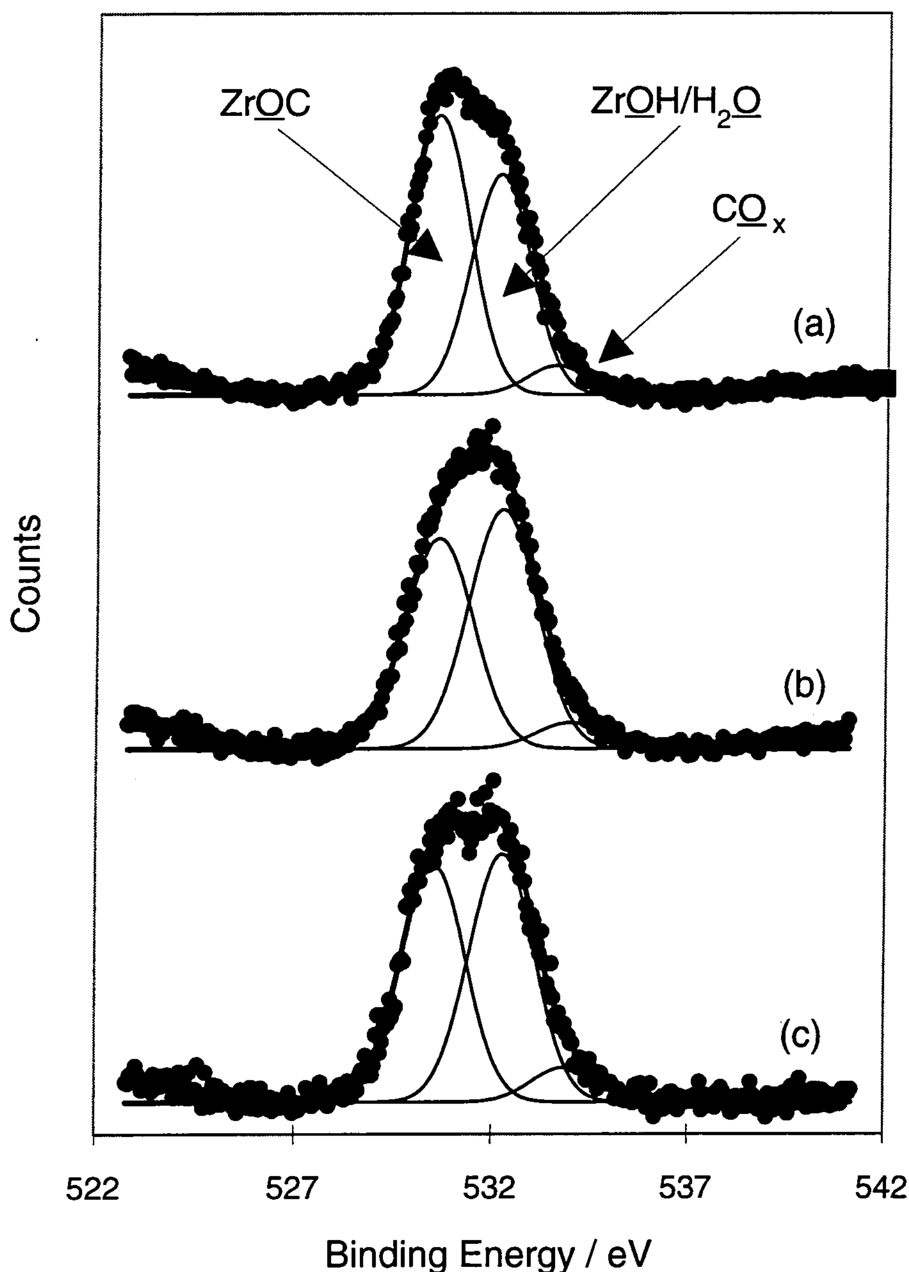


Figure 4.18 O(1s) XP spectra of $Zr(OBu)_4$ films on SDT PET: (a) untreated; (b) $H_2O$ plasma treated (20W, 2 min); and (c) $O_2$ plasma treated (20 W, 2 min).

*4.3.1.9 Oxygen Plasma Power Variation*

Strips of coated SDT PET were treated in an oxygen plasma for 2 min duration using RF powers up to 20 Watts; samples exposed for 2 min to plasmas greater than 20 W were found to be shriveled, discoloured and embrittled after treatment. XPS analysis indicated that the lowest power, 2 W, treatment, caused a decrease in carbon content of 20 %, an increase of approximately 10 % in zirconium and oxygen content, Figure 4.19. Treatments at higher powers,

however, caused carbon content to increase and oxygen content to decrease relative to the 2 W treated values, with no further change in zirconium content. Zr(3d) spectra show a gradual $Zr(OBu)_4$ increase of the higher binding energy environment with increasing plasma power, whilst O(1s) spectra indicate no clear trend with plasma power, Table 4.8.

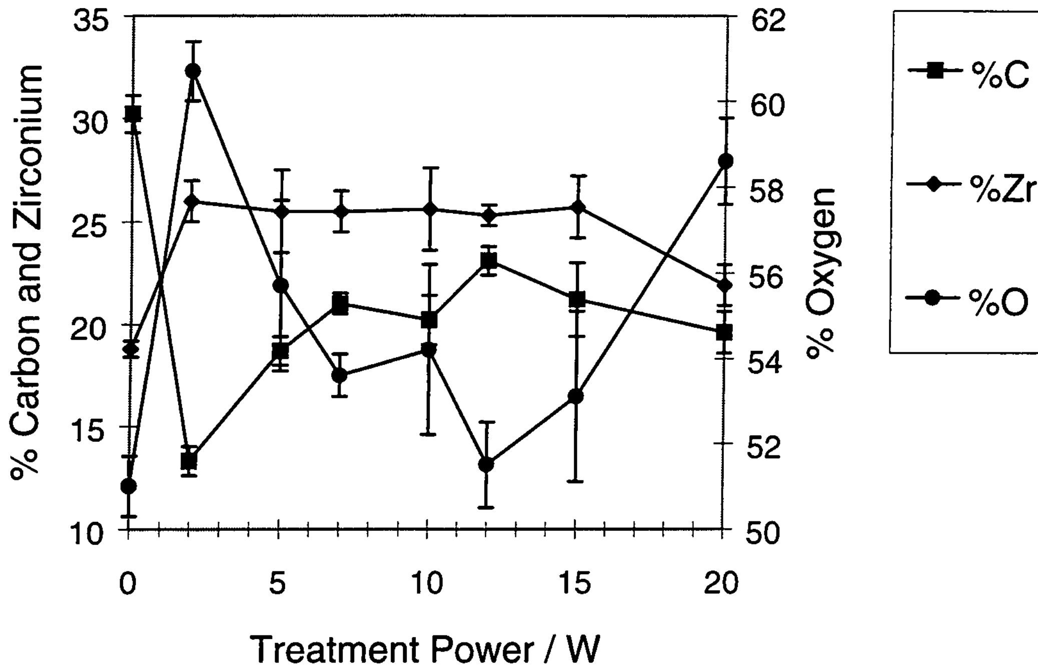


Figure 4.19 Carbon, zirconium and oxygen content of $Zr(OBu)_4$ films on SDT PET versus power of $O_2$ plasma treatment.

| Power / W | % Zr II | % O I | % O II | % O III | % CxHy | % C-Zr |
|---|---|---|---|---|---|---|
| 0 | 0 | 50.6 | 45.3 | 4.1 | 76.3 | 0 |
| 2 | 14.4 | 49.8 | 37.5 | 12.6 | 71.0 | 0 |
| 5 | 10.4 | 47.6 | 41.7 | 10.7 | 65.2 | 0 |
| 7 | 5.9 | 39.6 | 51.1 | 9.2 | 69.4 | 4.3 |
| 10 | 7.5 | 43.7 | 47.3 | 9.0 | 68.2 | 10.4 |
| 12 | 12.9 | 36.9 | 53.1 | 10.0 | 69.0 | 10.5 |
| 15 | 19.3 | 49.8 | 43.3 | 6.9 | 64.8 | 10.5 |
| 20 | 15.7 | 51.6 | 54.3 | 7.6 | 64.6 | 6.4 |

Table 4.8 Peak fit area proportions (errors ≤ 2 %) of $Zr(OBu)_4$ coated on SDT PET as a function of $O_2$ plasma treatment power.

### *4.3.1.10 Oxygen Plasma Duration Variation*

XPS of $Zr(OBu)_4$ films on SDT PET treated in a 10 W oxygen plasma for durations up to 10 minutes show that the significant change in composition occurred within the first 30 seconds of treatment, Figure 4.20; 8 min and 10 min treatments resulted in a less modified composition than shorter treatments. Zr(3d) spectra show that a maximum of 18 % of zirconium atoms were converted to a higher binding energy environment after 5 minutes of treatment, Table 4.9. Treatment times of 8 minutes and longer had a significant effect in increasing the middle binding energy peak in O(1s) spectra, Table 4.9. Hydrocarbon proportion of C(1s) area was lowest for short duration treatments, and carbide carbon was present for any oxygen plasma treatment, Table 4.9.

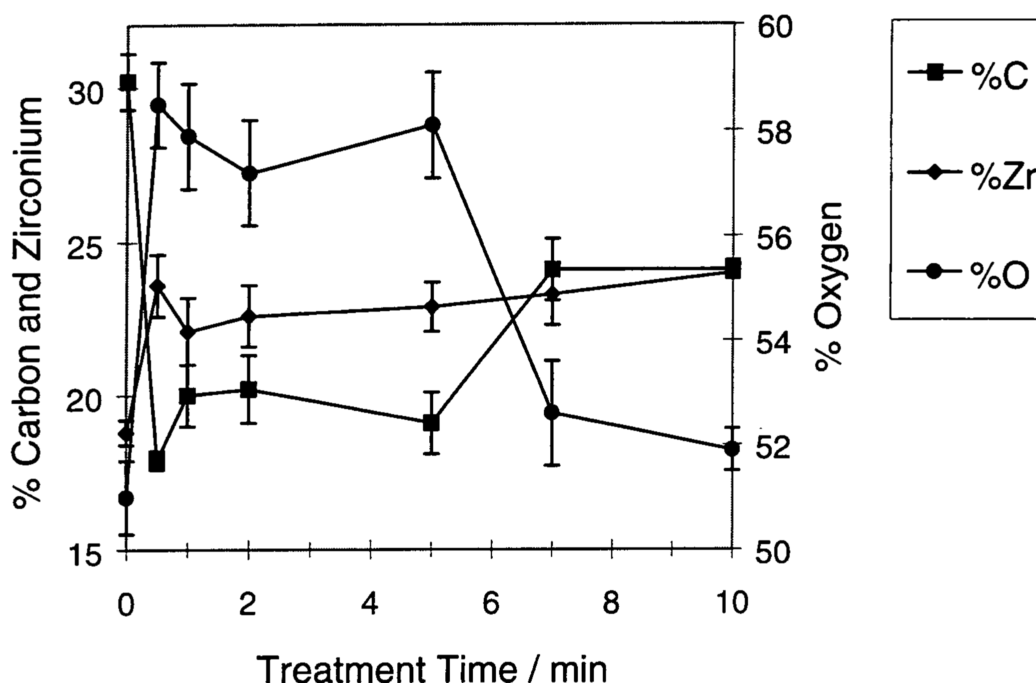


Figure 4.20 Carbon, zirconium and oxygen content of $Zr(OBu)_4$ films on SDT PET versus duration of $O_2$ plasma treatment.

| Duration / min | % Zr II | % O I | % O II | % O III | % CxHy | % C-Zr |
|---|---|---|---|---|---|---|
| 0 | 0 | 50.6 | 45.3 | 4.1 | 76.3 | 0 |
| 0.5 | 6.2 | 44.5 | 47.4 | 8.0 | 54.5 | 8.7 |
| 1 | 11.7 | 43.7 | 46.8 | 9.5 | 61.1 | 10.1 |
| 2 | 7.5 | 43.7 | 47.3 | 9.0 | 68.2 | 10.4 |
| 5 | 17.9 | 45.2 | 48.6 | 6.2 | 67.8 | 10.5 |
| 7 | 16 | 32.7 | 59.0 | 8.3 | 65.7 | 10.5 |
| 10 | 15.6 | 35.0 | 58.7 | 6.3 | 70.1 | 6.4 |

Table 4.9 Peak fit area proportions (errors ≤ 2 %) of $Zr(OBu)_4$ coated on SDT PET as a function of $O_2$ plasma treatment duration.

*4.3.1.11 Water Plasma Power Variation*

10 minutes purge of $Zr(OBu)_4$ films on SDT PET in 0.2 mbar water vapour increased carbon and decreased oxygen content. The extent of change was approximately the same as that for $Zr(OBu)_4$ films on glass purged in water vapour, Figure 4.21. Composition changes in the opposite direction from that observed for water purges occurred for water plasma treatments up to about 20 W, with no further significant modification for higher powers, Figure 4.21. Unlike $O_2$ plasma treatments, $H_2O$ plasma treatments of films on SDT PET caused no distortion nor embrittling of the samples.

Zr(3d) spectra show that 5 W water plasma treatment changes 36 % of zirconium atoms into the higher binding environment, Table 4.10; the highest proportion observed in this study. O(1s) spectra indicate a small increase in the proportion of the O II peak and a decrease in the O I peak up to plasma powers of approximately 10 W, Table 4.10. The C(1s) hydrocarbon peak proportion diminished up to powers of about 30 W, whilst no carbide peak was observed to the low binding energy of the hydrocarbon peak after any water plasma treatment, Table 4.10.

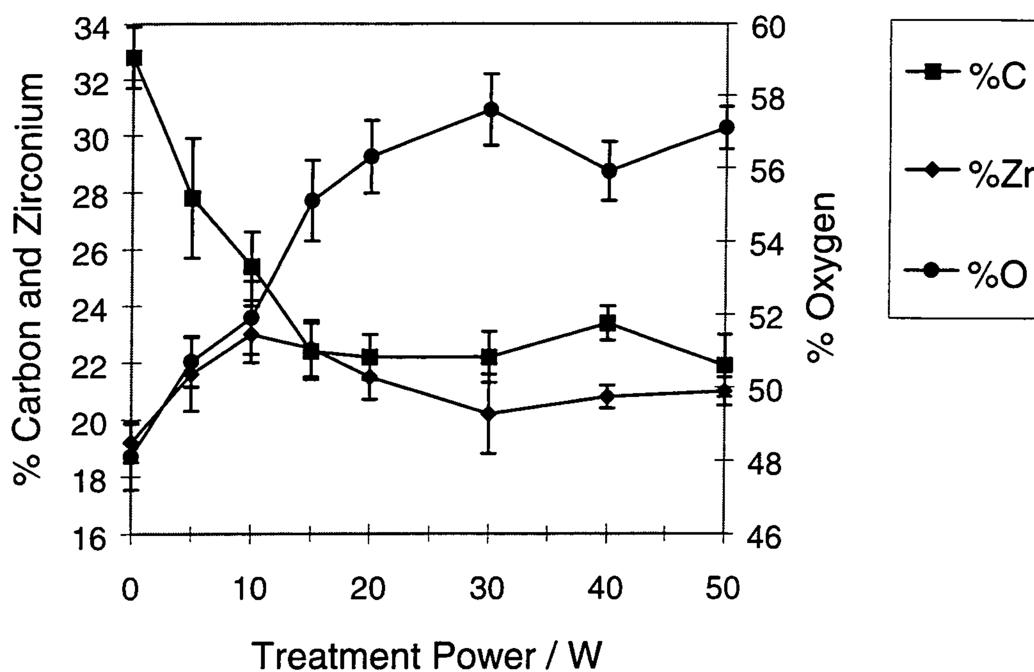


Figure 4.21 Carbon, zirconium and oxygen content of $Zr(OBu)_4$ films on SDT PET versus power of $H_2O$ plasma treatment.

| Power / W | % Zr II | % O I | % O II | % O III | % CxHy | % C-Zr |
|---|---|---|---|---|---|---|
| 0 | 4.9 | 50.3 | 44.9 | 4.6 | 78.8 | 0 |
| 5 | 36.1 | 47.0 | 47.1 | 5.9 | 63.9 | 0 |
| 10 | 28.9 | 38.5 | 51.3 | 10.3 | 71.1 | 0 |
| 15 | 31.2 | 47.6 | 47.5 | 4.9 | 68.8 | 0 |
| 20 | 33 | 44.2 | 50.2 | 5.6 | 67.0 | 0 |
| 30 | 36.6 | 46.2 | 48.7 | 5.1 | 63.4 | 0 |
| 40 | 35.5 | 43.7 | 51.4 | 4.9 | 64.5 | 0 |
| 50 | 36.8 | 46.7 | 47.4 | 5.9 | 63.2 | 0 |

Table 4.10 Peak fit area proportions (errors ≤ 2 %) of $Zr(OBu)_4$ coated on SDT PET as a function of $H_2O$ plasma treatment power.

*4.3.1.12 Water Plasma Duration Variation*

XPS analysis of films on SDT PET water plasma treated for up to 10 minutes duration showed that carbon content decreased and oxygen content increased during the first 2 minutes of treatment, to a final carbon content of about 25 %, Figure 4.22. Peakfits of Zr(3d) spectra show that 0.5 and 1 minute water plasma treatment modifies 25 % of surface zirconium to a higher binding energy chemical environment, and longer treatments result in less final modification, Table 4.11. An increase of the O II peak of roughly 7 %, at the expense of the O I peak, occurs gradually within the first 3 minutes of treatment, Table 4.11. Hydrocarbon proportion of C(1s) peak area decreases 12 % after 1 minute of treatment and increases slightly thereafter, whilst no carbide carbon is observed, Table 4.11.

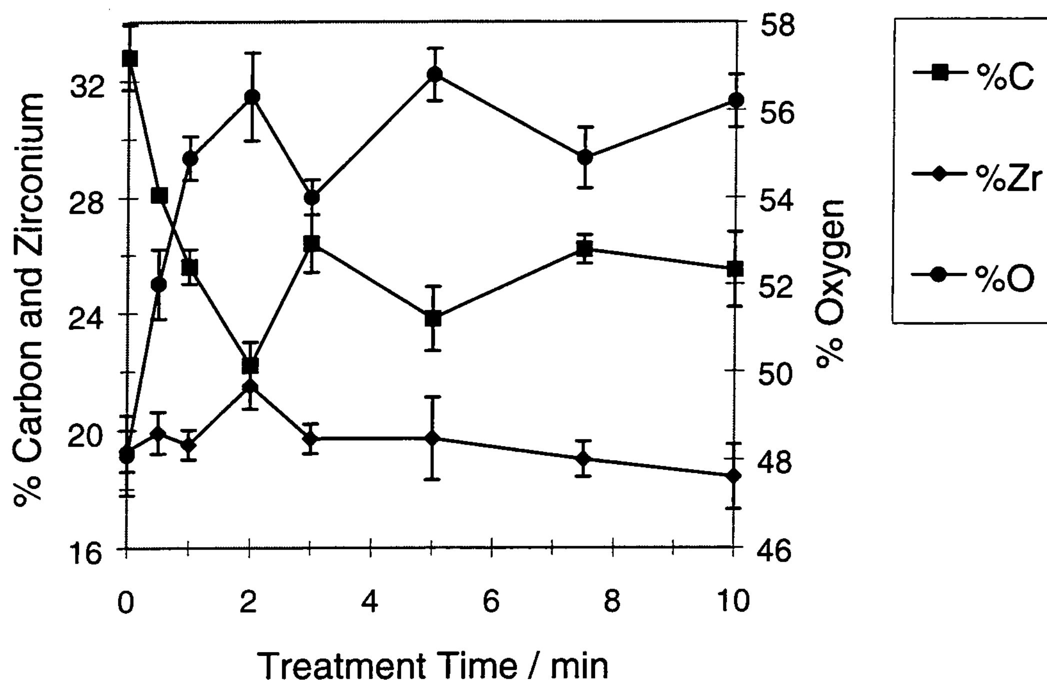


Figure 4.22 Carbon, zirconium and oxygen content of $Zr(OBu)_4$ films on SDT PET versus duration of $H_2O$ plasma treatment.

| Duration / min | % Zr II | % O I | % O II | % O III | % CxHy | % C-Zr |
|---|---|---|---|---|---|---|
| 0 | 4.9 | 50.3 | 44.9 | 4.6 | 78.8 | 0 |
| 0.5 | 24.4 | 46.9 | 45.6 | 7.5 | 70.7 | 0 |
| 1 | 24.9 | 44.0 | 48.4 | 7.5 | 63.5 | 0 |
| 2 | 6.8 | 44.2 | 50.2 | 5.6 | 67.0 | 0 |

| | | | | | | |
|---|---|---|---|---|---|---|
| 3 | 18 | 44.5 | 50.7 | 4.8 | 68.7 | 0 |
| 5 | 20.8 | 40.7 | 52.9 | 6.4 | 67.0 | 0 |
| 7 | 14.4 | 44.9 | 50.2 | 4.9 | 75.8 | 0 |
| 10 | 16.5 | 42.8 | 52.2 | 5.0 | 76.1 | 0 |

Table 4.11 Peak fit area proportions (errors ≤ 2 %) of $Zr(OBu)_4$ coated on SDT PET as a function of $H_2O$ plasma treatment duration.

### *4.3.2 Argon Ion Etch Depth Profiles*

XPS surface analysis after increasing times of ion etching provided the composition depth profile of a $Zr(OBu)_4$ film spin coated on glass, Figure 4.23. 50 s of argon ion etching untreated $Zr(OBu)_4$ on glass resulted in a film surface with 18 % less carbon, 8 % more oxygen and 10 % more zirconium than the untreated film. Surface composition remained constant for etch times between 50 s and 500 s, at which point silicon from the glass substrate was detected and oxygen content decreased slightly. The high binding energy shoulder of O(1s) spectra decreased with sputter time, Figure 4.24, and Zr(3d) spectra broadened for etch times of greater than 240 seconds, Figure 4.25.

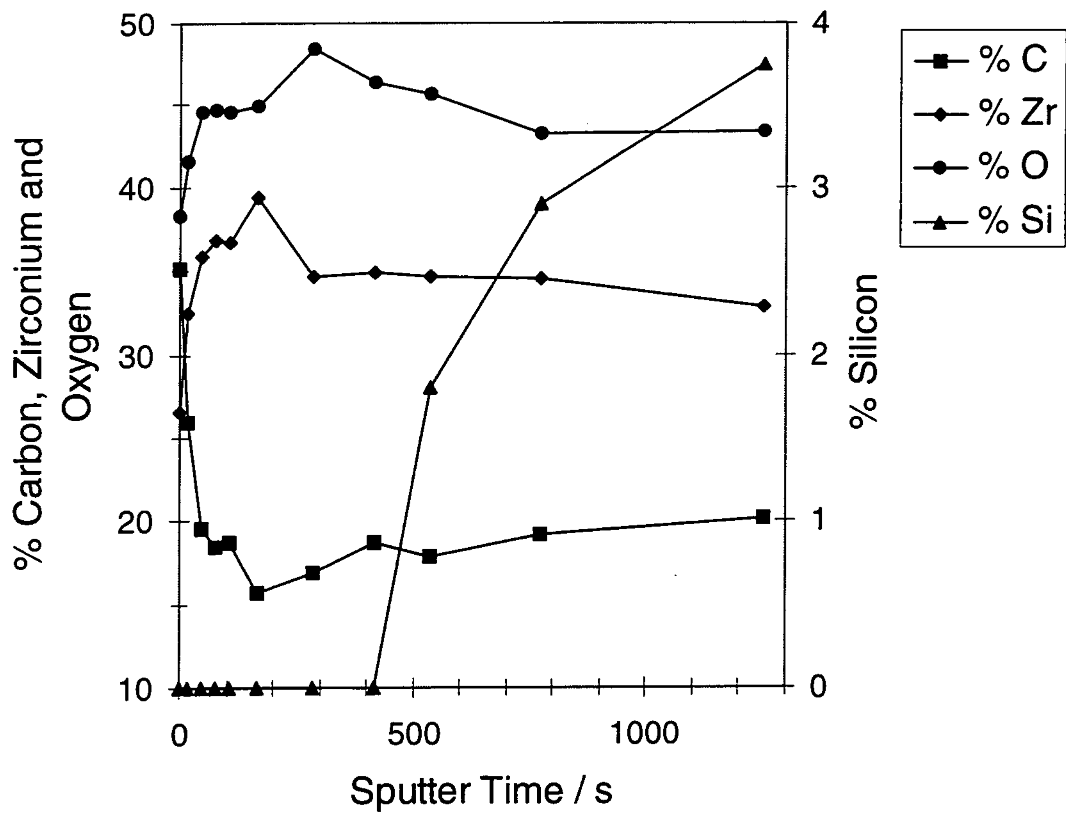


Figure 4.23 Ar Ion Etch Composition Depth Profile of $Zr(OBu)_4$ Spin Coated on Glass.

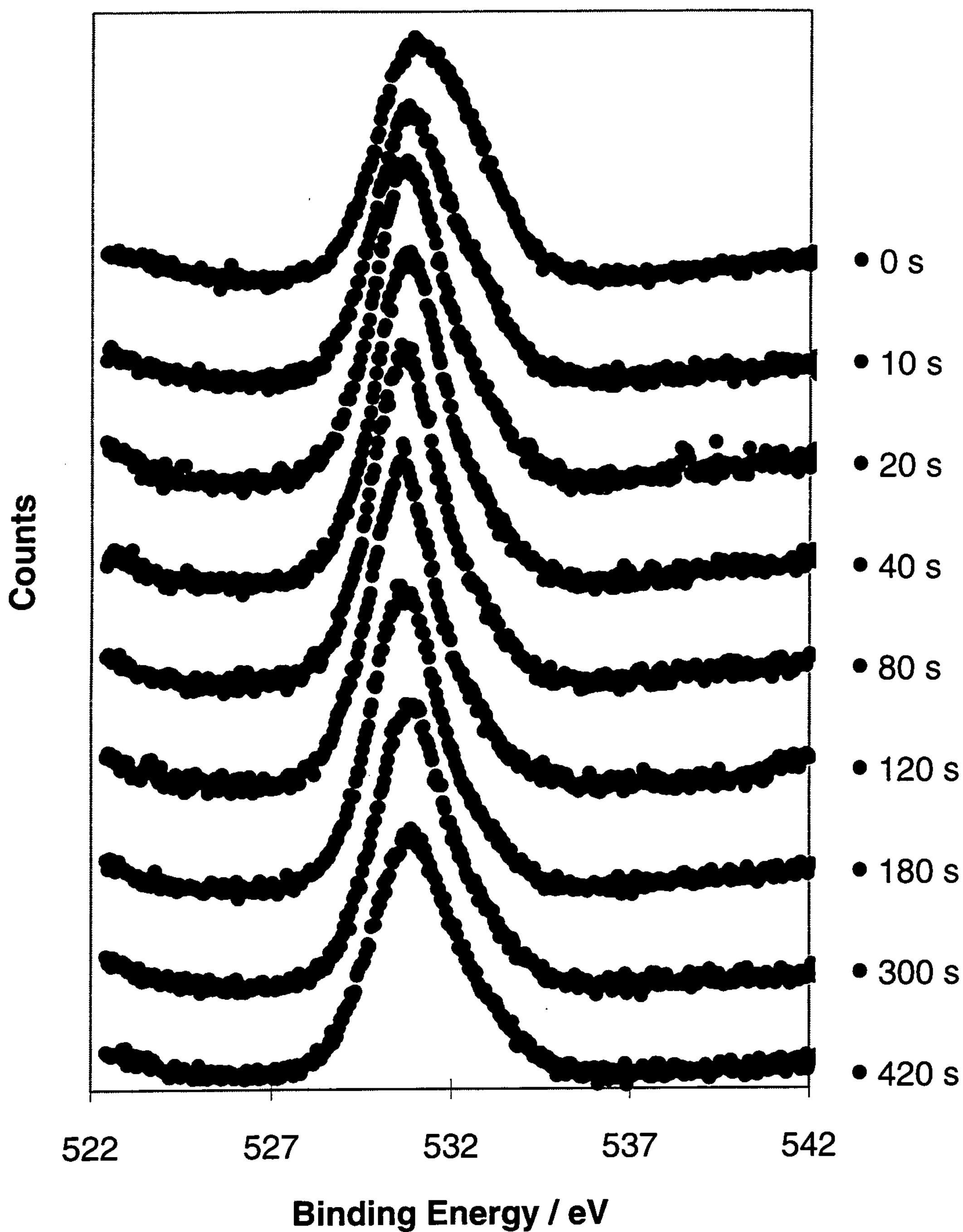


Figure 4.24 O(1s) spectra as a function of cumulative Ar ion etch time for untreated $Zr(OBu)_4$ spin coated on glass.

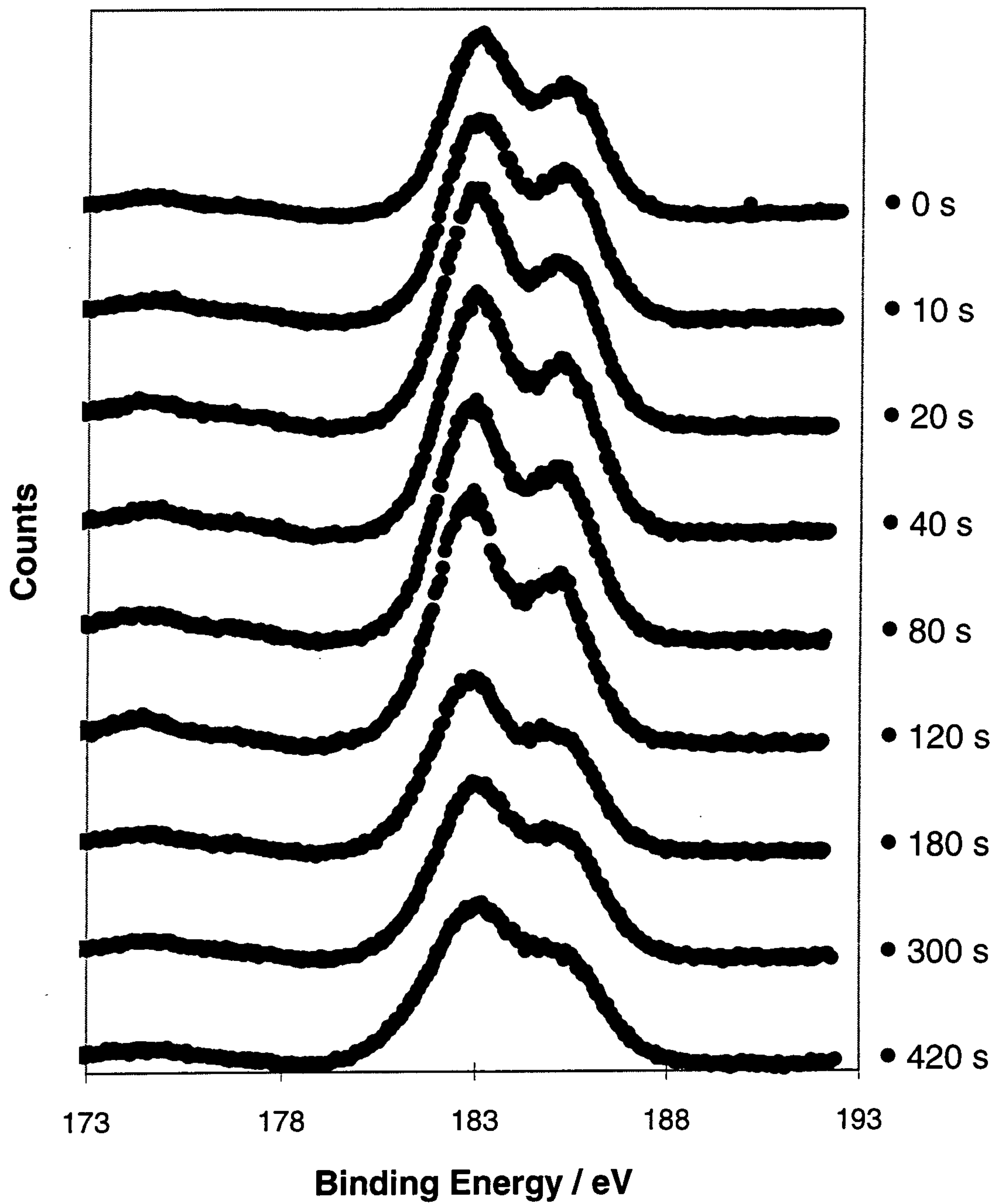


Figure 4.25 Zr(3d) spectra as a function of cumulative Ar ion etch time for untreated $Zr(OBu)_4$ spin coated on glass.

Argon ion etching of 30 W 2 min $O_2$ plasma treated $Zr(OBu)_4$ film on glass for 100 sec resulted in a surface composition with 26 % less carbon, 12 % more oxygen and 14 % more zirconium than the unetched film, Figure 4.26. Composition changed most rapidly up to 100 s etch time, after which surface zirconium content no longer changed, whilst carbon content decreased and oxygen content increased with etch time at a slower rate. No abrupt change in film composition was observed at the time when substrate silicon was detected. C(1s), Zr(3d) and O(1s) spectral lineshapes changed with etch time similarly to those for untreated $Zr(OBu)_4$ on glass, Figures 4.24 and 4.25.

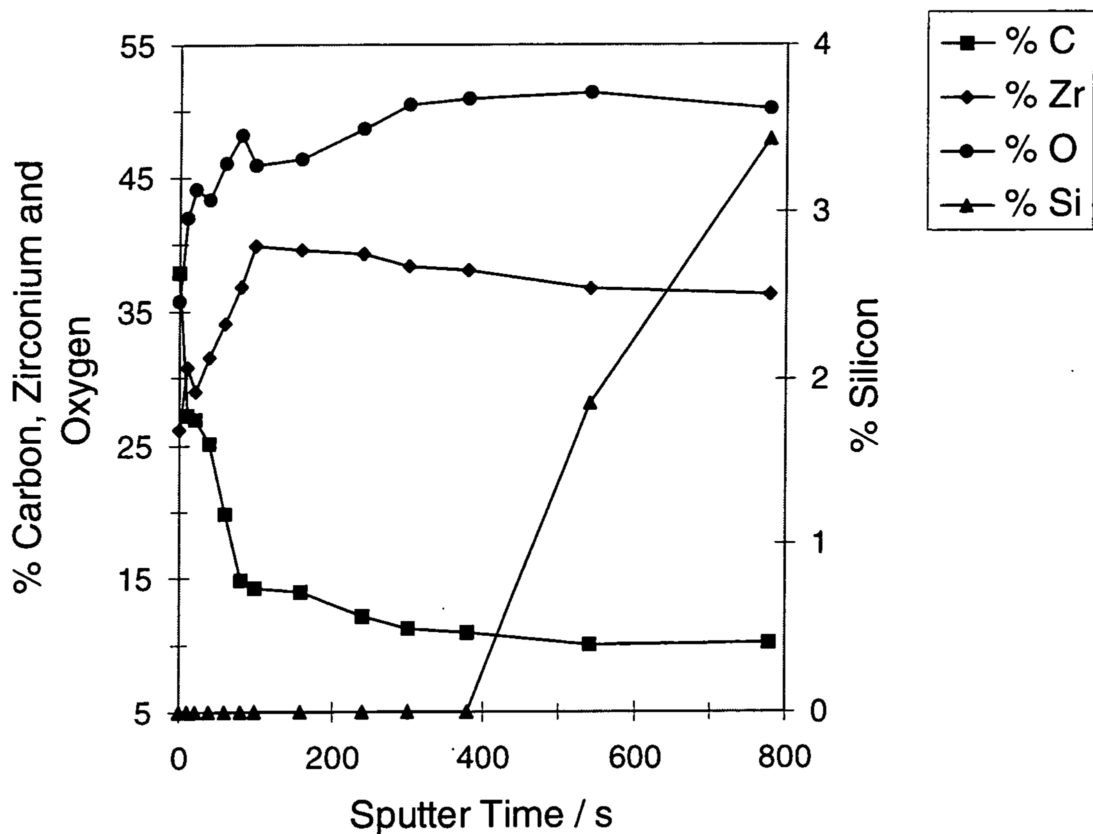


Figure 4.26 XPS Ar Ion Etch Depth Profile of Oxygen Plasma Treated $Zr(OBu)_4$ Spin Coated on Glass.

### 4.3.3 FTIR

Transmission FTIR spectra of 2 % weight / volume $Zr(OBu)_4$ solution spin coated on freshly pressed KBr discs, Figure 4.27(a), showed absorbances for: Zr-O (at 440 $cm^{-1}$ and 640 $cm^{-1}$)[33,34]; for CO(H) (at 1070 $cm^{-1}$, 1377 $cm^{-1}$ and 1458 $cm^{-1}$)[35]; for the butyl functionality (at 1136 $cm^{-1}$)[36]; for $CH_3$ (at 2876 $cm^{-1}$, 2928 $cm^{-1}$ and 2955 $cm^{-1}$)[33]; and for $OH/H_2O$ (at 1604 $cm^{-1}$ and 3316 $cm^{-1}$)[35] as previously reported for zirconium alkoxides[36,37]. FTIR spectra of $Zr(OBu)_4$ solution spin coated on KBr discs and $O_2$ plasma treated at 30 W for 2 minutes, Figure 4.27(b), showed absorption peaks only for Zr-O bonds, indicating that plasma treatment of the coated KBr disks removed all detectable carbon groups. Attenuated total internal reflection infrared (ATR-IR) spectra of $Zr(OBu)_4$ films spin coated on clean PET and silent discharge treated PET substrates did not differ from the ATR-IR spectra of clean PET film, Figure 4.28, indicating that spin coated films were insufficiently thick to produce infrared absorptions in addition to those of the substrate.

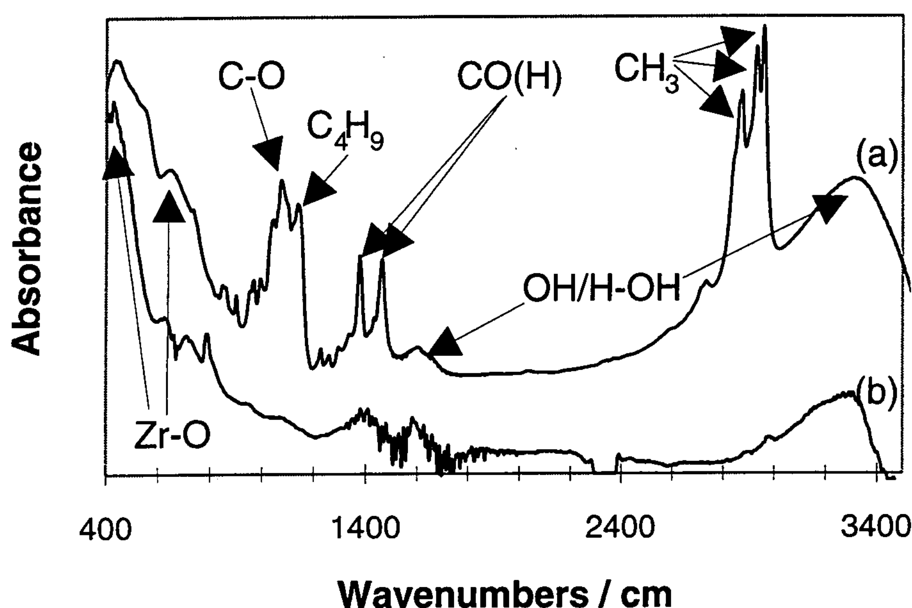


Figure 4.27 Transmission FTIR spectra of $Zr(OBu)_4$ spin coated on KBr: (a) untreated; and (b) $O_2$ plasma treated for 2 minutes at 30 W.

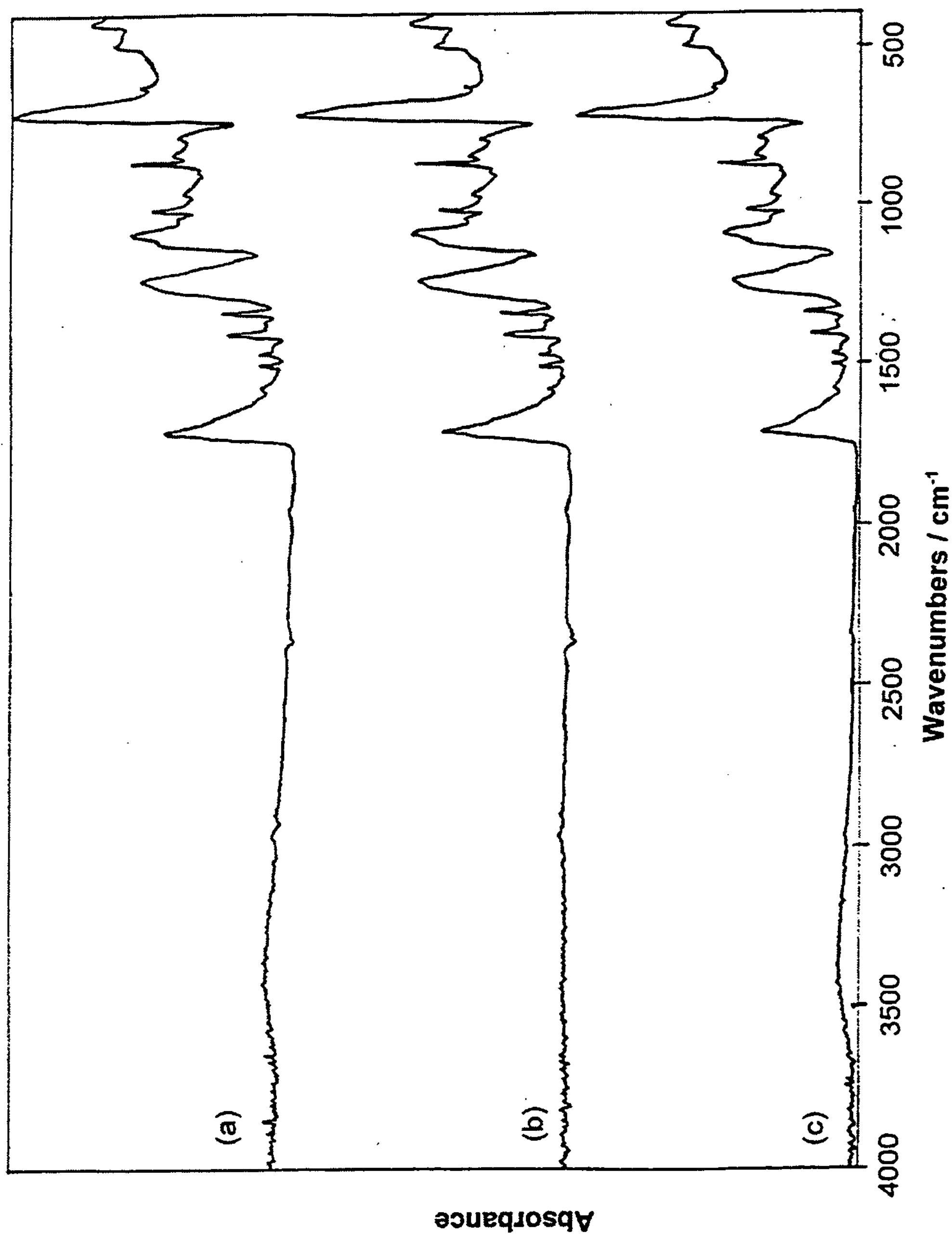


Figure 4.28 ATR-FTIR spectra of (a) clean PET; (b) SDT PET; and (c) $Zr(OBu)_4$ spin coated on SDT PET.

### *4.3.4 Gas Permeability Of $Zr(OBu)_4$ Coatings On PET Substrates*

Mean equilibrium partial pressures (MEPPPs) of oxygen, argon and helium for membranes of untreated PET and oxygen plasma treated $Zr(OBu)_4$ spin coated on PET, indicate that the plasma treated coating presents some barrier to helium and oxygen permeability, but does not significantly reduce argon permeability, Table 4.12.

| Membrane | $O_2$ MEPPP/ torr | Ar MEPPP/ torr | He MEPPP/ torr |
|---|---|---|---|
| Untreated PET | $0.160 \pm 0.002$ | $0.158 \pm 0.06$ | $7.32 \pm 0.08$ |
| SDT PET | $0.169 \pm 0.005$ | $0.156 \pm 0.04$ | $7.51 \pm 0.03$ |
| $O_2$ Plasma Treated $Zr(OBu)_4$ on SDT PET | $0.144 \pm 0.006$ | $0.150 \pm 0.002$ | $5.9 \pm 0.1$ |

Table 4.12 Mean equilibrium permeant partial pressures (MEPPPs) of $O_2$, Ar and He for untreated PET, silent discharge treated (SDT) PET and $O_2$ plasma treated $Zr(OBu)_4$ on SDT PET.

### *4.3.5 Film Thickness Estimation*

The change in mass of glass slides due to spin coating with 2% $Zr(OBu)_4$ solution was determined to be 150 ± 80 μg. An assumed density of 1 g/cm$^3$ and the slide surface area of 1.33 ± 0.05 cm$^2$ provided a thickness estimate of 1.1 ± 0.6 μm for films on glass. Profilometry measurements of the edge of a $Zr(OBu)_4$ film spin coated on glass indicated a film thickness of 0.4 μm. In contrast to the glass substrates, change in mass of a PET substrate due to spin coating with $Zr(OBu)_4$ solutions of various concentrations was not detectable with the electrobalance used, indicating that spin coated film thickness on PET is ≤ 0.25 μm.

### *4.3.6 AFM*

The topography of oxygen plasma treated $Zr(OBu)_4$ films spin coated on PET was shown by atomic force microscopy to be macroscopically rough and undulating on a hozontal scale of 5 μm, Figure 4.29, and less rough on length scales less than 1 μm, Figure 4.30.

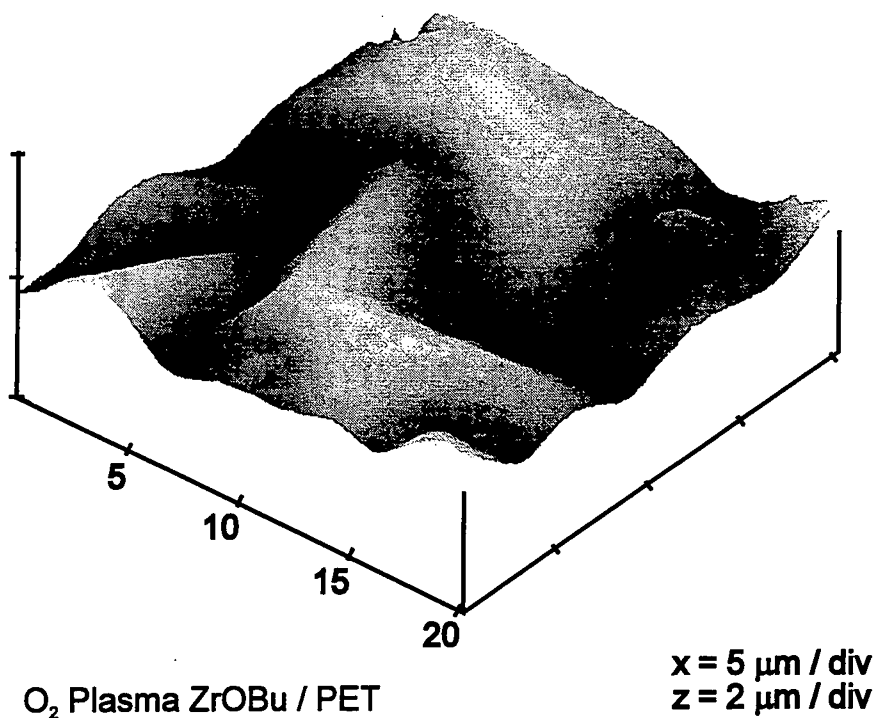


Figure 4.29 Atomic force micrographs of $O_2$ plasma treated $Zr(OBu)_4$ films spin coated on PET (1 μm per x-axis division).

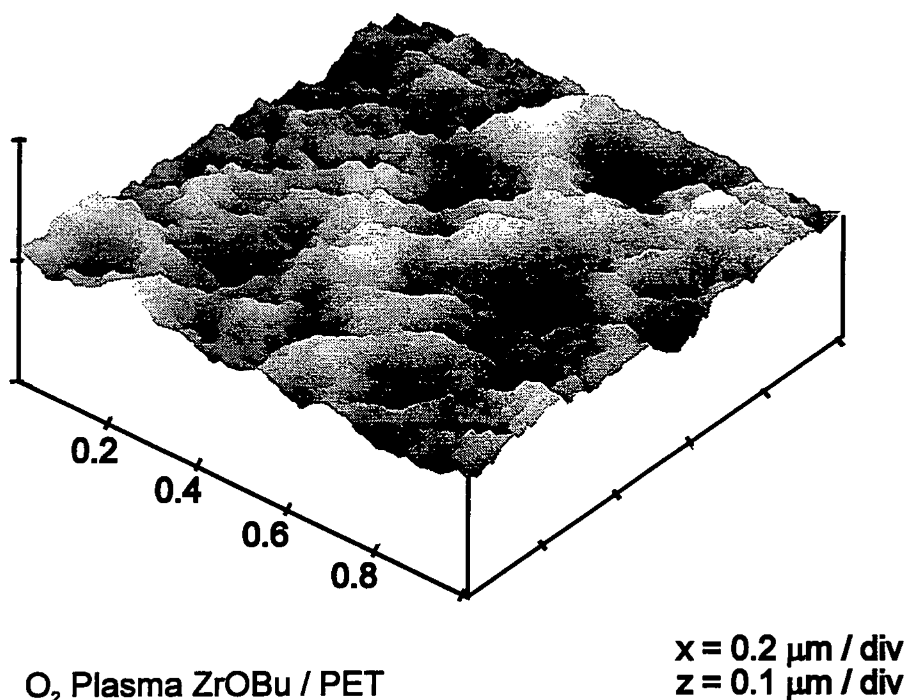


Figure 4.30 Atomic force micrograph of $O_2$ plasma treated $Zr(OBu)_4$ film spin coated on PET (0.2 µm per x-axis division).

## 4.4 DISCUSSION

Three distinct stages of the coating process are of interest: the behavior of $Zr(OBu)_4$ in alcohol solution; reactions of precursor molecules with substrate surface species and with atmospheric moisture during spin coating; and finally reactions of impinging plasma species with the solid precursor film surface.

The high reactivity of zirconium in its +4 coordination state drives solvation and oligomerization of monomeric alkoxide molecules in alcohol solution, resulting in solvated coordination complexes[13,15,16], Figure 4.31. Precursor polymerization may aid in complete substrate coverage and in forming well cross-linked gas barrier coatings upon oxidation. Alcoholysis reactions with propanol solvent modify $Zr(OBu)_4$ molecules by exchange of up to 4 butoxy ligands for propoxy groups, which induce a greater degree of oligomerization due to their lesser steric bulk[14,38]. Comparison of transmission

infrared absorbencies to previously reported spectra[36,37] confirmed the presence of only $Zr(OBu)_4$ species in the $Zr(OBu)_4$ solution diluted to 2 % concentration with propan-1-ol, Figure 4.27.

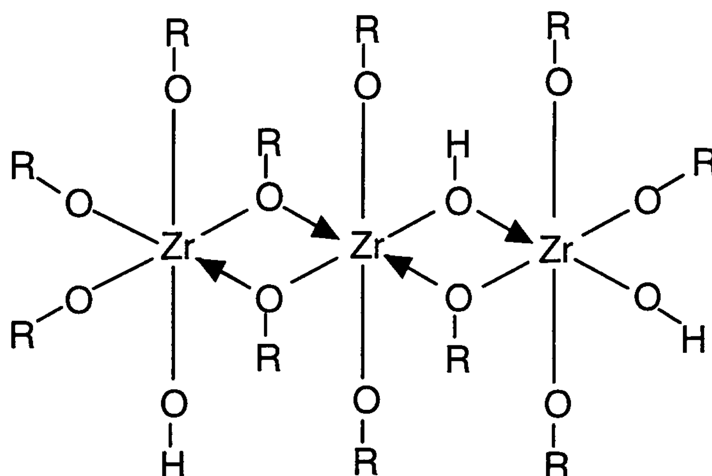


Figure 4.31. Structure of a trimeric solvated coordination complex of $Zr(OR)_4$ in alcohol solution[13,15].

Zirconium alkoxides are highly reactive towards hydrolysis: for use in sol-gel processing their functionality is usually reduced by complexation with β-diketonates to prevent premature precipitation of zirconia[14,41,42]. Uncontrolled hydrolysis of a *n*-butanol solution of $Zr(OBu)_4$ by atmospheric moisture occurs over a period of weeks producing caked powder[43], whilst accelerated hydrolysis can produce ultrafine powders[44] or gels[43] depending on solution pH and the proportion of water added. Despite efforts made in this study to limit precursor contact with atmospheric moisture, some hydrolysis, reaction 1, and condensation, reaction 2, probably occurred by the time of spin coating.

$Zr(OR)_4 + xH_2O \rightarrow [Zr(OR)_{4-x}(OH)_x] + xROH$ ($R = Pr^i$ or $Bu^n$) Reaction 1

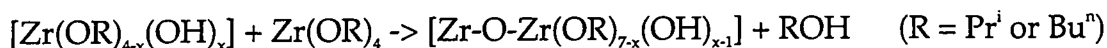

$[Zr(OR)_{4-x}(OH)_x] + Zr(OR)_4 \rightarrow [Zr\text{-}O\text{-}Zr(OR)_{7-x}(OH)_{x-1}] + ROH$ ($R = Pr^i$ or $Bu^n$)

Reaction 2

Spin coating is an established method for producing thin, uniform films of polymers and inorganic salts by dropwise addition of a volatile solution onto a substrate followed by high speed (>1000 rpm) spinning to remove the

solvent[20,45,46]. An estimation of film thickness of 1.1 ± 0.6 μm is inkeeping with the thickness of films spin coated from dilute solutions of sol-gel precursors[47]. Hydrolysis reactions during spin coating account for the large decrease in carbon and increase in zirconium and oxygen content, compared with stoichiometric $Zr(OBu)_4$, observed by XPS for spin coated films on each substrate, Table 4.1. Loss of a large proportion of the alkoxy ligands from adsorbing zirconium species as volatile butanol and propanol groups forms a film of hydroxylated zirconium oxo-polymers[14,40], some with unremoved pendant organic groups. Solvent and product alcohol molecules may become trapped in the growing spin coated film, further contributing to the film's organic content.

XPS studies of $Zr(OBu^{tert})_4$ adsorbing onto a hydroxylated aluminium surface at 105 Kelvin in UHV showed that the first monolayer adsorbed by loss of two butoxide ligands via proton transfer to give a surface bound di-butoxyzirconium species, and that subsequent multilayers of $Zr(OBu)_4$ adsorb intact[29]. During spin coating in air the rate of $Zr(OBu)_4$ hydrolysis is increased by atmospheric $H_2O$, and by hydroxyl groups and a residual water film on the substrate surface. Additionally, the surface of glass substrates catalyses dehydration of alcohol molecules[12,48], allowing a chain reaction hydrolysis of $Zr(OBu)_4$ to occur and explaining the greater composition change observed for this substrate over that for PET and SDT PET, Table 4.1.

Zirconium complexes react preferentially with carboxylate groups on oxidized polymer surfaces, forming Zr-O-C bonds[49,50]. These interactions enhance polymer surface adhesion of inks, paints and adhesives[51], cross-link polymers[50], and can, in some situations, block adhesive sites causing abhesion[52]. When $Zr(OBu)_4$ is deposited onto PET or silent discharge treated PET substrates, bonds form between polymeric zirconium alkoxy species and $C\text{-}O_x$ groups on the polymer surface. Oxidized species present on SDT PET cause removal of a larger number of organic ligands than during spin coating on untreated PET, Table 4.1.

A single resolved $Zr(3d)_{5/2}$ spin component peak at 183.0 eV in XP spectra of untreated films indicates a single oxygen-bound[24,29,30,53,54] or hydroxylated[55,56] zirconium environment, inkeeping with presence of a -Zr-(OR)-Zr-(OH)- type oxo-polymer structure shown in Figure 4.31. Peak fits of O(1s) spectra indicated three oxygen chemical environments present at untreated film surfaces;

predominantly O I at 530.5 eV, typical of oxygen covalently bound to zirconium[24,29,30]; O II at 532.3 eV, assigned to OH and adsorbed water[31,32]; and O III, of least intensity, at 534.2 eV attributed to C-$O_x$ species[24,29]. Intact alkoxide ligands together with hydrocarbon contamination at the surface of untreated films contributed to a C(1s) lineshape comprising mainly hydrocarbon, used as a charge reference at 285.0 eV, and a lesser C-O peak.

Bombardment of the film surface with 'streamers' of energetic electrons and reactive ozone molecules present during silent discharge treatment[57], appeared not to have a strong effect on $Zr(OBu)_4$ film composition, Table 4.3, nor, from XPS lineshapes, on chemical bonding. Ozone molecules are the most abundant chemically reactive species in atmospheric pressure plasma as opposed to oxygen radical species as in low pressure non-equilibrium plasmas. Such physico-chemical differences at the discharge-film interface account for a smaller film modification effect during silent discharge treatment.

Inductively coupled non-isothermal plasma reactors supply a high concentration of reactive species, such as radicals and metastable excited species, and only a low flux of ion bombardment, making them ideal for "ashing" of microelectronics resist rather than non-isotropic pattern etching[58]. Surface modification in such a plasma is likely to be dominated by the reaction of Zr-O-C groups at the precursor film surface with oxygen radicals; nucleophilic attack will break O-C bonds in preference to Zr-O bonds, since the latter are stronger[17,18], resulting in the removal of volatile oxidized organic molecules, such as $CO_x$ and $C_xH_yO_z$, and the formation of cross-linked zirconium oxide at the sample surface. Transmission infrared spectra of $Zr(OBu)_4$ films spin coated on freshly pressed KBr, Figure 4.27, indicate almost complete removal of carbon species during $O_2$ plasma treatment, whilst XPS results for $Zr(OBu)_4$ spin coated on glass show a decrease in surface carbon content of 11 ± 2 %, figure 4.7, and a depth profile of $O_2$ plasma treated films on glass confirm that carbon persists through to the film-substrate interface.

The ability of energetic oxygen atoms and ions in non-isothermal oxygen plasmas to oxidize and completely remove the organic component of metalorganic precursors has been demonstrated in studies of PECVD[59] and in surface treatment of organo-siloxane polymers[60]. Comparison of results in the present study with PECVD[59,60] and pyrolytic decomposition of $Zr(OBu)_4$ vapour at

350 °C[12,48], in which carbon-free $ZrO_2$ is produced, indicates that an energy barrier exists against removal of carbon containing groups from precursor molecules which is higher than the energy provided by plasma species. The higher binding energy Zr(3d) environment observed for plasma treated film surfaces indicates that $ZrO_2$ was produced, distinguishable by a chemical shift of +2.0 eV from Zr-O-C or Zr-O-H environments in the untreated film, Figures 4.8, 4.16. After plasma treatment, the dominant O(1s) oxygen environment changes from oxygen bound to zirconium, to oxygen in adsorbed water and OH groups; hydrated/hydroxylated oxide is formed from the solvated organo-oxo-zirconium polymer.

During $O_2$ plasma enhanced CVD using organometallics, the plasma concentration of carbon-rich atoms detected by mass spectrometry was reported to correlate with the final amount of carbon at the surface of deposited metal oxide films[61]. Above the spin coated film during plasma treatment in the present study, there exists a solid-plasma interface which consists of arriving plasma species and fragments removed from the film; carbon containing species may be re-deposited on the film surface as a result of carbon-rich fragments in the plasma-surface interface region. Recently, much interest has been shown in 'ormocer's (organically modified ceramics) in which residual organic molecules reduce the degree of oxo-polymer cross-linking, decreasing the necessary processing temperature, or create organic polymer networks, forming novel inorganic-organic composites[14,38,39]. Non-isothermal $O_2$ and $H_2O$ plasma treatments of what is conventionally a sol-gel precursor provides a new route to synthesize this class of materials.

Non-isothermal water plasma treatment of nickel oxide[31] and tin oxide[32], investigated as an alternative surface cleaning process, resulted in removal of all detectable surface carbon contamination and in surface hydration and hydroxylation. The attack of a spin coated film of $Zr(OBu)_4$ by $OH^+$ ions and radicals of a water plasma produce hydrolysis of Zr-O-R functionalities remaining at the film surface to give metal oxide or hydroxide groups on the surface with the loss of volatile organic groups.

Films coated on both glass and SDT PET substrates underwent greater changes in film composition and Zr(3d), O(1s) and C(1s) spectra during plasma treatment in $O_2$ gas than in $H_2O$ vapour, figures 4.7-4.22. Also notable were the

lower value of power and duration above which no further change occurred for oxygen plasma treatment, figures 4.19-4.22, and the absence of zirconium carbide production for water plasma treatment of $Zr(OBu)_4$ films on SDT PET, figure 4.18. These results may be explained by the higher reactivity of oxygen radicals than hydroxy radicals towards precursor molecules' alkoxy ligands.

Zr-C bonds form upon heating to 110°C, or argon ion bombardment, of a hydrocarbon overlayer on zirconia[24]; it has been proposed that as $ZrO_2$ bonds are broken, electrons are freed which allow Zr-C bond formation whilst oxygen atoms are adsorbed into the bulk. In the present study, carbide formation was observed for $O_2$ and $H_2O$ plasma treatment of $Zr(OBu)_4$ films upon glass, figure 4.10, and for $O_2$ plasma treatment of $Zr(OBu)_4$ films upon SDT PET, figure 4.18; the combination of $O^+$, $O^{2+}$, or $OH^+$ ion bombardment with heating of the film surface, due to bombardment by energetic plasma particles[60], is sufficient to break Zr-O bonds and allow zirconium carbide to form.

During formation of metal oxides by PECVD, deposition rate increases with R.F. plasma power at low power, and is independent of power at higher powers[59,63]. Increased plasma power provides greater energy for ionization, creating a greater density of free electrons and of reactive species[63]; during PECVD, the ratio of plasma power to flow rate determines film chemical structure[64,65]. As plasma treatment power was varied in the present study, the proportion of carbon in the film decreased and that of oxygen increased up to a certain value of power above which no further change occurred, figures 4.11, 4.15, 4.19 and 4.21. These trends suggest reaction rates for organic ligand removal and fragmentation depend, up to a saturation level, upon plasma ion energy and/or oxygen radical concentration. For films on glass, the effect of increasing $H_2O$ plasma power saturated at about 20 W, figure 4.15, whereas, for $O_2$ plasma the change of composition with power saturated at about 10 W, figure 4.11, confirming the greater reactivity of species in the latter treatment.

The effect upon film composition of varying plasma treatment duration was not as great as the effect of varying plasma treatment power, for both $O_2$ and $H_2O$ plasmas on both glass and SDT PET substrates. This indicates that an equilibrium is quickly established between surface modification, fresh surface exposure through ablation, and formation of a glassy oxidized plasma-resistant surface layer.

$O_2$ plasma treatment of films on SDT PET substrates yielded results unique from other combinations of plasma gas and substrate: the proportion of Zr at the film surface increased by 6 %, whereas this quantity remained unchanged for other treatments; the power and duration for greatest modification were the lowest values used (2 W and 0.5 min); at higher values than this the trend with power reversed and changed towards original film composition; at powers greater than 15 W the PET substrate appeared to be heat damaged; and finally, this treatment yielded the lowest carbon value observed and the greatest reduction in surface carbon content ($\Delta$%C=-16 %). More carbon is present at the surface of untreated films on SDT PET, accounting for the larger reduction in carbon content for this substrate during the more aggressive $O_2$ plasma treatment. Greater interaction of reactive oxygen plasma with organic substrate material also makes this treatment combination unique amongst those studied; films spin coated on SDT PET were thinner than those on glass and high power $O_2$ plasma treatment crinkled and embrittled the SDT PET substrate.

AFM investigation of the oxygen plasma treated film on SDT PET show the surface to be rough on a large scale, Figure 4.29, and relatively smooth on a smaller scale, Figure 4.30. The large scale topography is similar to siloxane films deposited by plasma enhanced CVD from HMDSO[66], which are reported to exhibit film stress and cracking.

The composition depth profile of both untreated and oxygen plasma treated $Zr(OBu)_4$ on glass indicates that a superficial hydrocarbon layer is present which is rich in carbon and poor in oxygen compared to the film bulk, figures 4.23 and 4.26. After removal of this contamination layer, the lower carbon and higher oxygen content of $O_2$ plasma treated $Zr(OBu)_4$ on glass persisted throughout the film thickness. No discontinuity in the depth profile was observed at the interface with the glass surface.

In the first 100 seconds of ion etching of untreated of $Zr(OBu)_4$ on glass, the high binding energy shoulder of O(1s) core lines diminished, figure 4.24, indicating that adsorbed water species or surface hydroxyl groups are preferentially removed. Zr(3d) and C(1s) spectra remained unchanged up to sputter times of about 250 seconds, after which these peaks broadened, through the creation of additional ion induced chemical environments.

The formation of an oxidized zirconium film on the surface of PET film reduced the substrate's gas permeability to oxygen and helium but not significantly to argon, Table 4.12. Barrier properties of polymer film are known to be improved by forming a continuous dense coating with low gas diffusion coefficient, or by blocking the sites of easiest diffusion through the polymer substrate[67-69]. The low barrier exhibited by oxygen plasma treated $Zr(OBu)_4$ films on SDT PET indicate that the oxide layer may be porous, cracked or have a coating component with high diffusion constant for the permeant gases, thus limiting its effectiveness as a gas barrier layer.

## 4.5 CONCLUSIONS

Treatment of the surface of $Zr(OBu)_4$ solid films in low pressure non-isothermal plasmas provides a novel low temperature alternative to conventional sol-gel calcination of ceramic precursors, allowing temperature sensitive organic substrates to be coated with an organic-inorganic composite film. The effect of a number of system parameters have been investigated, suggesting that oxygen radicals of a non-isothermal $O_2$ plasma are responsible for precursor film oxidation and alkoxy ligand removal. The highest level of film plasma surface chemical modification was achieved by $O_2$ plasma treatment of 2 W and 30 seconds duration; films treated at these conditions indicated a moderate decrease in permeability to $O_2$ and He gases. Future work using: other related precursors, such as zirconium tertiary butoxide; a combination of plasma treatment with moderate heating; and optimization of treatment conditions in terms of gas barrier performance may allow virtually all the film organic component to be removed, possibly creating competitive gas barrier coatings on polymer substrates.

## 4.6 REFERENCES

1. Wen J.; Wilkes, G. L. *J. Inorg. & Organometallic Polymers* **1995,** *5* 343.
2. Ritala, M.; Leskela, M. *Appl. Surf. Sci.* **1994,** *75,* 333.

3. Moles, P. J. *Catalysis Today* **1994**, *20*, R5.
4. Yamaguchi, T. *Catalysis Today* **1994**, *20*, 199.
5. Kim, J. S.; Marzouk, H. A.; Reucroft, P. J. *Thin Solid Films* **1995**, *254*, 33.
6. Kim, E.-T.; Yoon, S.-G. *Thin Solid Films* **1993**, *227*, 7.
7. Petitbon, A; Boquet, L.; Delsart, D. *Surf. Coatings Tech.* **1991**, *49*, 57.
8. Sherif, F. G. *Materials. Sci. & Eng. B - Solid State Materials* **1991**, *10*, 59.
9. Yoshitake, M.; Nosaka, T.; Okamoto, A.; Ogawa, S. *Thin Solid Films* **1993**, *230*, 482.
10. Choi, J.-H.; Kim, H.-G.; Yoon, S.-G. *J. Materials Science: Materials In Electronics* **1992**, *3*, 87.
11. Severin, K. G.; Ledford, J. S.; Torgerson, B. A.; Berglund, K. A. *Chem. Mater.* **1994**, *6*, 890.
12. Bradley, D. C. *Chem. Rev.* **1989**, *89*, 1317.
13. Bradley, D. C.; Mehrota, R. C.; Gaur, P. D. "*Metal Alkoxides*," Academic Press: London, 1978.
14. Sanchez, C.; Livage, J.; Henry, M.; Babonneau, F. J. *Non-crystalline Solids* **1988**, *100*, 65.
15. Bradley, D. C. *Nature* **1958**, *182*, 1211.
16. Bradley, D. C.; Mehrota, R. C.; Swanwick, J. D.; Wardlaw, W. *J. Chem. Soc.* **1953**, 2025.
17. Bradley, D. C.; Hillyer, W. *Trans. Farad. Soc.* **1966**, *62*, 2374.
18. Bradley, D. C.; Hillyer, W. *Trans. Farad. Soc.* **1966**, *62*, 2378.
19. Beer, H. F. *PhD Thesis*, Department of Chemistry, University of Durham, **1985**.
20. van Hardeveld, R. M.; Gunter, P. L. J.; van Ijzendoorn, L. J.; Wieldraaijer, W.; Kuipers, E. W.; Niemantsverdriet, J. W. *Applied Surface Science* **1995**, *84*, 339.
21. Seah, M. P. in "Practical Surface Analysis by Auger and X-ray Electron Spectrsocopy," 1st Edition, Ed. Briggs, D.; Seah, M. P., John Wiley & Sons, N. Y., 207, **1983**.
22. Royston, A. "XPSMin," data analysis program, Department of Chemistry, University of Durham, Durham, UK, 1988.
23. Clark, D. T.; Dilks, A. *J. Polym. Sci. Polym. Chem. Ed.* **1978**, *16*, 991.
24. Cocke, D. L.; Owens, M. S. *Appl. Surf. Sci.* **1988**, *31*, 471.

25. Barker, C. P.; Kochem, K.-P.; Revell, K. M.; Kelly, R. S. A.; Badyal, J. P. S. *Thin Solid Films* **1995**, *257*, 77.
26. Barker, C. P.; Kochem, K.-P.; Revell, K. M.; Kelly, R. S. A.; Badyal, J. P. S. *Thin Solid Films* **1995**, *259*, 46.
27. O'Hanlon, J. F. "A User's Guide To Vacuum Technology," 2nd Edition, J. Wiley & Sons, N. Y., **1989**.
28. Nanoscope III System Manual, Digital Instruments, Inc., santa Barbara, CA.
29. Miller, J. B.; Bernasek, S. L.; Schwartz, J. *J. Am. Chem Soc.* **1995**, *117*, 4037.
30. Eshelman, L. M.; de Jong, A. M.; Niemantsverdriet, J. W. *Catalysis Lett.* **1991**, *10*, 201.
31. Haasch, R. T.; Evans, J. F. *J. Vac. Sci. Tech.* **1988**, *6*, 1074.
32. Tarlov, M. J.; Evans, J. F.; Newman, J. G. *Appl. Surf. Sci.* **1993**, *64*, 115.
33. Wellbrock, U; Beier, W.; Frischat, G. H. *J. Non-Crystalline Solids* **1992**, *147*, 350.
34. Hsish C.-W.; Chiang, A. S. T.; Lee, C. C.; Yang, S. J. *J. Non-Crystalline Solids* **1992**, *144*, 53.
35. Schneider H; Voll, D.; Saruhan, B; Sanz, J.; Schrader, G.; Ruscher, C.; Mosset, A. *J. Non-Crystalline Solids* **1994**, *178*, 262.
36. Lynch, C. T.; Mazdiyasni, K. S.; Smith, J. S.; Crawford, W. J. *Anal. Chem.* **1964**, *36*, 2332.
37. Soraru, G. D.; Ravagni, A.; Dalmaschio, R.; Carturan, G.; Babonneau, F. *J. Mat. Res.* **1992**, *7*, 1266.
38. Livage, J.; Babonneau, F.; Sanchez, C. In "*Inorganic and Organometallic Oligomers and Polymers*," Editors Harrod, J. F.; Laine, R. M., Kluwer Academic Publishers, Dordrecht, **1991**, 217.
39. Schubert, U.; Hüsing, N.; Lorenz, A. *Chem. Mater.* **1995**, *7*, 2010.
40. Ueda, H. *J. Polym. Sci.: Part A: Polym. Chem.* **1989**, *27*, 263.
41. Mehrota, R. C. *Mater. Res. Soc. Symp.* **1988**, *121*, 81.
42. Gunji, T.; Goto, H.; Kimata, Y.; Nagao, Y.; Misono, T.; Abe, Y. *J. Polym. Sci.: Part A: Polym. Chem.* **1992**, *30*, 2295.
43. Lin, K.-L.; Wang, H.-C. *J. Mater. Sci.* **1988**, *23*, 3666.
44. Kumazawa, H.; Hori, Y.; Sada, E. *The Chem. Eng. J.* **1993**, *51*, 129.
45. Meyerhofer, D. *J. Appl. Phys.* **1978**, *49*, 3993.

46. Chinn, D.; Janata, J. *Thin Solid Films* **1994**, *252*, 145.

47. Klein, L. C. In *"Thin Film Processes II,"* Editors Vossen, J; Kern, L., Academic Press, Inc.: San Diego, **1991**, 501.

48. Bradley, D. C. *Phil. Trans. R. Soc. Lond.* **1990**, *A 330*, 167.

49. Palmer, D. M.; Straughan, B. P.; Treverton, J. A. *Appl. Surf. Sci.* **1993**, *68*, 243.

50. Moles, P. J, *J. Adh. Sci Tech.* **1992**, *6*, 61.

51. Moles, P. J, 2 *J. Oil and Colour Chemists Assoc.* **1989**, *72*, 301.

52. Comyn, J. *Int. J. Adhesion and Adhesives* **1994**, *14*, 109.

53. Wang, Y. M.; Li, Y. S.; Wong, P. C.; Mitchell, K. A. R. *Appl. Surf. Sci.* **1993**, *72*, 237.

54. Khawaja, E. E.; F. Bouamrane, F.; Hallak, A. B.; Daous, M. A.; Salim, M. A. J. Vac. Sci. Tech. **1993**, *A11*, 580.

55. Wong, P. C.; Li, Y. S.; Zhou, M. Y.; Mitchell, K. A. R. *Appl. Surf. Sci.* **1995**, *89*, 255.

56. Li, Y. S.; Wong, P. C.; Mitchell, K. A. R. *Appl. Surf. Sci.* **1995**, *89*, 263.

57. Eliasson, B.; Hirth, M.; Kogelschatz, U. *J. Phys. D: Appl. Phys.* **1987**, *20*, 1421.

58. Rossnagel, S. M. In *"Thin Film Processes II,"* Editors Vossen, J; Kern, L., Academic Press, Inc.: San Diego, **1991**, 34.

59. Frenck, H. J.; Oesterschulze, E.; Beckmann, R.; Kulisch, W.; Kassing, R. *Mater. Sci. & Eng.* **1991**, *A139*, 394.

60. Loy, D. A.; Shea, K. J.; Buss, R. J.; Assink, R. A. In "Inorganic and Organometallic Polymers" II Editors Wisian-Neilson, P.; Allcock, H. R.; Wynne, K. J., ACS Symp. Series: Washington D. C., ACS, **1994**, *572*, 122.

61. Breitbarth, F.-W.; Bald, J.; Rodemeyer, S.; Suhr, H. *Plasma Chem. & Plasma Processing* **1993**, *13*, 289.

62. Deshpandey, C. V.; Bunshah, R. F. In *"Thin Film Processes II,"* Editors Vossen, J; Kern, L., Academic Press, Inc.: San Diego, **1991**, 121.

63. Grill, A. *"Cold Plasma In Material Fabrication"*; IEEE Press: New York, **1993**, 203.

64. Kramer, P. W.; Yeh, Y.; Yasuda, H. *J. Membr. Sci.* **1989**, *46*, 1.

65. Park, N. Y.; Kim, N. in "Plasma Polymerization and Plasma Interactions With Polymeric Materials" Editor Yasuda, H. K.: J. Wiley & Sons; N. Y., **1990**, 91.

66. Fonseca, H. PhD Thesis, Durham **1993**.

67. Mercea, P.; Muresan, L.; Mercea, V.; Silipas, D. *J. Membrane Sci.* **1988**, *35*, 291.

68. Beu, T. A.; Mercea, P.-V. *Mater. Chem. & Physics* **1990**, *26*, 309.

69. Mercea, P.-V.; Bartan, M. *J. Membrane Sci.* **1991**, *59*, 353.

# Chapter Five : Plasma Modification Of Polyphenylsilsesquioxane Films

---

## 5.1 INTRODUCTION

In addition to their widely applied bulk attributes[1], organopolysiloxanes exhibit surface properties which make them useful as friction[2] and adhesion[3] modifiers, biomaterials[4], contact lens coatings[5,6], and in microelectronics as plasma etch resists[7-11]. Exposure of siloxanes to non-isothermal oxygen plasmas forms an oxygen-impermeable silica layer of 5 nm to 300 nm thickness, depending on plasma pressure and siloxane structure[8-11].

PVD[12] and PECVD[13,14] silica coatings as thin as 60 nm on polymer substrates exhibit extremely low oxygen permeability and have been developed as commercial gas barrier films. A threefold increase in oxygen barrier was reported for plasma treated PECVD siloxane films on polyethylene[15] indicating good potential for the presently studied process in which a solid siloxane film coating is plasma treated to yield a gas barrier film.

Polyphenylsilsesquioxane (PPSQ), Figure 5.1, is a highly cross-linked siloxane 'ladder-polymer'. PPSQ was selected as a promising solid precursor to $SiO_2$ gas barrier films for a number of reasons: pendant phenyl carbon atoms are highly susceptible to oxidative attack by oxygen plasma treatment[16]; the precursor backbone is already composed of crosslinked $SiO_2$ groups which are desirable for dense oxide gas barrier coating; and the ladder structure confers great stability against degradation of the polymer by chain scission[17,18].

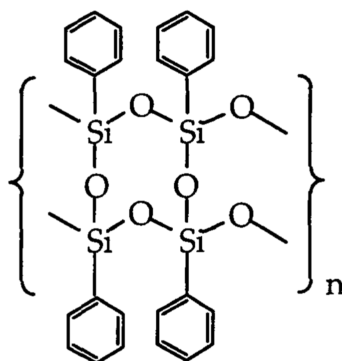


Figure 5.1 Ladder structure of polyphenylsilsesquioxane (PPSQ).

$O_2$ plasma modification of PPSQ films coated on polyester has been studied for various treatment conditions, and the gas barrier properties of the resultant coated film have been tested.

## 5.2 EXPERIMENTAL

Polyphenylsilsesquioxane (PPSQ) (Fluorochem, molecular weight 1600, high ladder content), Figure 5.1, was dissolved in toluene (analytical grade, Aldrich) by heating to 90°C for four hours. The saturated solution concentration was 0.9 ± 0.5 % weight/volume, as determined by the difference between the mass of undissolved solute and the total mass of PPSQ added to a known volume of toluene. PPSQ toluene solution was coated either by spin coating, as described in Section 4.2.3, or by evaporation in air of four drops of PPSQ solution. 50 mm x 7 mm strips of two substrate types were used: polyethyleneterephthalate (PET, ICI), 100 μm thickness, which was ultrasonically cleaned for 30 seconds in a mixture of propan-1-ol and cyclohexane (a polar and a non-polar solvent); and ultrasonically cleaned PET which had been treated for 30 seconds in a home built silent discharge reactor, Section 2.2, with an electrode gap of 3 mm and a voltage of 8.6 kV. PPSQ film thickness was estimated by weighing uncoated substrates, spin coated films on PET and evaporated films on PET.

PET substrates coated with PPSQ were treated inside and outside the glow region of an inductively coupled plasma, Section 2.2, at systematically varied levels of radio frequency (rf) power, duration and pressure. Silent discharge treatments of PPSQ films on PET were performed in a home built reactor, Section 2.2, with an electrode gap of 3 mm and a voltage of 8.6 kV for different treatment durations.

XPS analysis of untreated and plasma treated bulk PPSQ powder and spin coated films was performed. The XPS photoelectron take off angle was varied to gain depth information from plasma treated films. Gas permeability of untreated and $O_2$ plasma treated PET spin coated with PPSQ was measured using a laboratory built mass spectrometric method[19], Section 4.2.5.

## 5.3 RESULTS

The difference in mass of 2 $cm^2$ PET substrates before and after coating with toluene solution of PPSQ by spin coating was below the lower detectable limit of the electronic balance, and by evaporation coating was 0.33 ± 0.17 mg. The spin coated film was estimated to be less than 0.2 μm thick, and the evaporated film was estimated to be 1.35 ± 0.7 μm thick, using a PPSQ density value of 1.3 $g/cm^3$[20].

XPS analysis of PPSQ powder showed the surface to be richer in oxygen and poorer in carbon than predicted by the polymer's theoretical structure, Figures 5.2-5.4. The photoelectron signal intensity from powder PPSQ was low due to strong inelastic electron scattering from the rough powder surface. C(1s) spectra, Figure 5.5, showed a single $\underline{C}_xH_y$ environment with 9.1% $\pi$–$\pi^*$ shake-up intensity. Si(2p) and O(1s) peaks, Figure 5.6 and 5.7, were at 103.2 ± 0.02 eV and 532.6 ± 0.02 eV respectively, as expected for silsesquioxane $SiO_{3/2}$ groups[21].

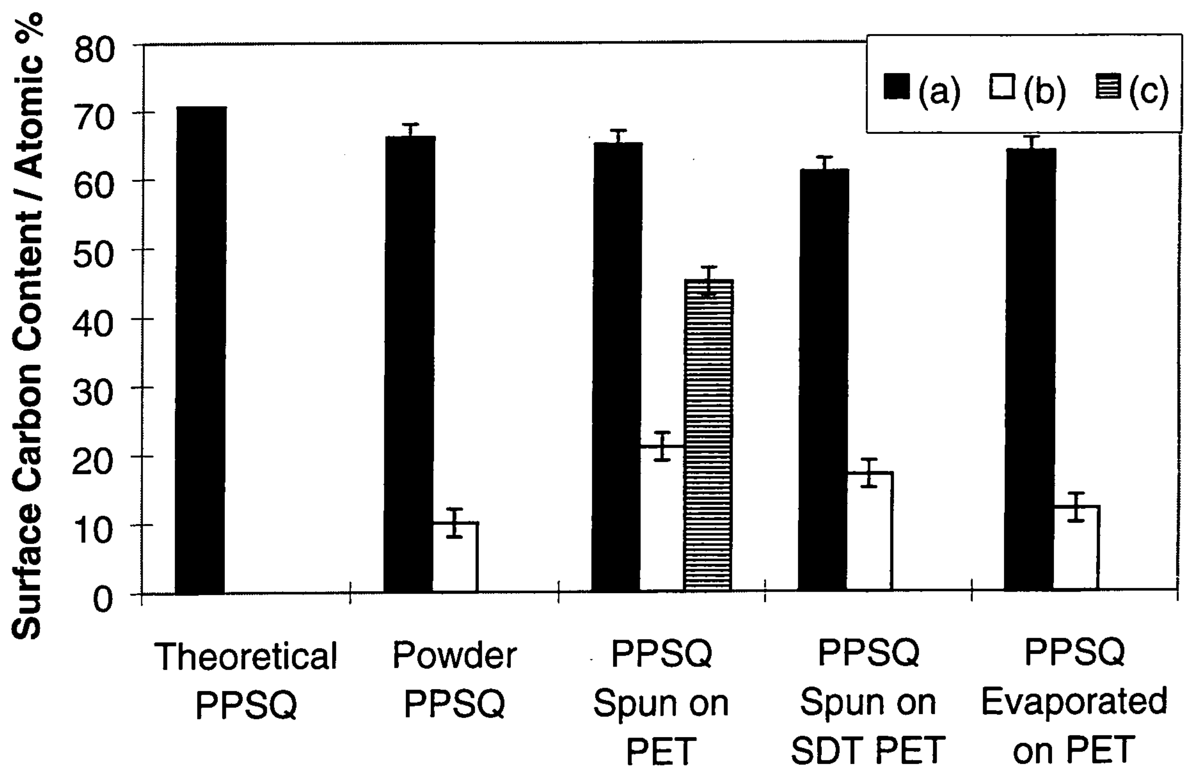


Figure 5.2 Surface % carbon for (a) untreated, (b) oxygen plasma treated, and (c) silent discharge treated PPSQ.

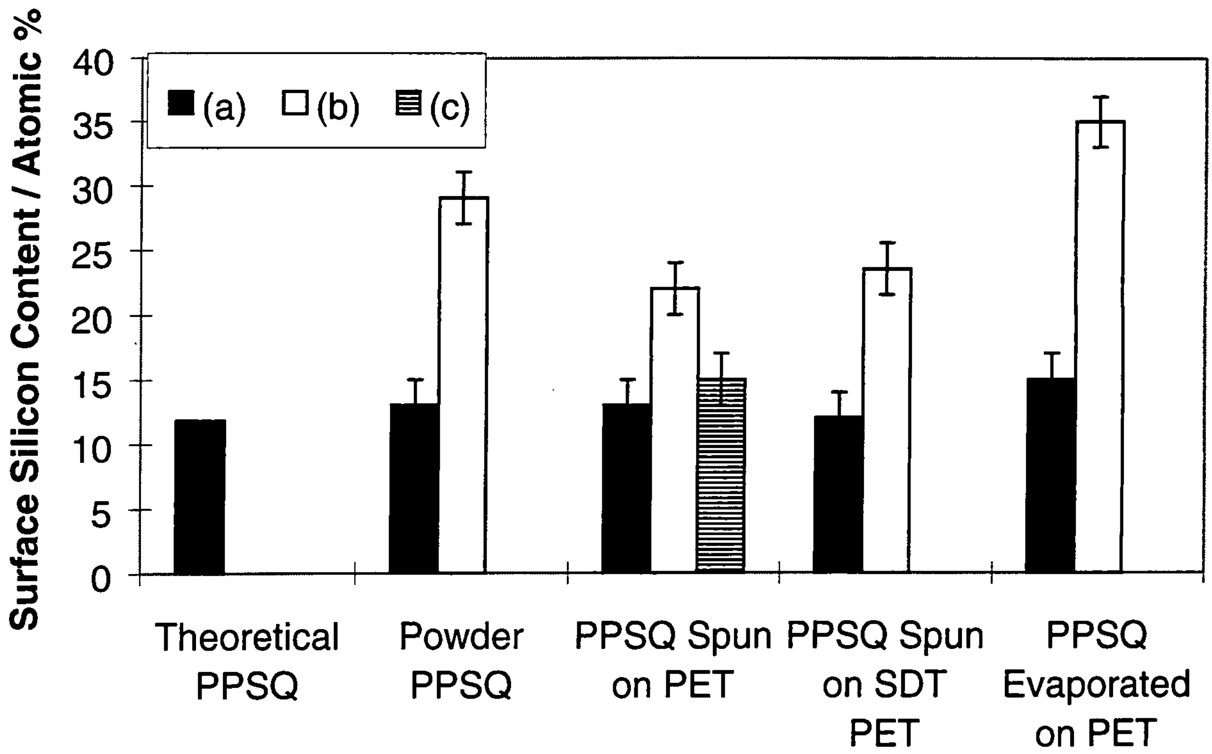


Figure 5.3 Surface % silicon for (a) untreated, (b) oxygen plasma treated, and (c) silent discharge treated PPSQ.

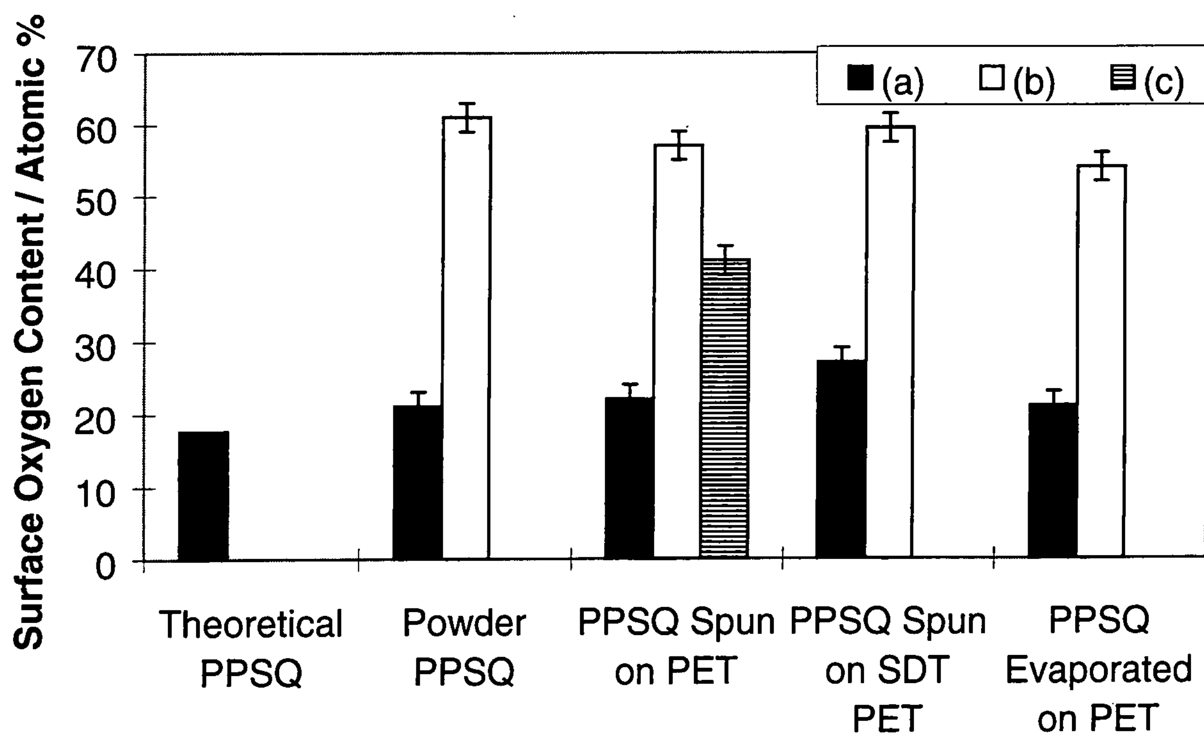


Figure 5.4 Surface % oxygen for (a) untreated, (b) oxygen plasma treated, and (c) silent discharge treated PPSQ.

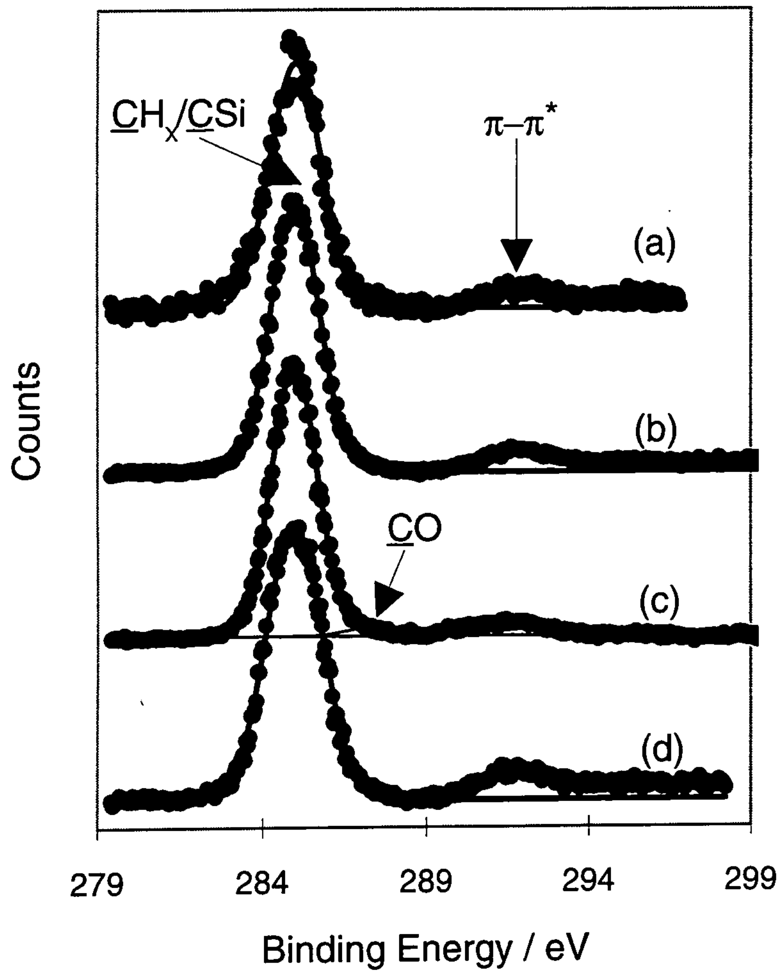


Figure 5.5 C(1s) spectra of untreated PPSQ: (a) powder; (b) spin coated on PET; (c) spin coated on SDT PET; and (d) evaporated on PET.

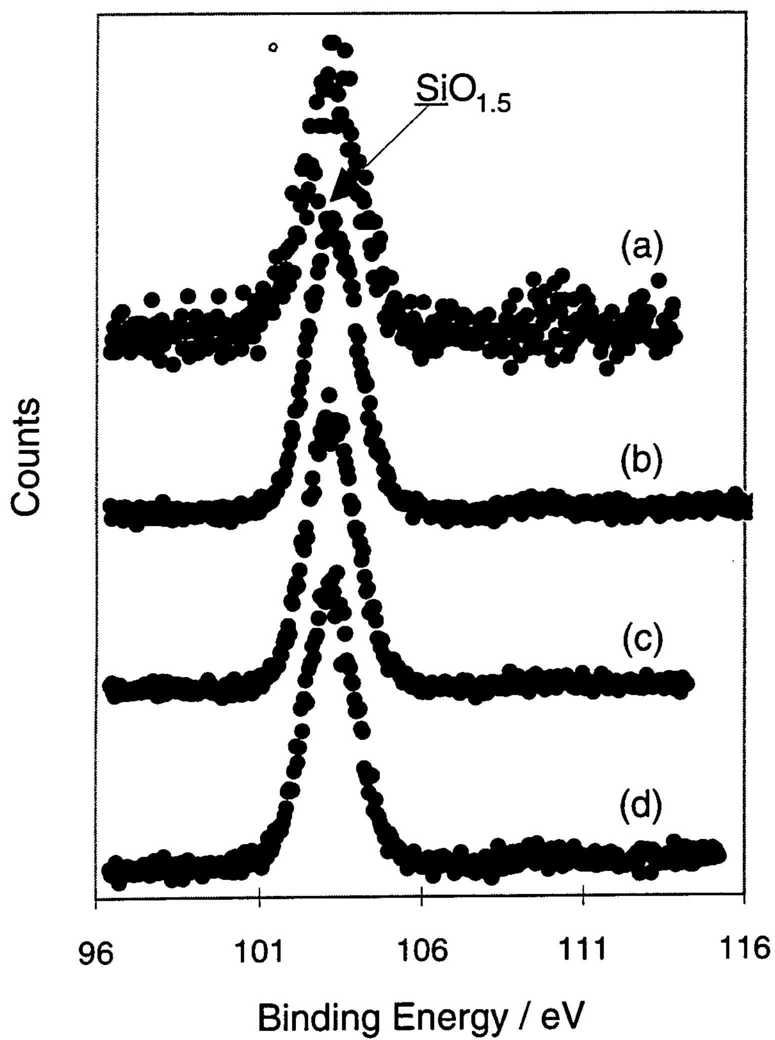


Figure 5.6 Si(2p) spectra of untreated PPSQ: (a) powder; (b) spin coated on PET; (c) spin coated on SDT PET; and (d) evaporated on PET.

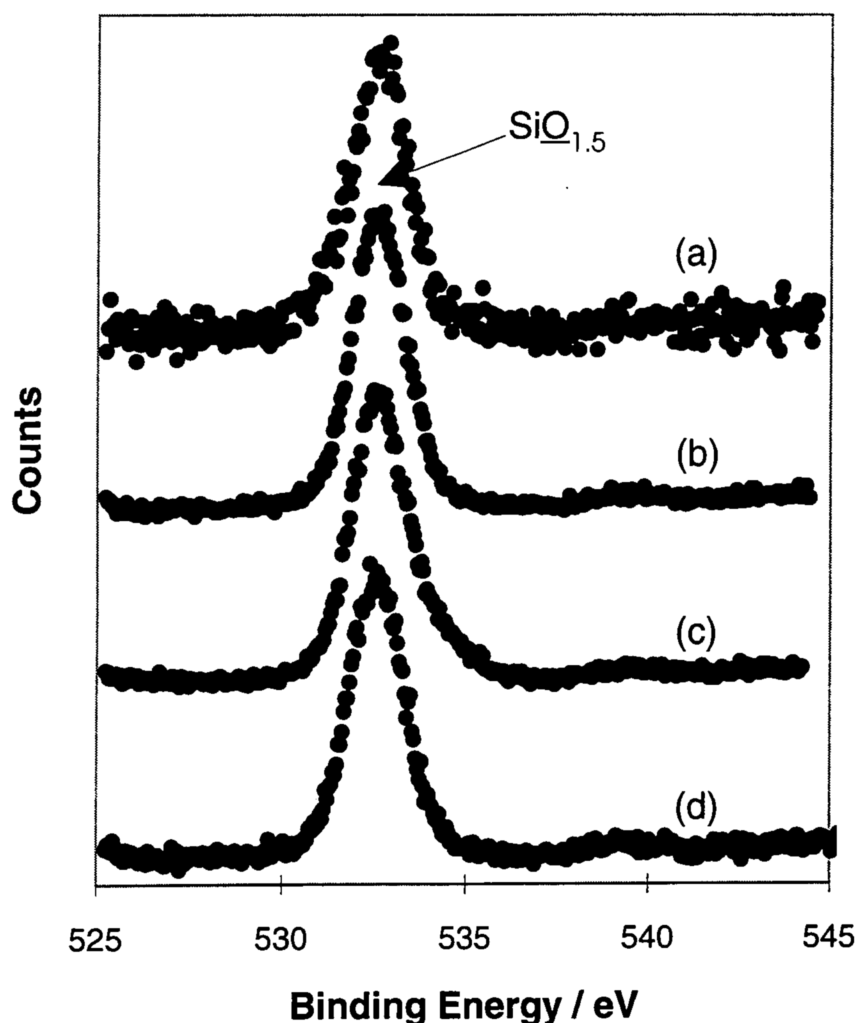


Figure 5.7 O(1s) spectra of untreated PPSQ: (a) powder; (b) spin coated on PET; (c) spin coated on SDT PET; and (d) evaporated on PET.

Films spin coated on solvent cleaned PET and silent discharge treated (SDT) PET, and films evaporated on clean PET, showed peaks only for carbon, silicon, and oxygen. The surface composition of PPSQ films spin coated and evaporated on untreated PET did not differ significantly from that of the surface composition of PPSQ powder, however, spin coated PPSQ films on SDT PET had lower carbon and higher oxygen contents, Figures 5.2 and 5.4. C(1s) spectra of PPSQ films spin coated on silent discharge treated (SDT) indicated that the pretreated polymer substrate interacted with the PPSQ coating resulting in a small proportion of surface oxidized carbon groups and 5 ± 1 % C(1s) $\pi$–$\pi^*$ shake up intensity, Figure 5.5(c). In contrast, the C(1s) spectrum of PPSQ spin coated on untreated PET showed a single C-H/C-Si carbon environment and 10 ± 1 % C(1s) $\pi$–$\pi^*$ shake up intensity Figure 5.5(b). XPS data from PPSQ films coated on

untreated PET substrates closely matched those of powder PPSQ, and so this substrate type was used in subsequent studies of PPSQ film plasma treatment. The PPSQ film XPS peak binding energies for O(1s), 532.6 ± 0.1 eV, and Si(2p), 103.2 ± 0.1 eV, did not differ for the two coating methods nor for different substrate preparations.

The surface of PPSQ powder, $O_2$ plasma treated for 2 minutes at a power of 20W, contained 56% less carbon, 16% more silicon and 40% more oxygen than untreated PPSQ powder, Figures 5.2-5.4. C(1s) spectra of $O_2$ plasma treated PPSQ powder, Figure 5.8(a), showed a broad range of oxidized functionalities and complete absence of a $\pi$–$\pi^*$ shake up peak, and the $O_2$ plasma treated PPSQ Si(2p) and O(1s) peak binding energies were higher than those of untreated PPSQ powder spectra by 0.8 ± 0.1 eV and 0.4 ± 0.1 eV respectively.

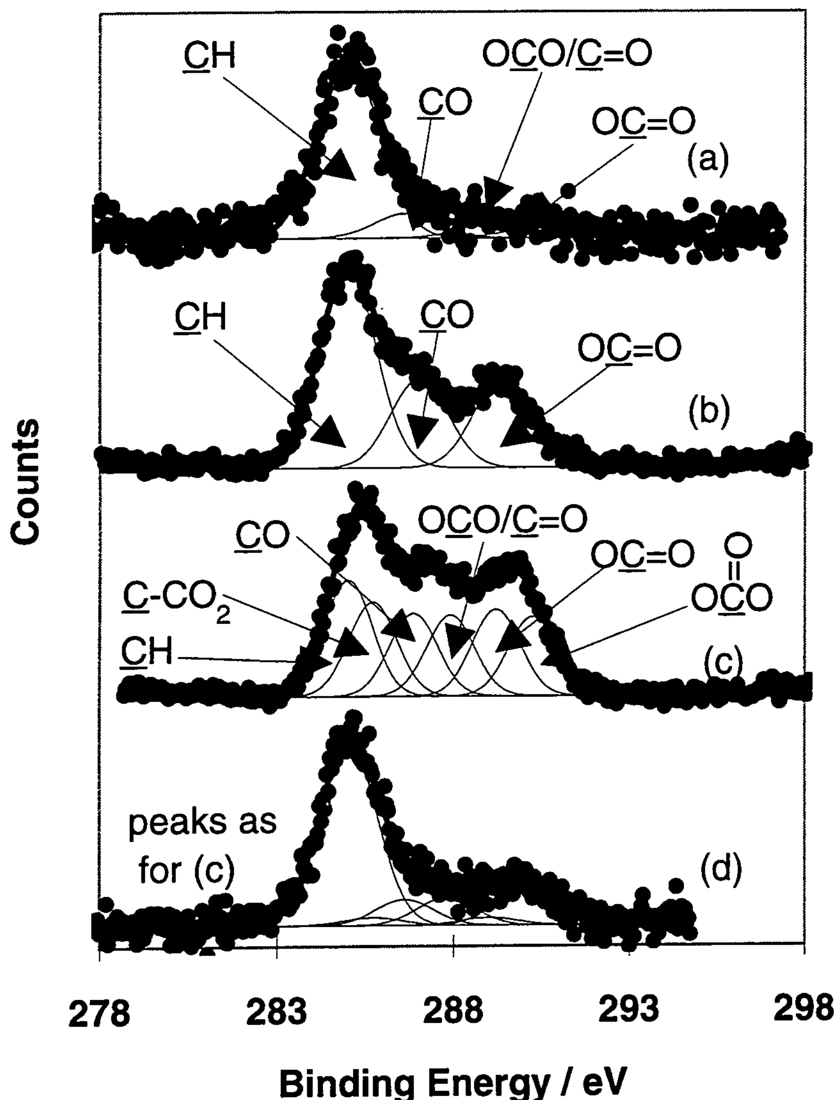


Figure 5.8 C(1s) spectra of $O_2$ plasma treated PPSQ: (a) powder; (b) spin coated on PET; (c) spin coated on SDT PET; and (d) evaporated on PET.

C(1s) spectra of $O_2$ plasma treated PPSQ spin coated on PET, figure 5.8(b), and on SDT PET, figure 8(c), match well with the C(1s) spectra for bare PET and bare SDT PET, section 3.2, suggesting that the spin coated PPSQ is removed from these substrates during $O_2$ plasma treatment. $O_2$ plasma treatment of spin coated and evaporated PPSQ films modified surface composition, Figures 5.2-5.4, and O(1s) and Si(2p) core level binding energies, by amounts similar to those for PPSQ powder, whilst silent discharge treatment had a lesser effect. The greatest change in surface composition was observed for $O_2$ plasma treatment of PPSQ films evaporated on untreated PET.

The extent of $O_2$ plasma modification of PPSQ films, both spun and evaporated on PET, peaked at approximately 20 W plasma power, Figures 5.9 and 5.10. C(1s) spectra of $O_2$ plasma treated spin coated PPSQ films showed a large proportion of oxidized carbon, Figure 5.8(b) and 5.8(c), relative to the C(1s) spectrum of $O_2$ plasma treated evaporated PPSQ, Figure 5.8(d). O(1s) spectra of oxygen plasma treated PPSQ films evaporated on untreated PET indicated the presence of two resolved environments present in roughly equal proportions, Figure 5.11.

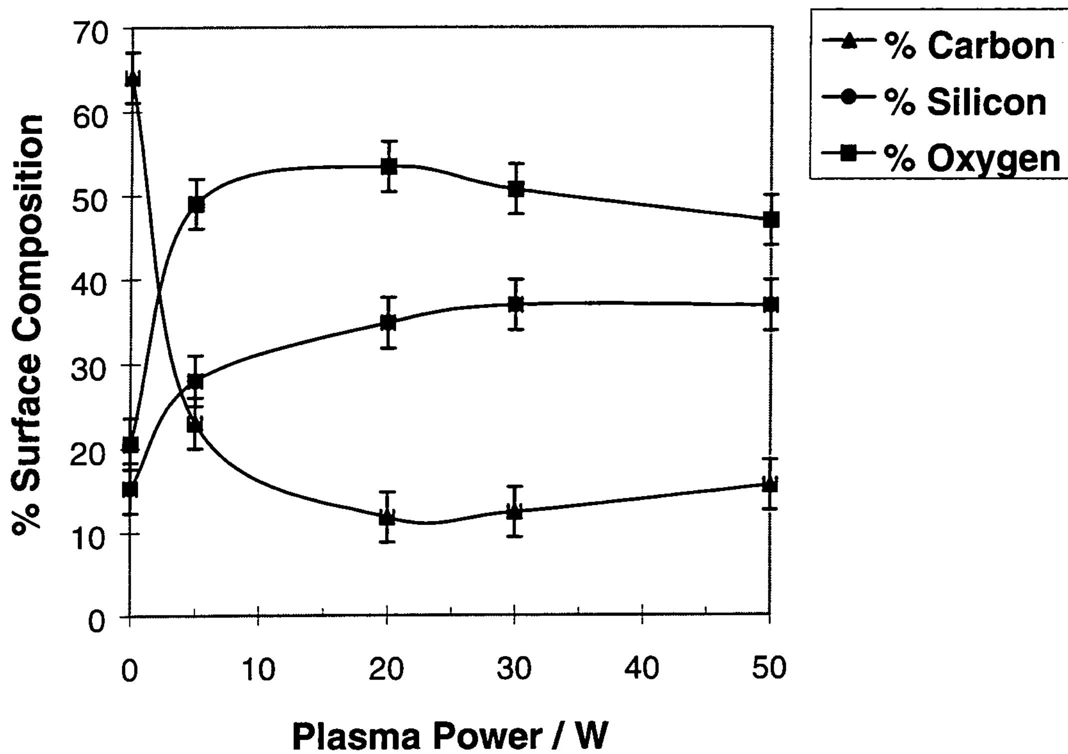


Figure 5.9 Composition of PPSQ evaporated on PET as a function of $O_2$ plasma treatment power.

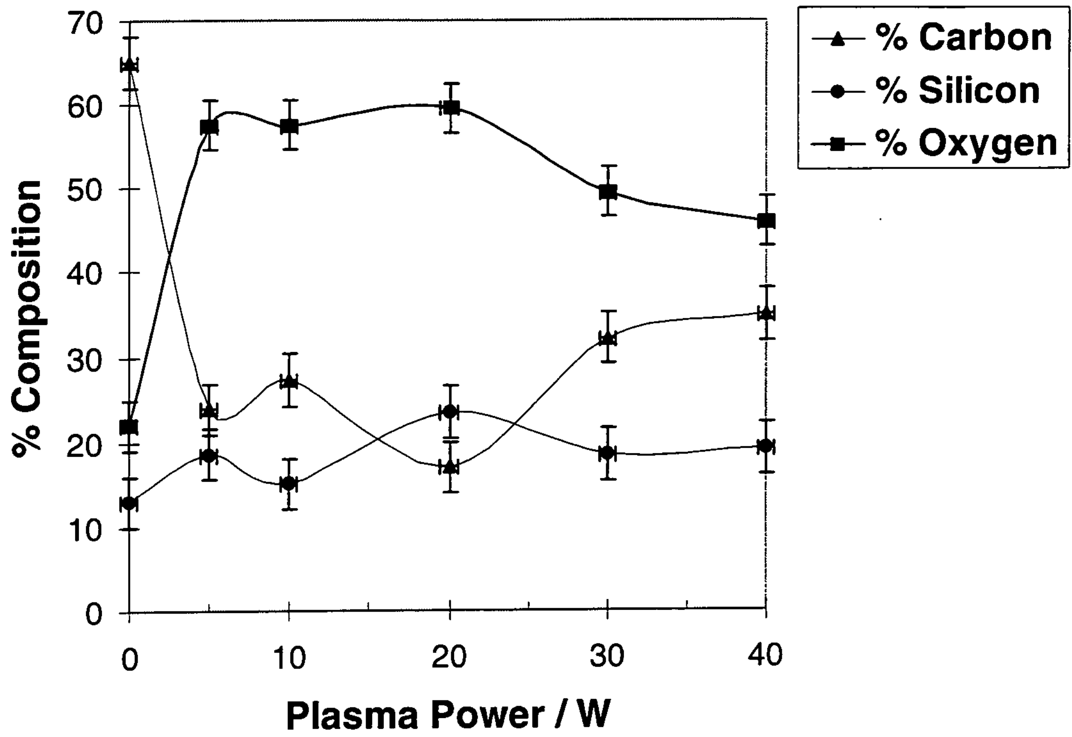


Figure 5.10 Composition of PPSQ spin coated on PET as a function of $O_2$ plasma treatment power.

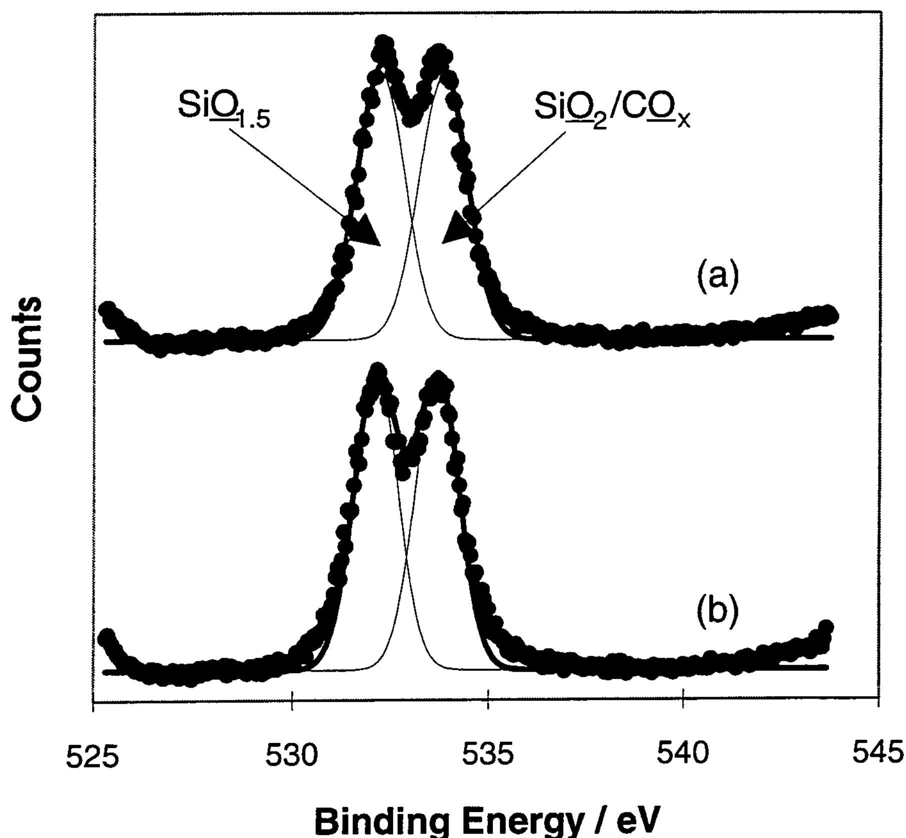


Figure 5.11 O(1s) XPS spectra of PPSQ evaporated on untreated PET and $O_2$ plasma treated at RF powers of (a) 20 W and (b) 30 W.

The composition of PPSQ films spin coated on PET, which were $O_2$ plasma treated for durations between 2 min and 10 min did not differ; surface modification is insensitive to duration in this range, in contrast to its strong dependence on plasma power.

PPSQ films evaporated on untreated PET, $O_2$ plasma treated at 50 W for 2 min and analyzed by XPS at 15°, 30°, and 45° electron take off angles, indicated that degree of film oxidation was greater at the film surface, and that more carbon remained from PPSQ molecules in the film subsurface, Table 5.1. O(1s) spectral lineshapes of 50 W treated samples varied considerably with electron take off angle, Figure 12: at 15° a single oxygen environment was observed at a binding energy of 532.9 ± 0.1eV; at 30° two environments were present at binding energies of 532.2 ± 0.1 eV and 533.8 ± 0.1 eV; and at 45° an asymmetric O(1s) peak indicated the presence of two environments at 532.3 and 533.6 eV in the ratio 1 to 0.9. These O(1s) binding energies correspond to $Si\underline{O}_{1.5}$ and $Si\underline{O}_2/C\underline{O}_x$

environments[21,22], respectively, and indicate that the less highly oxidized oxygen environment was dominant for the greatest electron take off angle, Figure 5.12(c), corresponding to deeper PPSQ film material.

| Sample | Electron Take-Off Angle | % C | % Si | % O |
|---|---|---|---|---|
| 50W 2min 0.2 mbar $O_2$ Plasma Treated | 15° | 13 | 29 | 58 |
| 50W 2min 0.2 mbar $O_2$ Plasma Treated | 30° | 16 | 37 | 47 |
| 50W 2min 0.2 mbar $O_2$ Plasma Treated | 45° | 19 | 31 | 50 |
| 50W 2min 0.5 mbar $O_2$ Plasma Treated | 30° | 17 | 33 | 50 |
| 50W 2min 0.5 mbar $O_2$ Plasma Treated | 45° | 18 | 30 | 51 |
| 50 W 2min 0.2 mbar $O_2$ Plasma Treated Outside Glow Region | 30° | 38 | 17 | 45 |

Table 5.1 Composition of $O_2$ Plasma Treated PPSQ films evaporated on PET analyzed at XPS electron take off angles of 15°, 30° and 45°.

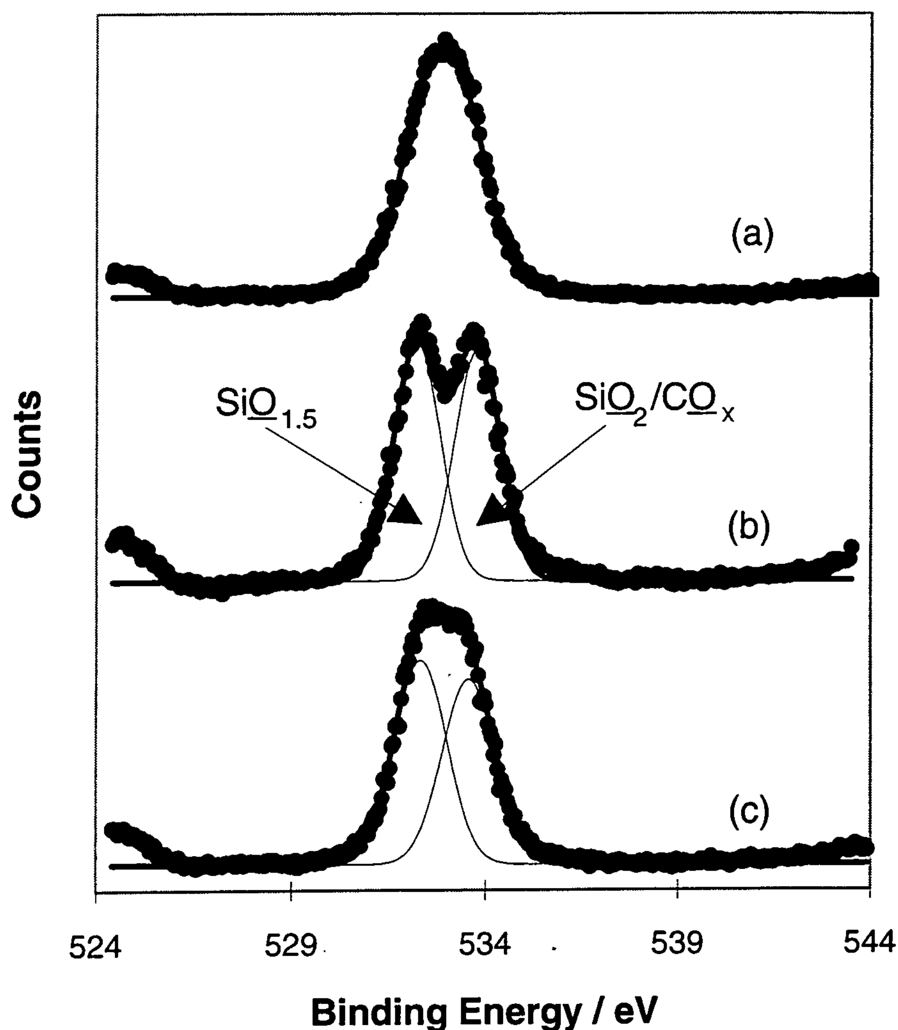


Figure 5.12 O(1s) XPS spectra of PPSQ evaporated on untreated PET and $O_2$ plasma treated at 50 W collected at electron take-off angles of (a) 15°, (b) 30°, and (c) 45°.

Analysis of films treated in 50 W $O_2$ plasmas at 0.2 mbar and 0.5 mbar indicated little variation in film composition with plasma treatment pressure in this range, Table 5.1. However, 45° electron take off angle O(1s) spectra showed a larger proportion of Si$\underline{O}_2$ environment for the higher pressure treatment, Figure 5.13, indicating that the depth of oxidative modification increased with plasma pressure in this range.

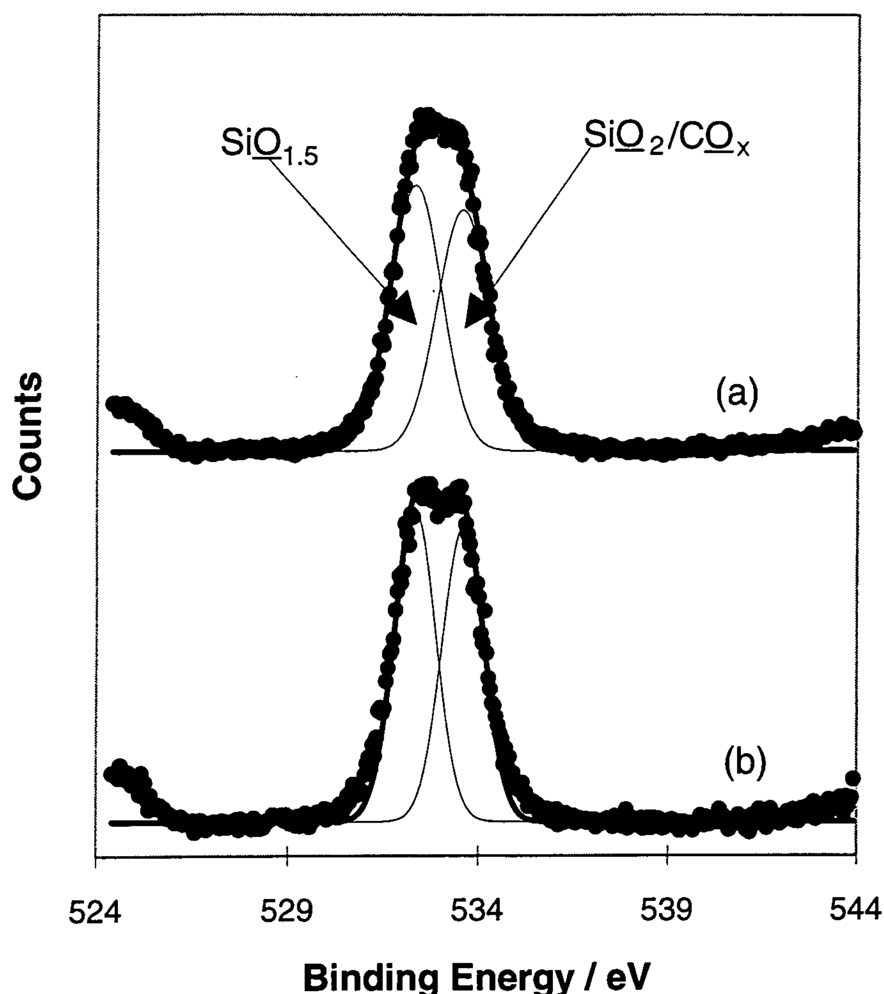


Figure 5.13 O(1s) XPS spectra collected at an electron take-off angle of 45° from PPSQ evaporated on untreated PET and $O_2$ plasma treated at 50 W in (a) 0.2 mbar $O_2$ and (b) 0.5 mbar $O_2$.

PPSQ films evaporated on PET and treated for 2 min in the downstream region of a 50 W $O_2$ plasma underwent less surface modification than for treatments inside the plasma glow, Table 5.1, demonstrating that a more reactive medium is present in the glow region.

Mean equilibrium partial pressures (MEPPPs) of oxygen, argon and helium permeant gases were measured for membranes of untreated PET and oxygen plasma treated PPSQ spin coated on PET, Table 5.2. $O_2$ plasma treated PPSQ coatings reduced oxygen and argon permeability of PET by 38% and 32% respectively, but did not significantly affect the helium permeability.

| Membrane | $O_2$ MEPPP /torr | Ar MEPPP /torr | He MEPPP /torr |
|---|---|---|---|
| Untreated PET | 0.160 ± 0.002 | 0.158 ± 0.06 | 7.32 ± 0.08 |
| $O_2$ Plasma Treated PPSQ on PET | 0.10 ± 0.02 | 0.108 ± 0.001 | 7.30 ± 0.6 |

Table 5.2. Mean equilibrium partial pressures of $O_2$, Ar and He for untreated PET and PPSQ evaporated on PET and $O_2$ plasma treated.

**5.4 DISCUSSION**

Films of PPSQ solution evaporated or spin coated on untreated PET showed the same composition, Figures 5.2-5.4, and C(1s), O(1s) and Si(2p) XPS spectral lineshapes, Figures 5.5-5.7, as PPSQ powder indicating that these film surfaces have the chemical structure of unmodified PPSQ. Films of PPSQ underwent some oxidative modification upon spin coating on silent discharge treated PET, Figures 5.2-5.4: reactive radicals introduced by silent discharge modification persist at the PET surface for a number of minutes after treatment[20], and react with phenyl groups in the spin coated PPSQ producing oxidized carbon products and reducing the amount of C(1s) $\pi-\pi^*$ shake-up intensity, Figure 5.5(c).

Si(2p) chemical shifts for $O_2$ plasma treatment of PPSQ were 0.8 ± 0.1 eV, corresponding to oxidation of silicon atoms from $SiO_{3/2}$ to $SiO_2$[21]. Oxygen plasma treatment of polyorganosiloxanes is reported in XPS[8], FTIR[9,23] and SIMS[5] studies, to cause progressive chemical modification of silicon atoms from organic R-Si-O environments to inorganic $SiO_2$ environments. The maximum level of oxygen plasma removal of siloxane hydrocarbon is reported to range from complete[11,23] to about 2/3 [7-9], compared with a maximum of 85% in this study, Figure 5.2. It has been proposed that oxygen ions are accelerated to the polymer surface and cleave Si-O and Si-C bonds, leaving radicals which trap and react with oxygen species from the plasma[11]. Plasma reactors usually used in such studies are of the RF diode etching type, in which high fluxes of ions, with energies in the range 50 to 200 eV, bombard samples placed on electrodes due to applied bias or self-bias[8]. In contrast, the inductively coupled plasma "asher" type reactor used in the

present study supplies to the sample surface a low ion flux[24] and a high flux of atomic oxygen atoms[25] and ultraviolet light[26].

The level of chemical modification in inductively coupled oxygen plasma treatment of phenyl ring containing organic polymer surfaces has been shown to depend upon the degree of $\pi$–$\pi$* shake-up in C(1s) XPS of the untreated polymer[15]; oxidation is hypothesized to proceed through atomic oxygen attack at phenyl ring sites excited by vacuum ultraviolet photons, section 3.4. PPSQ has all of its organic content in aromatic phenyl rings; $\pi$–$\pi$* shake-up electrons constitute 9% to 10% of the total C(1s) intensity, Figure 5.5, and shake-up peaks are also observed in Si(2p) spectra, Figure 5.6, and O(1s) spectra, Figure 5.7, indicating widely delocalized $\pi$-bonding in the polymer. Strong oxidative attack of phenyl rings in PPSQ is expected to break Si-C bonds, oxidizing silicon to $SiO_2$ and phenyl rings to smaller volatile fragments: the cessation of $CO_2$ optical emission has been used as an end point detector in $O_2$ plasma treatment of PPSQ gels[23].

Treatments performed 10 cm downstream from an inductive resonance coil, where atomic oxygen concentration is approximately 60% of that in the glow region[27] and vacuum ultraviolet radiation is also present[28], effected 66% of the hydrocarbon removal achieved in the glow region, Table 5.1, confirming that these two reactive components account for the majority of chemical modification. Variation of $O_2$ plasma power did not affect the level of chemical modification above a threshold value of about 20 W, Figures 5.9 and 5.10; a superficial $SiO_2$ layer formed by plasma oxidation at this power may prevent further reaction of subsurface PPSQ phenyl groups with increased concentrations of reactive species[11].

2 minutes $O_2$ plasma treatment of PPSQ films spin coated on PET and SDT PET yielded C(1s) spectra, Figure 5.8(b) and 5.8(c), which match those of the bare and SDT treated substrate surfaces, Chapter 3, Figure 3.1(a); the PPSQ film coverage appeared to be incomplete after plasma treatment. $O_2$ plasma etch rate of siloxanes at < 1 mTorr is approximately 50 nm / min[11] which may cause partial removal of the film. Alternatively, the large difference in density between untreated siloxane (1.3 g/cm$^3$) and silica (2.21 g/cm$^3$)[29] may cause extensive cracking of the thin film exposing low barrier substrate material between cracks[15].

In either case, such treated films would be unsuitable as gas barrier coatings. Evaporated films, 1.35 ± 0.7 μm thick, allowed $O_2$ plasma modification to proceed without apparent substrate exposure, Figure 5.8(d).

The thickness of the oxide layer created by $O_2$ plasma treatment of siloxanes is reported to depend on plasma pressure and siloxane structure; oxide growth is limited by atomic oxygen diffusion through the silica layer created and by diffusion into the siloxane polymer[11]. Oxygen plasma treatment of silicon containing polymer resists forms an oxide layer with a dynamic steady state thickness of 1 to 5 nm, as surface sputter rate is balanced by further oxidation[8,9]. Treatment of a polysiloxane of type $MeSiO_{1/2}$ in plasma pressures below 0.1 Torr is reported to produce a silica layer 7 nm thick, whilst increased content of cross-linked $RSiO_{3/2}$ groups or bulky phenyl side groups, both fully present in PPSQ, decreased the oxide thickness[11].

XPS spectra of 50 W $O_2$ plasma treated evaporated PPSQ films taken at electron take off angles of 15° and 30° yielded O/Si elemental ratios of 2.0 and 1.6 respectively, evidencing more extensive silicon oxidation at the outermost surface of the treated polymer, Table 5.1. The 15° electron take off angle O(1s) spectra showed a single peak at 532.9 eV, whilst the 30° O(1s) spectrum showed two peaks at energies for $SiO_{3/2}$ and $SiO_2$, confirming the presence of less highly oxidized silicon atoms deeper into the treated PPSQ film, Figure 5.12. These data indicate that full oxidation to $SiO_2$ occurred to a thickness less than the XPS sampling depth of ~ 5 nm, or three elastic mean free paths[8]. An oxide layer thickness calculation from angular dependent XPS data, as described for thermal oxidation of elemental silicon[30], is prohibited in this case by the small Si(2p) chemical shift for $SiO_{3/2}$ changing to $SiO_2$. Plasma treatments at 0.5 mbar yielded films with the same elemental composition as for films treated at 0.2 mbar for both 30° and 45° electron take off angle, however, the 45° take off angle O(1s) spectra for 0.2 mbar treatments showed a greater content of $SiO_{1.5}$ component than for 0.5 mbar treatments; the interface between the oxide layer and unmodified PPSQ was deeper in films treated at a higher pressure, inkeeping with previously proposed diffusion controlled oxidation[11].

PPSQ is reported to be more permeable and less perm-selective to $O_2$, $N_2$, $CO_2$ and $CH_4$ than expected from its high Tg and ladder structure[31]. The 38%

decrease in $O_2$ permeability of PET upon PPSQ coating and $O_2$ plasma treatment is about half the decrease reported for high density polyethylene (HDPE) substrate coated by PECVD using tetramethyldisiloxane and subsequently $O_2$ plasma treated[15], possibly due to the higher initial $O_2$ permeability of the HDPE, and possibly due to a denser, more highly cross-linked siloxane film deposited by PECVD. Silica coatings about 60 nm thick, deposited by electron beam evaporation of quartz, reactive sputtering of silicon and PECVD from organosiloxane monomers, have been employed commercially as oxygen barrier coatings on polymer substrates[12,13]. The decrease in the $O_2$ permeability of PET for such coatings is typically greater than two orders of magnitude and approaches that for single side aluminized PET[13]. The thinness or the discontinuity of the $SiO_2$ layer created at siloxane surfaces by $O_2$ plasma treatment forms a less effective gas barrier than $SiO_x$ coatings deposited by evaporation or CVD: firstly, oxide thickness may be limited to a few nanometers of the PPSQ coating presenting only a thin barrier layer; and secondly, cracks may appear in the silica layer to compensate for the near doubling of density upon modification from PPSQ to $SiO_2$ [15,20]. The absence of a change in helium permeability for the treated coating indicates that physical diffusion paths smaller than required by oxygen molecules may remain in the treated film surface.

Plasma modified silicon polymers tend to recover their original surface properties[32-36], full recovery taking from days to months depending upon polymer molecular weight, degree of cross-linking and storage conditions[35,36]. Minimization of free energy at the treated surface-air interface drives: elimination of polar groups by condensation of silanol groups[32]; reorientation of surface polar groups towards the subsurface[32,36]; and long range migrations of unmodified macromolecules to the surface[32,33,36]. $O_2$ plasma treated PPSQ is subject to these dynamics; its high degree of cross linking hinders recovery[37], whilst any cracks present in the treated layer provide easy migration paths for untreated PPSQ to reach the surface[33,34].

## 5.5 CONCLUSIONS

$O_2$ plasma treatment of PPSQ films coated on PET resulted in removal of up to 85% of silsesquioxane hydrocarbon content and oxidation of surface silicon atoms. The resultant silica-like film was thinner than the ~ 5 nm XPS sampling depth, and reduced $O_2$ and Ar permeability of the coated substrate by 37.5% and 31.6% respectively. Saturation of the level of chemical modification at a plasma power of approximately 20 W suggested that further reaction is prevented by an impermeable $SiO_2$ surface layer. Treatments downstream of the glow discharge indicated that a combination of atomic oxygen and ultraviolet light bombardment accounted for most of the chemical modification. Higher pressure treatment resulted in the same level of modification, but indicated a deeper interface between unmodified and oxidized PPSQ. Future optimization of plasma treatment conditions with topographical characterization to produce a crack-free $SiO_2$ layer[33] may yield coatings with significantly lower gas permeability.

## 5.6 REFERENCES


1. Rochow, E. G. *Silicon and Silicones;* Springer-Verlag: Berlin, **1987**.
2. Zaichenko, L. P; Rassadina, T. N.; Abramzon, A. A.; Proskuryakov, V. A.; Khudobin, Y. I.; Kharitonov, N. P. *J. Appl. Chem. USSR* **1980,** *53,* 1231.
3. Lin, S.B. *J. Adh. Sci. & Tech.* **1996,** *10,* 559.
4. Tunney, M. M.; Keane, P. F.; Jones, D. S.; Gorman, S. P. *Biomaterials* **1996,** *17,* 1541.
5. Fakes, D. W.; Davies, M. C.; Brown, A.; Newton, J. M. *Surf. & Interface Anal.* **1988,** *13,* 233.
6. Munro, H. S.; McBriar, D. I. *J. Coating Tech.* **1988,** *60,* 41.
7. Watanabe, F.; Ohnishi, Y. *J. Vac. Sci. Tech. B* **1986,** *4,* 422.
8. Hartney, M. A.; Chiang, J. N.; Hess, D. W.; Soane, D. S. *Appl. Phys. Lett.* **1989,** *54,* 1510.
9. Chou, N. J.; Tang, C. H.; Paraszczak, J.; Babich, E. *Appl. Phys. Lett.* **1985,** *46,* 31.

10. Jurgenstein, C. W.; Shugard, A.; Dudash, N.; Reichmanis, E.; Vasile, M. J. *J. Vac. Sci. Tech. A* **1988**, *6*, 2938.

11. Namatsu, H. *J. Electrochem. Soc.* **1989**, *136*, 2676.

12. Jones, J. W. *U. S. Patent* # 3,442,686, 1969.

13. Lopata, E.; Felts, J. *U. S. Patent* #4,888,199, **1989**.

14. Felts, J; Lopata, E. *European Patent Office, Publication* #0299754 A2.

15. Morra, M.; Occhiello, E.; Garbassi, F. *J. Appl. Polym. Sci.* **1993**, *48*, 1331.

16. Greenwood, O. D.; Hopkins, J.; Badyal, J. P. S. *Macromolecules* **1997**, *30*, 1091.

17. Baney, R. H.; Itoh, M.; Sakakibara, A.; Suzuki, T. *Chem. Rev.* **1995**, *95*, 1409.

18. Mark, J. E.; Allcock, H. R.; West, R. *Inorganic Polymers*, Prentice Hall: New Jersey, **1992**, 156.

19. Barker, C. P.; Kochem, K.-P.; Revell, K. M.; Kelly, R. S. A.; Badyal, J. P. S. *Thin Solid Films* **1995**, *257*, 77.

20. Itoh M.; Suzuki, T. *private communication*, **1997**.

21. Alfonsetti, R.; Simone, G. De; Lozzi, L.; Passacantando, M.; Picozzi, P.; Santucci, S. *Surf. Interface Anal.* **1994** , *22*, 89.

22. Beamson, G.; Briggs, D. *High Resolution XPS of Organic Polymers, The Scienta ESCA300 Database*; J. Wiley and Sons: New York, 1992.

23. Loy, D. A.; Shea, K. J.; Buss, R. J.; Assink, R. A. in *Inorganic and Organometallic Polymers II*, Ed. Wisian-Neilson, P; Allcock, H. R.; Wynne, K. J. *ACS Symp. Ser. 572*, Washington D.C. **1994**, 122.

24. Rossnagel, S. M. in *Thin Film Processes II,* Editors Vossen, J; Kern, L., Springer-Verlag, **1989**, 34.

25. McTaggart, F. K. *Plasma Chemistry In Electrical Discharges*; Elsevier: Amsterdam **1967**.

26. Clark, D. T.; Dilks, A. *J. Polym. Sci., Polym. Chem. Ed.* **1980**, *18*, 1233.

27. Mano, T.; Hozumi, K.; Tatsuta, T.; Sawai, M.; Tsuji, O. *Anal. Lett.* **1992**, *25*, 1365.

28. Granier, A; Chereau, D.; Henda, K.; Safari, R.; Leprince, P. *J. Appl. Phys.* **1994**, *75*, 104.

29. CRC handbook of Chemistry & Physics, Ed. Weast, R. C.; Astle, M. J.; Publ. CRC Press , 60$^{th}$ edition, **1981**, F-1.

30. Hill, J. M; Royce, D. G.; Fadley, C. S.; Wagner, L. F. *Chem. Phys. Lett.* **1976,** *44,* 225.

31. Mi, Y.; Stern, S. A. *J. Polym. Sci.: Part B: Polym. Phys.* **1991,** *29,* 389.

32. Morra, M.; Occhiello, E.; Marola, R.; Garbassi, F.; Humphrey, P.; Johnson, D. *J. Colloid & Interface Sci.* **1990,** *137,* 11.

33. Owen, M. J.; Smith, P. J. *J. Adh. Sci. & Tech.* **1994,** *8,* 1063.

34. Everaert, E. P.; Vandermei, H. C.; Busscher, H. J. *J. Adh. Sci. & Tech.* **1995,** *9,* 1263.

35. Everaert, E. P.; Vandermei, H. C.; Busscher, H. J. *J. Adh. Sci. & Tech.* **1996,** *10,* 351.

36. Toth, A.; Bertoti, I.; Blazso, M.; Banhegyi, G.; Bognar, A.; Szaplonczay, P. *J. Appl. Polym. Sci.* **1994,** *52,* 1293.

37. Occhiello, E.; Morra, M.; Cinquina, P.; Garbassi, F. *Polymer* **1992,** *33,* 3007.

# Chapter Six : Conclusions

---

Investigations have been presented into the dependence of chemical and physical modifications of organic and inorganic polymer surfaces upon polymer chemical structure and upon the nature of the gas plasma used for modification. These studies have increased mechanistic understanding of plasma modification of polymer surfaces, allowing more accurate choices of system parameters to be made for desired surface properties. The presented research has also quantified differences which exist between low pressure and atmospheric non-isothermal plasmas and explored their potential for use in producing gas barrier polymer coatings from thin films of precursors.

Polymers containing chromophoric phenyl groups were more readily oxidized by low pressure plasma than by atmospheric discharge, due to the abundance of vacuum ultraviolet light and atomic oxygen radicals in the former. The level of oxygenation of phenyl containing organic polymers in a low pressure $O_2$ plasma followed the intensity of electronic excitation of phenyl groups in the unmodified polymers, confirming a VUV initiated atomic oxygen nucleophilic attack mechanism for chemical modification. In contrast, polymers such as polyisoprene which are highly susceptible to ozonolysis were most highly oxygenated by silent discharge treatment, which follows an activated ozonolysis reaction mechanism. Solvent rinsing of low pressure plasma modified polymers indicated that highly oxidized polymers such as PPO had a greater proportion of scissioned ring and chain molecules at the surface than less highly modified polymers such as PET.

Modification of polymer surface topography, such as roughening, was greatest in the case of silent discharge treatment, and for saturated polymers such as PIB, which easily undergoes chain scission. The level of chemical modification of phenyl containing polymers by low pressure $O_2$ plasma appeared to control the size of globular features on their surfaces, via agglomeration of high surface energy modified material on low surface energy substrates. Zirconium butoxide films appeared very rough on a large scale following plasma treatment; physical modification accompanied chemical changes and may have

reduced the gas barrier capabilities of the coating. AFM data from plasma physical modification of polymers showed an advantage of this imaging technique over SEM, in which necessary metallization of insulators may obscure such features.

Zirconium butoxide ($Zr(OBu)_4$) and polyphenylsilsesquioxane (PPSQ), which are oligomeric and macromolecular respectively, both showed potential as precursors to gas barrier oxide coatings though plasma oxidation. This process is additionally an alternative to sol-gel production of inorganic-organic composite coatings on temperature sensitive substrates. $O_2$ plasma treatment of films of both precursors, and $H_2O$ plasma treatment in the case of $Zr(OBu)_4$, converted metal centres from their initial state to metal dioxide environments and reduced film hydrocarbon content. Oxygen or hydroxy radicals at the plasma-precursor film interface, and possibly ions and VUV photons, play an important role in this conversion from organic to inorganic material: maximum PPSQ oxygenation occurred at the position in the discharge where the flux of both plasma VUV radiation and plasma atomic oxygen was high, indicating a synergistic modification mechanism.

PPSQ films were more reactive than $Zr(OBu)_4$ films towards $O_2$ plasma treatment, and $Zr(OBu)_4$ films underwent greater chemical modification for $O_2$ than $H_2O$ plasma treatment, suggesting a higher reactivity of this precursor with atomic oxygen than with hydroxy radicals. Oxidation extended throughout $Zr(OBu)_4$ films but was constrained to the surface-most layers in PPSQ, due to formation of an oxygen impermeable $SiO_2$ overlayer. Plasma pressure dependence of PPSQ modification depth confirmed a diffusion limited oxidation mechanism.

Decreases of 38 % and 32 % in $O_2$ and Ar permeability for $O_2$ plasma treated PPSQ and of 10 % and 19 % in $O_2$ and He gas permeability for $O_2$ plasma treated $Zr(OBu)_4$ coatings on PET confirmed the possibility of creating perm-selective or reduced permeability coatings by a novel process of non-isothermal plasma treatment of a solid precursor film. Limitations on gas barrier may have been due to cracks formed in plasma treated coatings and the thinness of $SiO_2$ films on plasma treated PPSQ films. Further work in this area may profit from the use of: alternative zirconium alkoxide precursors such as zirconium tertiary butoxide[1] which hydrolyze more easily than $Zr(OBu^n)_4$; siloxane precursors such

as polydimethylsiloxane which form thicker oxide layers than PPSQ[2]; treatment in plasmas which operate at higher pressure, such as diode discharge reactors; and moderate heating during plasma treatment, as in PECVD, which may reduce the final organic content of the film.

## REFERENCES

1. Bradley, D. C. *Chem. Rev.* **1989**, *89*, 1317.
2. Namatsu, H. *J. Electrochem Soc.* **1989**, *136*, 2676.

# Appendix One: Surface Analysis Techniques

## 1 INTRODUCTION

Analysis techniques which provide information about surface chemistry and morphology are well suited to the study of non-isothermal plasma-material interactions, since these interactions selectively modify the outermost few atomic layers of materials[1-4]. Furthermore, since the gas barrier and adhesive properties of a material depend directly on the physico-chemical state of its surface[5-7], detailed knowledge of surface properties allows mechanistic understanding of how these properties may be controlled.

Analyses of surfaces and sub-surfaces by photoelectron and infrared photon spectroscopies have been combined in this thesis with scanning probe atomic force microscopy, to provide complementary chemical and topographical data on the nature of surface modification by cold plasmas.

## 2 X-RAY PHOTOELECTRON SPECTROSCOPY

### *2.1 Introduction*

When atoms or molecules are illuminated with photons of sufficient energy, electrons are emitted according to the *photoelectric effect* first observed by Hertz in 1887. A photon's energy, hν, is used to overcome the ionization potential (in a solid, the binding energy $E_b$ plus the work function $\Phi$) and excess energy is conserved as kinetic energy $E_k$ of the photoelectron[8]:

$$E_k = h\nu - E_b - \Phi$$

Photons with an energy of hν can liberate electrons from levels up to a binding energy of $h\nu-\Phi$; X-radiation is used to probe core electrons (X-ray photoelectron spectroscopy, or XPS) whilst far-ultraviolet light can only release low-lying valence electrons (ultraviolet photoelectron spectroscopy, or UPS).

X-rays incident on the sample surface excite electrons at a series of energies representative of the binding energies of electron levels in the sample. A

vacuum of $10^{-7}$ torr or better ensures that most emitted electrons reach the energy analyzer without suffering energy loss, thus a spectrum is recorded which is characteristic of the sample[8]. Electrons that do undergo such inelastic losses contribute to the spectrum a step on the low kinetic energy side of the 'elastic' peak; these dominate the spectrum at low kinetic energy whilst electrons released by *Bremsstrahlung* radiation dominate the spectrum at high kinetic energy[9].

Following the removal of a core electron, radiationless decay is highly probable for atoms of atomic number less than 30, whilst X-ray fluorescence may be observed for heavier atoms[9]. In the former, an electron is demoted in energy to take the place of an emitted core electron and the excess energy is converted into kinetic energy of a second emitted electron, known as an Auger electron. The kinetic energies of Auger electrons are dependent only on the atoms energy levels which allows unique elemental identification from a series of Auger electron spectral peaks[10]. The binding energy of photoelectrons varies with their atom's chemical environment, leading to a shift in the energy spectrum of photoelectrons, which can be used to identify chemical species present in the analyzed surface[11].

### *2.2 Instrumentation*

A water cooled anode, typically magnesium or aluminium, is bombarded by 12 keV electrons in ultra high vacuum, emitting X-ray lines characteristic of transitions in the anode material in addition to a background of broad, continuous *Bremsstrahlung* radiation due to electrons de-accelerated at the anode. Mg K$\alpha$ radiation, used for XPS analyses in this thesis, is emitted from magnesium atoms when electron vacancies created in the K shell (orbital quantum number of 1) are filled by electrons in the L shell (orbital quantum number of 2). Emitted photons have an energy of 1253.6 eV, allowing core electrons to be released, and a linewidth of 0.7 eV, allowing spectral resolution of less than an electronvolt[9].

Energy dispersion of photoelectrons from the sample is achieved by an electrostatic field between concentric hemispherical surfaces. An electromagnetic

lens transfers electrons to the analyzer and reduces electron energy by a constant factor of $^{1}/_{22}$ to improve the analyzer's absolute energy resolution. This 'fixed retarding ratio' mode allows constant relative resolution (constant $^{\Delta E}/_{E}$) across the spectrum of kinetic energy[8].

Having traversed the analyzer, electrons are detected by a multi-electrode electron multiplier whose signal, after pre-amplification, is recorded as the number of counts per second at a certain kinetic energy.

### *2.3 Spectral Interpretation*

X-ray photoelectron spectra are direct representations of the core-electron structure of atoms in the sample surface[8]. Quantitative information regarding the elemental composition of the sample surface is obtained by calculating the area of each photoelectron peak after background removal. Sensitivity factors, which correct for differing photoionization cross-section of different elements, and for the transmission function of the lens-analyzer system, are obtained for a spectrometer by recording spectra of samples of known composition and stoichiometry[12].

Photoelectron binding energy can be used to distinguish between atoms differing in oxidation state, molecular environment, lattice site and type of bonds[9-11]. Gaussian peaks are statistically fitted to the recorded spectral envelope to allow calculation of the proportion of atoms in various environments[13].

### *2.4 Valence Band Spectral Features*

The loss of a core photoelectron causes a substantial reduction in electronic screening of valence electrons from nuclear charge. As a result, valence electrons may be promoted to a vacant orbit of higher energy, and the original photoelectron is emitted with a correspondingly lower kinetic energy[14]. This is referred to as a 'shake-up' transition and is commonly observed in the spectra of unsaturated molecules, in which $\pi$–$\pi^*$ transitions occur in the valence band[15].

*2.5 Sampling Depth*

Photoelectrons are liberated down to the depth of penetration of the X-rays (into the bulk), but the inelastic mean free path of free electrons in the solid is so small that only electrons released in the upper 20 to 50 Å escape into the surrounding vacuum. The cross section for inelastic scattering of electrons, $\sigma$, is a function of electron kinetic energy: $\sigma = f(Ek)$[9-11,16] therefore escape depth and surface sensitivity vary with kinetic energy of the observed electron peak as shown in figure A1.1[9]. Mean free paths are generally in the range 5 to 20 Å for the energy range 100 to 1000 eV used in XPS[9], therefore one can assume analysis of less than 60 atomic layers.

Inelastic loss processes for electrons include the excitation of lattice vibrations (phonons with energy of about $10^{-2}$ eV), of collective oscillations of the electron gas (plasmons with energy from 5 to 25 eV) and of electron interband transitions or ionization. At very low kinetic energy ($\ll 1$ eV) electrons are unable to excite any of the above quantized transitions and their mean free paths are long whilst at high kinetic energies the cross-sections for such processes are again low and escape depths large. In the intermediate (100 to 1000 eV) energy range used in XPS, electron escape depth is approximately linear with kinetic energy. Consequently, there is a tendency for photoelectrons with low kinetic energy to be released from the shallow, near surface region[16].

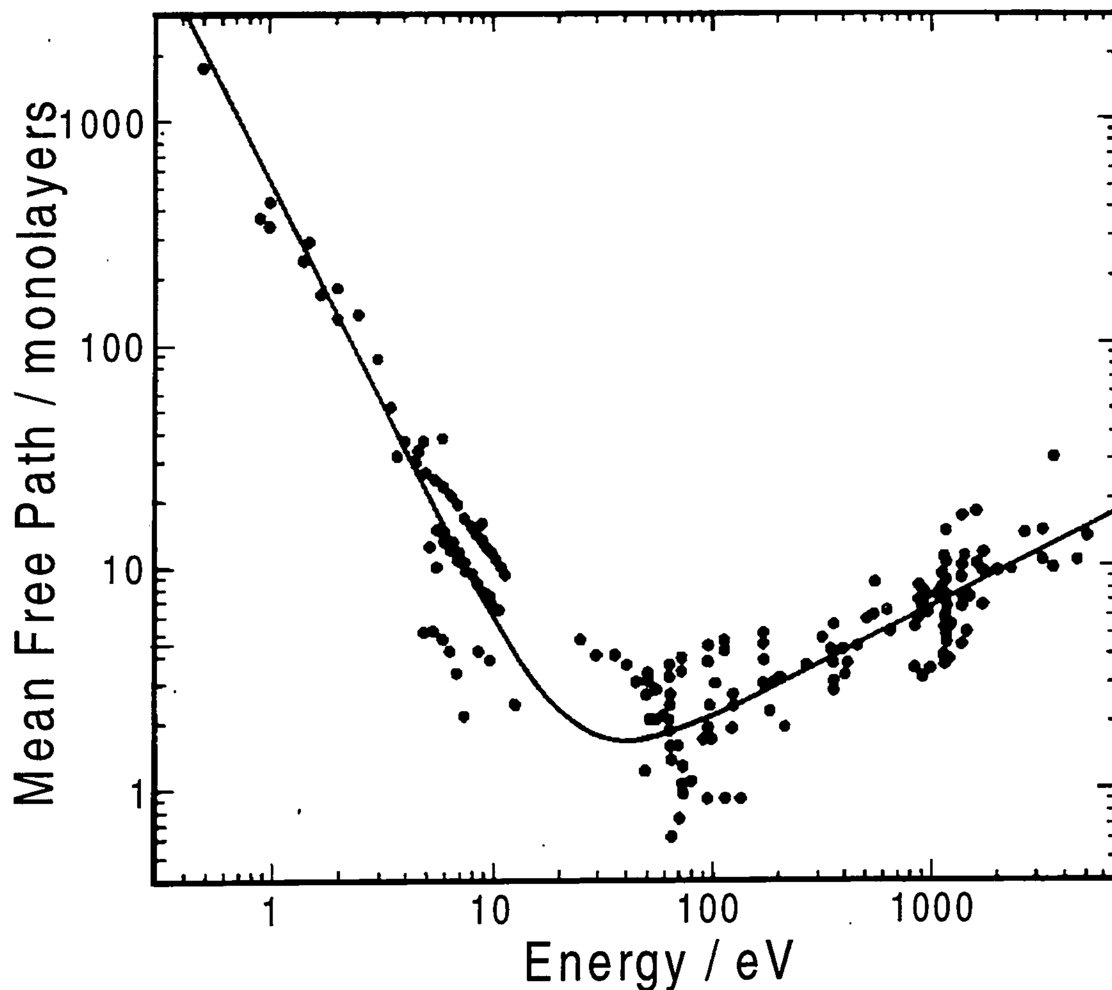


Figure A1.1 Variation of electron mean free path with kinetic energy[9].

*2.6 XPS Depth Profiling*

Composition and chemical states of subsurface material are important in understanding the behaviour of ultrathin films, functionally graded films, and multilayer coatings, and in probing the depth of chemical modification by plasmas[17]. A number of techniques use XPS non-destructively to provide chemical information from material beneath the sample surface: photoelectron sampling depth may be varied continuously by changing the angle, from the surface plane, at which electrons are detected[18]; sampling depth may be varied discretely by using more than one X-ray anode source material, such as magnesium and aluminium; photoemission core levels at different energies give depth resolved information[19-21] due to the dependence of electron escape depth with kinetic energy, Figure A1.1[9]. These techniques are limited to a profiling depth of about 5 nm from the surface[20].

Alternatively, analysis by XPS may be used between periods of energetic inert-ion sputtering to yield chemical information as the surface recedes[19-23]. Quantitative analysis in this destructive mode of depth profiling is limited by: differential sputter rates of different elements[24]; ion induced reduction of valence band electrons[25]; modification of surface composition by ion induced cascade mixing[26]; changes in surface microtopography[27]; and XPS analysis of a surface area greater than that evenly eroded by the ion beam[20].

### *2.7 Advantages and Disadvantages of XPS*

XPS is very widely used in surface research, so it is has good technical support and well developed data bases exist for comparison of data. During the relatively rapid collection of XPS data (about 5 minutes for each energy region of interest) the sample suffers very little damage and sample charging can be kept to a minimum by earthing through the sample holder. XPS peaks can be located to an accuracy of about 0.1 eV; the line width of the X-ray source is the limiting factor. The sensitivity of the technique varies by only about one order of magnitude amongst all elements, allowing good quantitative compositional analysis of all elements except hydrogen.

Disadvantages of XPS include the requirement of an ultra high vacuum; in some cases, the limited resolution of different chemical species due to small shifts in binding energy; and the variation of surface depth information with photoelectron kinetic energy.

## 3 SURFACE INFRARED SPECTROSCOPY

### *3.1 Introduction*

Absorption spectroscopy using radiation in the mid infrared region (4000 $cm^{-1}$ to 666 $cm^{-1}$) is commonly used to identify compounds and functional groups present in a sample[28]. Frequencies of absorption depend on the relative masses of atoms in the molecule, the bond strength (force constant for oscillation) and atomic geometry of chemical groups, allowing unique deduction of atomic groups within a molecular structure[29]. Comparison of a sample spectrum with

standard spectra in extensive libraries takes advantage of the complex nature of even simple molecules' spectra rather like fingerprinting; a spectral match at all infrared frequencies can yield positive identification[30].

Far infra-red (below 100 $cm^{-1}$) radiation absorbed by a molecule is stored as quantized rotational energy; this results in discrete lines in the absorption spectrum. Absorption of higher energy infrared radiation leads to a change in vibrational energy of the molecule, accompanied by a series of rotational energy transitions. These broaden the range of energies of all possible transitions, resulting in energy bands of various widths (about 10 $cm^{-1}$ wide)[31].

If an absorption causes a vibration which does not change the dipole moment of the molecule then no band will appear in the infrared spectral region, illustrated by the infrared inactive symmetrical stretches of $CO_2$. Conversely, functional groups with a strong dipole moment, such as carbonyls, have strong infrared absorption bands[29].

Vibrational modes of the molecule may be stretching or bending[29], Figure A1.2. The former involves regular vibrations along bond axes in which the interatomic distance oscillates but bond angles are constant; the latter is an oscillation in the angle between bonds with a common atom. Alternatively, the bend may be at a bond between a pendant group and the rest of the molecule.

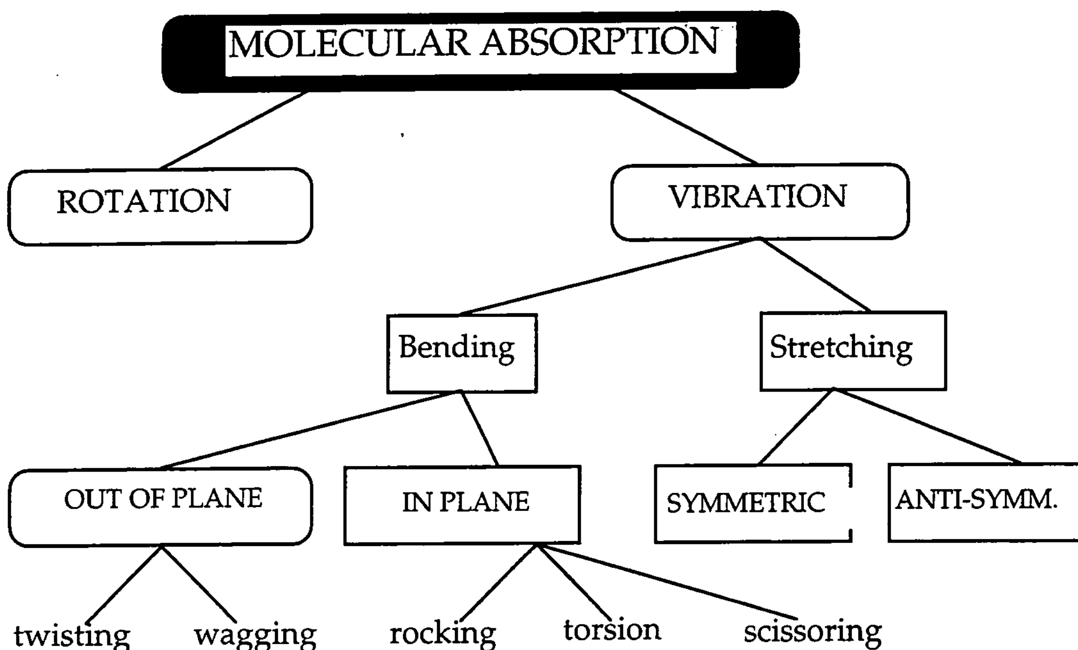


Figure A1.2 Modes of molecular excitation following infrared absorption.

### *3.2 Instrumentation*

Absorption experiments require a source of radiation, tunable or with a dispersing element, a sample holder and an intensity detector to register the radiant power transmitted by the sample at a certain frequency[28]. Mid and near infrared spectroscopy does not need vacuum conditions and high intensity sources are readily available. Dispersion can be performed by a diffraction grating or a Michelson-type interferometer, where the beam is split by a calcium fluoride or quartz crystal coated with silicon or germanium[28].

### *3.3 Attenuated Total Internal Reflection*

Transmission spectroscopy is a bulk analysis technique: multiple reflection of infrared may be used instead to obtain absorptions of surface species[32]. The sample, of refractive index $n_1$, is placed in good contact with an infrared transparent crystal, of high refractive index $n_2$, such as KRS-5 (thallium bromide - thallium iodide)[33]. Infrared radiation is directed into the crystal so that the angle of incidence at the crystal-sample interface, $\theta_i$, is greater than the critical angle for internal reflection, $\theta_c$:

$$\theta_i > \theta_c = \sin^{-1}(n_2/n_1)$$

Whilst being internally reflected, the radiation penetrates into the sample surface a short distance, d, determined by the refractive indices of the crystal and sample, the angle of incidence and the frequency of the radiation[33]. Electromagnetic energy in the form of a evanescent wave passes into the sample, to satisfy the condition of continuity of the normal electric field component at the media boundary, and probes the sample surface infrared spectrum[32]. The evanescent wave in the sample is not polarized so it can interact with dipoles in all directions. The refractive index of the sample is wavelength dependent and varies rapidly around the region that an absorption band occurs; this enhances the attenuation of reflected intensity and gives rise to the absorption spectrum.

Multiple reflections of the incident radiation along the crystal-sample interface increases attenuation at absorbed frequencies.

Penetration depth is typically about $10^{-6}$ m, providing surface chemical information which is complementary to that of XPS[31]. The sampled depth is greater at lower wavenumbers as radiation is more strongly absorbed at higher frequencies[34].

## A1.4 ATOMIC FORCE MICROSCOPY

### *A1.4.1 Introduction*

An experimental apparatus was developed *circa* 1970 for the direct measurement of forces between curved surfaces as a function of Angstrom level separations[35]. The technique relies upon extremely close positioning of surfaces, using a piezoelectric crystal, and the optical detection of deflection of springs on which the samples are mounted[36,37].

The atomic force microscope (AFM) is a related instrument, invented in 1986[38], in which a microscopically sharp tip attached to a cantilever is scanned laterally at Angstrom level distances from a surface; an image of the surface is produced using deflection of the cantilever as height contrast. Tip deflection has been measured by a variety of methods including a reflected laser beam, laser interferometry, variation of capacitance, and tunneling current from the cantilever[39].

The technique rapidly provides topographical images of non-conducting samples in air, without sample preparation, down to the scale of atomic resolution[40]. Practical limitations of the AFM are sample lateral motion noise[41,42] and interpretation of image features[40].

### *A1.4.2 Modes of Operation*

The AFM may be operated in a number of modes, using different types of cantilever, measuring forces of different magnitudes, and at different surface-tip distances[43]. In the 'contact mode' of operation, where tip-surface separation is

about $10^{-10}$ m, deflection of the tip measures relatively large ionic repulsive forces of about $10^{-9}$ N[40]. Cantilever deflection is proportional to the tip-surface force in the Hookean regime, and is used as the image contrast. Soft cantilevers are used in this mode[43], with spring constants of $10^{-3}$ $Nm^{-1}$ to 1 $Nm^{-1}$ [44]. Although atomic resolution is possible[45], there is significant chance of deforming soft sample surfaces and creating topographical artifacts such as 'smearing'[46,47], or of damaging the tip resulting in multiple tip imaging[44].

The 'non-contact mode' uses small amplitude (about 1 nm) oscillation of a relatively stiff tip[43], near to its resonant frequency of around 100 kHz, at tip-surface separations of about 10 nm[40]. Repulsive and attractive surface-tip forces have the effect of increasing and decreasing the oscillation frequency respectively[39], providing image contrast. Forces exerted on the surface by the tip are much smaller than in contact mode, but lateral resolution is poorer[43] and oscillations are often halted by the capillary force of an adsorbed surface water layer[48].

'Tapping Mode' AFM uses larger amplitude tip oscillations to ensure that the tip remains oscillating[48]. Lateral resolution may be as high as in contact mode, since the tip momentarily contacts the surface force many times at each of its scanned positions[49]. This mode is advantageous for imaging of easily deformed surfaces such as polymers[50], whilst damage to a tip may be checked by the inspection of its resonance response curve[48].

### A1.5 REFERENCES


1. Strobel M.; Corn, S; Lyons, C. S.; Korba, G. A. *J. Polym. Sci.: Polym. Chem. Ed.* **1985,** *23,* 1125.
2. Gerenser L. *J. Adh. Sci Tech.* **1987,** *1,* 303.
3. Nakayama Y.; Soeda F.; Ishitani A. *Polym. Eng. & Sci.* **1991,** *31,* 812.
4. Coopes I. H.; Grifkins K. J. *J. Macromol. Sci. Chem. Ed.* **1982,** *17,* 217.
5. Barker C. P.; Kochem K.-H.; Revell K. M.; Kelly R. S. A.; Badyal, J. P. S. *Thin Solid Films,* **1995,** *259,* 46.
6. Barker C. P.; Kochem K.-H.; Revell K. M.; Kelly R. S. A.; Badyal, J. P. S. *Thin Solid Films,* **1995,** *257,* 77.

7. Mittal K. L. *J. Vac. Sci. Tech.* **1976**, *13*, 19.
8. J.M. Walls Ed., "Methods OF Surface Analysis", Cambridge University Press, (1989).
9. D. Briggs and M.P. Seah *Practical Surface Analysis Volume 1 Auger and X-ray Photoelectron Spectroscopy*, 2$^{nd}$ Ed.; Wiley: N.Y., **1990**.
10. T. A. Carlson *Photoelectron and Auger Spectroscopy*; Plenum Press: N.Y., **1975**.
11. P. K. Ghosh, *Introduction To Photoelectron Spectroscopy*; Wiley & Sons: N. Y., **1983**.
12. Seah, M. P. *Appl. Surf. Sci.* **1993**, *70-71*, 1.
13. Beamson, G.; Briggs, D. *High Resolution XPS of Organic Polymers, The Scienta ESCA300 Database*; J. Wiley and Sons: New York, **1992**.
14. Clark, D. T.; Thomas, H. R. *J. Polym. Sci: Polym. Chem. Ed.* **1978**, *16*, 791.
15. Keane, M. P.; Naves de Brito, A.; Correia, N.; Svensson, S.; Lunell, S. *Chem Phys.* **1991**, *155*, 379.
16. M. Prutton, *Surface Physics*; 2$^{nd}$ Ed., Oxford Uni. Press, **1983**.
17. Le, Q. T.; Pireaux, J. J.; Caudano, R. *J. Adh. Sci. & Tech.* **1997**, *11*, 735.
18. McCaslin, P. C.; Young, V. *Scanning Microscopy* **1987**, *1*, 1545.
19. Hofmann, S. Ch. 4 in *Practical Surface Analysis Volume 1 Auger and X-ray Photoelectron Spectroscopy* Ed. Briggs D. and Seah M. P. 2$^{nd}$ Ed.; Wiley: N.Y., **1990**.
20. Ghosh, P. K. in *Introduction to Photoelectron Spectroscopy* J. Wiley & Sons: New York, **1983**, 160.
21. Ertl, G.; Kuppers, J. in *Low Energy Electrons and Surface Chemistry, Monographs in Modern Chemistry* Ed. Ebel, H. F. **1974**, *4*, 45 Verlag Chemie: Weinheim.
22. Zinner, E. *J. Electrochem. Soc.* **1983**, *130*, C199.
23. Hofman S. *Progress Surf. Sci.* **1991**, *36*, 35.
24. Mathieu, H. J.; Landolt, D. *Surf. Sci.* **1975**, *53*, 228.
25. Holm, R.; Storp, S. *Appl. Phys.* **1976**, *9*, 217.
26. Sigmund, P. in *Sputtering By Ion Bombardment*, Ed. Behrisch, Topics In Appl. Phys. **1981**, *1*, Springer Verlag, Heidelberg.
27. Hofman, S. *Appl. Phys.* **1976**, *9*, 59.

28. J. M. Hollas, *Modern Spectroscopy;* J. Wiley & Sons: New York, **1987**.
29. R. M. Silverstein, G. C. Bassler and T. C. Morril *Spectrometric Identification Of Organic Compounds;* Fourth Ed., Wiley & Sons: N. Y., **1981**.
30. Durig, J. R. *Vibrational Spectra And Structure, A Series Of Advances, Volume 18;* Elsvier: Amsterdam, **1990**.
31. Banwell, C. N. *Fundamentals Of Molecular Spectroscopy;* McGraw-Hill: London, **1983**.
32. Harrick, N. J. *Internal Reflection Spectroscopy;* John Wiley: N. Y., **1967**.
33. Winnograd, N. *Prog. Solid State Chem.* **1981**, *13*, 285.
34. Mirabella F. M. Jr.*Appl. Spec. Rev.* **1985**, *21*, 45.
35. Tabor, D.; Winterton, R. H. S.*Proc R. Soc Lond. A* **1969**, *312*, 435.
36. Israelachvili, J. N.; Tabor, D. *Proc R. Soc Lond. A* **1972**, *331*, 19.
37. Israelachvili, J. N.; Tabor, D. *Prog. Surf. Membrane Sci.* **1973**, *7*, 1.
38. Binig, G; Quate, C. F. Geber, Ch. *Phys. Rev. Lett.* **1986**, *56*, 930.
39. Sarid D.; Elings, V. *J. Vac. Sci. Tech. B* **1991**, *9*, 431.
40. Quate, C. F. *Surf. Sci.* **1994**,*299-300*, 980.
41. Goh, M. C.; Markiewiecz, P. *Chem. & Industry* **1992**,*September*, 687.
42. Rugar, D.; Hansma, P. *Physics Today* **1990**,*October*, 23.
43. Topometrix Tecnical Report *AFM Imaging Modes;* Topometrix Corporation: Santa Clara, **1993**.
44. Meyer, E. *Prog. Surf. Sci.* **1992**, *41*, 3.
45. Ohnesorge, F.; Binig, G. *Science* **1993**, *260*, 1451.
46. Hues, S. M.; Colton, R. J.; Meyer, E.; Guntherodt, H.-J. *MRS Bulletin* **1993**, *18*, 41.
47. Burnham, N. A.; Colton R. J.; Pollock, H. M. *J. Vac. Sci. Tech. A*, **1991**, *9*, 2548.
48. *Nanoscope Optical Viewing System Manual;* Digital Instruments Inc.: Santa Barbara, **1991**.
49. Elings, V.; Gurley, J. U. S. Patent No. 5,266,801, **1993**.
50. Hansma, P. K.; Cleveland, J. P.; Radmacher, M.; Walters, D. A.; Hillner, P. E.; Bezanilla, M.; Frtiz, M.; Vie, D.; Hansma, H. G.; Pratner, C. B.; Massie, J.; Fukunaga, J.; Gurley, J.; Elings V. *Appl. Phys. Lett.* **1994**, *64*, 1738.

# APPENDIX TWO: Courses, Conferences, Colloquia, Lectures and Seminars Attented

---

## COURSES ATTENDED

1. Chemistry Department induction courses;
2. Laboratory techniques, 6 lectures;
3. Electronic structure and bonding, 6 lectures.

## RESEARCH CONFERENCE ATTENDED

12th International Symposium of Plasma Chemistry, Loughborough University, August, 1993.

## COLLOQUIA, LECTURES AND SEMINARS ATTENDED

**1992**

Oct. 28 Dr. J. K . Cockcroft, University of Durham
Recent Developments in Powder Diffraction

Nov. 5 Dr. C. J. Ludman, University of Durham
Explosions, A Demonstration Lecture

Nov. 18 Dr. R. Nix, Queen Mary College, London
Characterisation of Heterogeneous Catalysts

Nov. 26 Dr. D. Humber, Glaxo, Greenford
AIDS - The Development of a Novel Series of Inhibitors of HIV

**1993**

Feb. 18 Dr. I. Fraser, ICI Wilton
Reactive Processing of Composite Materials

March 11 Dr. R. A. Y. Jones, University of East Anglia
The Chemistry of Wine Making

May 13 Prof. J. A. Pople, Carnegie-Mellon University, Pittsburgh, USA
Applications of Molecular Orbital Theory

| | |
|---|---|
| Sept. 13 | Dr. K.J. Wynne, Office of Naval Research, Washington, USA<br>Polymer Surface Design for Minimal Adhesion |
| Oct. 20 | Dr. P. Quayle, University of Manchester<br>Aspects of Aqueous ROMP Chemistry |
| Oct. 27 | Dr. R.A.L. Jones, Cavendish Laboratory, Cambridge<br>Perambulating Polymers |
| Nov. 10 | Prof. M.N.R. Ashfold, University of Bristol<br>High Resolution Photofragment Translational Spectroscopy : A New Way to Watch Photodissociation |

**1994**

| | |
|---|---|
| Jan. 26 | Prof. J. Evans, University of Southampton<br>Shining Light on Catalysts |
| Feb. 2 | Dr. A. Masters, University of Manchester<br>Modeling Water Without Using Pair Potentials |
| March 9 | Prof. F. Wilkinson, Loughborough University of Technology<br>Nanosecond and Picosecond Laser Flash Photolysis |
| Oct. 5 | Prof. N. L. Young, Brigham Young Univerity, Utah, USA<br>Determining Molecular Structure - the INADEQUATE NMR way |
| Dec. 7 | Prof. D. Briggs, ICI and University of Durham<br>Surface Mass Spectrometry |

**1995**

| | |
|---|---|
| Jan. 18 | Dr. G. Rumbles, Imperial College, London<br>Real or Imaginary Third Order Non-Linear Optical Materials |
| Feb. 1 | Dr. T. Cosgrove, Bristol University<br>Polymers do it at Interfaces |
| March 1 | Dr. M. Rosseinsky, Oxford University<br>Fullerene Intercalation Chemistry |
| May 3 | Prof. E. Randall, Queen Mary and Westfield College<br>New Perspectives In NMR Imaging |